DASA 2698
July 1971

UNCLASSIFIED

TRIAXIAL TESTS ON LARGE ROCK SPECIMENS

by

Peter Jay Huck
Madan M. Singh

for

HEADQUARTERS
Defense Atomic Support Agency
Washington, D.C. 20305

IIT RESEARCH INSTITUTE
Technology Center
Chicago, Illinois 60616

Contract No. DASA01-69-C-0134

Unclassified

Security Classification

DOCUMENT CONTROL DATA - R & D

(Security classification of title, body of abstract and indexing annotation must be entered when the overall report is classified)

1. ORIGINATING ACTIVITY (Corporate author)

IIT Research Institute, Chicago, Illinois

2a. REPORT SECURITY CLASSIFICATION

Unclassified

2b. GROUP

3. REPORT TITLE

TRIAXIAL TESTS ON LARGE ROCK SPECIMENS

4. DESCRIPTIVE NOTES (Type of report and inclusive dates)

Draft Final Report No. D6051-23

5. AUTHOR(S) (First name, middle initial, last name)

Peter J. Huck and Madan M. Singh

6. REPORT DATE	7a. TOTAL NO. OF PAGES	7b. NO. OF REFS
April 1971	165	45

8a. CONTRACT OR GRANT NO.	9a. ORIGINATOR'S REPORT NUMBER(S)
DASA-01-69-C-0134	
b. PROJECT NO. ARPA Order Number 1397	DASA 2698
c. Program Code 9F10	9b. OTHER REPORT NO(S) (Any other numbers that may be assigned this report)
d.	

10. DISTRIBUTION STATEMENT

Approved for public release, distribution unlimited

11. SUPPLEMENTARY NOTES	12. SPONSORING MILITARY ACTIVITY
	Director, Advanced Research Projec Agency, 1400 Wilson Blvd., Arlingt Virginia 22209

13. ABSTRACT

A study was conducted to determine the effect of specimen size on the mechanical response of rock. Specimens of Cedar City tonalite (Cedar City, Utah) and Charcoal Black granite (Cold Springs, Minnesota ranging in size from 2 in. dia. to 32 in. dia. (24 in. dia. for the tonalite) were tested in triaxial compression. In addition to the standard triaxial test stress trajectory, one specimen of each rock type was loaded uniaxial strain to simulate true one-dimensional compression. Test data included axial and circumferential strain at up to 30 locations on the largest specimens, surface wires to indicate crack propagation on the 12 inch and larger specimens, axial and radial stresses and the confining pressure media temperature. Data were recorded under loading, unloading and reloading conditions. The test data for each specimen size and rock type were fit to a non-linea hysteretic model to determine variation in the model parameters as a function of specimen size.

KEY WORDS	LINK A		LINK B		LINK C	
	ROLE	WT	ROLE	WT	ROLE	WT
Large Triaxial Tests						
Scale Effect						
Cedar City Tonalite						
Charcoal Black Granite						
Non-Linear Hysteretic Model						

IIT RESEARCH INSTITUTE
Technology Center
Chicago, Illinois 60616

IITRI Project No. D6051
Final Report No. D6051-23
Contract No. DASA-01-69-C-0134

TRIAXIAL TESTS ON LARGE ROCK SPECIMENS

by

Peter Jay Huck
Madan M. Singh

for

Department of Defense
Advanced Research Projects Agency
Washington, D.C.

July 1971

DASA 2698

TRIAXIAL TESTS ON LARGE ROCK SPECIMENS

by

Peter Jay Huck
Madan M. Singh

IIT Research Institute
Technology Center
Chicago, Illinois 60616

ARPA Order Number	ARPA 1397
Program Code Number	9F10
Name of Contractor	IIT Research Institute
Effective Date of Contract	15 May 1969
Contract Expiration Date	15 Aug 1971
Amount of Contract $	$99,000
Contract Number	DASA01-69-C-0134
Principal Investigator and Phone Number	Madan M. Singh AC312/225-9630 Ext. 4784
Project Scientist or Engineer and Phone Number	Peter J. Huck AC312/225-9630 Ext. 4735
Short Title of Work	Triaxial Tests Large Rock Specimens

Sponsored by
Advanced Research Projects Agency
ARPA Order No. 1397

FOREWORD

This is a final report on IIT Research Institute (IITRI) Project D6051 (IITRI Report No. D6051-23) entitled, "Triaxial Tests on Large Rock Specimens". This research was supported by the Advanced Research Projects Agency of the Department of Defense and was monitored by Mr. Clifton McFarland under Contract No. DASA 01-69-C-0134.

The project was conducted under the supervision of Dr. Madan M. Singh, who served as program manager. Mr. Peter J. Huck was project engineer. Other IITRI staff members who contributed to the overall research effort include Dr. R. H. Cornish and Messrs. F. W. Dew, L. A. Finlayson, P. A. Hettich, S. Martin, R. D. Nelson and J. J. Vosatka.

Respectfully submitted,
IIT Research Institute

Peter Jay Huck
Project Engineer

APPROVED:

R. H. Cornish
Director
Mechanics of Materials Division

PJH:bk

TABLE OF CONTENTS

Section		Page
1	INTRODUCTION	2
2	PREVIOUS STUDIES	4
	2.1 Effect of Size	4
	2.2 Effect of Confinement	7
3	EXPERIMENTAL APPARATUS	9
	3.1 Small Test Cells	11
	3.2 48-Inch Test Cell	11
	3.3 Specimen Preparation	17
	3.4 Instrumentation and Data Reduction	18
4	EXPERIMENTAL PROGRAM	21
5	DISCUSSION OF RESULTS	30
	5.1 Theoretical Considerations for Constitutive Equations	30
	5.1.1 Formulation of Constitutive Equations	30
	5.1.2 Limit Surface	31
	5.1.3 Elastic Equations	33
	5.2 Typical Behavior of Rock	34
	5.2.1 Hydrostatic Behavior	34
	5.2.2 Triaxial Compression	39
	5.2.3 Uniaxial Strain	43
	5.2.4 Poisson's Ratio and Young's Modulus	43
	5.2.5 Yield and Fracture Criteria	45
	5.3 Analysis of Experimental Results	47
	5.3.1 Charcoal Black Granite	47
	5.3.2 Cedar City Tonalite	59
	5.3.3 Uniaxial Strain Tests	66
	5.4 Strength Properties	72
6	SUMMARY AND CONCLUSIONS	74

TABLE OF CONTENTS (Cont'd.)

Section		Page
	REFERENCES	78
	APPENDIX A - COMPUTER PLOTS OF TEST DATA	A-1

LIST OF FIGURES

Figure		Page
1	Typical Triaxial Cell Schematic	10
2	Schematic of System for 2 in., 4 in., and 12 in. Triaxial Specimens	12
3	48 in. dia. Cell with 32 in. dia. Specimen Being Loaded	13
4	Schematic of 48 in. dia. Triaxial Cell	14
5	Radial Strain Gages for Uniaxial Strain Tests	16
6	Typical Gage Layout	19
7	Loading Specimen Into 48 in. dia. Triaxial Cell	23
8	Inserting Sliding Piston Into 48 in. dia. Triaxial Cell	24
9	Removing Fractured Specimen From 48 in. dia. Triaxial Cell	25
10	32 in. dia. Charcoal Black Granite Specimen After Tests 27-28 (σ_c = 5000 psi)	26
11	32 in. dia. Charcoal Black Granite Specimen After Tests 29-30 (σ_c = 10,000 psi)	27
12	32 in. dia. Charcoal Black Granite Specimen After Test 31 (uniaxial strain)	28
13	22 in. dia. Cedar City Tonalite Specimen After Test 32 (uniaxial strain)	29
14	Yield Surface for Mises' Yield Criterion	32
15	Typical Compressibility Curve for Rock, After Paulding (40)	35
16	Compressibility of Granite, Gabbros and Diabases, After Clark (41)	36
17	Stress Strain Curve for Nonlinear Hysteretic Model	38

LIST OF FIGURES (Cont'd.)

Figure		Page
18	Idealized Stress Strain Behavior of Rock After Swanson (21)	41
19	Variation of Shear Modulus with Mean Stress	42
20	Yield Criteria	46
21	Mean Stress vs. Volumetric Strain, Typical Response for Charcoal Black Granite	48
22	Bulk Modulus vs. Mean Stress - 2" Ø and 4" Ø CBG	49
23	Bulk Modulus vs. Mean Stress - 12" Ø and 32" Ø CBG	50
24	Deviator Stress vs. Strain, Charcoal Black Granite	54
25	Tangent Moduli for Charcoal Black Granite, 2-In. Dia.	55
26	Tangent Moduli for Charcoal Black Granite, 4-In. Dia.	56
27	Tangent Moduli for Charcoal Black Granite, 12-In. Dia.	57
28	Tangent Moduli for Charcoal Black Granite, 32-In. Dia.	58
29	Poisson's Ratio vs. Mean Stress for 2" Ø and 4" Ø Charcoal Black Granite	61
30	Poisson's Ratio vs. Mean Stress for 12" Ø Charcoal Black Granite	62
31	Poisson's Ratio vs. Mean Stress for 32" Ø Charcoal Black Granite	62
32	Bulk Modulus for 2" Cedar City Tonalite	63

LIST OF FIGURES (Cont'd.)

Figure		Page
33	Bulk Modulus for 4" Cedar City Tonalite	63
34	Variation of Bulk Modulus for Cedar City Tonalite, 2-in., 4-in. and 12-in. dia.	64
35	Volumetric Strain for Cedar City Tonalite Models	64
36	Bulk Modulus for Cedar City Tonalite Models	65
37	Tangent Moduli for Cedar City Tonalite	67
38	Poisson's Ratio for Cedar City Tonalite	68
39	Uniaxial Strain Test	70
40	Shear Behavior for Uniaxial Strain Tests	71
41	Volumetric Strain for Uniaxial Test	71
42	Maximum Value of $\sqrt{J_2'}$ Reached for All Tests	73

ABSTRACT

A study was conducted to determine the effect of specimen size on the mechanical response of rock. Specimens of Cedar City tonalite (Cedar City, Utah) and Charcoal Black granite (Cold Springs, Minnesota) ranging in size from 2 in. dia. to 32 in. dia. (22 in. dia. for the tonalite) were tested in triaxial compression. In addition to the standard triaxial test stress trajectory, one specimen of each rock type was loaded under uniaxial strain to simulate true one-dimensional compression. Test data included axial and circumferential strain at up to 30 locations on the largest specimens, surface wires to indicate crack propagation on the 12 inch and larger specimens, axial and radial stresses and the confining pressure media temperature. Data were recorded under loading, unloading and reloading conditions. The test data for each specimen size and rock type were fit to a non-linear hysteretic model to determine variation in the model parameters as a function of specimen size.

TRIAXIAL TESTS ON LARGE ROCK SPECIMENS

1. INTRODUCTION

Currently a number of structures are being located underground, many of which are in rock. It is anticipated[1,2] that the number of such underground structures will increase enormously in the next two decades. It may be concluded that the number of structures in rock will increase correspondingly. In spite of this anticipated underground construction activity, little is known about the mass behavior of rock. It is qualitatively recognized, of course, that the rock mass behaves distinctly differently from the matrix in small samples, but this effect of size is not well understood, and cannot be predicted, to date, with any degree of confidence. These variations are attributed to joints and other weakness planes in the rock mass. Yet, most of the test procedures for determining strength and elastic moduli information about rocks are based on these properties on small samples[3-6]. It is both difficult and expensive to try to perform properties tests on larger specimens. Hence some relationships between the various sizes need to be established. It was the intent of this program, to study the mechanical behavior of rock specimens of different sizes, and to determine how these relate to each other.

During this program, two varieties of rock, Charcoal Black granite from Cold Springs, Minnesota and Cedar City tonalite from Cedar City, Utah, were investigated. Four sizes of rock cores, 2-in. dia., 4-in. dia. 12-in. dia., and 32-in. dia. (22-in. in case of the tonalite) were subjected to triaxial compression tests. The specimens were strain gaged to determine the elastic modulii. One test on the large core samples of each rock type was uniaxial strain only. The data obtained was correlated to ascertain trends.

Accumulation of sufficient data on size effects with various rock types may be expected to finally lead to predictive equations for the rock mass. It should be borne in mind, however, that the strength properties of smaller rock samples are governed by microflaws such as crystal lattice disturbances, grain boundaries, minute voids (pores) and weak cementing material. The strength of the rock mass is dependent on macroflaws, i.e. failure planes, joints, cavities, and intrusions. It also appears probable that the rock mass is more affected by environmental conditions than the matrix. In general, environmental factors induce a time-dependent reduction in strength by chemical alteration, rheological deformation, and structural failure. The roles of residual stresses in the rock matrix and orogenic forces on the mass are not well understood; hence their effect on rock behavior requires further study. The presence of water significantly affects the behavior of the rock mass as well as the matrix. In general it tends to reduce the structural strength, but whether the manner in which this is accomplished in the two cases is the same, has not been clearly established. Finally, it should be mentioned that the configuration of the rock mass, and the base material on which it rests probably controls its gross behavior. It would be difficult to simulate these conditions in laboratory samples, but the overall effects maybe estimated by varying size and end conditions.

2. PREVIOUS STUDIES

2.1 Effect of Size

Several studies have been conducted to determine the effect of size of specimens. Most of these have been with unconfined compressive tests. Rice and Enzian[7] showed that the compressive strength of 2 1/2 - 4 in. coal cubes was about 2500 psi, whereas a 54 in. cube of the same coal failed at 300 psi. Greenwald, Howard, and Hartmann[8] related the size of coal pillars to their compressive strength at an experimental face by over-cutting and side-cutting. There was a decrease in strength with increasing pillar height relative to the cross-sectional area, the breaking stress σ_c for small pillars approximately satisfying the relationship

$$\sigma_c \propto \left(\frac{b}{h}\right)^{0.5},$$

where b is the lateral dimension of the pillar and h is its height. Burton and Phillips[9] studied the relationship between size and compressive strength of cubes of anthracite over the range 1/4 in. to 4 in. and found that

$$\sigma_c \propto a^{-0.45 \pm 0.05},$$

where a is the linear dimension of the cubes. Millard, Newman and Phillips[10] extended the range of these observations, and used Griffith's theory of crack propagation to explain the failure phenomenon. Both these investigations by Phillips and his associates may be said to show that approximately

$$\sigma_c \propto a^{-0.5},$$

Evans and Pomeroy[11] found that the relation between the mean crushing load (φ) and the side of the cube (a) is of the

form

$$\varphi \propto a^{\beta},$$

where β = constant varies between 1.5 and 2, i.e.,

$$\sigma_c \propto a^{-0.5 \text{ to } 0}$$

Holland[12] has suggested a coal pillar design formula as follows:

$$\sigma = \frac{ka^{0.5}}{h}$$

where a = least width of pillar (inches), h = thickness of pillars (inches), and k = coefficient depending on type of coal. This is valid for a/h ratios between 1 and 10.

For rocks, the types of relationships developed are slightly different. According to the Weibull theory[13],

$$\left(\frac{\sigma}{\sigma_m}\right)^{\alpha} = \left(\frac{v_m}{v}\right)$$

where σ = tensile or compressive strength of the rock from a standard laboratory test,

σ_m = equivalent strength of the rock mass,

v_m = volume of the rock mass,

v = volume of the test sample, and

α = constant (with values near 10 for rocks).

The relation established by Protodyakonov[14] was of the type

$$\frac{\sigma}{\sigma_m} = 1 + \frac{s(\gamma - 1)}{s + a}$$

where s = spacing between major discontinuities in the rock mass, e.g., joints, beds.

a = dimension of the test specimen, usually diameter for compression tests, and

δ = mass fracture coefficient (in compression:1-2 for igneous rocks, 1-3 for competent sedimentary rocks, 3-10 for weak rocks; in tension: approximately double these values).

Grobbelaar[15], based on the work of Epstein[16], Bieniawski[17], and others, found that the formulae relating the modal strength of the weakest elements and its standard deviation, based on the weakest link theory, are

$$\sigma_N = \sigma_u - \sigma_s \ (2\log N)^{0.5} - 1/2 \ \{\log(\log N) + \log(4\ )\} \ (2\log N)^{-0.5}$$

and $\sigma_s(N) = \sigma_s \times \pi (12\log N)^{-0.5}$

or $\sigma_s(N) = \sigma_s(N_o) \ (\log N_o / \log N)^{0.5}$

where N = number of flaws in the large cubic specimen,

N_o = number of flaws in the small cubic specimen or unit cube,

σ_N = modal strength of the weakest link in a sample containing N elements,

σ_u = average strength of a unit cube of material containing N_u elements,

σ_s = standard deviation of the modal strength of samples containing N_o elements,

and $\sigma_s(N)$ = standard deviation of the modal strength of the weakest element in a sample containing N elements.

These formulae are based on the "weakest link theory", which can be analyzed mathematically if it is assumed that the frequency of occurrence of events is a continuous function (e.g. Weibull[13] or normal distribution). The "links" in this case are the macroflaws (or cracks) in the bulk material; not the microflaws.

Glucklich and Cohen[18,19] have indicated that effects other than statistical exist, since the total stored elastic energy increases with specimen volume. The energy released at onset of fracture is related to initiate fracture; in other words, this reduces the rock strength. This phenomenon has been recently discussed by Baecher[20].

2.2 Effect of Confinement

There have been numerous studies investigating the effects of various aspects of confinement on rocks. It is not intended to review all of these completely in this section. Most of the pertinent work has been briefly discussed by Swanson[21]. The earliest experimental work was performed by Adams[22] and von Karman[23]. However, significant headway was not made until the initiation of work by Griggs[24] and his coworkers[25-26]. Since then a number of researchers have conducted various types of studies under pressure several of which were presented at a symposium on rock deformation[27]. Baidyuk[28] has summarized some of the Russian and American work. Research in this area is still very active[21,29,30]. All of this work has been performed with small rock specimens, a few inches in diameter. As a result considerable light has been shed on the behavior of the rock matrix and the criteria of failure. Refinements to the Griffith hypothesis have been proposed[31-33] and appear to explain the rock fracture process under confinement fairly well. The extrapolation of these theories to larger rock masses is of doubtful value and hence large scale field testing has to be resorted to[34]. The U. S. Bureau of Mines has undertaken a rather comprehensive program to collect field data with the intention of correlating it into a hypothesis[35]. The contributions of Hoek[36], Bieniawski[37], Cook[7], Wawersik[38] and Houpert[39] to the mechanism of brittle failure in rock deserve to be noted even though the studies

were not conducted under a confined state of stress.

To the best of the authors' knowledge no experimental investigations on large rock samples under confinement have been performed.

3. EXPERIMENTAL APPARATUS

In order to conduct triaxial tests for the range of specimen sizes used on this project, four triaxial cells were set up as shown below:

Chamber I.D. (in.)	Specimen Diameter (in.)	Maximum Chamber Pressure (ksi)	Maximum Axial Load lb. x 10^6
4.0	2.06	30	0.375
6.5	3.65	30	0.990
14.7	10-12	20	3.40
48.3	22-32	20 axial 10 confining	36.5

In a standard triaxial cell the axial load is supplied by an external loading machine. However, in order to achieve the large end loads required for the tests in this program, these chambers were separated into two regions by sliding pistons. The general configuration is shown in Fig. 1. One region contained the specimen, and was pressurized to the desired confining pressure. Axial load was transmitted to the rock by the sliding piston. The maximum axial stress in the rock depends upon the ratio of the rock and piston areas and the difference in the confining pressure and the axial chamber pressure. The specimen stresses are given by the following equations:

$$\sigma_2 = \sigma_3 = P_3$$

$$\Delta\sigma_1 = (P_1 - P_3)\,\frac{Ap}{Ar}$$

$$\sigma_1 = \sigma_3 + \Delta\sigma_1$$

where

A_p = piston area

A_r = specimen area

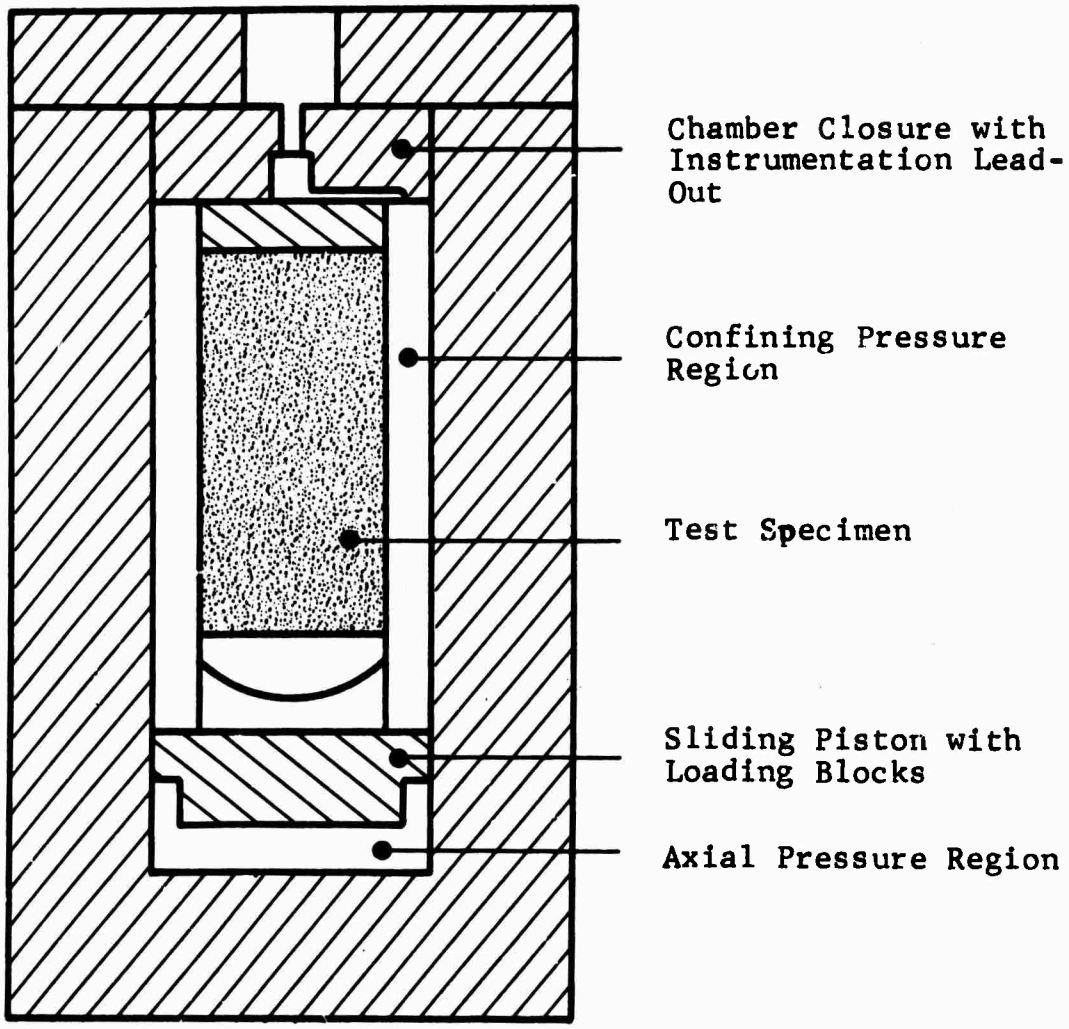

Fig. 1 TYPICAL TRIAXIAL CELL SCHEMATIC

P_1 = axial chamber pressure

P_3 = confining chamber pressure

$\Delta\sigma_1$ = deviator stress

σ_1, σ_2 and σ_3 = principal stresses.

Reference to Figure 1 and the above equations confirms that if $P_1 = P_3$, $\Delta\sigma_1 = 0$ and the specimen is under hydrostatic stress ($\sigma_1 = \sigma_2 = \sigma_3$). For $P_3 = 0$, the specimen is unconfined, with $\sigma_2 = \sigma_3 = 0$ and $\sigma_1 = \Delta\sigma_1 = P_1 A_p/A_r$.

3.1 Small Test Cells

The three smaller test cells are incorporated into a testing system with centralized controls, instrumentation, and pumping systems. A schematic of this system is shown in Fig. 2. The tests conducted in this system consisted of initial hydrostatic loading up to the desired confining pressure, followed by triaxial compression at constant σ_3 above that pressure. At least one load-unload-reload cycle was observed for each test. Provision was made for pressure cross-connections between the confining pressure and axial pressure chamber volumes to insure hydrostatic conditions during the hydrostatic test phases.

3.2 48-Inch Test Cell

This test cell is shown in Figs. 3 and 4. The basic unit is a 48" I.D. by 86" working length chamber having 20,000 psi design working pressure. The chamber walls are built up from rings 12" long which are held in place by a 3/4" thick liner on the inside diameter. The entire axial load is carried by a flexible reaction frame which was built up from steel strap. The 140 ton weight of this chamber is substantially less than the weight that would have been required by conventional chamber design. This is the

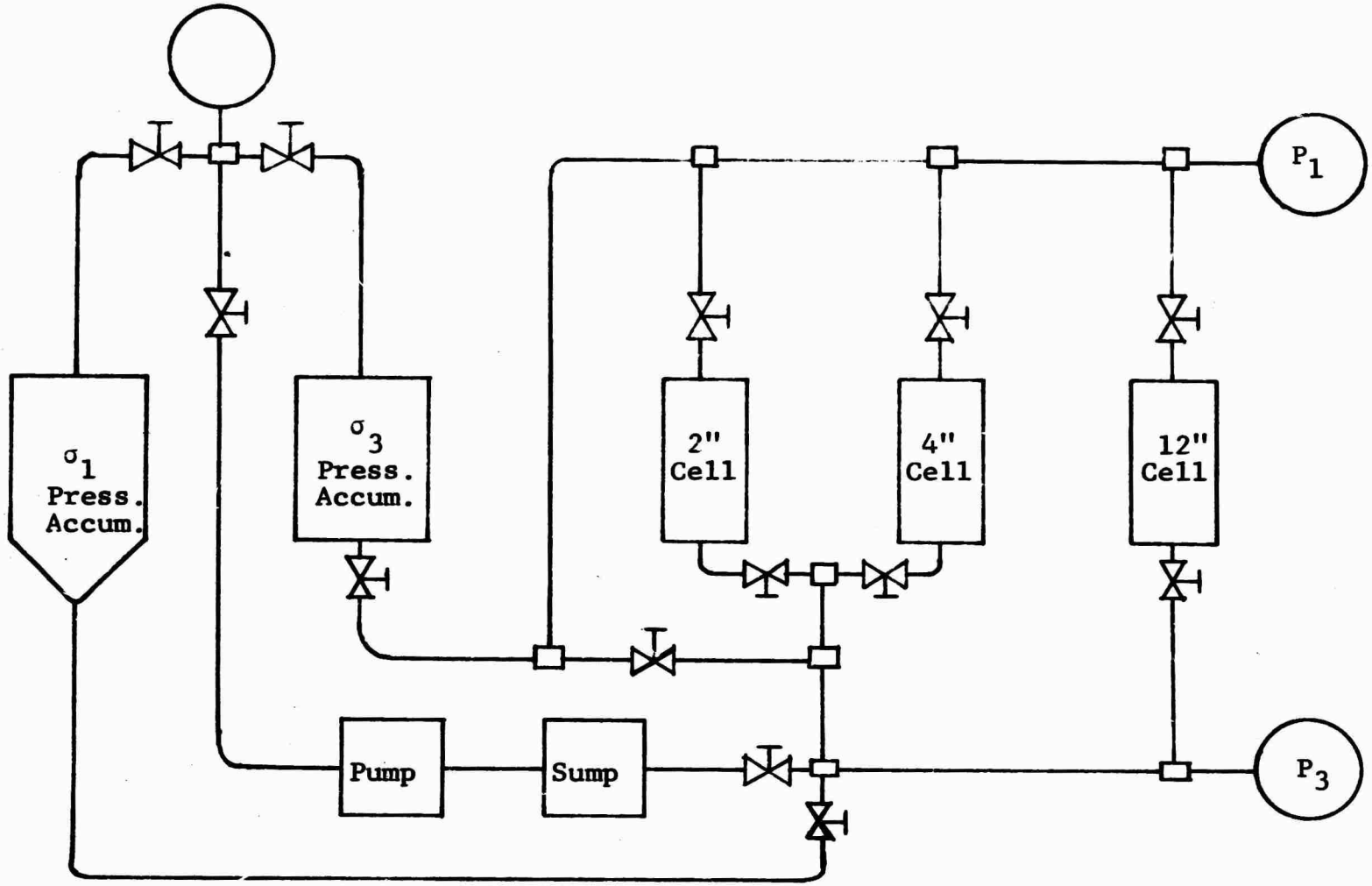

Fig. 2 SCHEMATIC OF SYSTEM FOR 2 IN., 4 IN., AND 12 IN. TRIAXIAL SPECIMENS

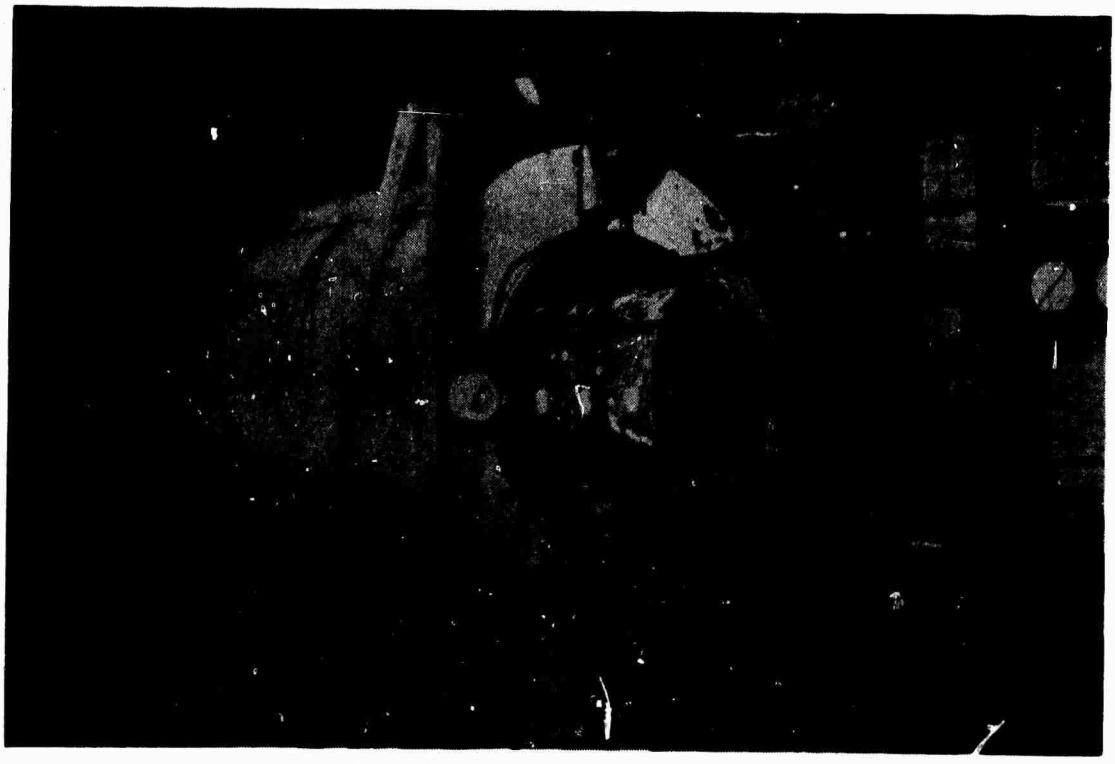

NOT REPRODUCIBLE

Fig. 3 48 IN. DIA. CELL WITH 32 IN. DIA. SPECIMEN BEING LOADED

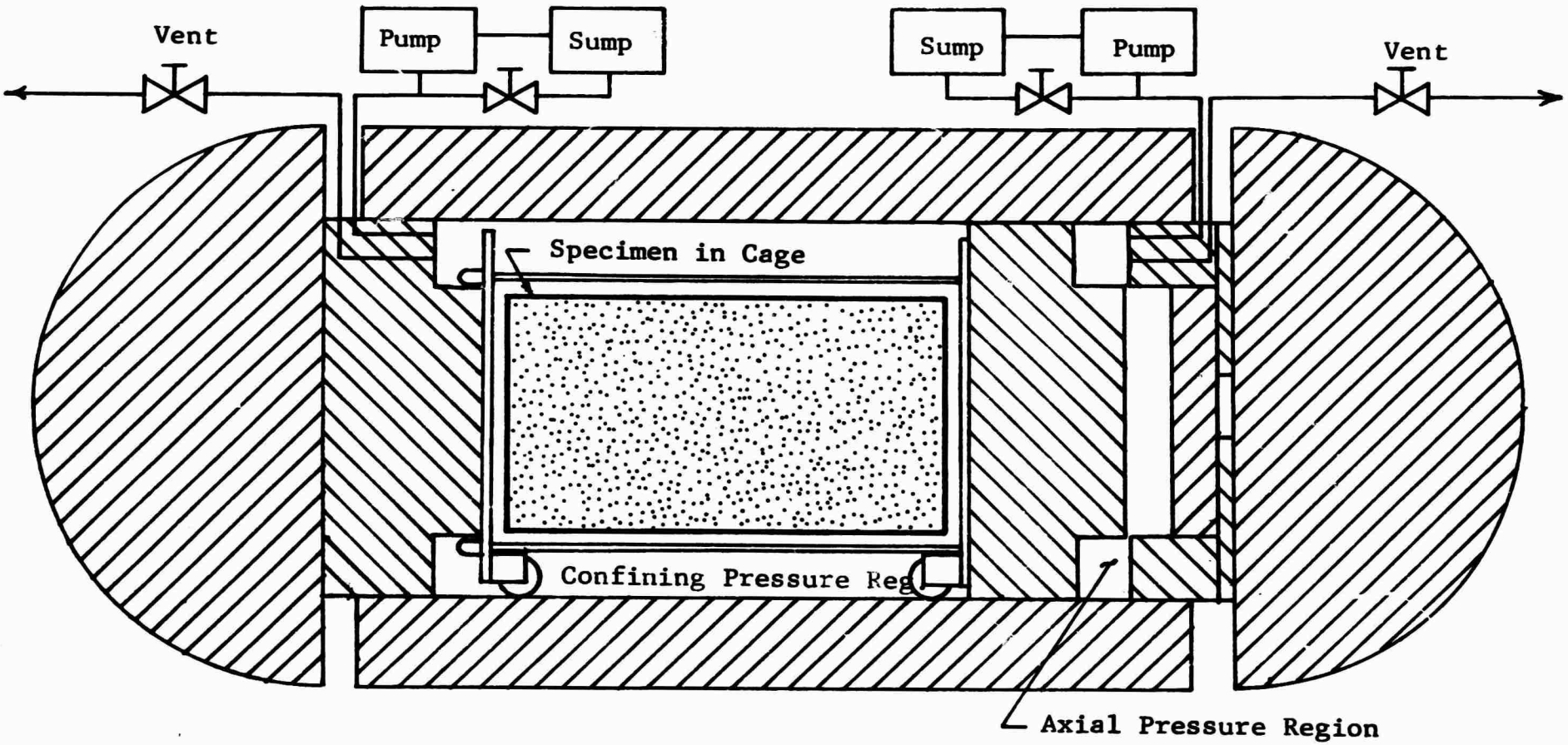

Fig. 4 SCHEMATIC OF 48 IN. DIA. TRIAXIAL CELL

largest chamber currently available at IIT Research Institute, and is capable of applying axial loads of 36 million pounds to rock specimens as large as 3 1/2 ft. in diameter.

As can be seen in the schematic, the pumping and control systems for this unit are simpler than for the small chambers. A separate pump was used at each end of the chamber. Accumulators were not used because the chamber volume itself is large in comparison with other available pressure chambers.

The operation of this chamber is similar to that of the smaller chambers, except that the turn-around time between tests in on the order of a week instead of an hour. The tests in this chamber differed slightly from those in the smaller test cells. In order to maintain seal integrity, a positive pressure differential of about 200 psi was maintained across the sliding piston during the "hydrostatic" portions of the triaxial tests, and the axial pressure was not allowed to drop below 400 psi at the bottom of the load-unload-reload cycle. Had these precautions not been taken, there would have been danger of upsetting the piston seal, thus aborting the remainder of the test.

Two of the large specimens were loaded to produce uniaxial strain. Figure 5 shows the two transducers were designed to provide measurements of average radial strain. One transducer consisted of a full strain gage bridge using manganin wire elements. The active elements each consisted of 4 turns of manganin wire wound tightly around, but not bonded to, the specimen. Temperature and pressure compensation were achieved by similar elements loosely wound on the specimen next to the active elements. The second transducer consisted of an open steel loop pinned to the specimen. The open ends of the loop were jointed by a flexible strap mounting foil strain gages as shown in Figure 5b. Small

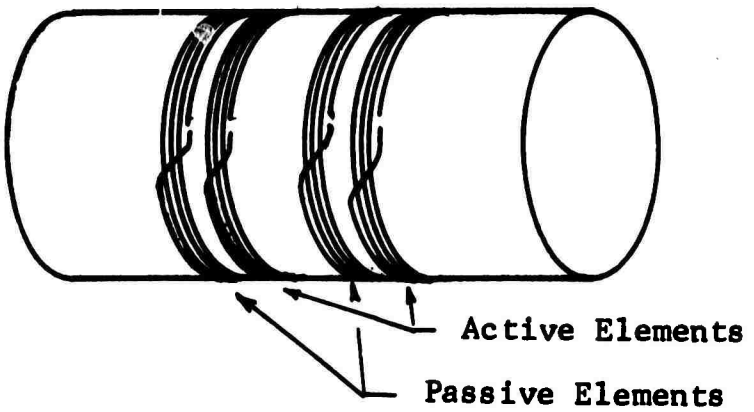

5a - Manganin Wire Gages

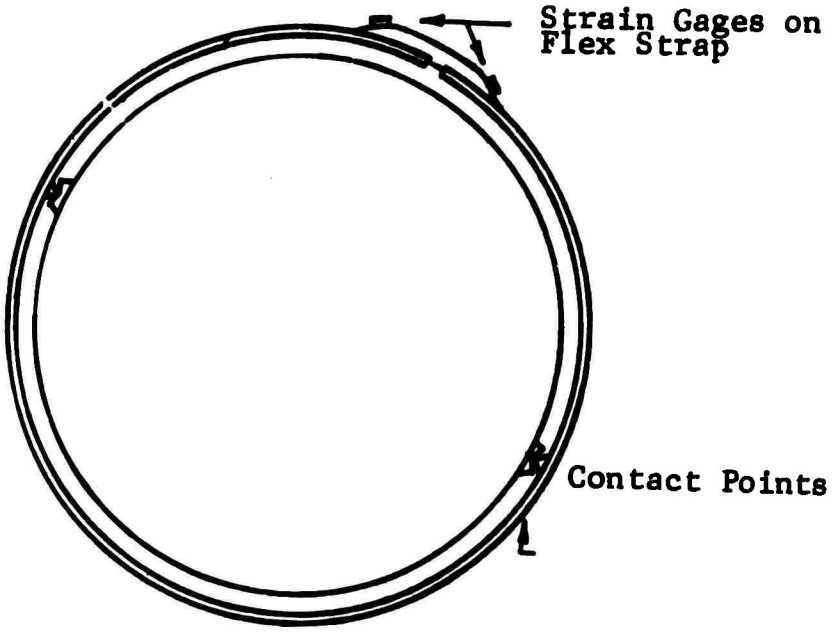

5b Beam Type Gage

Fig. 5 RADIAL STRAIN GAGES FOR UNIAXIAL STRAIN TESTS

deflections at the diametrically opposed pins cause relatively large bending strains in the flexible strap. This transducer suffered from somewhat erratic operation, as is usual with any point-to-point gages on rock specimens.

3.3 Specimen Preparation

Specimens of the Charcoal Black Granite were bought from Cold Spring Granite Co. in Cold Spring, Minnesota, but the Cedar City tonalite was supplied by DASA. In both cases, the larger cores (10 or 12-in. and 22 or 32-in. dia.) were obtained as such from the source, but the 2-in. and 4-in. dia. specimens were cored in the laboratory from extra rock obtained in each case. These smaller cores were cut parallel to the axis of the larger cores so as not to introduce complications because of anisotropy.

End preparation of the 2-in. and 4-in. dia. cores consisted of facing on a lathe until the ends were plane and parallel to 0.001 inches. The larger cores were capped in a specimen cage to permit handling. The capping material used was a steel-filled epoxy. Figures 3 and 7 each show an assembled 32 inch specimen in its cage. The cage tie rods were designed with end fittings that would accept tensile load only. Since the maximum tensile load that could be applied to the cage by these tie rods corresponded to 30 psi compressive stress in the rock specimen, the effect of the cage on the rock was negligible.

An array of foil strain gages were mounted on each specimen. The number used ranged from three rosettes on the 2 in. cores to thirty rosettes on the 32 in. cores. These were two element rosettes with 1/4 in. gage length placed with the direction of rolling parallel to the specimen axis. The gage placement procedure included the following steps:

* grind the rock surface
* apply two thin coats of gage cement

* visual inspection for voids in the cement base
* affix and wire gage
* apply two coats of gage cement for water proofing
* check gage for continuity and response (soft eraser) and replace if necessary.

In several cases it was necessary to move a rosette slightly away from its pre-determined location because of local flaws or drill shot embedded in the surface (especially in the case of the tonalite).

In addition to the gages, break wires were cemented to the surface of the 12-in. and greater diameter specimens. This wire was No. 36 manganin wire well bonded to the surface so that the wire would break if a crack propagated across it during a test. Figure 6 shows typical instrumentation for a 12-in. core.

The instrumented cores were waterproofed with latex cement over the foil gages, and at least two coats of latex paint with a thickening agent spread over the entire rock surface. Waterproofing is very important in a triaxial test since both the loading conditions and the character of the rock can be changed by intrusion of oil into the rock voids. In those tests where the specimens could not be loaded to failure on the second load cycle, the specimen was recovered intact and stripped of paint for visual inspection. In several cases, traces of oil were found under the paint, but typically the specimens were completely dry. In no case was there enough oil to do more than dampen a very small area on the specimen surface.

3.4 Instrumentation and Data Reduction

The instrumentation on this program included foil strain gages, temperature transducers, pressure gages and break wires on the larger specimens. All instrumentation except the pressure gages were recorded using an automatic

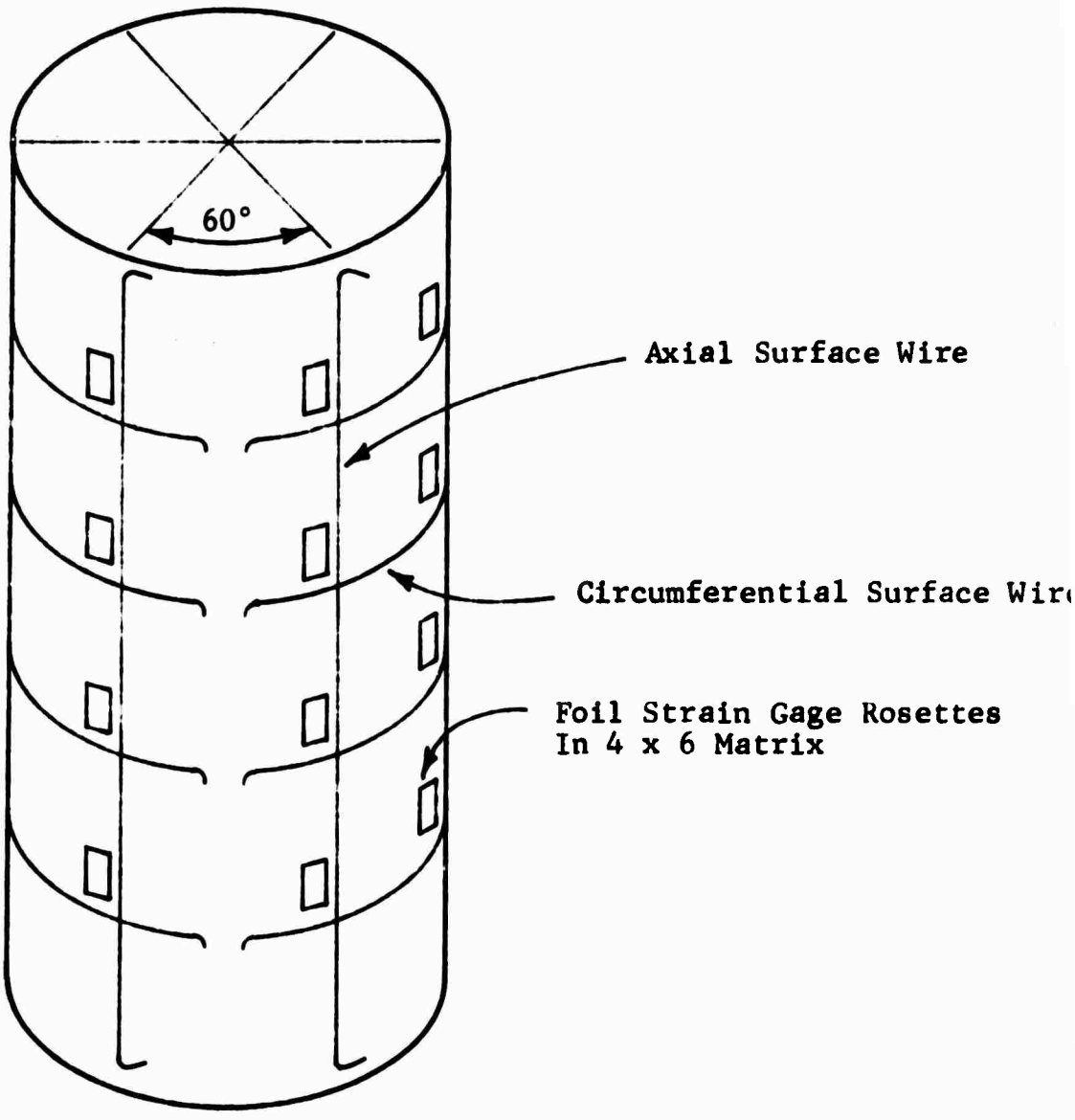

Fig. 6 TYPICAL GAGE LAYOUT

data acquisition system. The pressures were read using Hiese Super Accurate bourdon gages and inserted manually onto the data system output as they were read.

Due to the bulk of data involved, the data were reduced and plotted using the 1108 Univac computer at IITRI. In addition to printed output, the following plots were produced for each test:

Shear strain vs. deviator stress
Volumetric strain vs. mean stress
Poisson's ratio vs. mean stress
Octahedral shear stress vs. mean stress
Circumferential and axial strain vs. axial stress
Elastic, shear and bulk moduli vs. mean stress.

Data from each test was then assembled by hand to show trends from test to test.

4. EXPERIMENTAL PROGRAM

The program included triaxial tests on specimens ranging from 2-in. to 32-in. dia. One uniaxial strain test was conducted on the largest available specimen for each rock type, these being a 32-in. dia. granite and a 22-in. dia. tonalite. The uniaxial tests were conducted by monitoring mean radial strain and maintaining sufficient confining pressure to hold this strain as near zero as possible. The experimental program is summarized in Table 1. IITRI was able to procure the granite core from Cold Springs Quarry, Minnesota. The tonalite specimens were delivered by DASA which was unable to obtain more than one large specimen of tonalite.

The loading and unloading sequence in the large chamber is shown by the photographs in Figs. 7, 8 and 9. Typical failures are seen in Figs. 10 thru 13.

Table 1

TEST NUMBERS IN EXPERIMENTAL PROGRAM

Rock Type	Core Dia.	Confining Pressure σ_o			Uniaxial Strain
		5 ksi	10 ksi	15 ksi	
Charcoal Black Granite	2	12	14	34	
	4	9	11	19	
	12	16,21, 37	10		
	32	27-28	29-30		31
Cedar City Tonalite	2	24,25	26	33	
	4	35,36	18	22,23	
	12	17	38		
	22				32

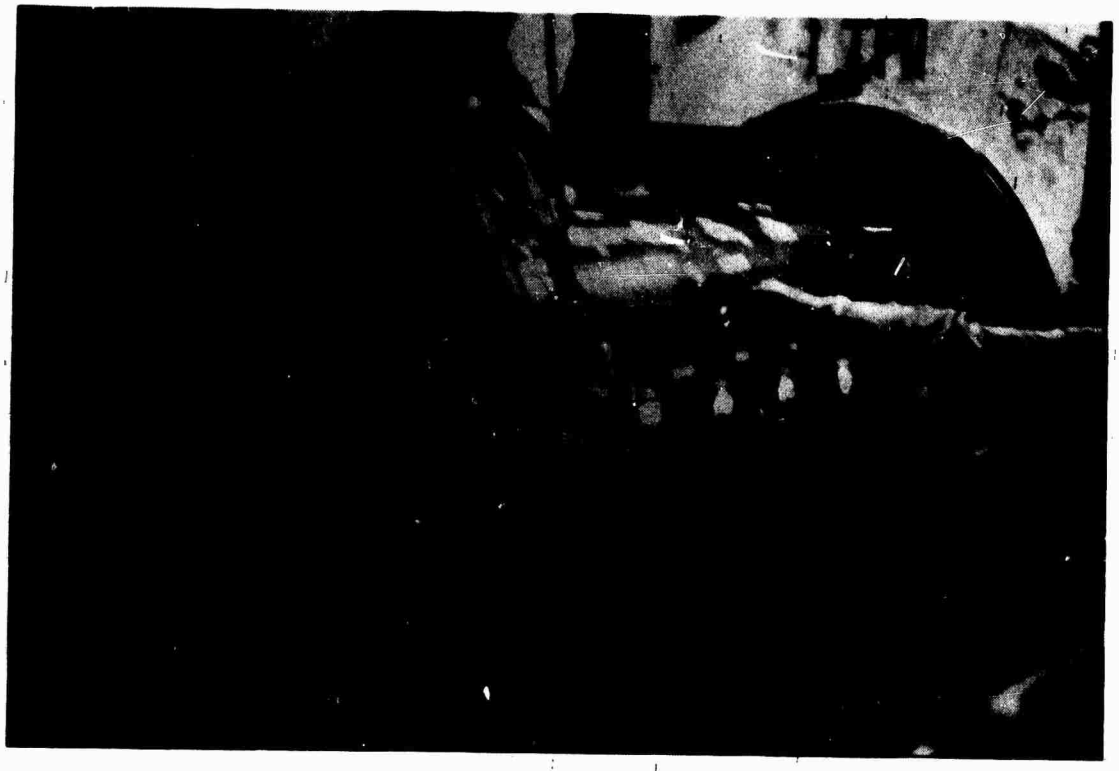

Fig. 7 LOADING SPECIMEN INTO 48-IN. DIA. TRIAXIAL CELL

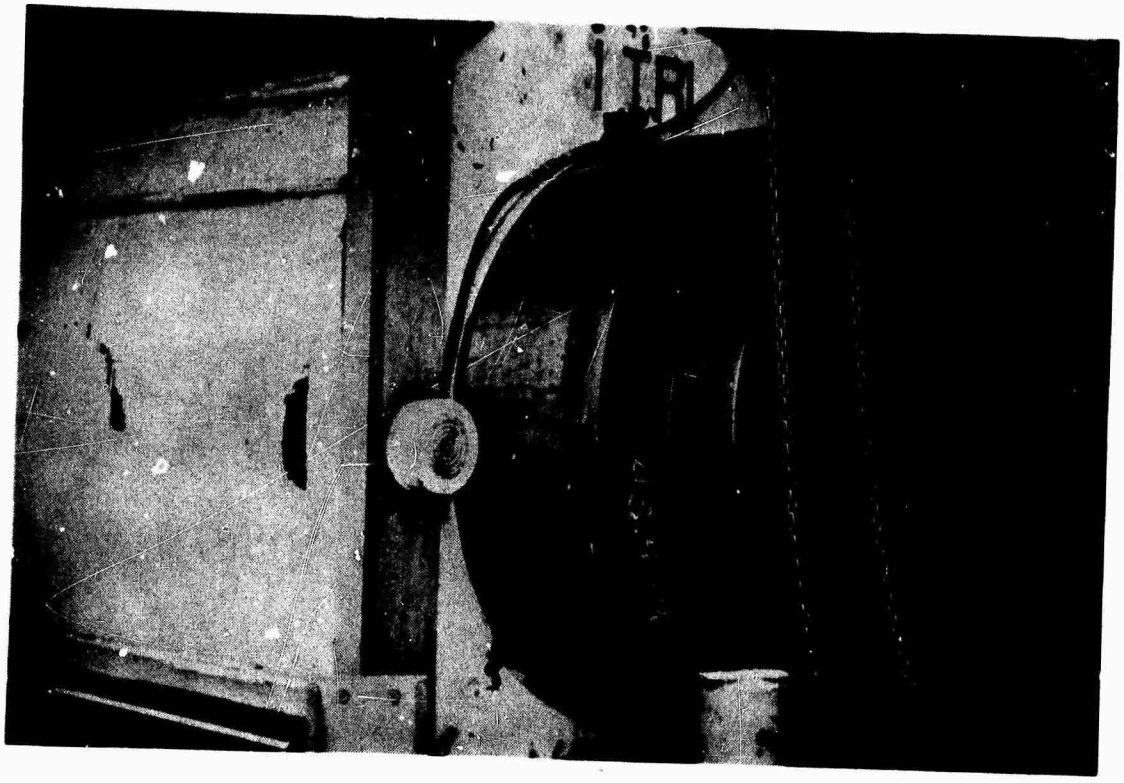

Fig. 8 INSERTING SLIDING PISTON INTO 48-IN. DIA. TRIAXIAL CELL

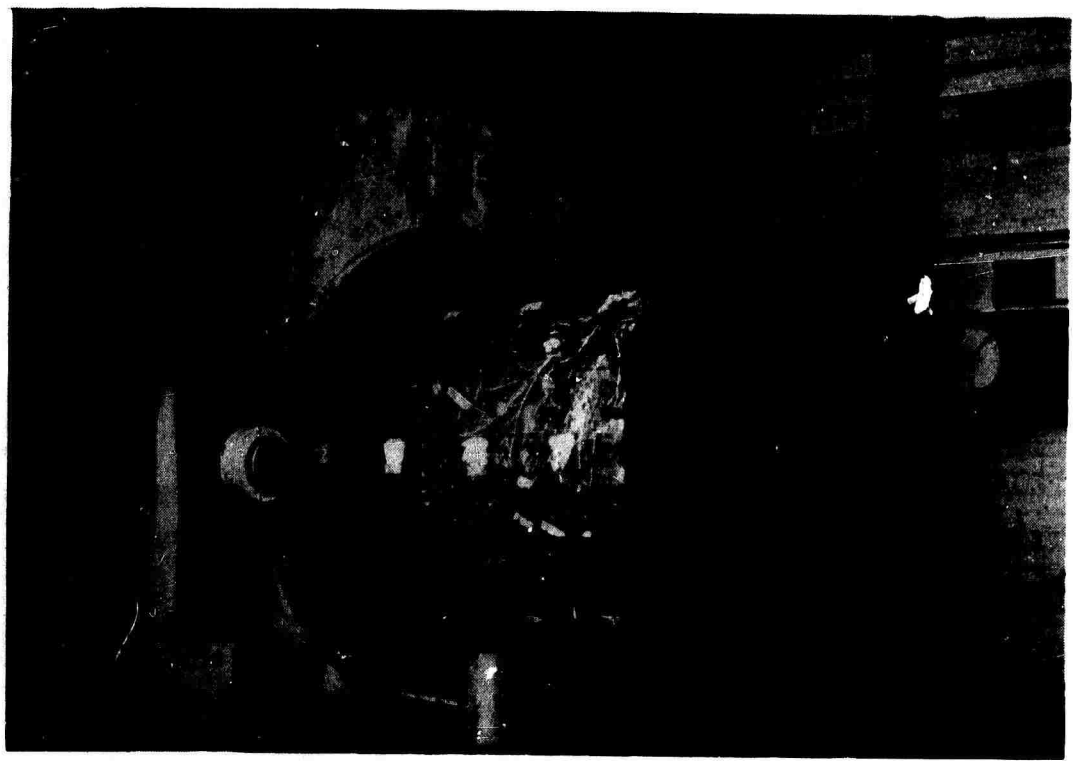

Fig. 9 REMOVING FRACTURED SPECIMEN FROM 48-IN. DIA. TRIAXIAL CELL

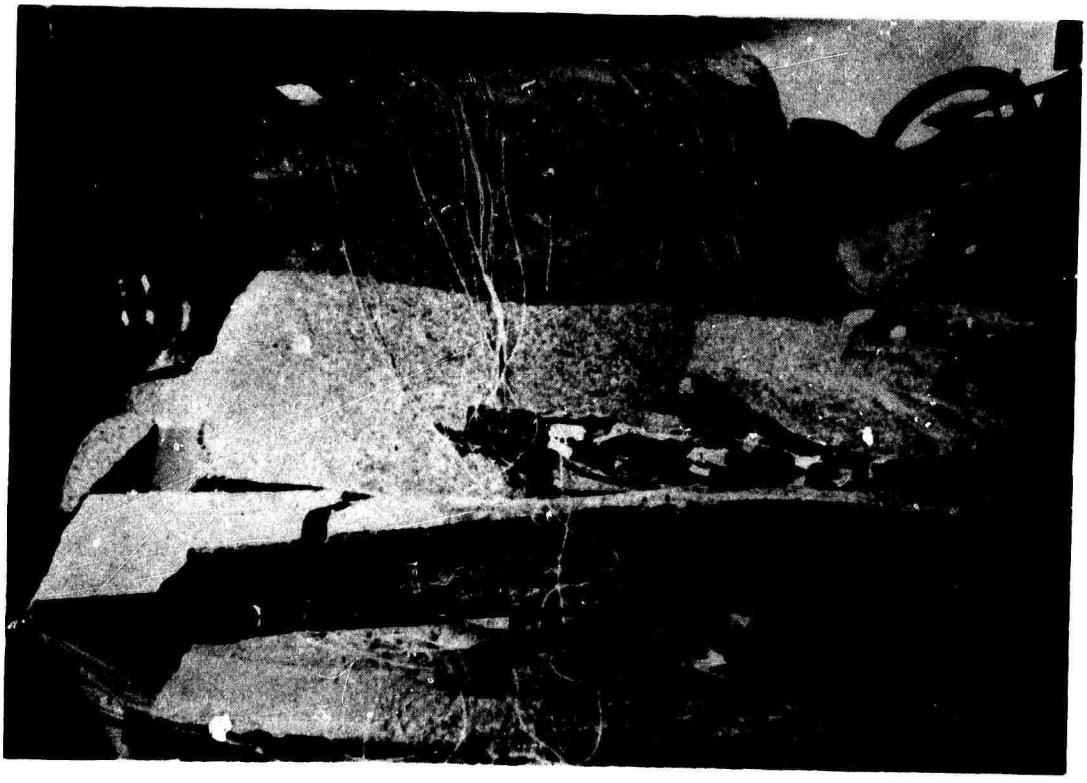

Fig. 10 32-IN. DIA. CHARCOAL BLACK GRANITE SPECIMEN AFTER TESTS 27-28 (σ_c = 5000 psi)

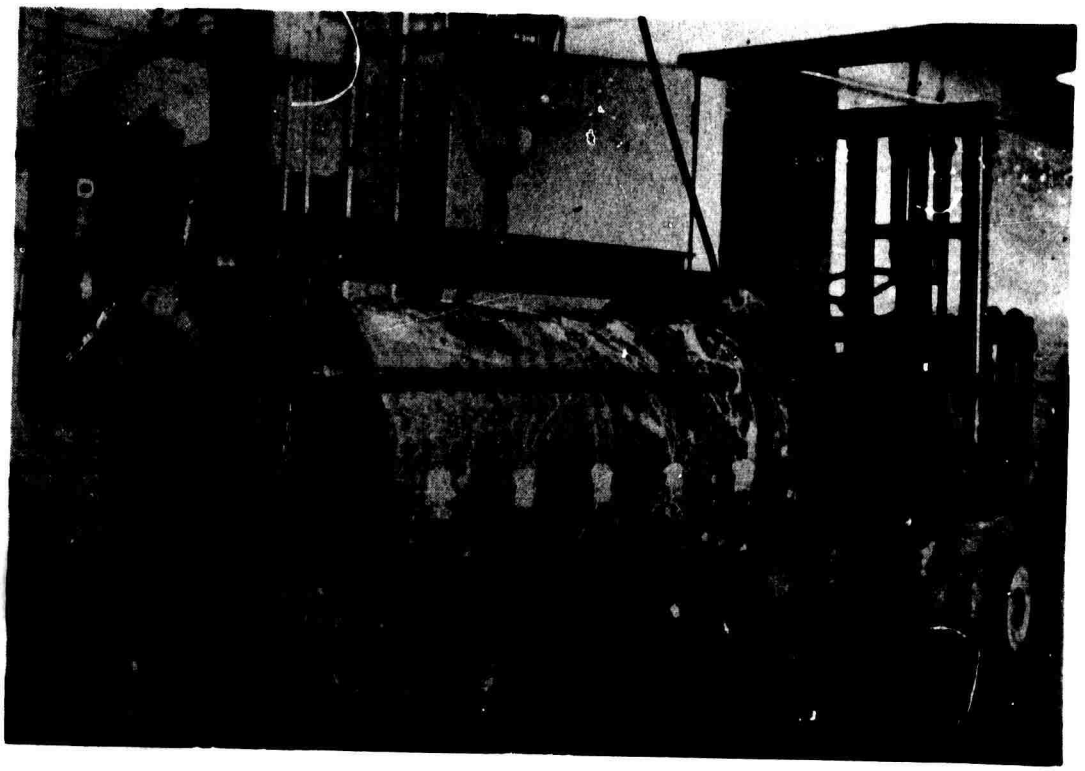

Fig. 11 32-IN. DIA. CHARCOAL BLACK GRANITE SPECIMEN AFTER TESTS 29-30 (σ_c = 10,000 psi)

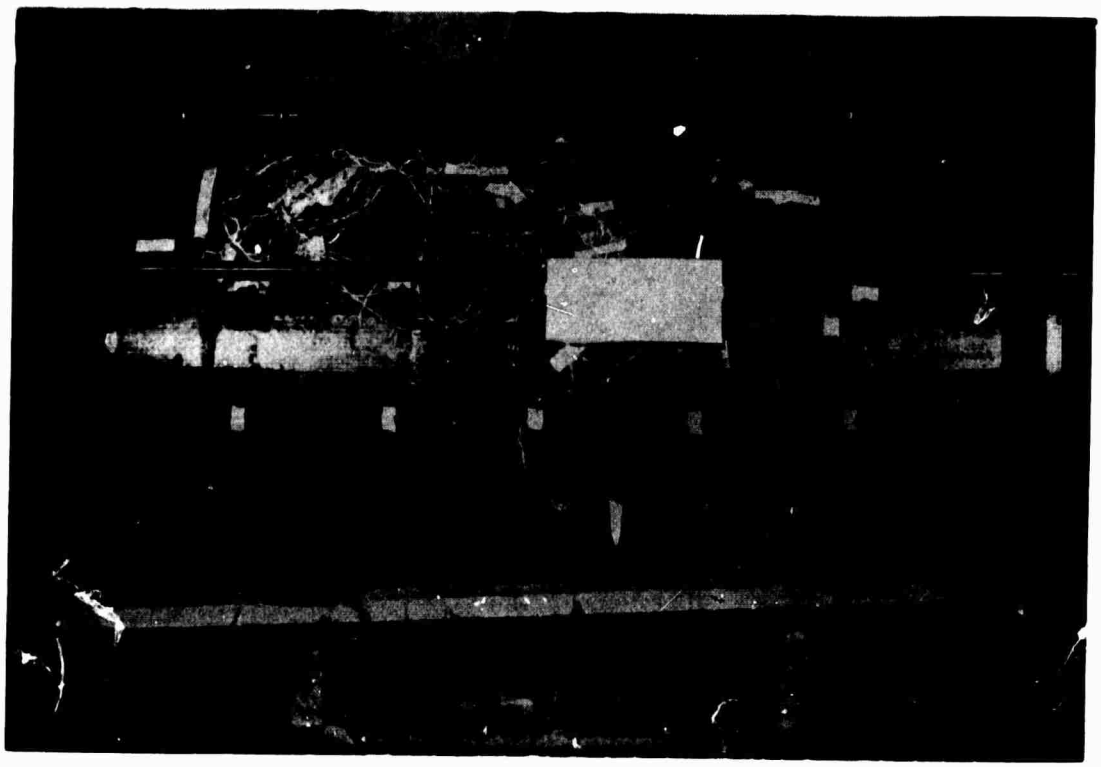

Fig. 12 32-IN. DIA. CHARCOAL BLACK GRANITE SPECIMEN AFTER TEST 31 (UNIAXIAL STRAIN)

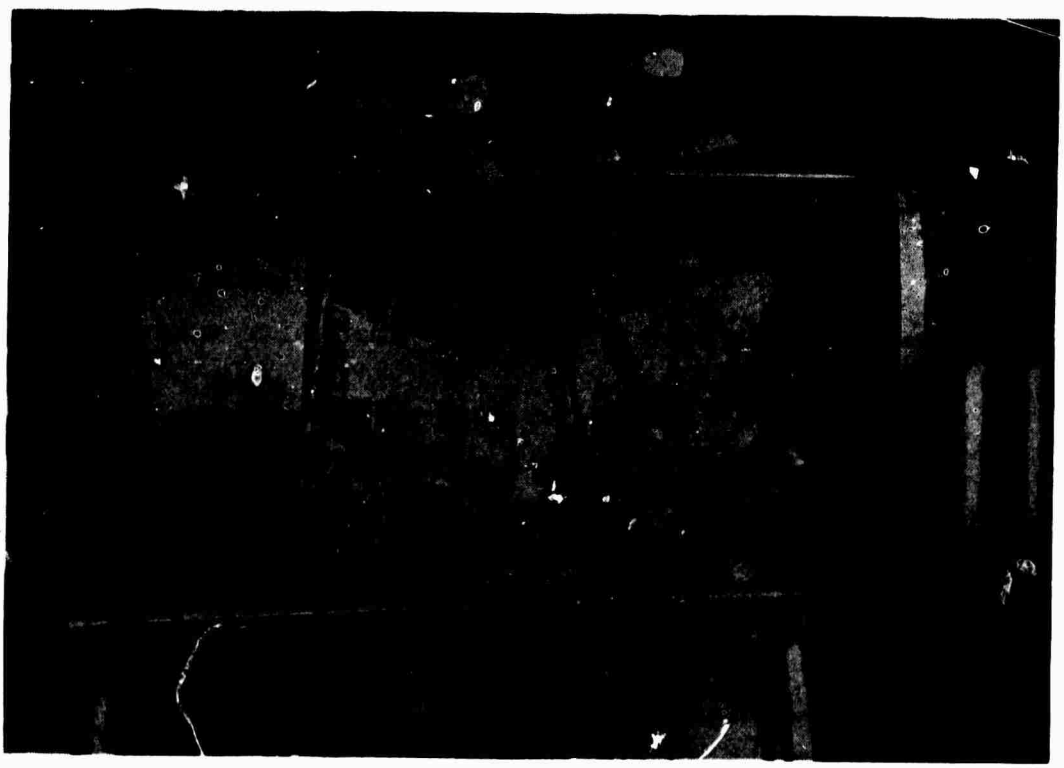

Fig. 13 22-IN. DIA. CEDAR CITY TONALITE SPECIMEN AFTER TEST 32 (UNIAXIAL STRAIN)

5. DISCUSSION OF RESULTS

5.1 Theoretical Considerations for Constitutive Equations

The large amount of data generated during this program makes a simple report of experimental data inappropriate. The reduced data itself consists of an 8 1/2 inch thick stack of printed computer output. Since it was obvious at the start of the program that this would be the case, parallel computer output in the form of graphical plots was provided for inclusion in the report as an appendix. In order to summarize the data for discussion in the text of the report, it was felt that the most convenient form would be a comparison of the test data with a model. The model parameters can then be evaluated as a function of specimen size much more easily than the actual data.

5.1.1 Formulation of Constitutive Equations

Concepts from the theory of plasticity have recently been used to describe the behavior of particulate materials such as soil and rock. If a stress space is constructed with coordinate axes representing the three principal stresses, the state of stress of an element of material is described by a point in this stress space. The locus of all possible stress states which cause yielding of the material is a surface called the yield or limit surface. This surface separates the stress states attainable in the material from those which are not attainable. An elastic-plastic material is one which behaves as an elastic material at stress states within the limit surface, and as a plastic material at stress states on the limit surface. A material model thus must include both a description of the limit surface and the elastic equations that hold within the limit surface.

5.1.2 Limit Surface

The limit surface in principal stress space is usually expressed by

$$\sqrt{J_2'} = f(J_1) \tag{1}$$

in which J_1 is the first invariant of the stress tensor and J_2' is the second invariant of the deviatoric stress tensor. These invariants are defined by

$$J_1 = \sigma_1 + \sigma_2 + \sigma_3 \tag{2}$$

$$J_2' = \frac{1}{6}\left[(\sigma_1-\sigma_3)^2 + (\sigma_1 - \sigma_2)^2 + (\sigma_2 - \sigma_3)^2\right] \tag{3}$$

in which σ_1, σ_2, and σ_3 are the three principal stresses. An equivalent method of describing the yield surface is to write the octahedral shear stress, τ_{oct}, as a function of the octahedral normal stress, σ_{oct}, or

$$\tau_{oct} = f(\sigma_{oct}) \tag{4}$$

in which

$$\sigma_{oct} = \frac{1}{3}(\sigma_1 + \sigma_2 + \sigma_3) \tag{5}$$

and

$$\tau_{oct} = \frac{1}{3}\left[(\sigma_1-\sigma_2)^2 + (\sigma_1-\sigma_3)^2 + (\sigma_2-\sigma_3)^2\right]^{1/2} \tag{6}$$

One form of a yield surface commonly used is the Mises' yield criteria given by

$$J_2' = K_o^2 \tag{7}$$

in which K_o is the yield limit of the material in simple shear. Equation (7) describes the surface of a cylinder in principal stress space with the axis inclined equally to all three principal stress axes as shown in Fig. 14. According to Mises' yield criterion the shear strength of a material is independent

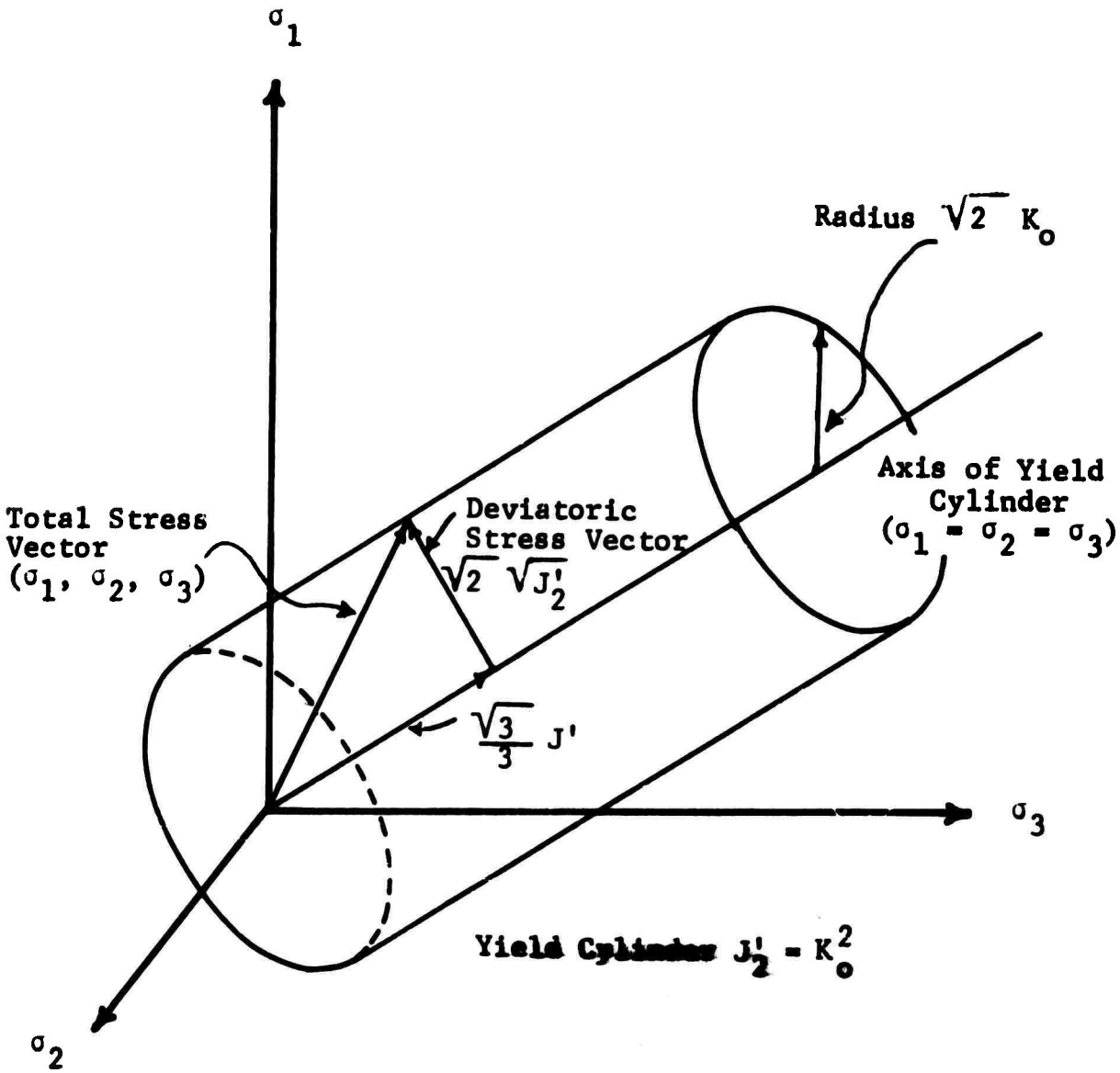

Fig. 14 YIELD SURFACE FOR MISES' YIELD CRITERION

of the mean stress σ_m, where

$$\sigma_m = \frac{1}{3} J_1 \tag{8}$$

In granular materials, including most soils and rocks, it has been established that shear strength increases with mean stress due to frictional behavior. For these materials the Coulomb-Mohr yield surface is more applicable, and is given by

$$\sqrt{J_2'} = A + B\, J_1 \tag{9}$$

in which A and B are constants. Equation (9) describes the surface of a cone in principal stress space with the same axis as the Mises' yield criteria shown in Fig. 14.

5.1.3 Elastic Equations

Constitutive equations for an isotropic linear elastic material are given by

$$\sigma_{ij} = \lambda \delta_{ij} \varepsilon_{kk} + 2\mu \varepsilon_{ij} \tag{10}$$

in which

σ_{ij} = stress tensor

ε_{ij} = strain tensor

δ_{ij} = Kronecker's delta

λ, μ are Lame's constants.

It is sometimes convenient to separate the volumetric response which is produced by mean stress from the distortional response which is produced by shear stress. This is accomplished through the deviator strain tensor, ε'_{ij}, and the deviator stress tensor, σ'_{ij}, which are defined as

$$\varepsilon'_{ij} = \varepsilon_{ij} - \frac{1}{3} \varepsilon_{kk} \delta_{ij} \tag{11}$$

$$\sigma'_{ij} = \sigma_{ij} - \frac{1}{3} \sigma_{kk} \delta_{ij} \tag{12}$$

The constitutive equations (10) may then be rewritten in the form

$$\sigma_{ij} = k\,\delta_{ij}\,\varepsilon_{kk} + 2G\varepsilon'_{ij} \qquad (13)$$

in which k and G are respectively the bulk modulus and shear modulus. These moduli are defined by

$$k = \frac{1}{3}\,\frac{\sigma_{kk}}{\varepsilon_{kk}} = \frac{\sigma_1 + \sigma_2 + \sigma_3}{3(\varepsilon_1+\varepsilon_2+\varepsilon_3)} \qquad (14)$$

$$G = \frac{1}{2}\,\frac{\sigma'_{ij}}{\varepsilon'_{ij}} \qquad (15)$$

Nonlinear behavior may be incorporated by using an incremental constitutive relation and defining k and G as functions of one or more of the stress invariants. Inelastic behavior may be incorporated by using separate values of k and G for loading and unloading. The unloading moduli must be greater than the loading moduli to prevent energy generating hysteresis loops.

5.2 Typical Behavior of Rock

5.2.1 Hydrostatic Behavior

Past work has shown that the stress-strain behavior of rock subjected to hydrostatic pressure is non-linear. A typical curve of mean stress versus volumetric strain from Paulding[40] is shown in Figure 15. In an unloaded state a rock specimen usually has an initial porosity, including some small cracks. As hydrostatic pressure increases, the cracks begin to close and the porosity decreases, causing the rock to become stiffer and less compressible. At higher pressures the response becomes linear and compressibility of the rock may be predicted from the individual compressibilities of its constituent minerals. The initial porosity may be determined by extending the linear portion of the curve back to the strain axis. Based on data presented by Clark[41], shown in Fig. 16, it appears that the influence of the initial

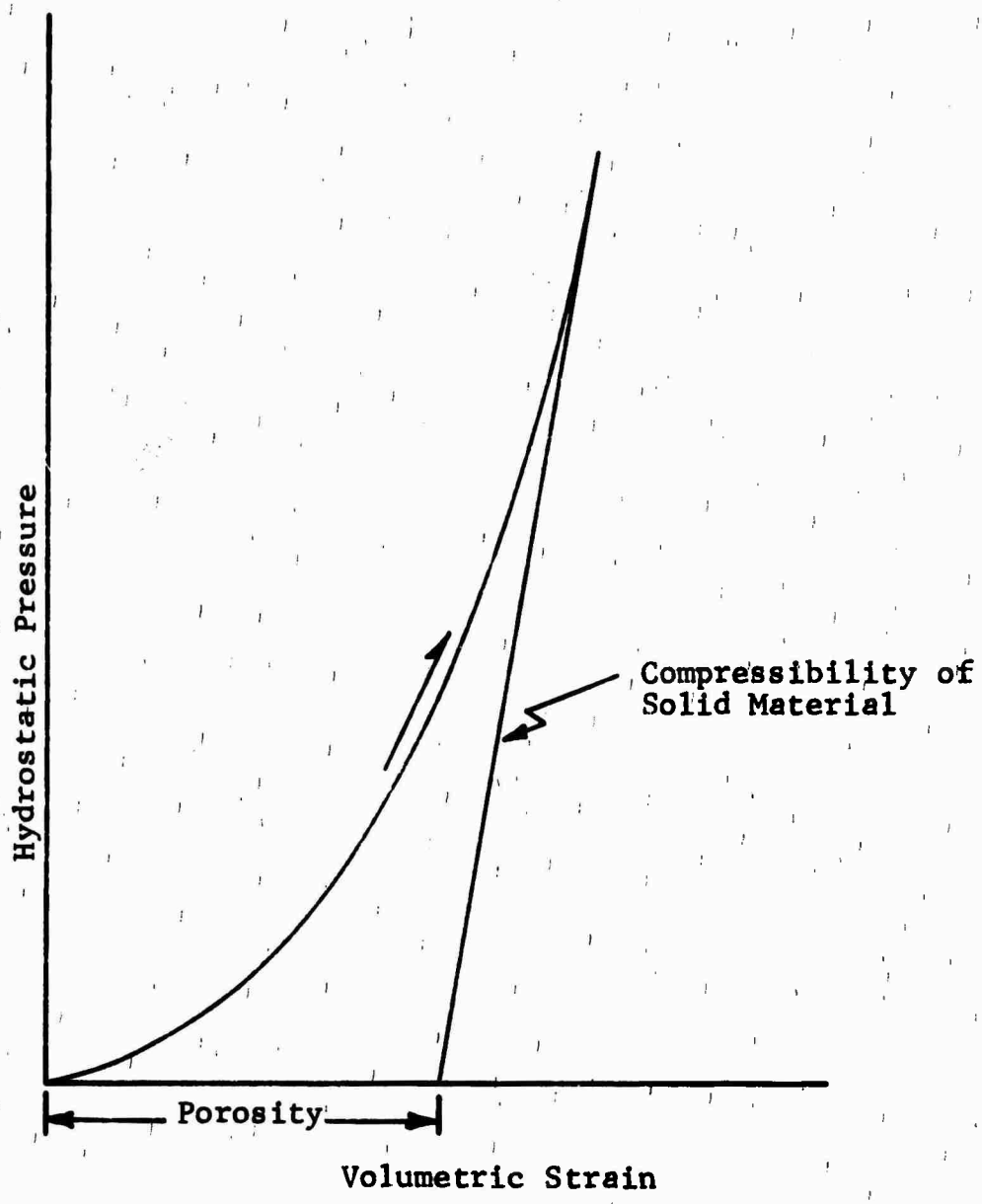

Fig. 15 TYPICAL COMPRESSIBILITY CURVE FOR ROCK, AFTER PAULDING[40]

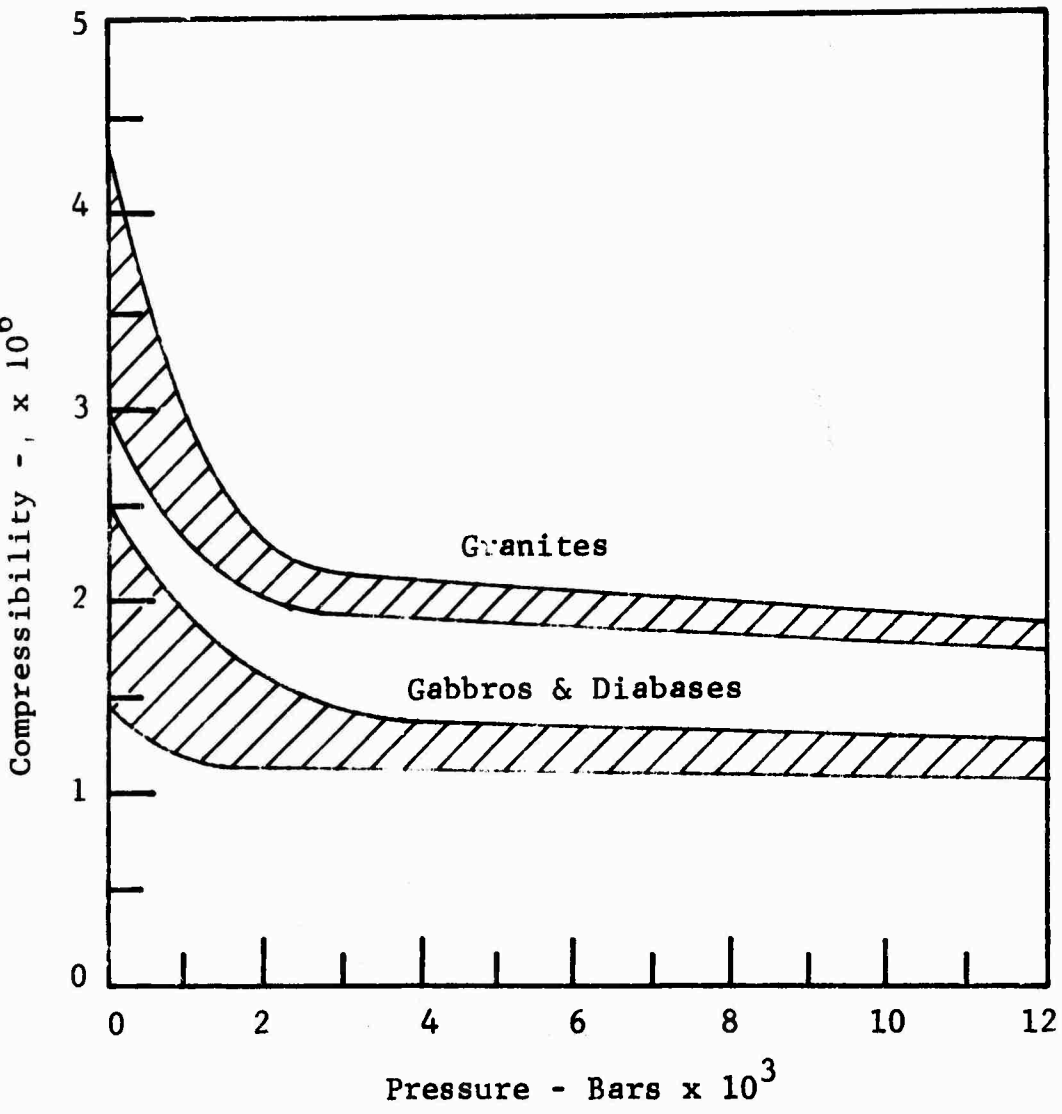

Fig. 16 COMPRESSIBILITY OF GRANITE, GABBROS, AND DIABASES; FROM CLARK[41]

porosity on compressibility becomes negligible at a pressure of about 2000 bars or 29 ksi.

The behavior of granular materials under hydrostatic pressure has been studied analytically through the use of models consisting of various packings of elastic spheres[42]. Hertz's contact theory[43] has been used and has shown that the volumetric strain is directly proportional to mean stress to the two-thirds power. This nonlinearity in response is due to the geometry of the packing of the individual particles and not the properties of the material comprising the spheres. The Hertz theory may be applicable if rock may be considered as a granular material.

A nonlinear hysteretic model used by Seaman and Whitman[44] to study the behavior of sand appears to be suitable for representing the hydrostatic behavior of rock. The stress-strain curve for this model is shown in Fig. 17. For virgin loading

$$\sigma_m = A_1 \ \varepsilon_v^n \tag{16}$$

and for unloading and reloading

$$\sigma_m = A_2 \ (\varepsilon_v - \varepsilon_{v\ell})^n \tag{17}$$

in which

σ_m = mean stress

ε_v = volumetric strain

$\varepsilon_{v\ell}$ = residual volumetric strain

A_1 and A_2 = material properties

This model represents both the nonlinear and the inelastic behavior of the rock observed under hydrostatic loading.

Application of the mathematical model in a computer code would perhaps be most convenient in an incremental form using tangent values of bulk modulus,

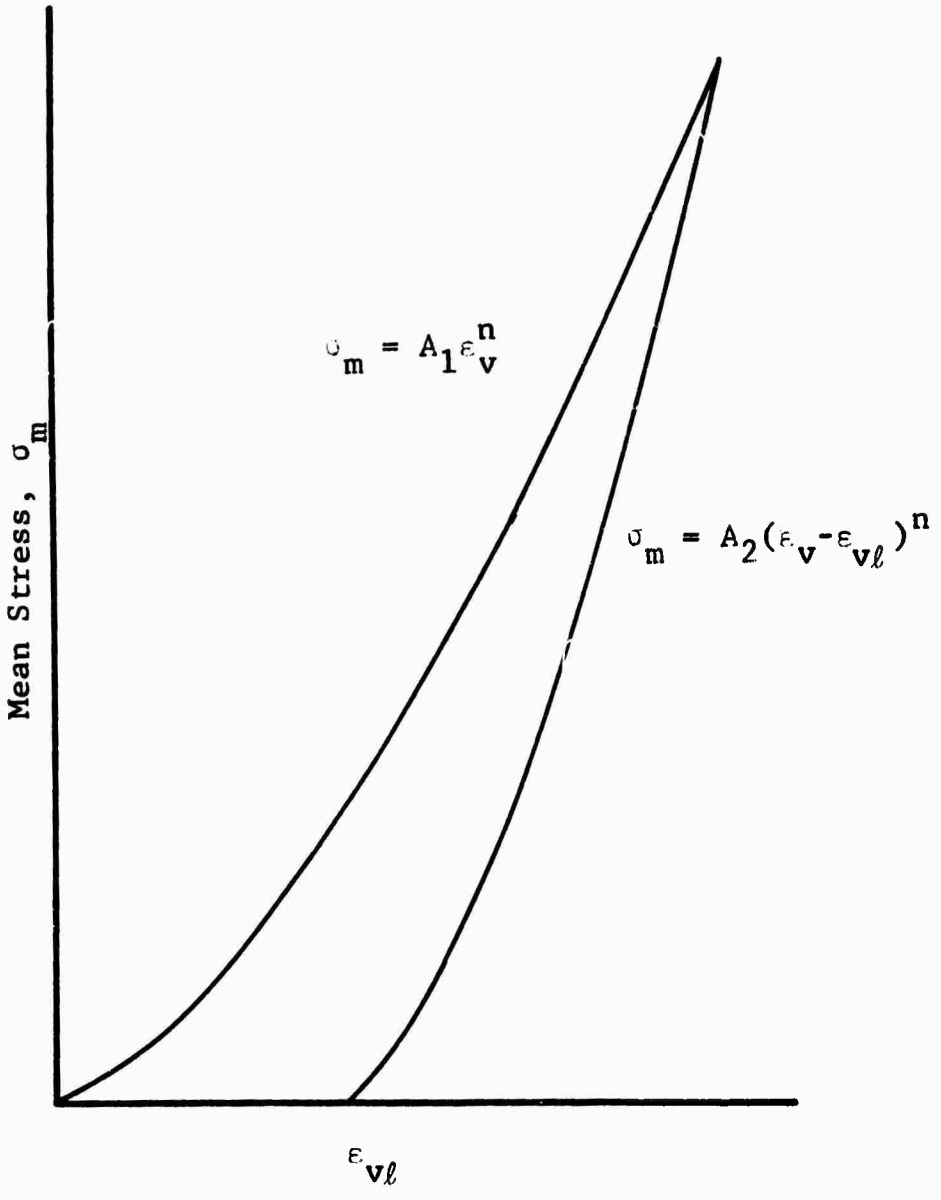

Fig. 17 STRESS-STRAIN CURVE FOR NONLINEAR HYSTERETIC MODEL (after Seaman & Whitman[44])

k_t. This modulus is a function of mean stress and for a given stress represents the slope of the curve at that stress level.

For loading

$$k_t = \frac{d\sigma_m}{d\varepsilon_v} = n\, A_1^{1/n}\, \sigma_m^{n-1/n} \tag{18}$$

and, for unloading and reloading

$$k_t = \frac{d\sigma_m}{d\varepsilon_v} = n\, A_2^{1/n}\, \sigma_m^{n-1/n} \tag{19}$$

Note that in this model the modulus for unload-reload is larger than the modulus for virgin loading at any given stress level.

5.2.2 Triaxial Compression

A triaxial compression test normally consists of two phases. First, a hydrostatic confining stress, σ_c, is applied to the specimen so that the principal stresses are all equal to σ_c. Then, two principal stresses, σ_2 and σ_3, are kept constant at σ_c while the third principal stress, σ_1, is increased. For these conditions one of the components of the deviator stress is

$$\sigma'_{11} = \sigma_1 - 1/3\ (\sigma_1 + 2\sigma_3) = 2/3\ (\sigma_1 - \sigma_3) \tag{20}$$

If the material is isotropic two principal strains, ε_2 and ε_3, are also equal, meaning that the corresponding component of deviator strain is

$$\varepsilon'_{11} = \varepsilon_1 - 1/3\ (\varepsilon_1 + 2\varepsilon_3) = 2/3\ (\varepsilon_1 - \varepsilon_3) \tag{21}$$

Thus, for triaxial conditions the shear modulus may be determined from

$$\frac{\sigma'_{11}}{2\varepsilon'_{11}} = \frac{\sigma_1 - \sigma_3}{2(\varepsilon_1 - \varepsilon_3)} \tag{22}$$

Idealized behavior of a rock specimen loaded in triaxial compression as presented by Swanson[21] is shown in Fig. 18. The relation between deviator stress and strain is linear up to yield. At stress states beyond yielding the relation becomes nonlinear and plastic behavior occurs. The modulus for unloading is equal to that for virgin loading to the yield point.

Volume change behavior is the same as that for hydrostatic loading at stress states below yield. At yield the volume of the specimen begins to increase even though the mean stress is compressive and also increasing. This tendency for rock to expand when yielding is termed dilatancy and is characteristic of almost all particulate materials.

At low stress levels shear modulus increases relatively rapidly with mean stress; however, at higher stresses it remains relatively constant. Torsional wave velocities were measured in cylinders of different granites exposed to hydrostatic pressure between 1 kg/cm^2 and 4,000 kg/cm^2 by Birch and Bancroft[45]. From the wave velocities the modulus of rigidity, which is identical to the shear modulus, was determined and is shown as a function of mean stress in Fig. 19. Also shown in Fig. 19 are values of shear moduli for specimens of Charcoal Black granite and Cedar City tonalite determined from triaxial tests performed during this study. The moduli determined by Birch and Bancroft[45] and those for the Charcoal Black granite are in good agreement and increase approximately with the 1/10 power of the mean stress. Values of shear modulus for the Cedar City tonalite are, however, radically different. At mean stress levels below about 5 ksi, the shear modulus increases with the 5/6 power of mean stress. At higher stress levels, the shear modulus increases less rapidly. One probable cause for this change in behavior is the relatively high initial porosity of the tonalite.

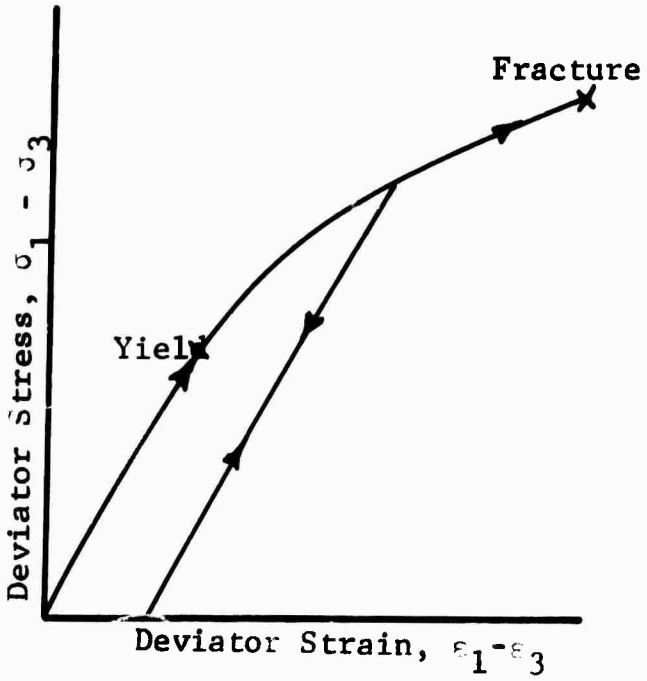

a) Shear Stress-Strain

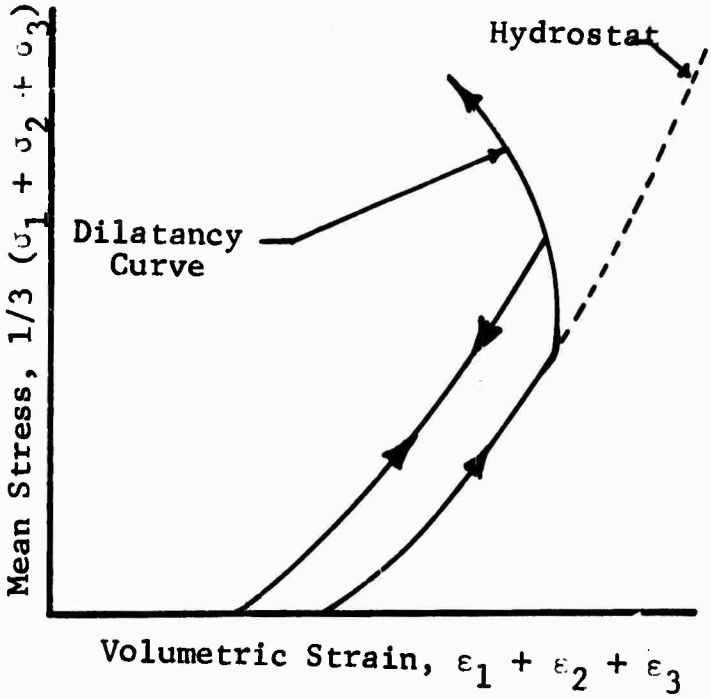

b) Volume Behavior

Fig. 18 IDEALIZED STRESS-STRAIN BEHAVIOR OF ROCK, FROM SWANSON[21]

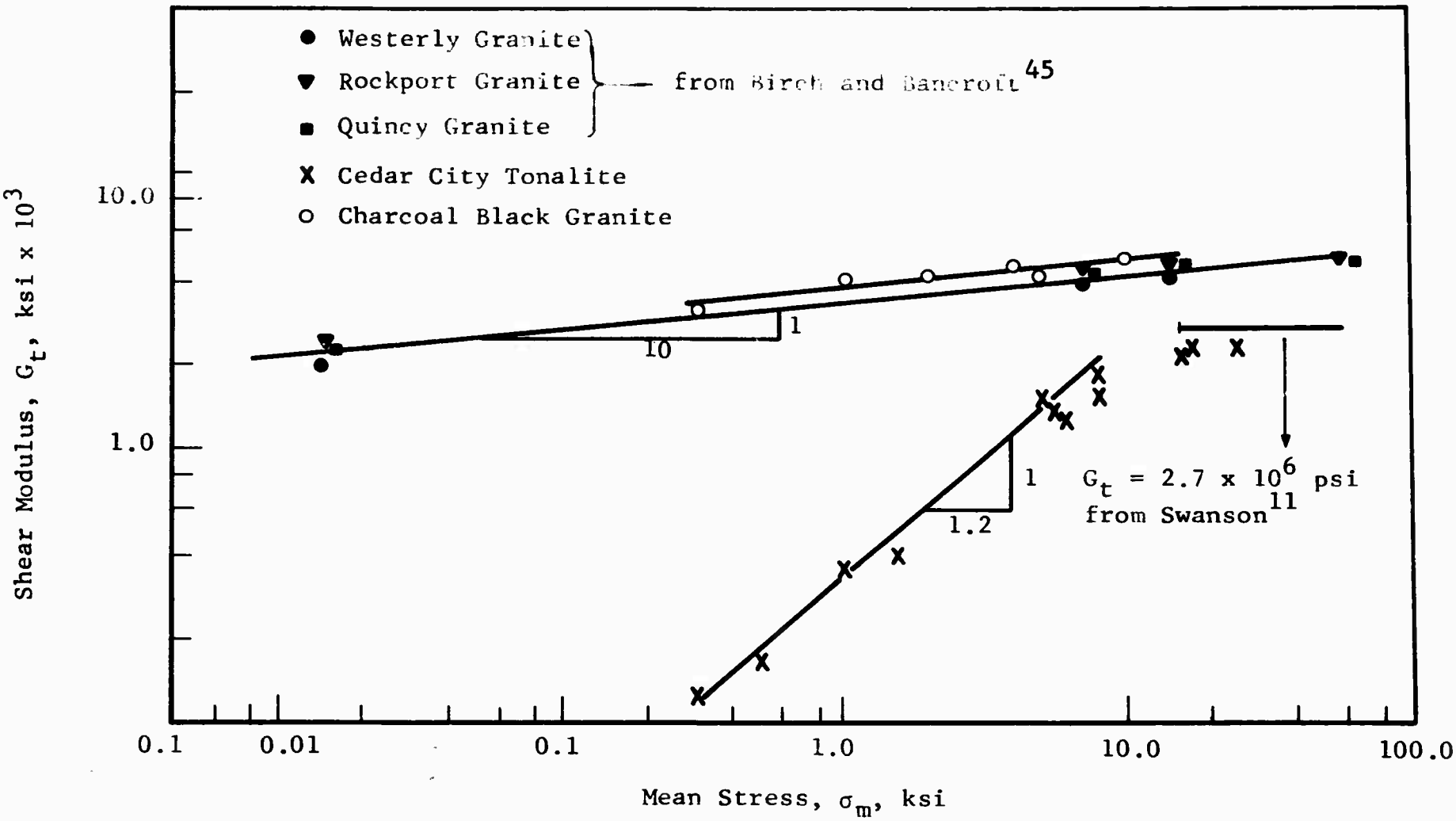

Fig. 19 VARIATION OF SHEAR MODULUS WITH MEAN STRESS

Values of shear modulus shown in Fig. 19 are tangent values, G_t, which refer to the slope of the deviator stress-strain curve at a given stress value. For nonlinear behavior the tangent shear modulus is a function of mean stress and may be calculated from

$$G_t = 1/2 \frac{d(\sigma_1 - \sigma_3)}{d(\varepsilon_1 - \varepsilon_3)} \tag{23}$$

The functional relationship with mean stress may be written as

$$G_t = c\,\sigma_m \tag{24}$$

in which c is a constant.

5.2.3 Uniaxial Strain

The uniaxial strain test is a special type of triaxial test in which the lateral strains, ε_2 and ε_3, are equal to zero throughout the test. One method of obtaining this condition is through monitoring the lateral strains and controlling the lateral stresses, σ_2 and σ_3, to maintain zero strain. In soil mechanics, for the uniaxial strain loading, the ratio between the lateral and axial stress is called the coefficient of earth pressure at rest, K_o, where

$$K_o = \frac{\sigma_3}{\sigma_1} \quad . \tag{25}$$

Data from this test may be used to compute bulk and shear moduli from the following equations:

$$G = 1/2 \frac{\sigma_1}{\varepsilon_1} (1 - K_o), \text{ and} \tag{26}$$

$$k = 1/3 \frac{\sigma_1}{\varepsilon_1} (1 + 2K_o). \tag{27}$$

5.2.4 Poisson's Ratio and Young's Modulus

Two constants are necessary to describe the stress-strain behavior of an isotropic elastic material. One set

of constants, k and G, which separate volumetric and deviatoric behavior have been described previously. Another pair of constants which are commonly used are Poisson's ratio, ν, and Young's modulus, E. The constants E and ν are derived directly from a triaxial test in which the lateral stresses, σ_2 and σ_3, are equal to zero. For this special test condition.

$$E = \frac{\sigma_1}{\varepsilon_1}, \text{ and} \tag{28}$$

$$\nu = -\frac{\varepsilon_3}{\varepsilon_1} \tag{29}$$

For more general test conditions

$$E = \frac{9kG}{3k + G}, \text{ and} \tag{30}$$

$$\nu = \frac{3k - 2G}{2(3k+G)} . \tag{31}$$

The use of tangent values of bulk and shear moduli, k_t and G_t, in equations (30) and (31) will result in tangent values for Poisson's ratio, ν_t, and Young's modulus, E_t.

For hydrostatic loading the deviatoric stresses and strains are zero and G is undetermined. Therefore, E and ν are also indeterminate from a hydrostat. For a triaxial test with σ_3 equal to zero, E and ν may be computed from equations (28) and (29). For a triaxial test with σ_3 unequal to zero but constant, tangent values of E and ν may be computed from

$$E_t = \frac{d\sigma_1}{d\varepsilon_1}, \text{ and} \tag{32}$$

$$\nu_t = -\frac{d\varepsilon_3}{d\varepsilon_1} . \tag{33}$$

For more general conditions equations (30) and (31) must be used.

For uniaxial strain tests the following expressions may be used

$$E = \frac{\sigma_1}{\varepsilon_1} \quad \frac{(1 + 2\,K_o)\,(1 - K_o)}{(1 + K_o)} \quad , \text{ and} \qquad (34)$$

$$\nu = \frac{K_o}{1 + K_o} \quad . \qquad (35)$$

5.2.5 Yield and Fracture Criteria

In principal stress space the restraint $\sigma_2 = \sigma_3$ defines a plane which includes the σ_1-axis and the axis of the yield surface shown in Fig. 14. As $\sigma_2 = \sigma_3$ is a condition maintained during the triaxial test all stress states in this test lie in the $\sigma_2 = \sigma_3$ plane. Thus, yield and fracture criteria may be described by a curve in this plane. Curves representative of different failure criteria are shown in Fig. 20 with J_1 plotted vs. $\sqrt{J_2'}$ on orthogonal axes. The stress path for a constant σ_3 triaxial test is also shown in Fig. 13.

A thorough discussion of yield and fracture surfaces as they apply to the behavior of rock has been given by Swanson[21]. The yield surface defines all stress states at which the rock ceases to be an elastic material. At stress states within the yield surface some form of elastic equations govern the material behavior. At states on the yield surface equations from plasticity govern the behavior. It has been shown[21] that most rocks exhibit strain-hardening behavior; i.e., the increase of stress beyond initial yield causes the yield surface to move outward. Continued increase of stress causing outward movement of the yield surface will eventually result in failure of the rock. The locus of all stress states causing failure is called the fracture

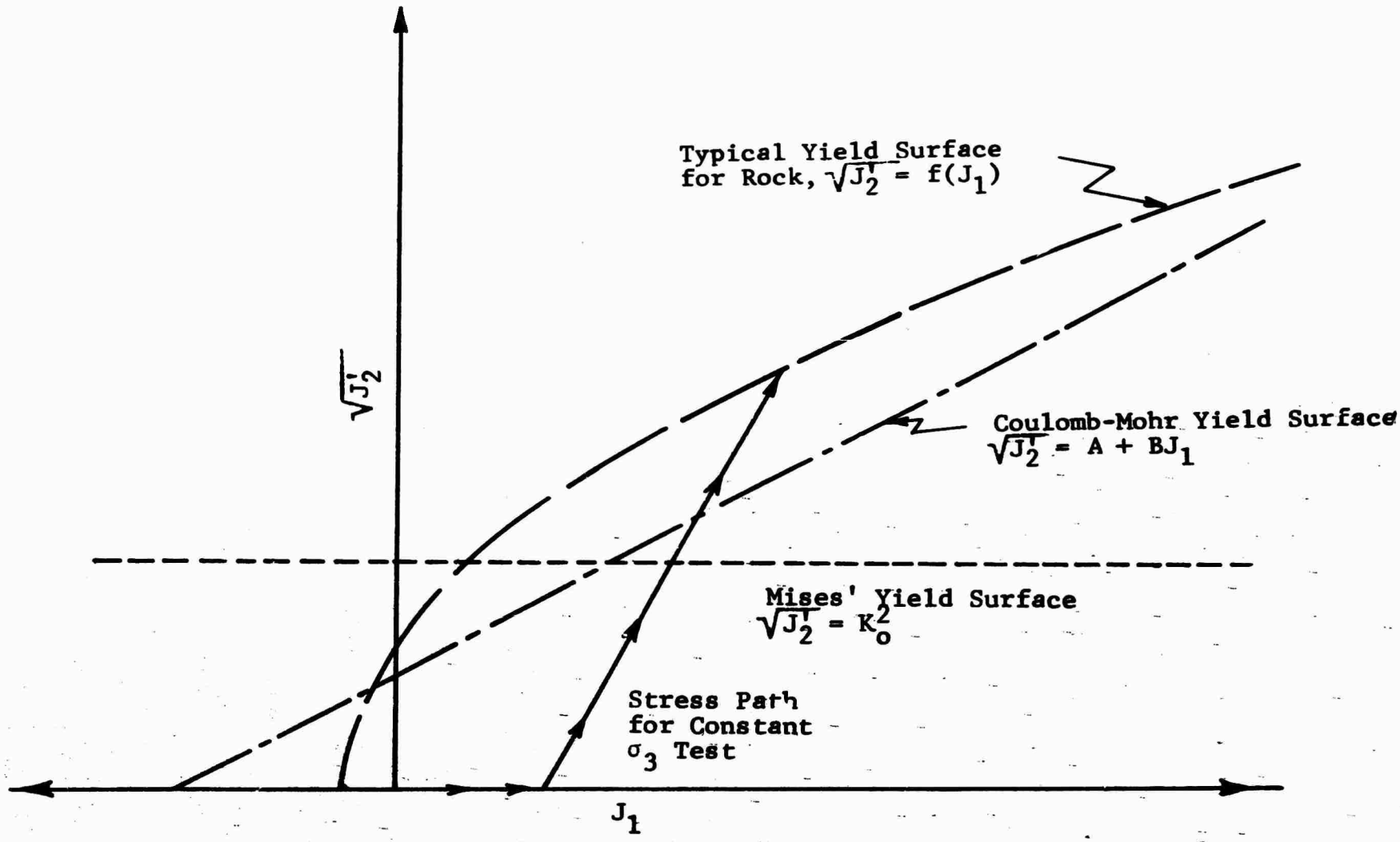

Fig. 20 YIELD CRITERIA

surface or failure surface.

5.3 Analysis of Experimental Results

Experimental results are presented in a form consistent with the elastic-plastic constitutive model presented earlier. Elastic properties are presented as functions of mean stress and are given in terms of tangent values which are compatible with a nonlinear incremental form of elasticity equations. Yield and fracture criteria are presented in the form $J_2' = (J_1)$.

5.3.1 Charcoal Black Granite

Typical volume change data from a constant confining pressure triaxial test is shown in Fig. 21 along with a curve representing the nonlinear hysteretic model fitted to the experimental data. The constants for the model were conveniently determined from logarithmic plots of the data. In the middle portion of the curves experimental results and the model are in close agreement. At relatively low stress levels, less than 2 ksi, the model predicts stresses that are smaller than those measured. Fracture of this specimen occurred at a mean stress of 17 ksi and yielding had begun at about 14 ksi which results in dilatant behavior of the specimen at these stress levels. Thus, as would be expected the model and experimental results do differ at stress levels greater than 14 ksi for this particular specimen.

Tangent values of bulk modulus, K_t, were determined from the experimental data and plotted as a function of mean stress in Figs. 22 and 23. These values represent the computed slope between actual consecutive data points rather than the slope of a smooth curve drawn through the data points. This procedure introduces "noise" in the plots since the data points are rather close together and the uncertainity in the computed volumetric strain is rather large in comparison with the change in volumetric strain over

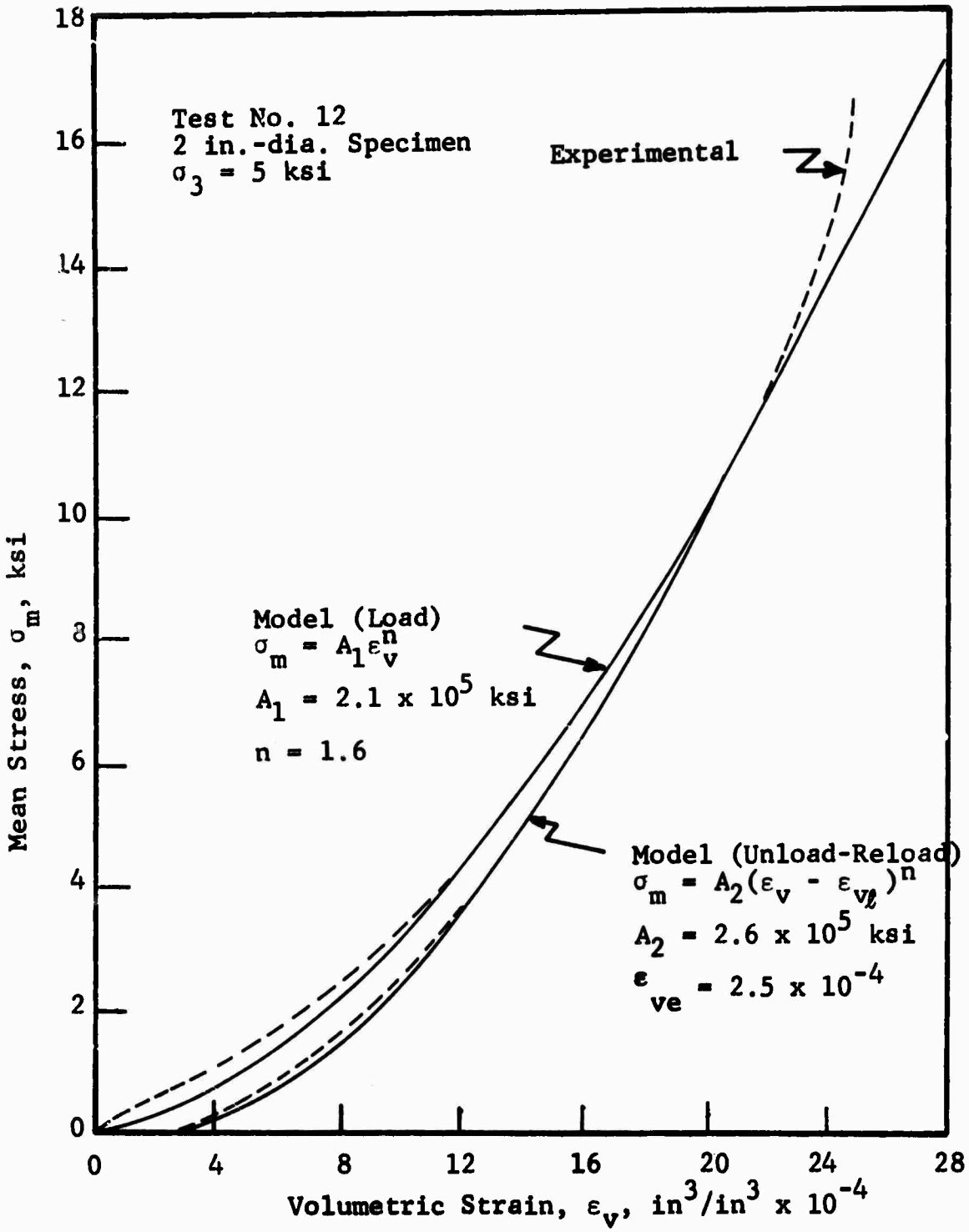

Fig. 21 MEAN STRESS VS. VOLUMETRIC STRAIN, CHARCOAL BLACK GRANITE

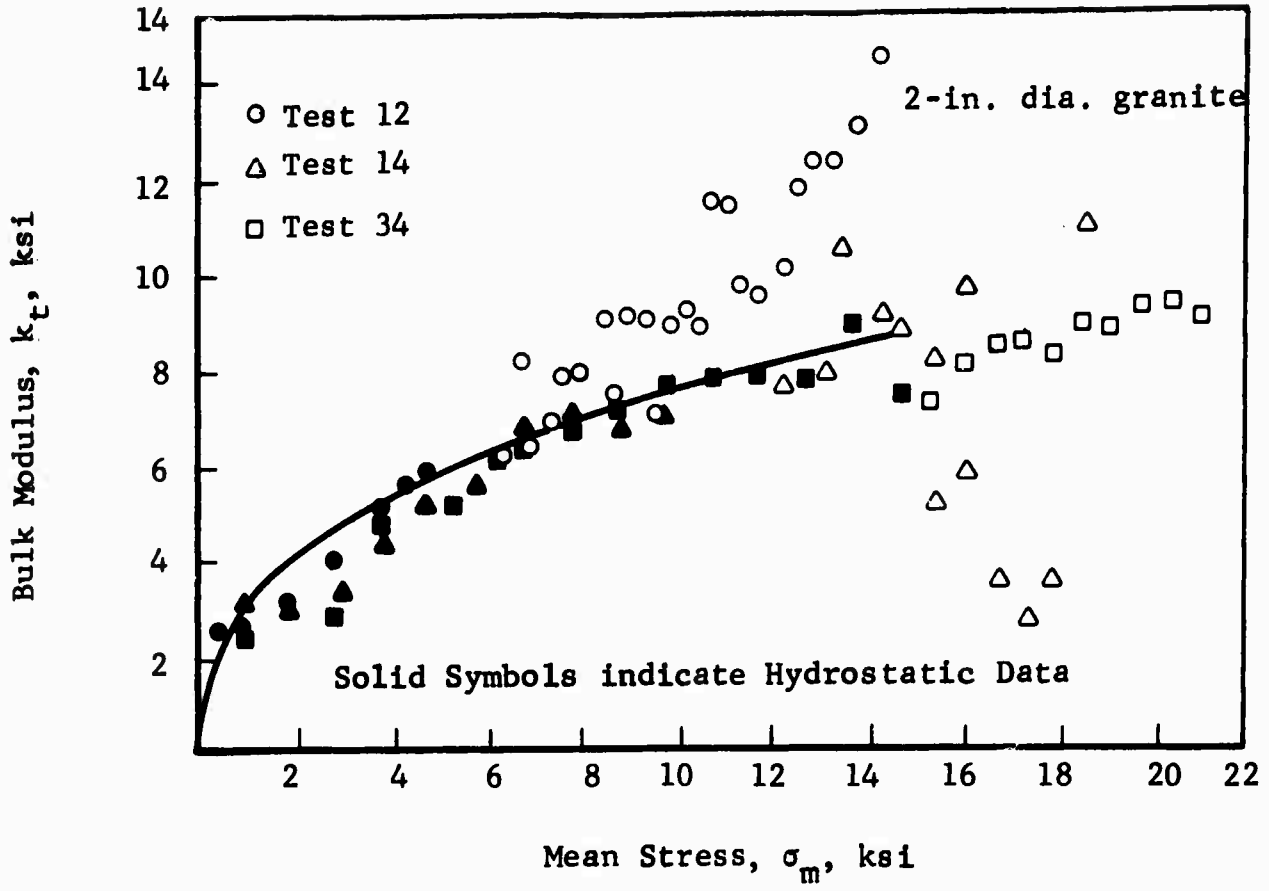

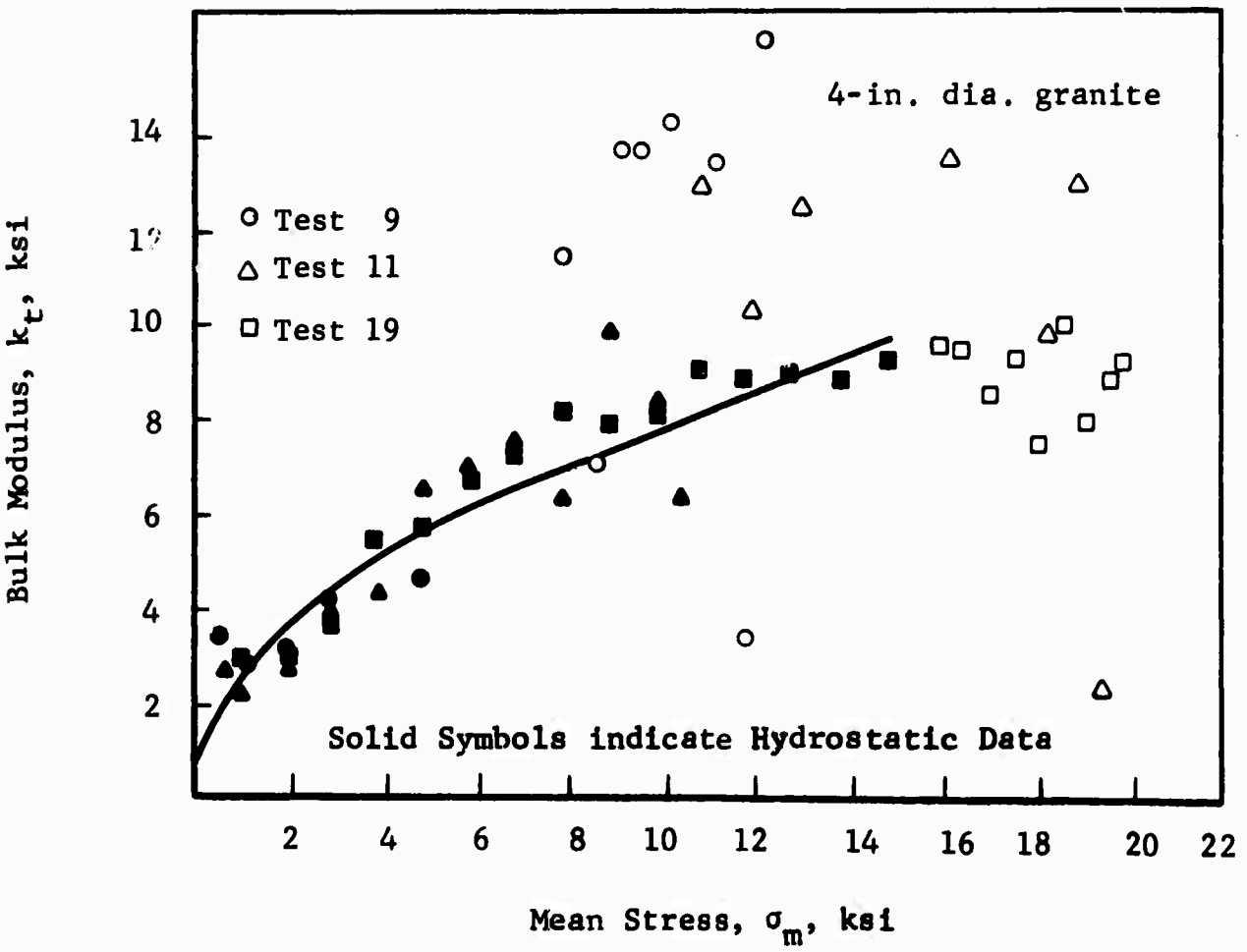

Fig. 22 BULK MODULUS VS. MEAN STRESS - 2" Ø AND 4" Ø CBG

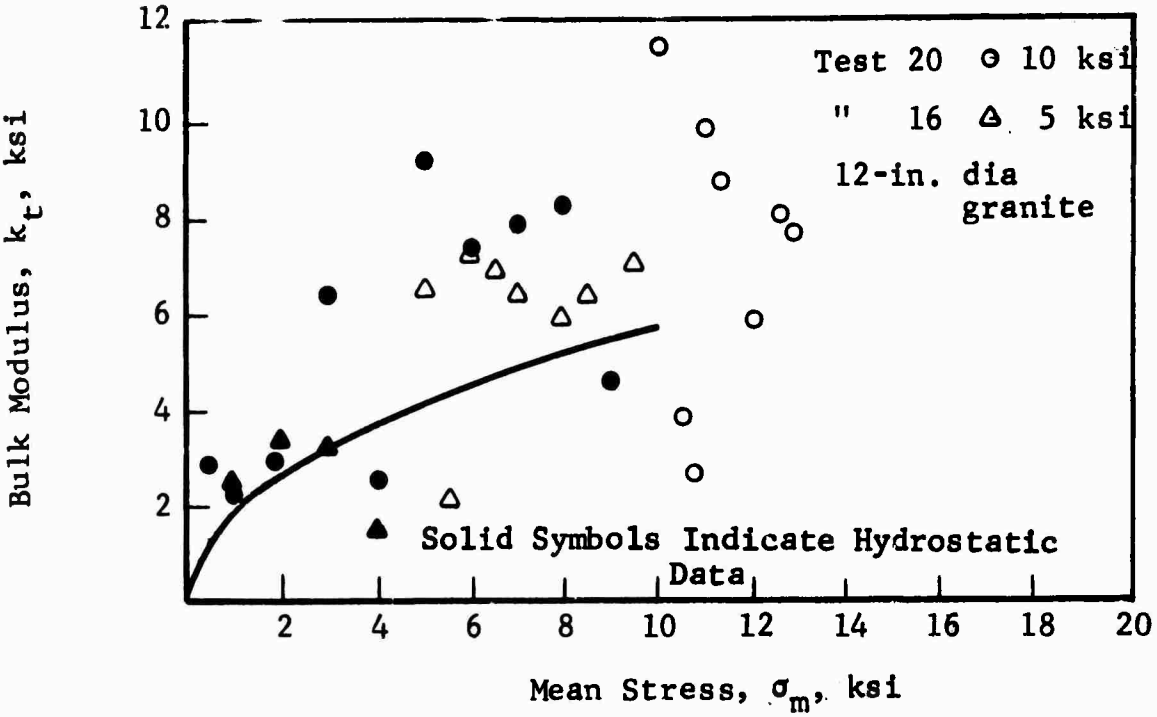

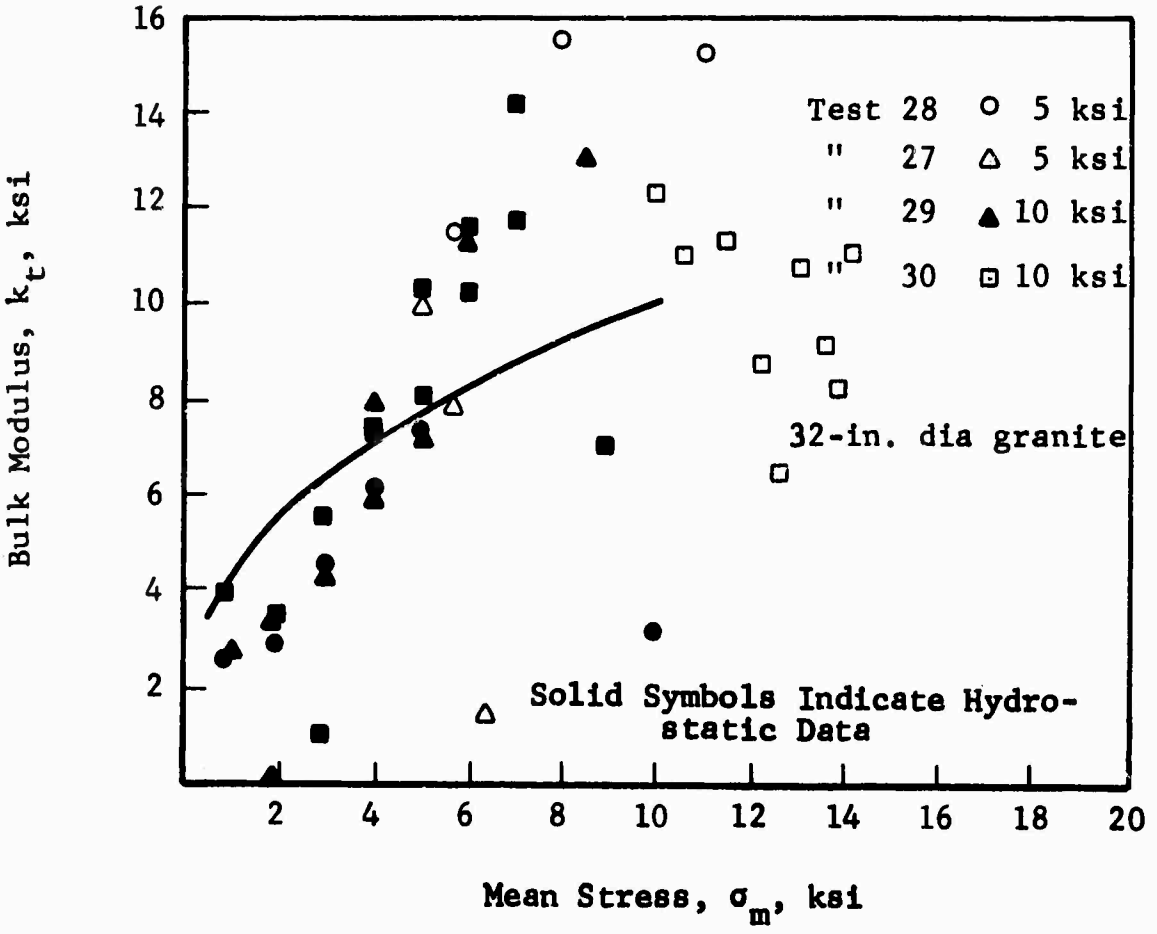

Fig. 23 BULK MODULUS VS. MEAN STRESS - 12" Ø AND 32" Ø CBG

the short interval between data points. Each plot is superimposed on the values of bulk modulus predicted by the nonlinear hysteretic model for the particular core size. Several trends are immediately apparent. First, the experimental data fits the model best in the hydrostatic range of each test, and departs from the model at low stress levels and at high stress levels where yielding is to be expected. Second, the fit to the model is best for the small specimens and worse for the large specimens. This is probably a result of the relatively early slippage that took place in the larger specimens. The larger specimens began slippage at low levels of deviator stress, so that earlier departure from the model is to be expected. Of course, it is to be remembered that the model was developed for small rock specimens.

Table 2 is a summary of the model parameters for the tests on Charcoal Black granite. The smaller cores behaved quite consistently, and the model parameters were simply averaged to produce the final parameters for each test. The larger tests were less consistent, particularly with respect to the values for A_1. The final parameters for the 32-in. specimens were obtained from a composite log-log plot of data for tests 27, 28 and 30.

An interesting comparison may be made between the analysis of an ideal packing of elastic spheres as discussed earlier and the observed hydrostatic behavior of the rock specimens. Values of "n" in the nonlinear hysteretic model vary from 1.59 to 1.93 with an average of 1.74 for the specimens of Charcoal Black granite. The corresponding values of "n" for the ideal packing is 1.5. For granular soils n values between 1.5 and 2.0 have been observed[44].

Table 2

NONLINEAR HYSTERETIC MODEL PARAMETERS FOR TEST ON CHARCOAL BLACK GRANITE

Diameter	Test	J_o ksi	n	A $\times 10^6$	Mean for Core Size n	A' $\times 10^6$
2	12	5	1.61	0.208	1.59	0.172
	14	10	1.52	0.113		
	34	15	1.63	0.194		
4	9	5	1.86	1.24	1.89	0.905
	11	10	1.90	1.25		
	19	15	1.61	0.216		
12	16	5	1.98	1.19	1.93	0.534
	37	5	2.03	.03		
	20	10	1.78	0.38		
32	27	5	1.53	.24	1.56	0.237
	28	5	1.85	1.90		
	29	10	4.05	-		
	30	10	1.80	1.68		

Typical deviatoric stress and strain data from a constant confining pressure triaxial test, $\sigma_3 = 5$ ksi, are shown in Fig. 24. The curves are very nearly linear at stresses less than approximately 30 ksi which is the level at which initial yielding of the specimen occurs. Also the unload curve is nearly elastic with a very small residual strain. Similar data was obtained from tests at other confining pressures except the unconfined compression test, $\sigma_3 = 0$. For this test the slope of the deviatoric stress vs. deviatoric strain curve increased slightly as the stress increased meaning that the shear modulus, G, also increases with stress at low stress levels.

Tangent values of shear modulus, G_t, were determined from the experimental data and are shown in Fig. 24 (b), 25 (b), 26 (b) and 27 (b) for specimen diameters of 2 in., 4 in., 12 in. and 32 in. respectively. The stress paths of the particular tests considered for each diameter are shown in Figs. 25 (a), 26 (a), 27 (a), and 28 (a). As observed from the data the shear modulus increases with mean stress especially at the low stress levels. An equation of the form

$$G_t = c\sigma_m^{1/10}, \tag{36}$$

in which "c" is a constant, was fitted to the experimental results and is shown in Fig. 25 through 28. As relatively little inelastic behavior was observed in the shear deformations the model for shear modulus is the same for both loading and unload-reload. Model predictions are in agreement with observed behavior except at low stresses.

A summary of the mathematical models for bulk and shear moduli along with the constants determined from the experimental results is presented in Table 3. Values of Young's modulus were computed from equation (30) using the predicted values of bulk and shear modulus and are shown

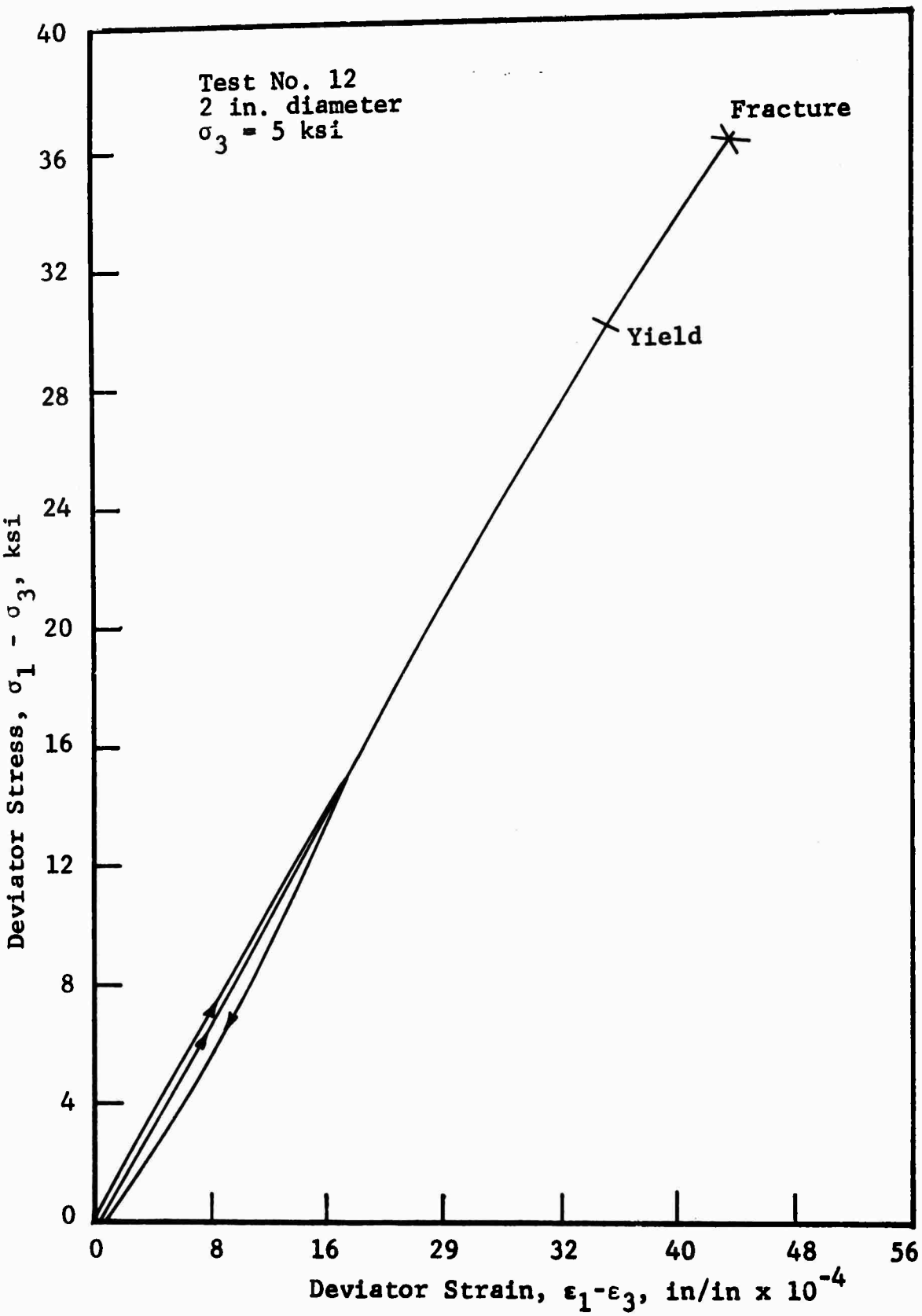

Fig. 24 DEVIATOR STRESS VS. STRAIN, CHARCOAL BLACK GRANITE

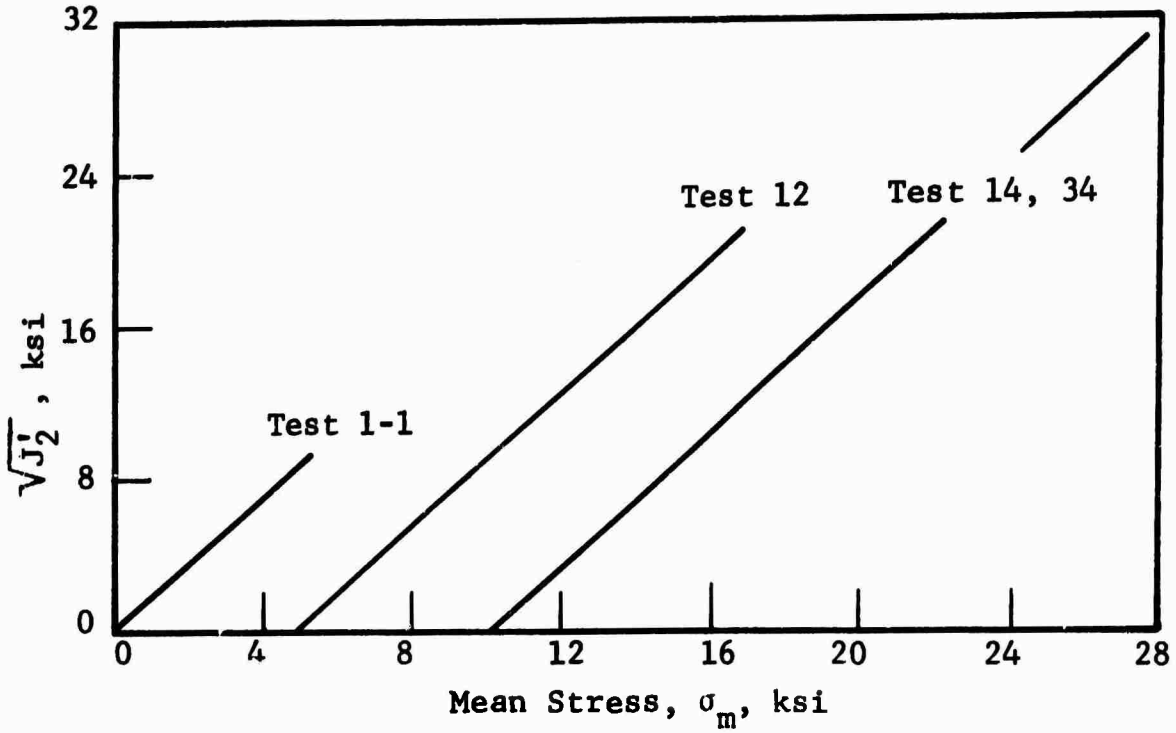

a) Stress Path

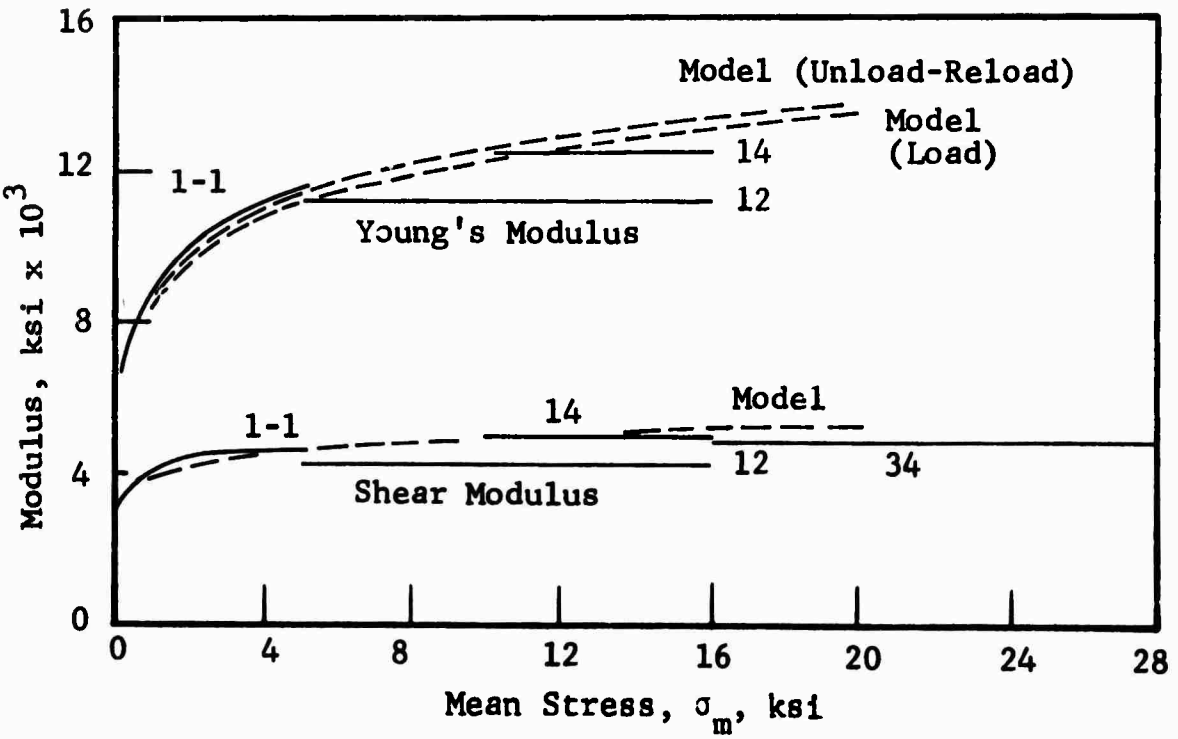

b) Shear Modulus and Young's Modulus

Fig. 25 TANGENT MODULI FOR CHARCOAL BLACK GRANITE, 2-IN. DIA.

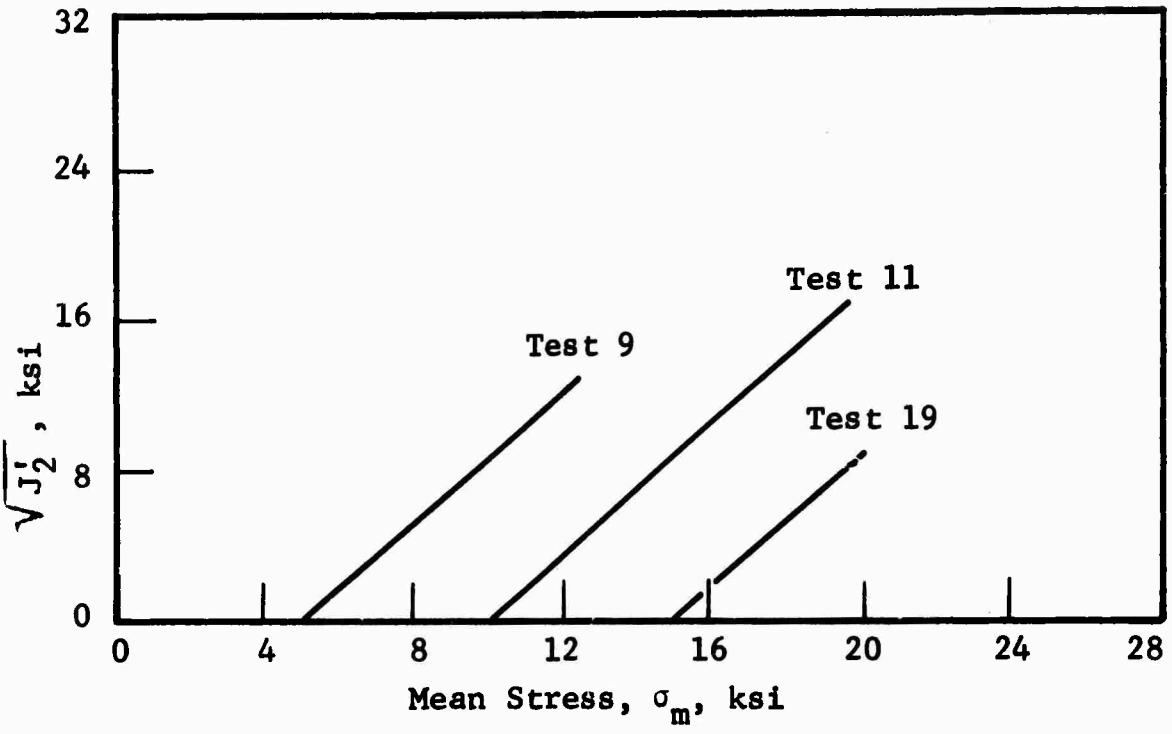

a) Stress Path

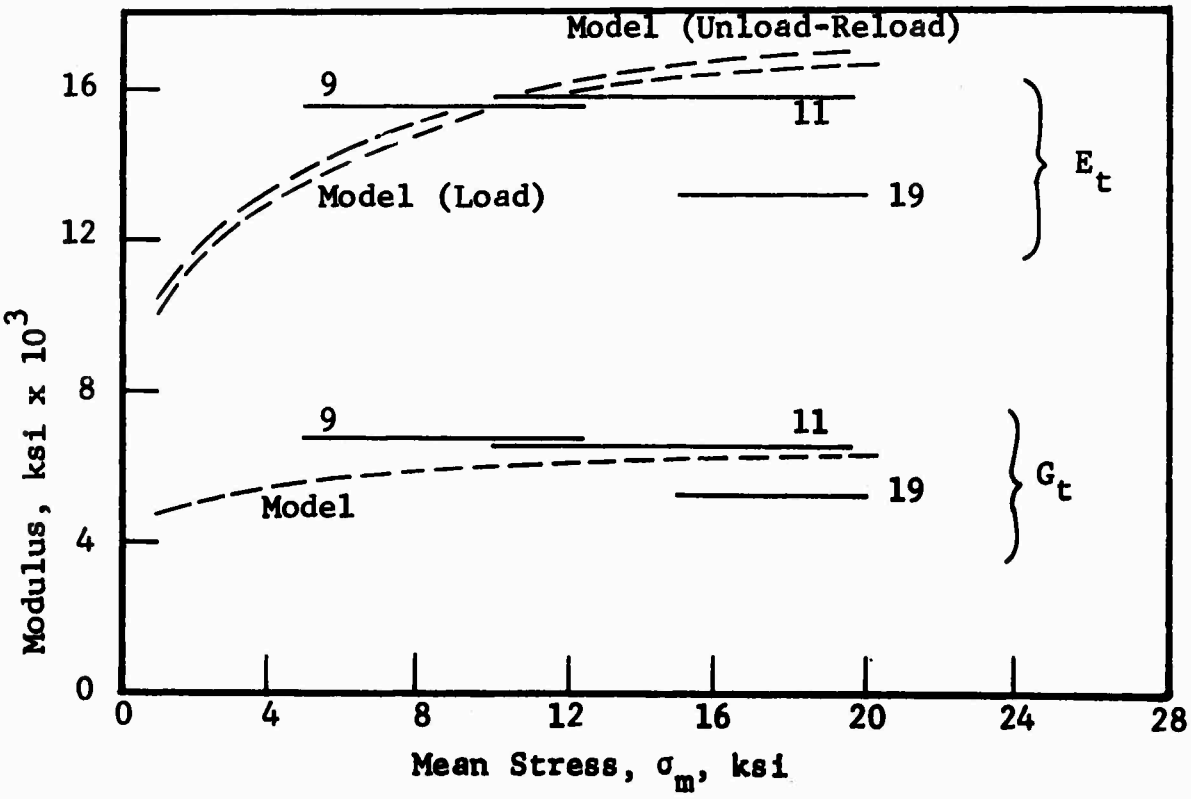

b) Shear Modulus and Young's Modulus

Fig. 26 TANGENT MODULI FOR CHARCOAL BLACK GRANITE, 4-IN. DIA.

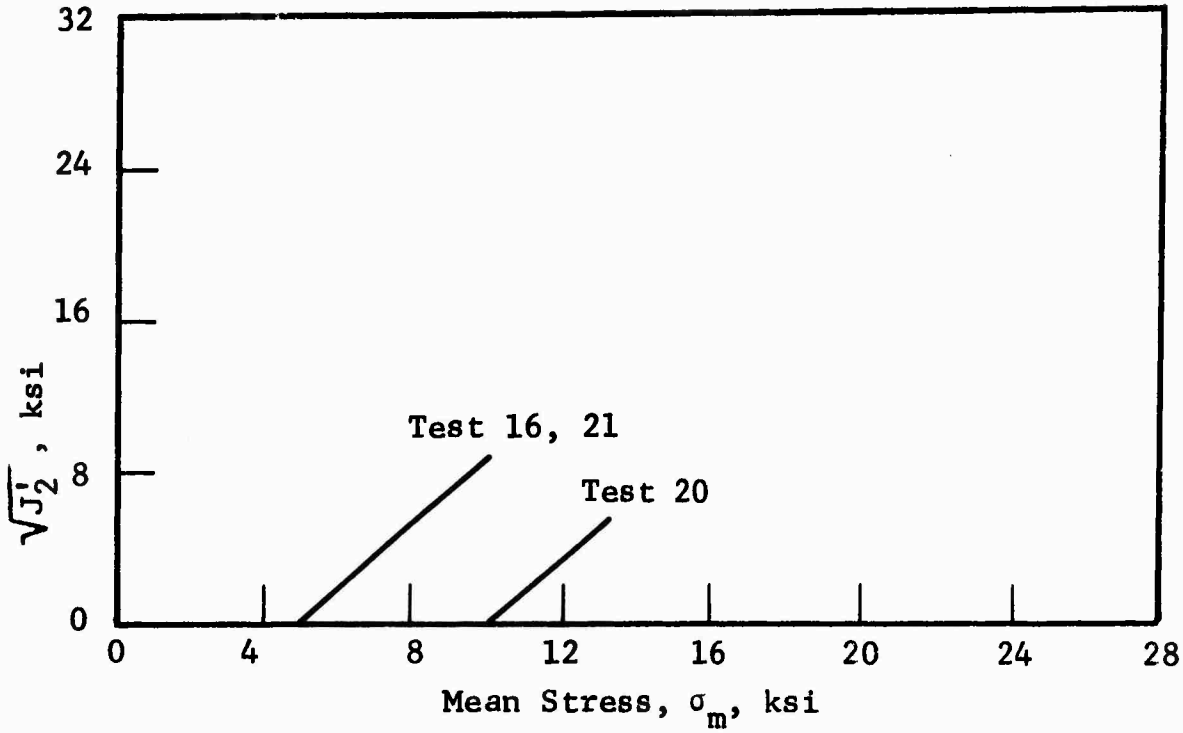

a) Stress Path

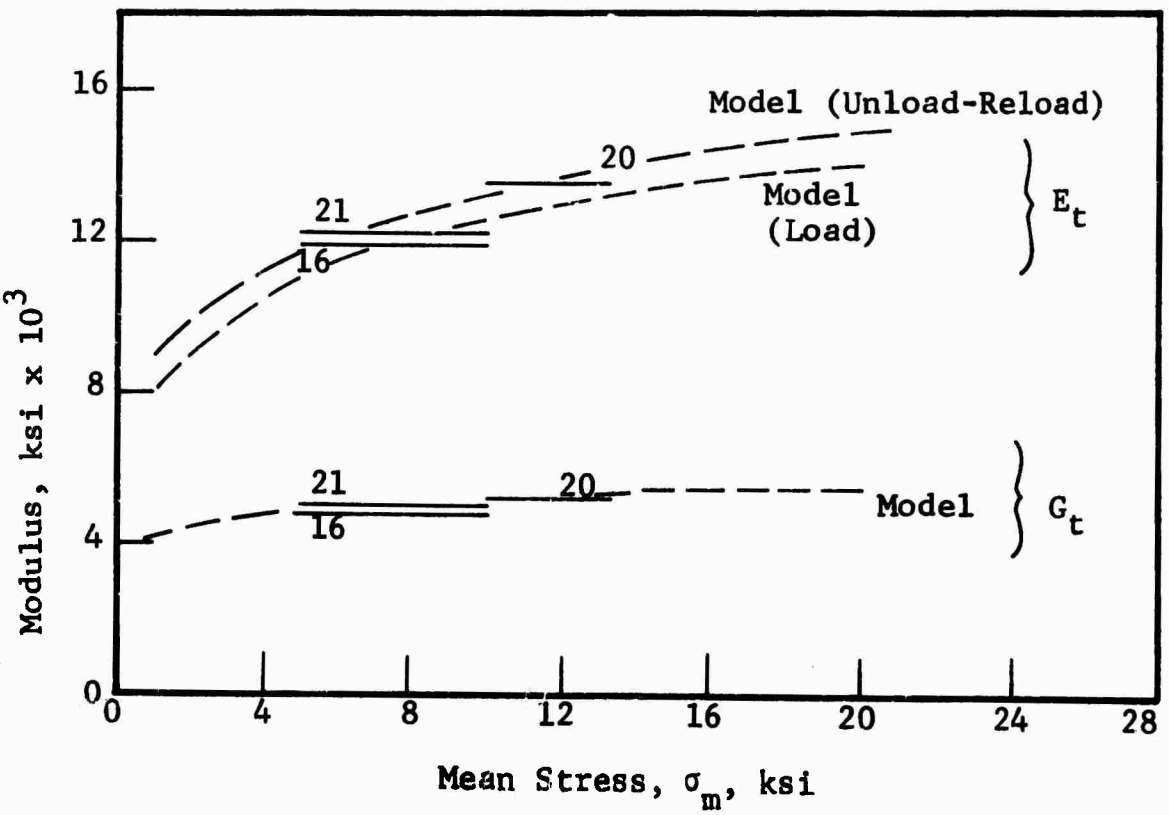

b) Shear Modulus and Tangent Modulus

Fig. 27 TANGENT MODULI FOR CHARCOAL BLACK GRANITE, 12-IN. DIA.

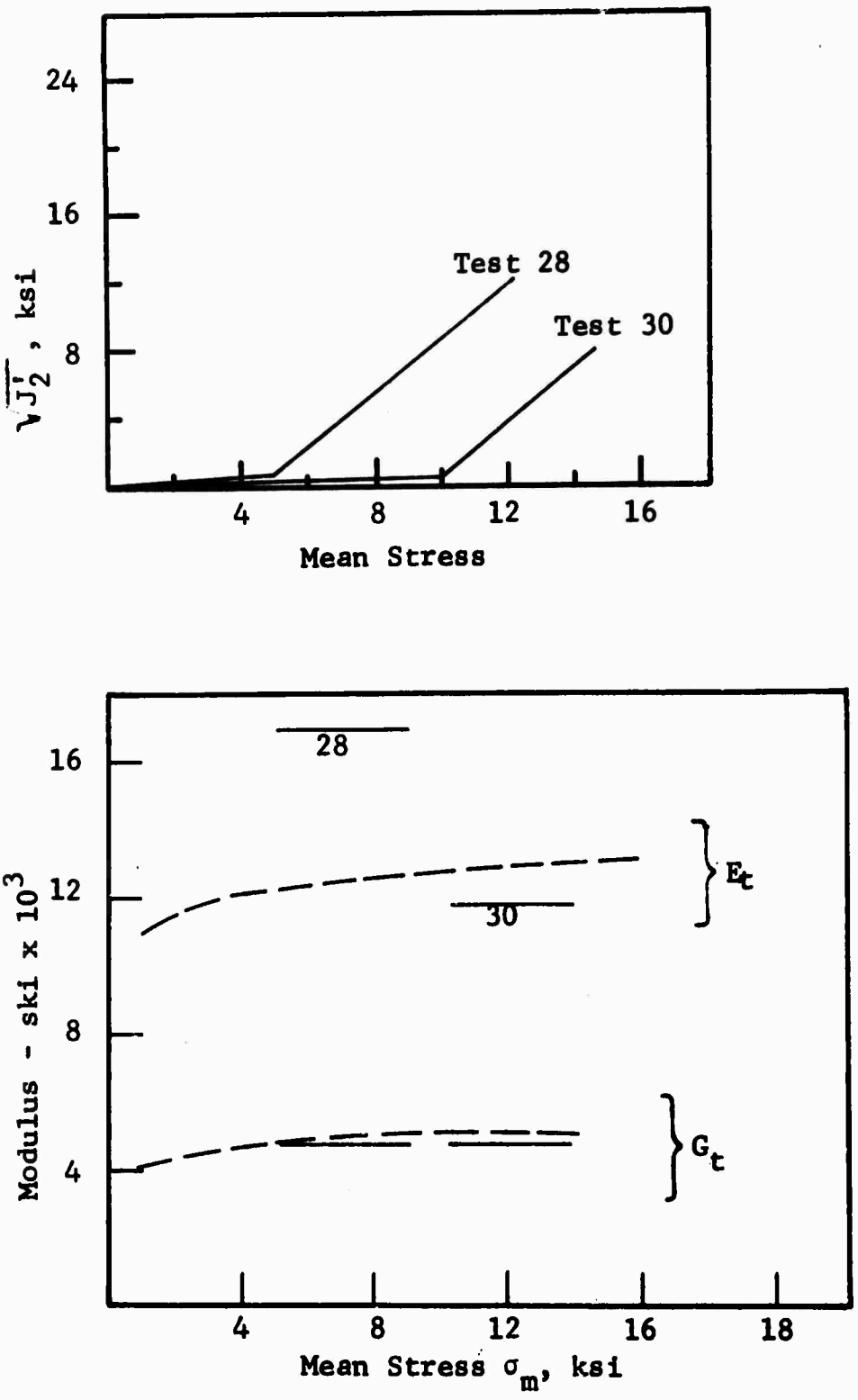

Fig. 28 TANGENT MODULI FOR CHARCOAL BLACK GRANITE, 32-IN. DIA.

Table 3

ELASTIC PROPERTIES OF CHARCOAL BLACK GRANITE

Bulk Modulus

loading, $k_t = nA_1^{1/n} \sigma_m \frac{n-1}{n}$

unload - reload, $k_t = nA_2^{1/n} \sigma_m^{n-1/n}$

Shear Modulus

loading, $G_t = C \sigma_m^{1/10}$, G_t and σ_m in ksi

unload - reload, $G_t = C \sigma_m^{1/10}$, G_t and σ_m in ksi

Young's Modulus

$$E_t = \frac{9 k_t G_t}{3 k_t + G_t}$$

Poisson's Ratio

$$V_t = \frac{3 k_t - 2G_t}{2(3k_t + G_t)}$$

Specimen Diameter in inches	n	A_1 in ksi	A_2 in ksi	C
2	1.59	1.72×10^5	1.72×10^5	3,900
4	1.89	9.05×10^5	10.7×10^5	4,800
12	1.93	5.34×10^5	13.5×10^5	4,100
32	1.56	2.37×10^5		

as a function of mean stress in Fig. 25 through 28. Poisson's ratio values were computed from equation (31) and are shown in Figs. 29, 30, and 31 for the different specimen diameters. Again, except at stresses below 1 ksi the model fits the experimental data.

5.3.2 Cedar City Tonalite

The nonlinear hysteretic model was fitted to the various core sizes of Cedar City tonalite by use of log-log plots of mean stress versus volumetric strain. The resulting model parameters were used to compute bulk moduli in the same fashion as was done for the Charcoal Black granite. Figures 32, 33 and 34 show the actual bulk moduli as a function of mean stress. The solid symbols indicate data from the hydrostatic portions of the various tests, the open symbols the triaxial compression portions. In general, the hydrostatic data fall near the model and the triaxial data depart from the model. The data points do not scatter symmetrically about the model because the model was fit to the volumetric strains rather than the bulk moduli.

The same observations apply to this data as to the corresponding Charcoal Black granite data. The model for each core size fits best in the intermediate stress ranges, and the data scatter increases with specimen size. The nonuniformity of this rock type is particularly noticeable in the 12-in. cores. Tests 17 and 38 had quite different moduli below 5 ksi, but appeared to converge to the same stiffness above 7 ksi. This may be expected if the existing cracks are closing in this pressure range.

The scale effect is shown in Figs. 35 and 36. Figure 35 is a plot of the mean stress versus volumetric strain predicted by the model for the three specimen sizes. Figure 36 is a common plot of the bulk moduli. The major difference between the 2-in. and 4-in. models is that the 4 in. model is slightly

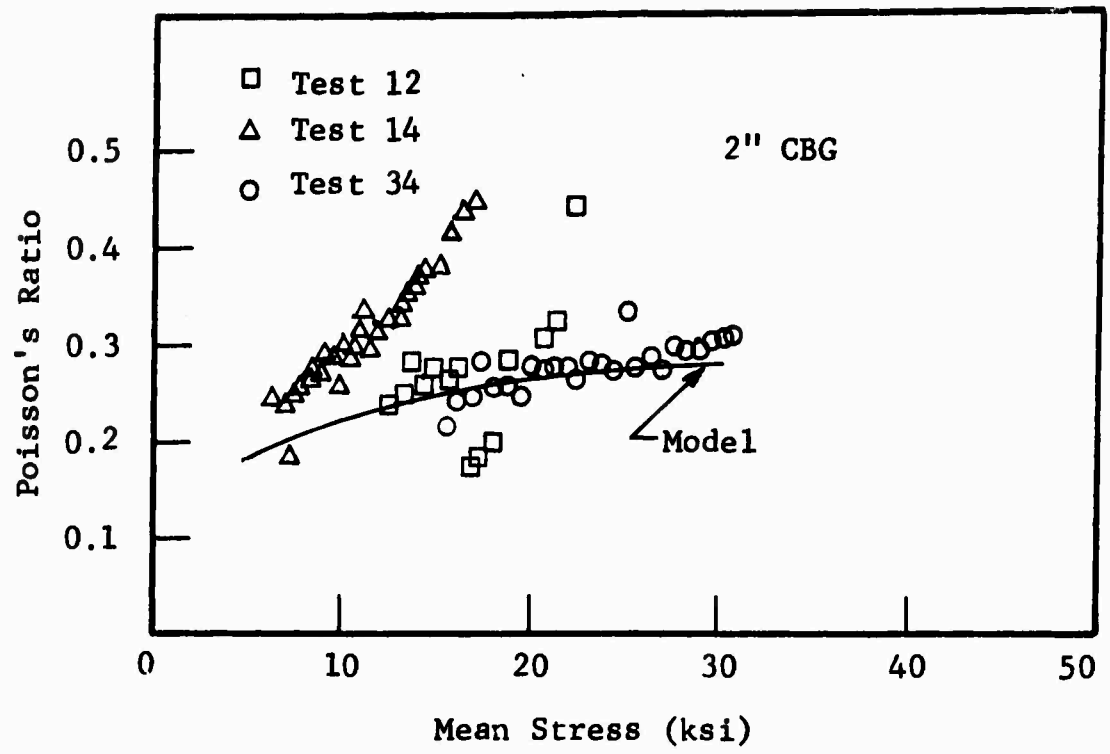

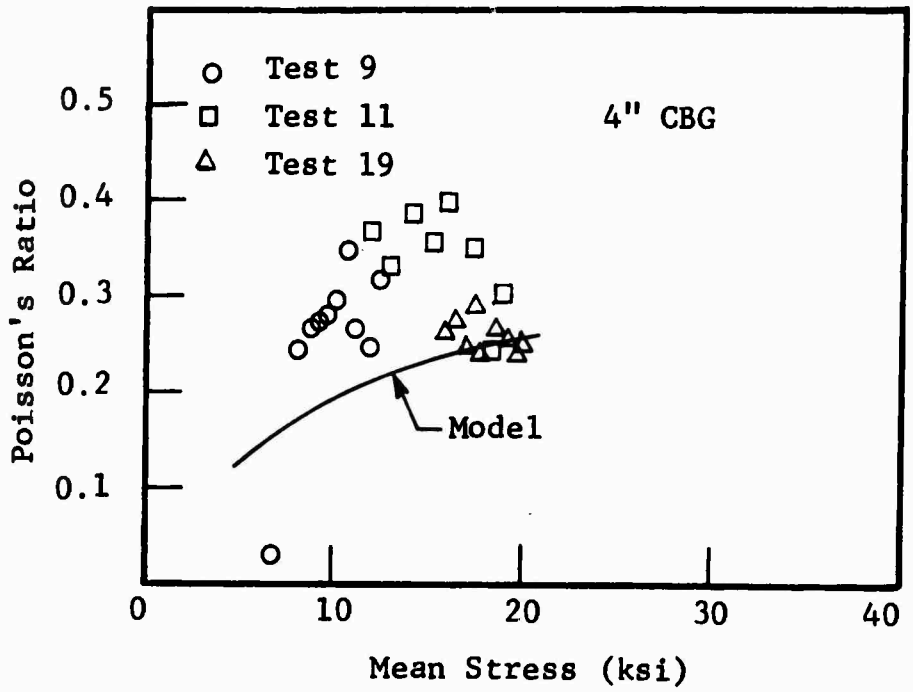

Fig. 29 POISSON'S RATIO VS. MEAN STRESS FOR 2 IN. Ø AND 4" Ø CHARCOAL BLACK GRANITE

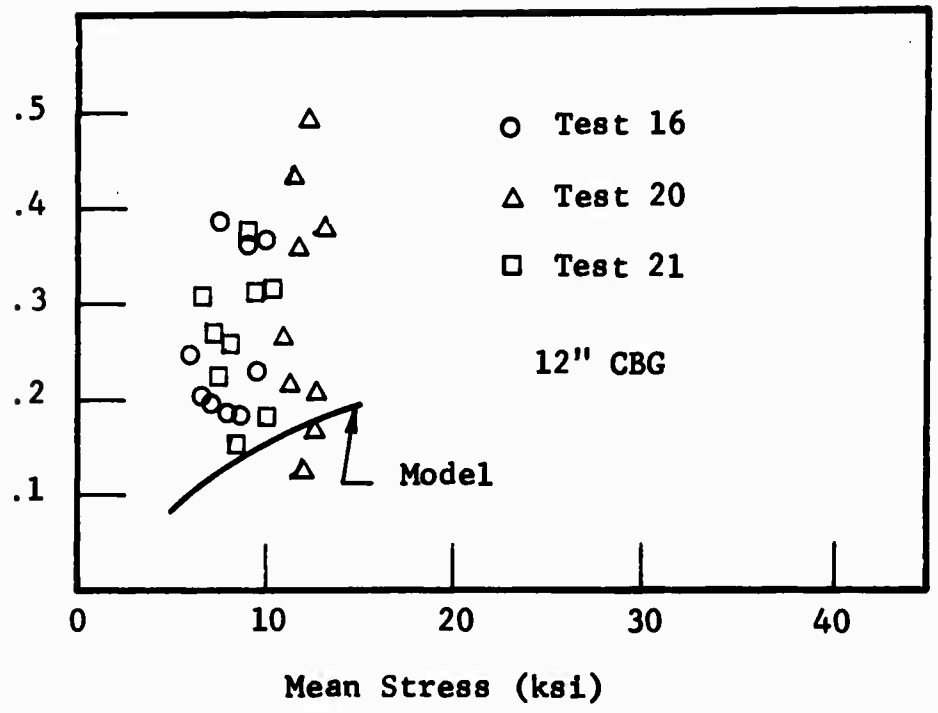

Fig. 30 POISSON'S RATIO VS. MEAN STRESS FOR 12" Ø CHARCOAL BLACK GRANITE

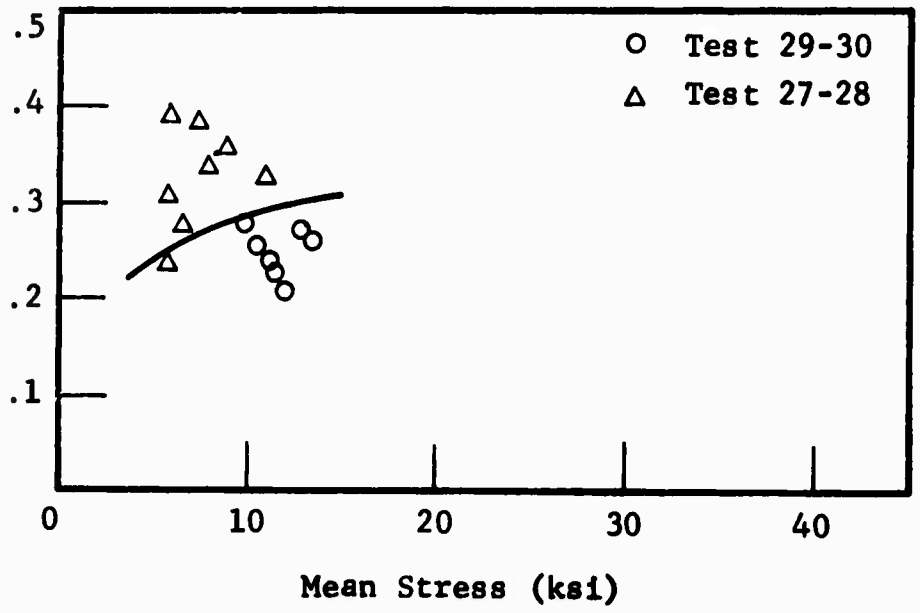

Fig. 31 POISSON'S RATIO VS. MEAN STRESS FOR 32" Ø CHARCOAL BLACK GRANITE

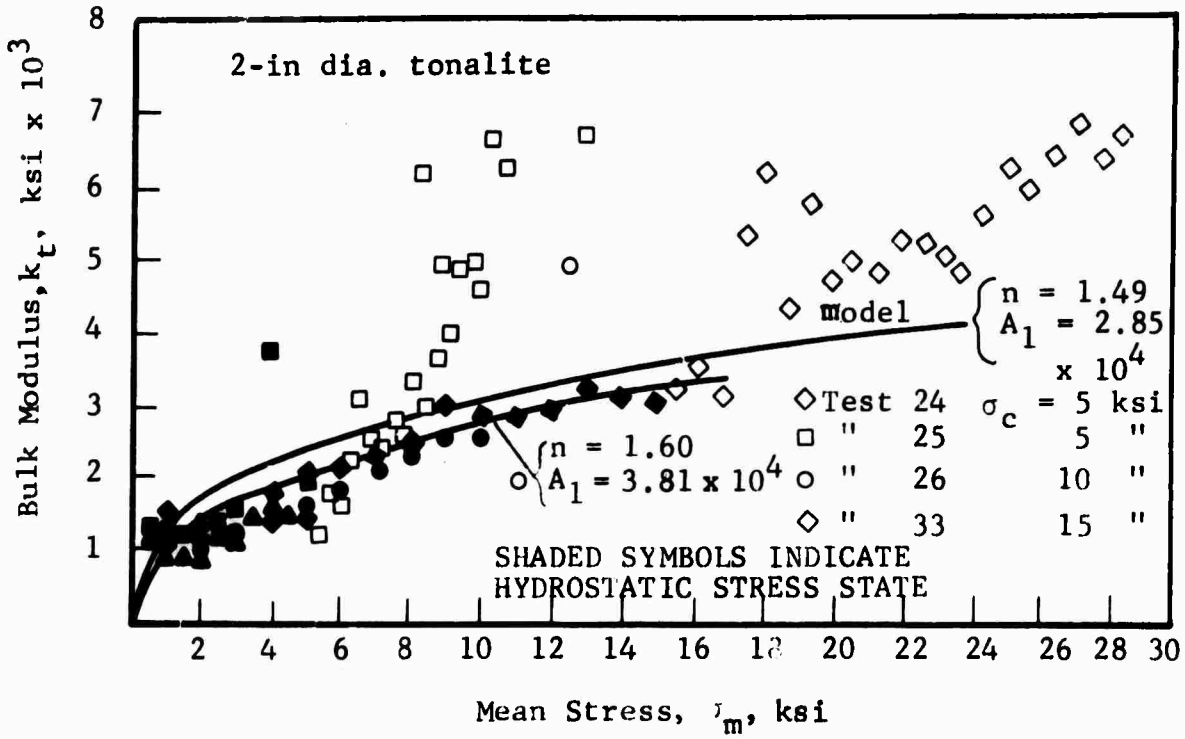

Fig. 32 BULK MODULUS FOR 2" CEDAR CITY TONALITE

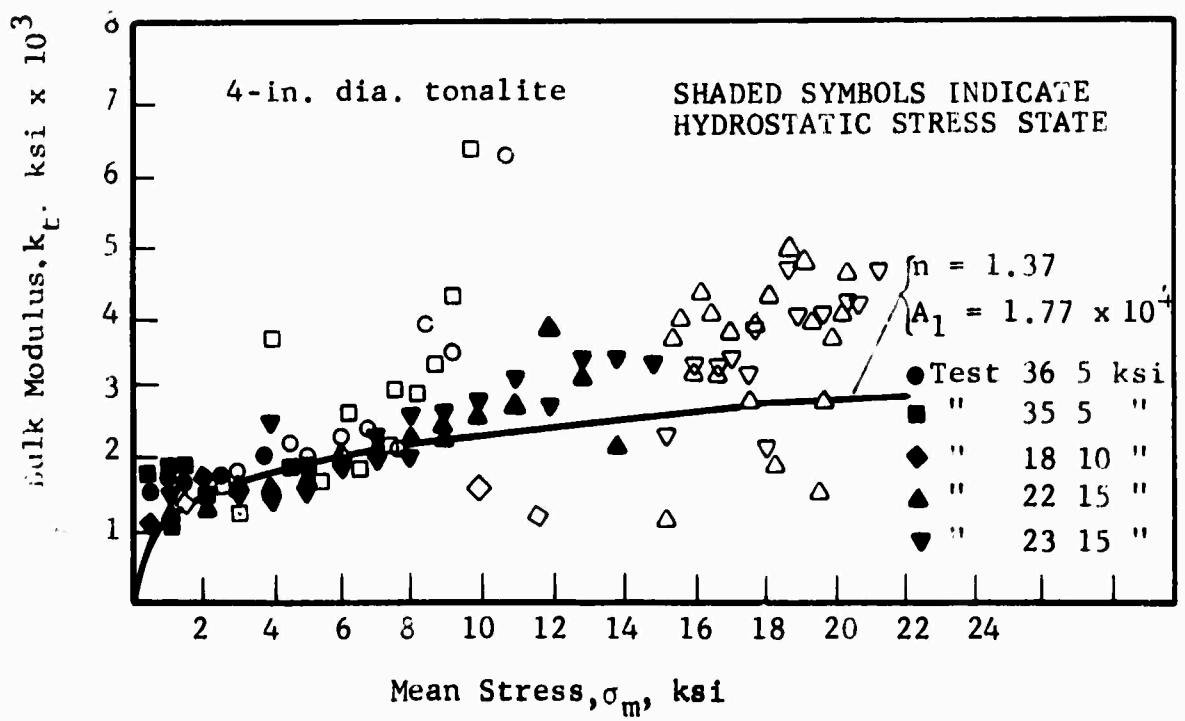

Fig. 33 BULK MODULUS FOR 4" CEDAR CITY TONALITE

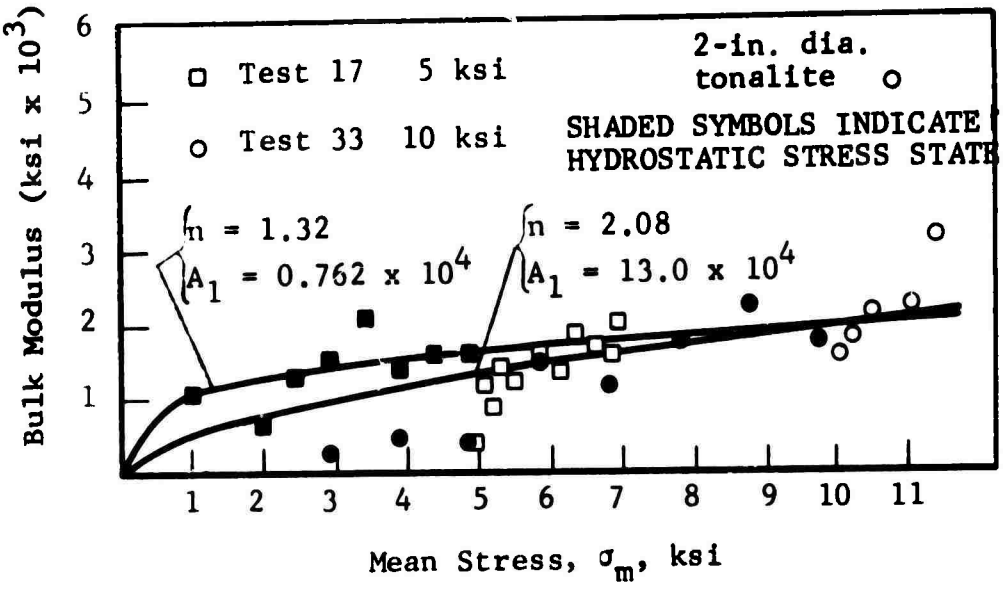

FIG. 34 VARIATION OF BULK MODULUS FOR CEDAR CITY TONALITE, 2-in, 4-in. and 12-in. DIAMETER

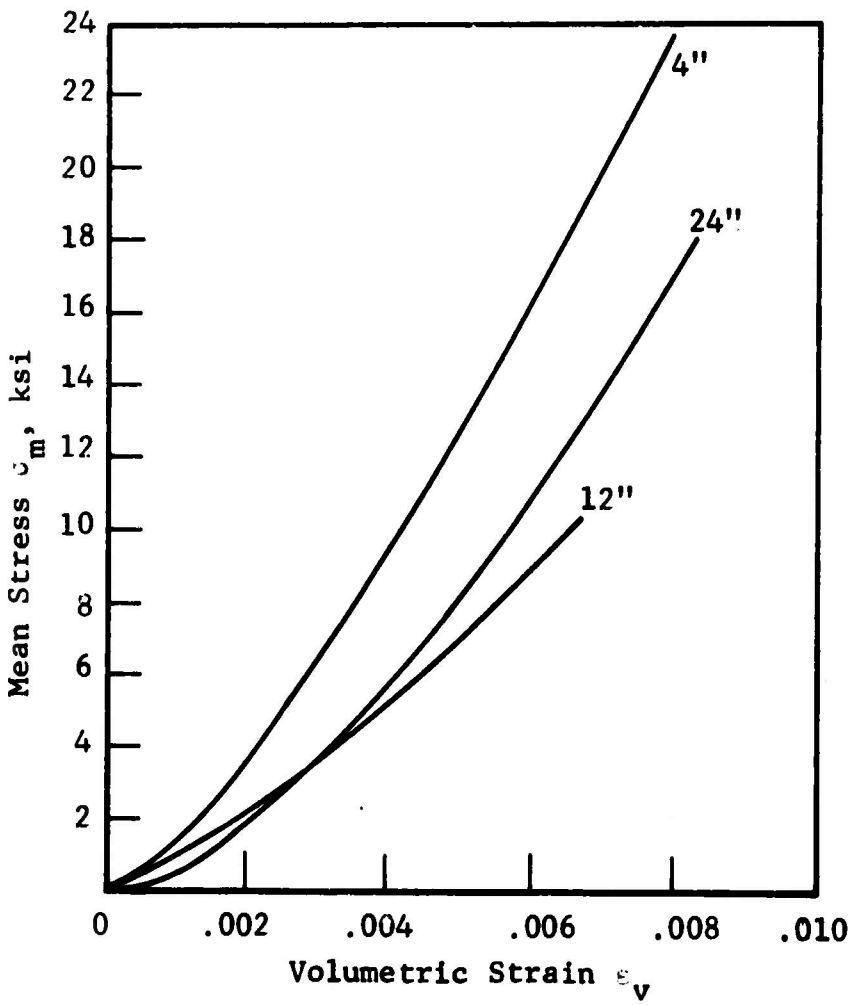

Fig. 35 VOLUMETRIC STRAIN FOR CEDAR CITY TONALITE MODELS

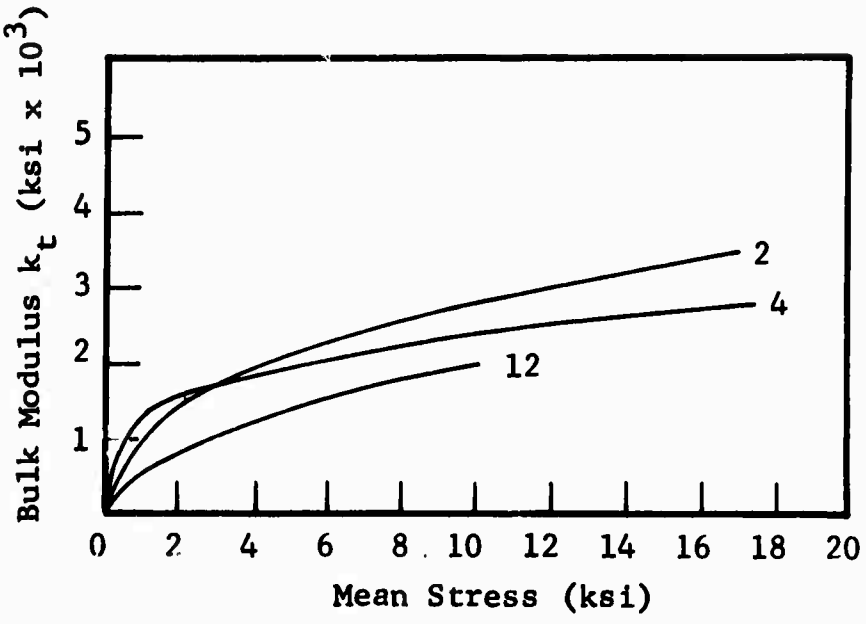

Fig. 36 BULK MODULUS FOR CEDAR CITY TONALITE MODELS

stiffer below 3 ksi. This results in a horzontal displacement of the curves in Fig. 35. If Fig. 35 were extended to higher stress levels, the 2-in. and 4-in. curves would cross as a result of the higher 2-in. bulk modulus. The actual differences in these curves are probably a result of specimen variation rather than scale effects. The 12-in. specimens appear to be significantly less stiff than the smaller specimens.

Figure 37 shows the scale effect upon shear modulus G_t and elastic modulus E_t. Data from all tests are included, and again the scatter is caused by the short interval between data points. It can be seen that the 2-in. and 4-in. specimens were not significantly different, and that the 12-in. specimens were less stiff at lower mean stress values. The shear modulus did not fit the one-tenth power of mean stress model, so fair lines were passed through the data by eye. The elastic modulus model was computed using values of the bulk modulus models in Figs. 32, 33 and 34, and appears to represent the experimental elastic moduli well.

Figure 38 shows plots at Poisson's ratio for the various size specimens. The typical behavior is to start out somewhat below the model and rapidly increase to a value greater than would be predicted by this model. The tests having 15 ksi confining pressure maintain a value of approximately 125% of the model value for a period before yielding begins, while the tests at lower confining pressures appear to maintain a monotonic increase. As the yield point approaches, the value of Poisson's ratio may increase because of the dilatancy of the specimen.

5.3.3 Uniaxial Strain Tests

Uniaxial strain tests were conducted on two specimens, a 22-in. dia. Cedar City tonalite specimen and a 32-in. dia. Charcoal Black granite specimen. The results from this type of test should be applicable to unidirectional compression

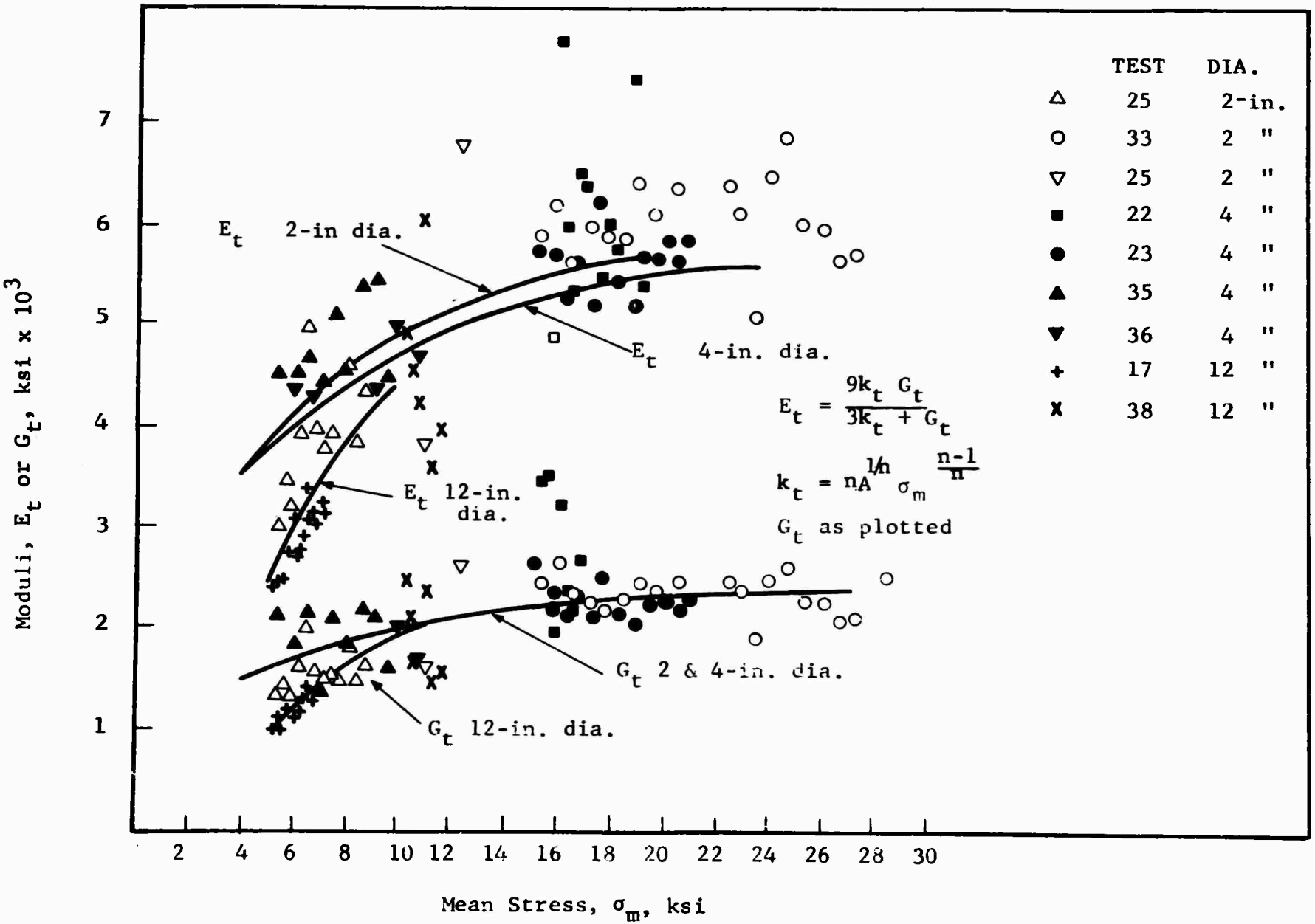

Fig. 37 TANGENT MODULI FOR CEDAR CITY TONALITE

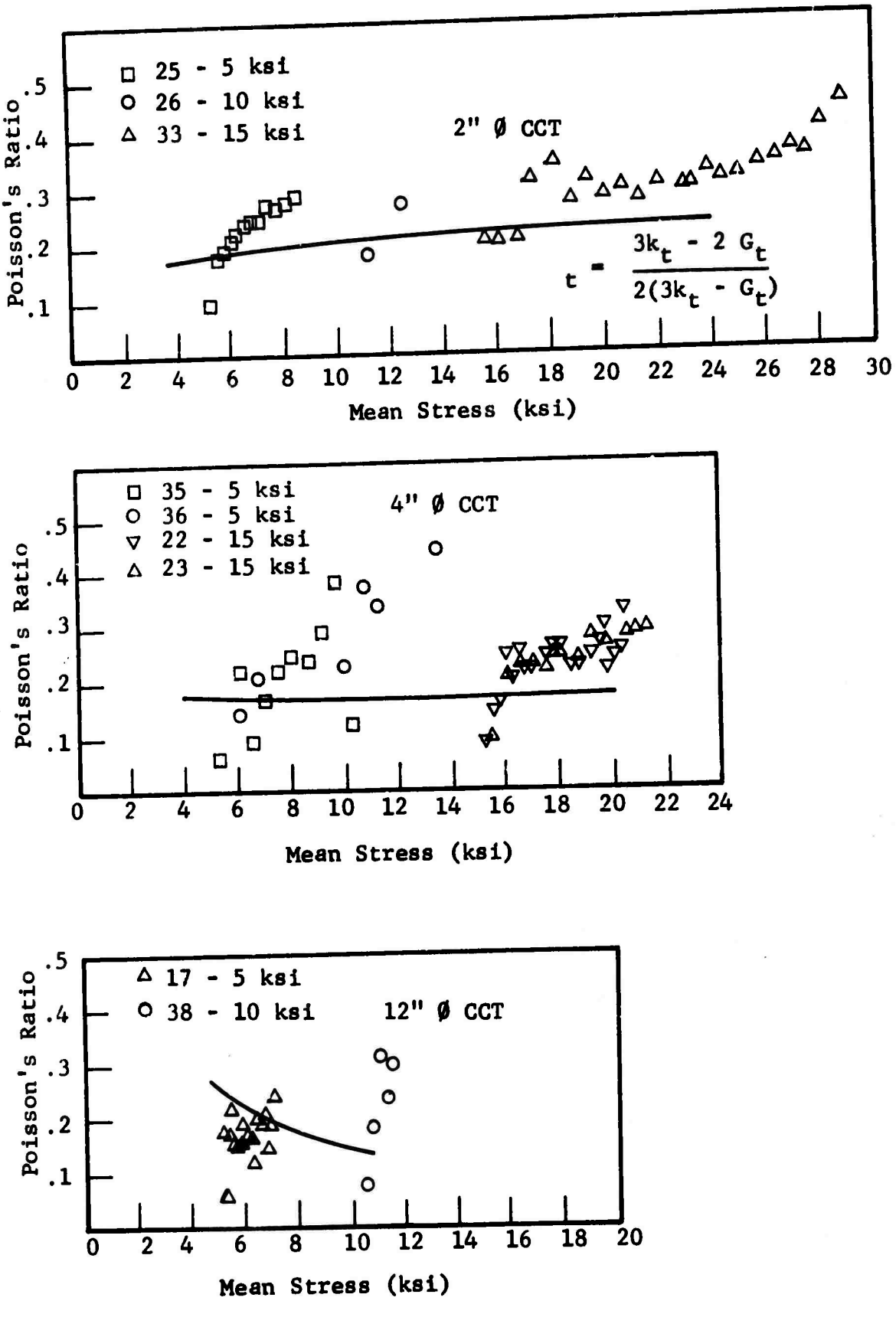

Fig. 38 POISSON'S RATIO FOR CEDAR CITY TONALITE

of an element in a rigidly confined mass or plane-wave propagation. The radial strains were monitored during the test by the auxiliary averaging strain gages described in the experimental apparatus section of this report. Confining pressure was controlled to maintain these gage readings as near zero as possible.

Figure 39 shows the axial and lateral strains and the stress trajectories for both tests. As can be seen, the radial strains did go tensile by about 250 microstrains in test 31 and 100 microstrains in test 32. The Cedar City tonalite (test 32) failed at an axial stress of 20 ksi.

The behavior of the Charcoal Black granite was somewhat more complex, primarily because this specimen was able to support load after slippage, and the test was continued for two full cycles. The offset on the unload cycle at 11.5 ksi was caused by a gage failure. The offset on the reload cycle at 26.5 ksi was accompanied by a major rock shift.

Figures 40 and 41 show the shear strain and volumetric strain for both tests. Note that for this test condition there appears to be little difference between the two rock types. Both have shear moduli G_t between 4×10^6 and 5×10^6. Any curvature in the Charcoal Black granite shear modulus is swallowed by the initial zero offset, which may or may not be real. The bulk modulus for the Cedar City tonalite increases from 1.6×10^6 to 5.2×10^6 ksi as mean stress goes from zero to 9 ksi. The Charcoal Black granite bulk modulus ranged from 1.7×10^6 ksi at 1.5 ksi to 4×10^6 ksi at a mean stress of 10 ksi. Corresponding values for elastic modulus and Poisson's ratio are listed below:

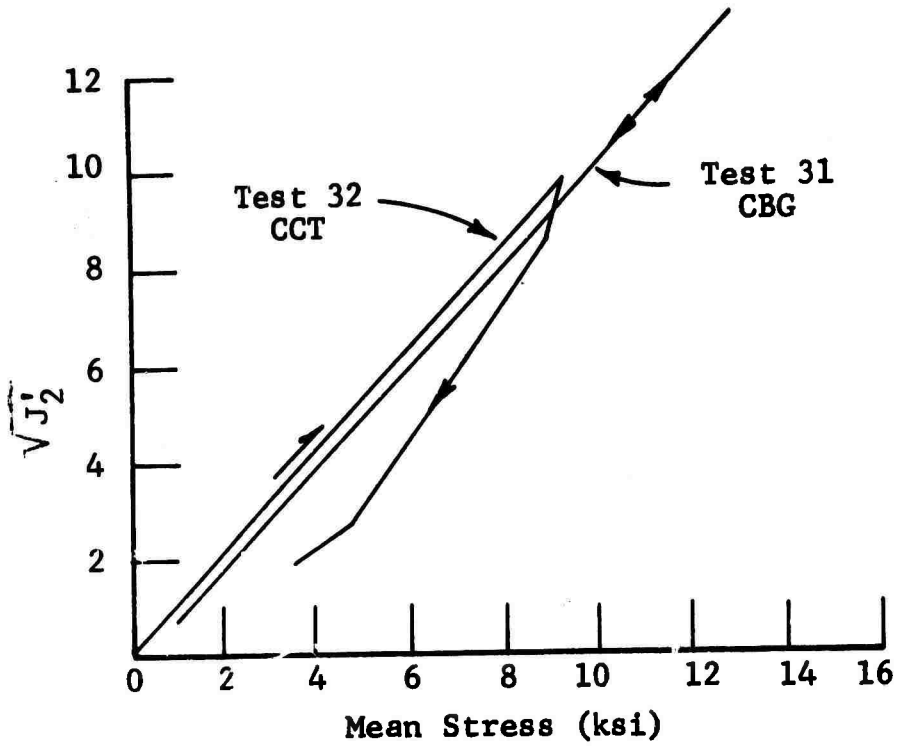

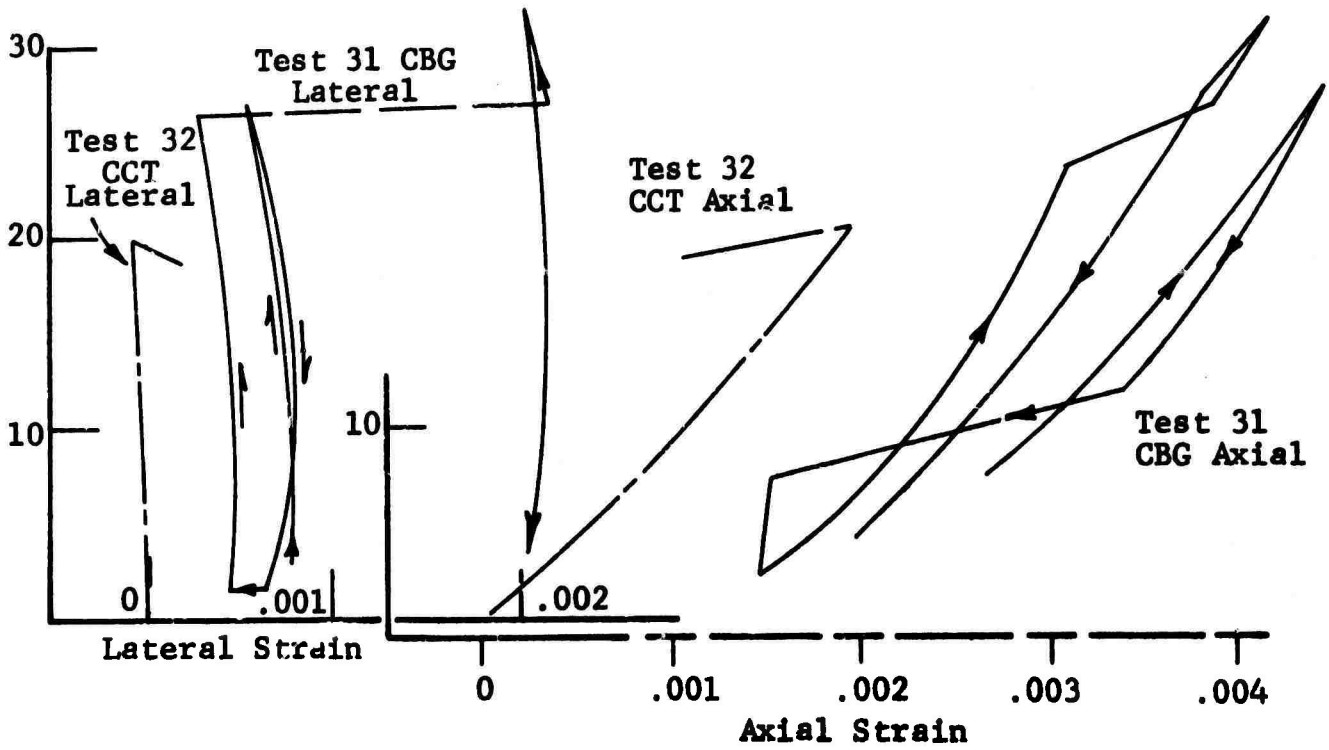

Fig. 39 UNIAXIAL STRAIN TEST

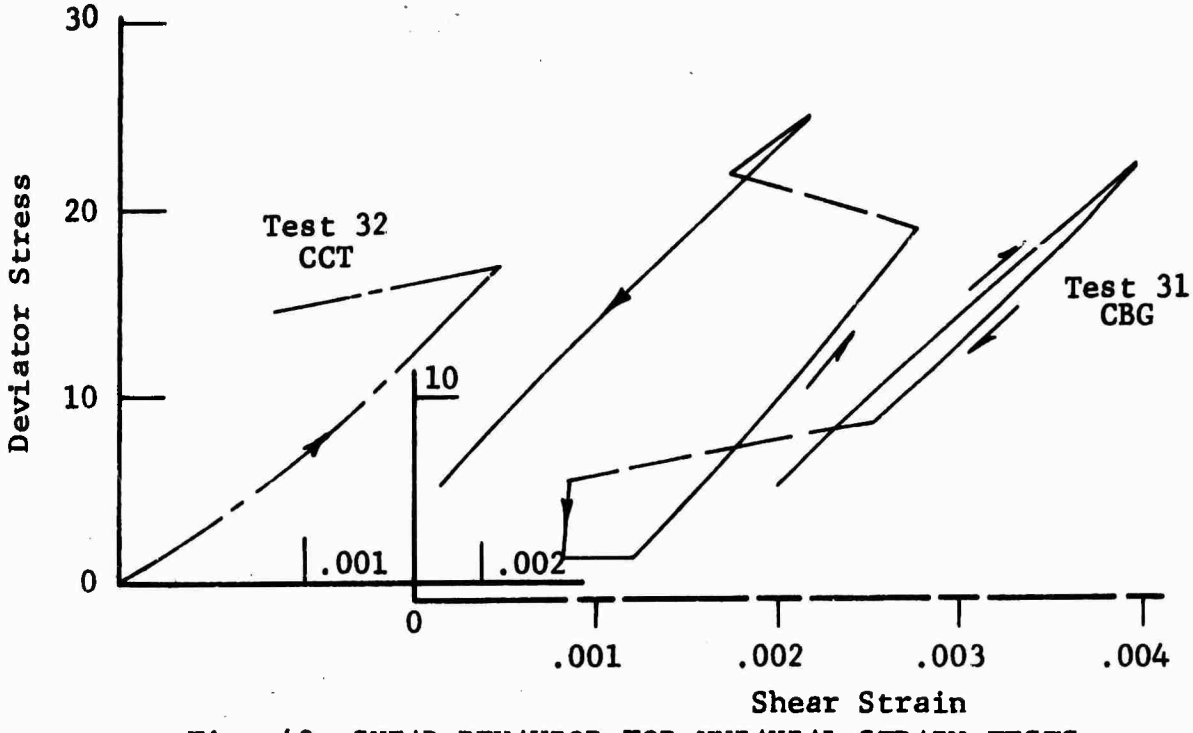

Fig. 40 SHEAR BEHAVIOR FOR UNIAXIAL STRAIN TESTS

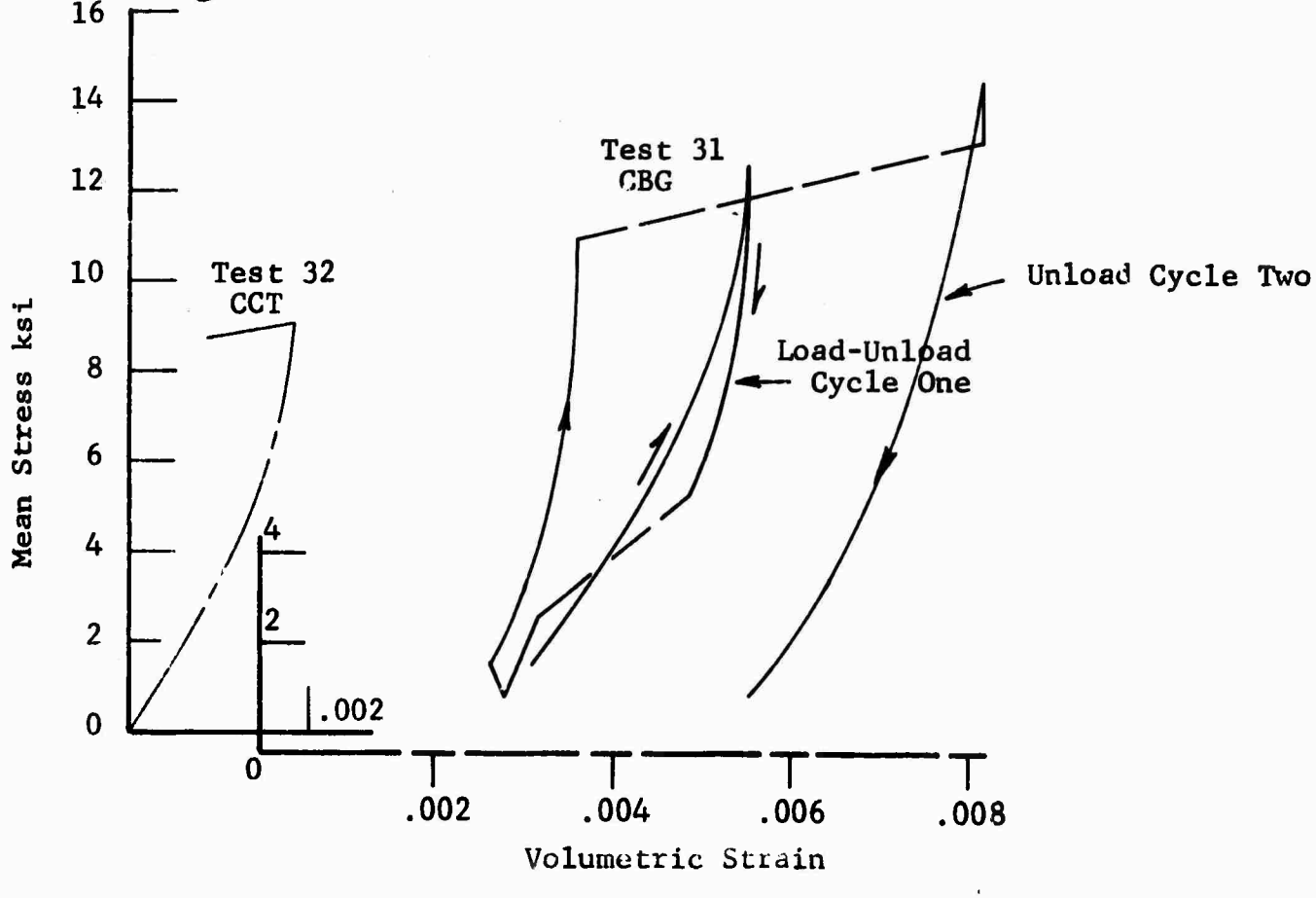

Fig. 41 VOLUMETRIC STRAIN FOR UNIAXIAL TEST

	Charcoal Black Granite				Cedar City Tonalite			
σ_m	G	K	E	ν	G	k	E	ν
2	4	2.9	8.3	.03	4.5	3.5	9.5	.05
4		3.3	8.5	.07		4.4	10	.12
6		3.8	8.9	.11		7.0	11	.24
8		4.2	9.1	.14		10.5	12	.31

5.4 Strength Properties

Figure 42 indicates the maximum stress levels attained by each specimen. Due to a less favorable intensification ratio in the 14-in. triaxial cell, there were no failures of the 12-in. specimens. Future programs would need to employ higher stress levels to insure failure.

The 32-in. dia. Charcoal Black granite specimens reached maximum stress levels of about one half that of the 2-in. specimens. The actual scale effect is probably somewhat greater. Slippage along a joint plane will produce instant failure in a 2-in. specimen, while a 32-in. specimen not only survives minor slippage, but can be loaded to greater stress levels.

The Cedar City tonalite was much more variable. As might be expected from a weathered rock, the strength at low mean stress levels is quite low. This corresponds to a low "c" value on a plot of the Mohr-Coulomb failure envelope.

Enough data was not obtained in this program to apply any statistical theories, such as those of Weibull[13] or Grobbelaar[15]. It is hoped this will become possible when more data is accumulated.

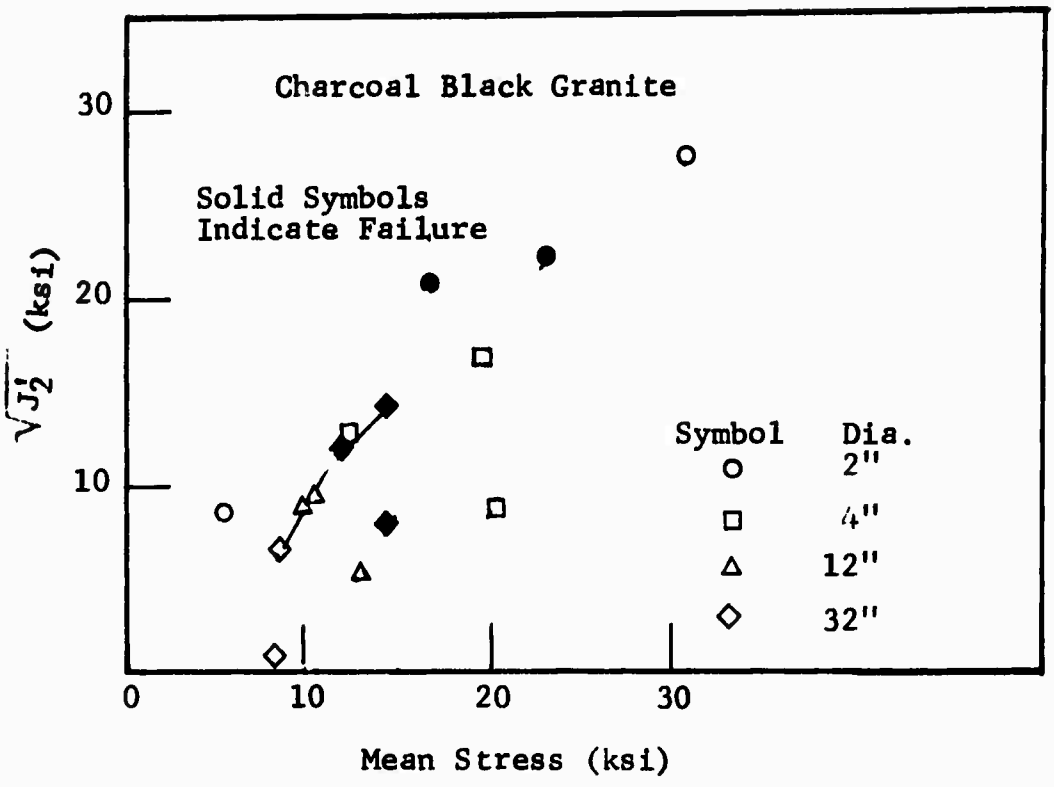

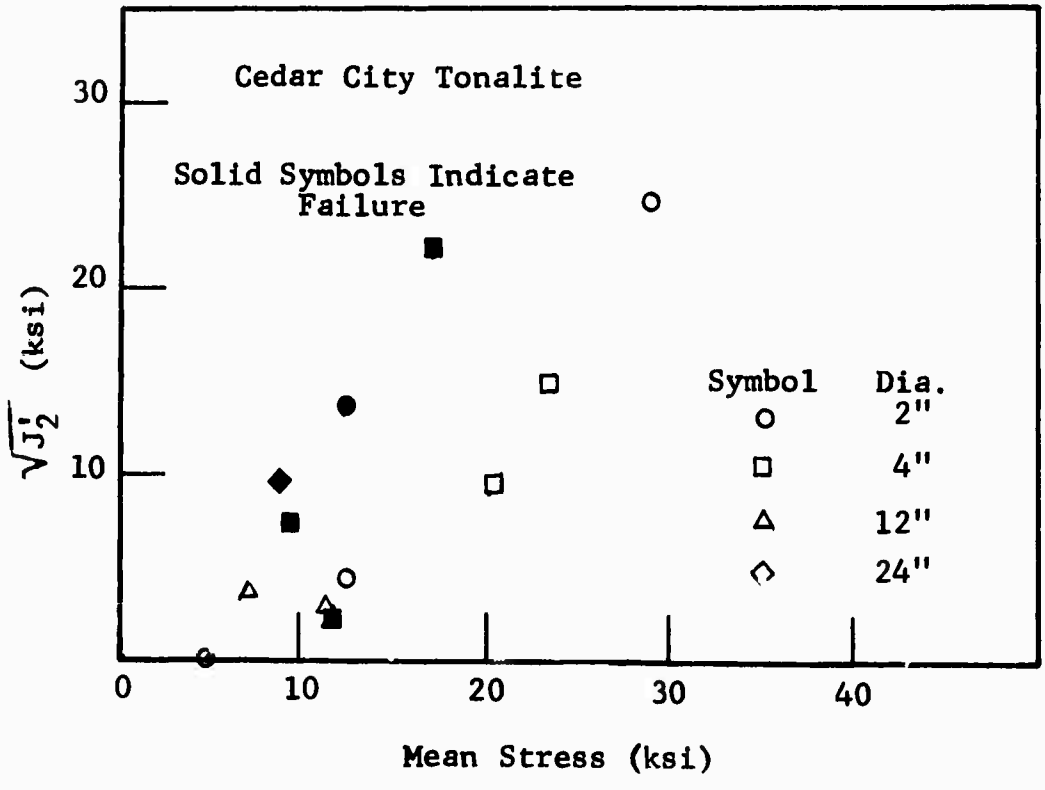

Fig. 42 MAXIMUM VALUE OF $\sqrt{J_2'}$ REACHED FOR ALL TESTS

6. SUMMARY AND CONCLUSIONS

Over the course of this program, 27 triaxial tests were run on samples ranging from 2 in. to 32 in. dia. This is the first time that specimens of this size have ever been tested under laboratory conditions. Because of the large volume of data collected, the results of this program are presented in term of a nonlinear hysteretic model proposed by Seaman and Whitman[44] and having the form

$$\sigma_m = A_1 \varepsilon_v^n \quad \text{loading}$$

$$\sigma_m = A_2 (\varepsilon_v - \varepsilon_{v\ell})^n \quad \text{unloading}$$

where

σ_m is mean stress

ε_v is volumetric strain

$\varepsilon_{v\ell}$ is residual volumetric strain.

The data fit this model well at intermediate stresses. However, the model predicts that bulk modulus is zero when mean stress equals zero, and bulk modulus goes to infinity at infinite mean stress. In fact, rocks display a finite bulk modulus at zero mean stress and a constant bulk modulus under high stresses. In spite of this, the data depart from the model only below stresses of about 3 ksi and at higher stresses when yielding occurs.

The model parameters as fitted to each core size are summarized in Tables 4 and 5. Up to 12-in. dia. it seems the influence of specimen size on the mechanical properties is small. There is not enough data on the larger samples to draw definite conclusions. The largest scale effect was found in the Cedar City tonalite at mean stress levels below 5 ksi. Both the model and the experimental data indicated low bulk modulus and elastic modulus in this

range, although these parameters increase rapidly with mean stress.

The influence of specimen size on strength is pronounced on both rock types. The 32-in. Charcoal Black granite specimens failed at stress levels about one half those of the 2-in. specimens. The mode of failure also was markedly different. The 2-in. specimens failed catastrophically, while the 32-in. specimens failed initially by a series of small slips.

With the accumulation of more test data it may become possible to develop a model which more clearly predicts the behavior of the large rock cores. It may also become meaningful to verify statistical hypotheses.

It should be noted that with the larger cores, the rock depicted a load carrying capacity even after failure had initiated. This is often observed in the field. Besides, the mechanism of failure was different in these larger cores. This is significant in that at about 30-in. dia. or larger perhaps the type of rock failure obtained appears to be similar to that observed in the field. Perhaps models developed for this size can predict results closer to field observations.

Table 4

CHARCOAL BLACK GRANITE

Diameter	Test	σ_3	n	A_1 x10^6	A_2 x10^6
2	12	5	1.61	0.208	0.206
	14	10	1.52	0.113	0.137
	34	15	1.63	.194	
4	9	5	1.86	1.24	1.11
	11	10	1.90	1.25	1.75
	19	15	1.61	0.216	0.223
12	16	5	1.98	1.19	2.01
	37	5	2.03	.0298	
	21	5	reloaded	specimen	test 20
	20	10	1.78	0.381	0.692
32	27	5	1.53	0.244	
	28	5	1.85	1.90	
	29	10	4.05		
	30	10	1.80	1.68	
	31	$\bar{\varepsilon}_3$			

Table 5

CEDAR CITY TONALITE

Diameter	Test	σ_3	n	$A_1 \times 10^5$	$A_2 \times 10^5$
2	24	5	1.28	0.565	
	25	5	1.64	5.06	6.85
	26	10	1.60	3.81	4.59
	33	15	1.43	1.95	
4	35	5	1.27	.855	
	36	5	1.23	.756	
	18	10	1.35	1.03	
	22	15	1.64	4.8	6.23
	23	15	1.35	1.42	
12	17	5	1.32	0.762	1.25
	38	10	2.08	13.0	
24	32	$\bar{\varepsilon}_3$			

REFERENCES

1. Rapid Excavation, National Academy of Sciences, Wash. D.C., Publ. 1690, 1968, 48p.

2. Proc. Advisory Conference on Tunneling, Rept. on Tunneling, 1960-1980, Organization for Economic Cooperation and Development, Washington, D.C. June 22-26, 1970, 26p, Appendices and Comments.

3. Standard Method of Test for Triaxial Compressive Strength of Undrained Rock Core Specimens Without Pore Pressure Measurements, ASTM Test Designation D2664-67.

4. Standard Method of Test for Direct Tensile Strength of Rock Core Specimens, ASTM Test Designation D2936-71.

5. Standard Method of Test for Unconfined Compressive Strength of Rock Core Specimens, ASTM Designation D2938-71.

6. Standard Method of Test for Deformation Moduli of Rock Core Specimens in Compression, ASTM Test (In Preparation).

7. Rice, G. S. and Enzian, C., Tests of Strength of Roof Supports Used in Anthracite Mines of Pennsylvania, U. S. Bureau of Mines Bull. n303, 1929, 44p.

8. Greenwald, H. P., Howath, H. C., and Hartmann, Experiments on the Strength of Small Pillars of Coal in the Pittsburgh Bed, U. S. Bureau of Mines Tech. Paper n605, 1939, 22p.

9. Burton, L. D. and Phillips, J. W., Communication to Evans and Pomeroy (11).

10. Millard, D. J., Newman, P. C. and Phillips, J. W., The Apparent Strength of Extensively Cracked Materials, Proc. Phys. Soc. (London), v68, ser B, 1955, p. 723-728.

11. Evans, I. and Pomeroy, C. D., The Strength of Cubes of Coal in Uniaxial Compression, Mechanical Properties of Non-Metallic Brittle Materials, ed. W. H. Walton,

Interscience Publishers, New York, N.Y., 1958, p. 5-28.

12. Holland, C. T., The Strength of Coal in Mine Pillars, Proc. Sixth Symp. on Rock Mech., U. of Missouri at Rolla, Rolla, Mo., 1964, p. 450-466.

13. Weibull, W., A Statistical Theory of Strength of Materials, Ingretensk Akad. Handl., n151, 1939, p. 5-45.

14. Protodyakonov, M. M., Methods for Evaluating of Cracks and Strength of Rocks in Depth, Fourth Intl. Conf. Rock Mech. and Strata Control, Columbia U., New York, N.Y., 1964, Addendum.

15. Grobbelaar, C., A Theory for the Strength of Pillars, Pillarco, Pretoria, S. Africa, June 1970, 103p.

16. Epstein, B., Statistical Aspects of Fracture Problems, Jour. Appl. Phys. v 19, n2, Feb. 1948, p. 140-147.

17. Bieniawski, Z. T., Mechanism of Brittle Fracture of Rock, D.Sc (Eng.) Thesis, U. of Pretoria, S. Africa, 1968.

18. Glucklich, J., Cohen, L. J., Size as a Factor in the Brittle-Ductile Transition of Some Materials, Int. Jour. of Fract. Mech. v 3, n4, Dec. 1967, p. 278-289.

19. Glucklich, J., Cohen, L. J., Strain-Energy and Size Effects in a Brittle Material, ASTM Materials Research and Standards, v 8, n10, Oct. 1968, p. 17-22.

20. Baecher, G. B., The Size Effect in Brittle Fracture, M. S. Thesis, Mass. Inst. Tech. June 1970, 190p.

21. Swanson, S. R., Development of Constitutive Equations for Rocks, Ph.D. Thesis, Univ. of Utah, Dec. 1969, 140p.

22. Adams, F. D. and Nicholson, J. T., An Experimental Investigation into the Flow of Marble, Phil. Trans. Roy. Soc. (London), Ser. A, v 196, 1901, p. 363-401.

23. von Karman, T., Festigkeitversuche unter Allseitigem Druck, Zeitschr. des Vereins deut. Ing., v 60, 1911, p. 1749-1757.

24. Griggs, D. T., Deformation of Rocks Under High Confining Pressures, J. Geol., v. 44, 1936, p. 541-577.

25. Griggs, D. T., and Miller, W. B., Deformation of Yule Marble: Part I--Compression and Extension Experiments on Dry Yule Marble at 10,000 Atmospheres Confining Pressure, Room Temperature, Geol. Soc. Am. Bul., v. 62, 1951 p. 853-862.

26. Handin, J. W. and Griggs, D., Deformation of Yule Marble: Part II--Predicted Fabric Changes, Geol. Soc. Am. v. 62, 1951, p. 863-886.

27. Griggs, D. and Handin, J., Rock Deformation, Geol. Soc. Am., Mem. 79, March 1, 1970, 382p.

28. Baidyuk, B. V., Mechanical Properties of Rocks at High Temperatures and Pressures, Consultants Bureau, Plenum Pub. Corp. New York, 1967.

29. Morgenstern, N. R. and Tamuly Phukan, A. L., Non-linear Stress-Strain Relations for a Homogeneous Sandstone, Intl. Jour. Rock Mech. Mng. Sci., v. 6, 1969, p. 127-142.

30. LaMori, P. N., Static Determination of the Equation of State of Cedar City Tonalite, DASA Rept. No. 01-69-C 0053, May 1970, 78p.

31. McClintock, F. A., Walsh, J. B., Friction on Griffith Cracks in Rock under Pressure, Proc. 4th Nat. Cong. Appl. Mech., Berkeley, 1962, p. 1015-1022.

32. Brace, W. F., Brittle Fracture of Rocks, Proc. Intl. Conf. on State of Stress in the Earth's Crust, American Elsevier Publ. Co., New York, 1964, p. 111-174.

33. Murrell, S. A. F., The Effect of Triaxial Stress Systems on the Strength of Rocks at Atmospheric Temperatures, Geophys. Jour., v. 10, 1965, p. 231-282.

34. Pfefferle, W. and Smith, C. R., Phase I Flatjack Tests, Air Force Rept. No.: SAMSO-TR-70-381, Oct. 6, 1970, 42p.

35. Obert, L., Personal communication.

36. Hoek, E., Brittle Failure of Rock, Chapter 4 in Rock Mechanics in Engineering Practice (ed. Stagg and Zienkiewicz), J. Wiley, London, 1968, p. 99-124.

37. Wawersik, W. R., Detailed Analysis of Rock Failure in Laboratory Compression Tests, Ph.D. Thesis, University of Minnesota, 1968.

38. Cook, N. G. W., The Failure of Rock, Int. Jour. Rock Mech. Mng. Sci., v. 2, 1965, p. 389-403.

39. Houpert, R., La résistance à la rupture des granites, Revue de l'industrie minérale, May 15, 1968, p. 21-23.

40. Paulding, B. W. Jr., Techniques Used in Studying the Fracture Mechanics of Rock, Testing Techniques for Rock Mechanics, ASTM STP 402, Am. Soc. Testing Mats., 1966, p. 73-86.

41. Clark, G. B., Deformation Moduli of Rocks, Testing Techniques for Rock Mechanics, ASTM STP 402, Am. Soc. Testing Mats., 1966, p. 133-174.

42. Ko, Hon-Yinn, and Scott, R. F., Deformation of Sand in Hydrostatic Compression, Journal of the Soil Mechanics and Foundation Division, ASCE, vol. 93, No. SM3, May, 1967.

43. Timoshenko, F., and Goodier, J. N., Theory of Elasticity, McGraw-Hill Book Co., New York, 1951.

44. Seaman, L., and Whitman, R. V., Stress Propagation in Soils, Final Report-Part IV, Stanford Research Institute, Menlo Park, California, for Defense Atomic Support Agency, DASA 1266-4, June 1964.

45. Birch, F., and Bancroft, D., The Effect of Pressure on the Rigidity of Rocks. Jour. Geol. v 46, n1, Jan-Feb 1938, p. 59-87; n2, Feb-Mar 1938, p. 113-141.

APPENDIX A - COMPUTER PLOTS OF TEST DATA

Data was reduced and plotted using the Univac 1108 at IITRI. This appendix includes the three most significant plots for each test, these being:

shear strain vs. deviator stress
volumetric strain vs. mean stress
axial and lateral strains vs. axial stress.

In several cases, e.g. test 19 σ_m vs. ε_v, the data went off-scale during the plotting subroutines. When this occurred, the data was plotted at an arbitrary value with in the plot scale.

The plots are arranged in order of rock type, core diameter, confining stress and test number.

Rock Type	Diameter	Confining Stress	Test	Page
CBG	2	5	12	A-3
		10	14	A-6
		15	34	A-9
	4	5	9	A-12
		10	11	A-15
		15	19	A-18
	12	5	16	A-21
		5	21	A-24
		5	37	A-28
		10	20	A-31
	32	5	27	A-34
		5	28	A-37
		10	29	A-40
		10	30	A-43
		uniaxial strain	31	A-46

Rock Type	Diameter	Confining Stress	Test	Page
CCT	2	5	24	A-49
		5	25	A-52
		10	26	A-55
		15	33	A-58
	4	5	35	A-60
		5	36	A-63
		10	18	A-66
		15	22	A-69
		15	23	A-72
	12	5	17	A-75
		10	38	A-78
	24	uniaxial strain	32	A-81

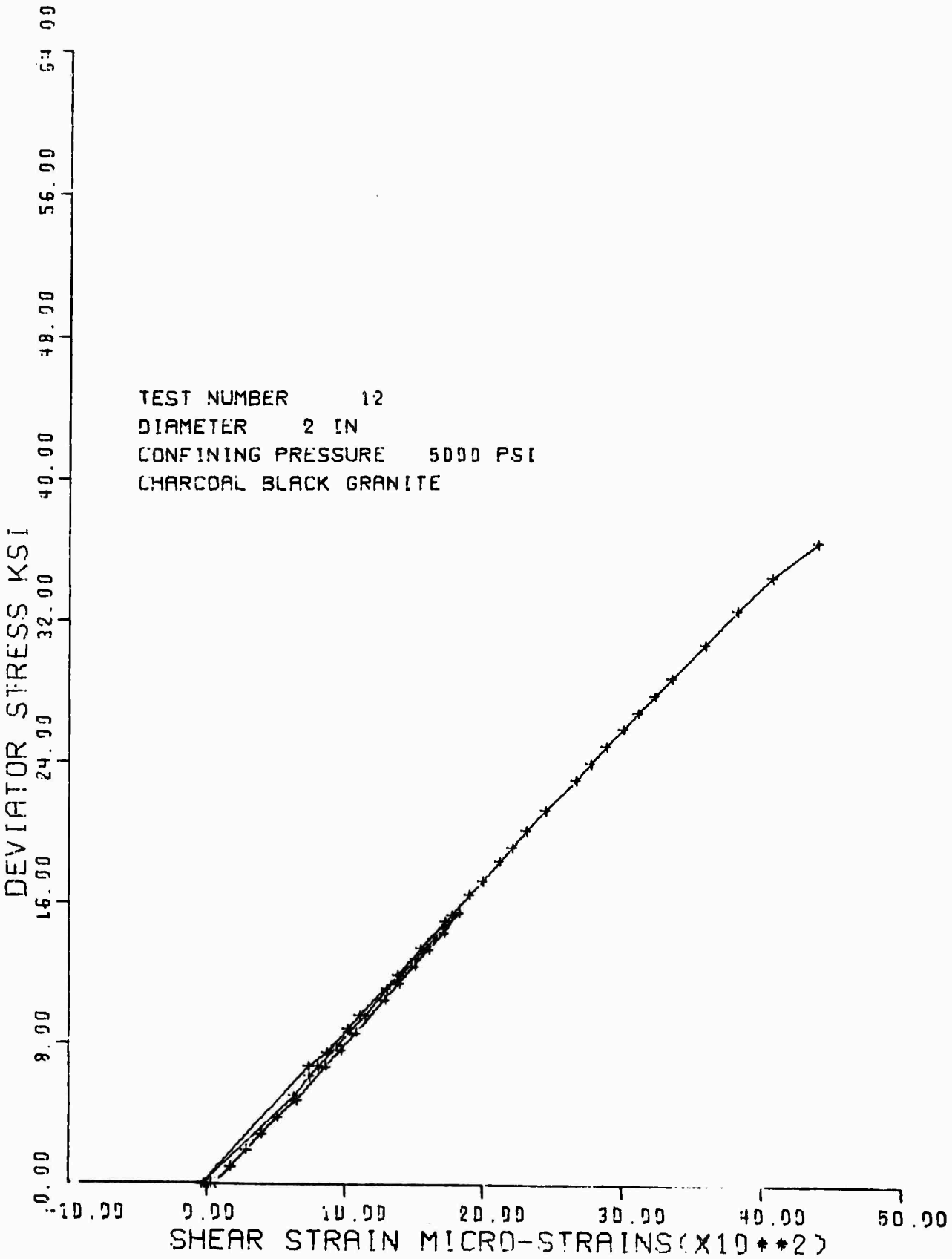
TEST NUMBER 12
DIAMETER 2 IN
CONFINING PRESSURE 5000 PSI
CHARCOAL BLACK GRANITE
DEVIATOR STRESS KSI
0.00
8.00
16.00
24.00
32.00
40.00
48.00
56.00
64.00
-10.00
0.00
10.00
20.00
30.00
40.00
50.00
SHEAR STRAIN MICRO-STRAINS(X10**2)

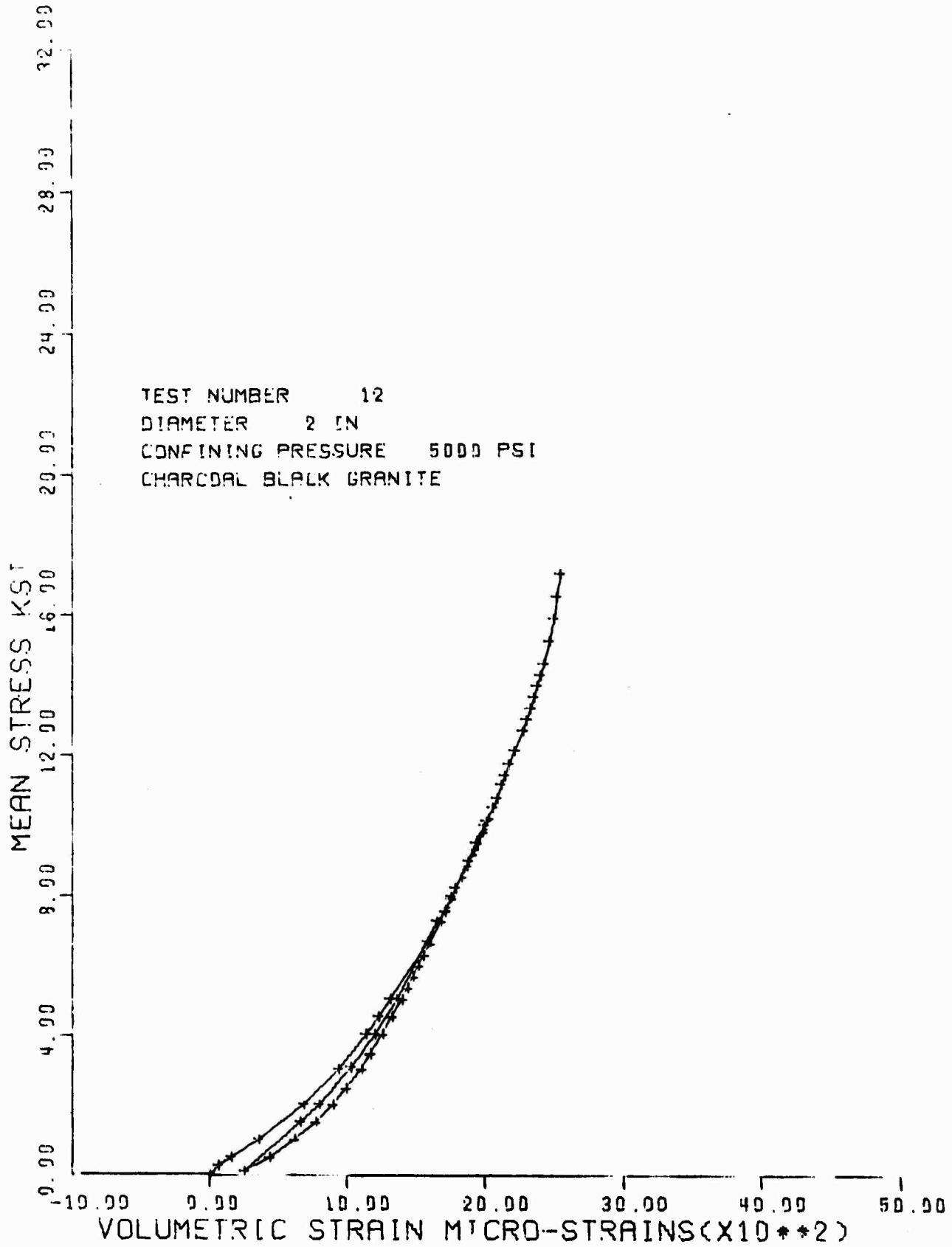
TEST NUMBER 12
DIAMETER 2 IN
CONFINING PRESSURE 5000 PSI
CHARCOAL BLACK GRANITE
MEAN STRESS KSI
0.00
4.00
8.00
12.00
16.00
20.00
24.00
28.00
32.00
-10.00
0.00
10.00
20.00
30.00
40.00
50.00
VOLUMETRIC STRAIN MICRO-STRAINS(X10**2)

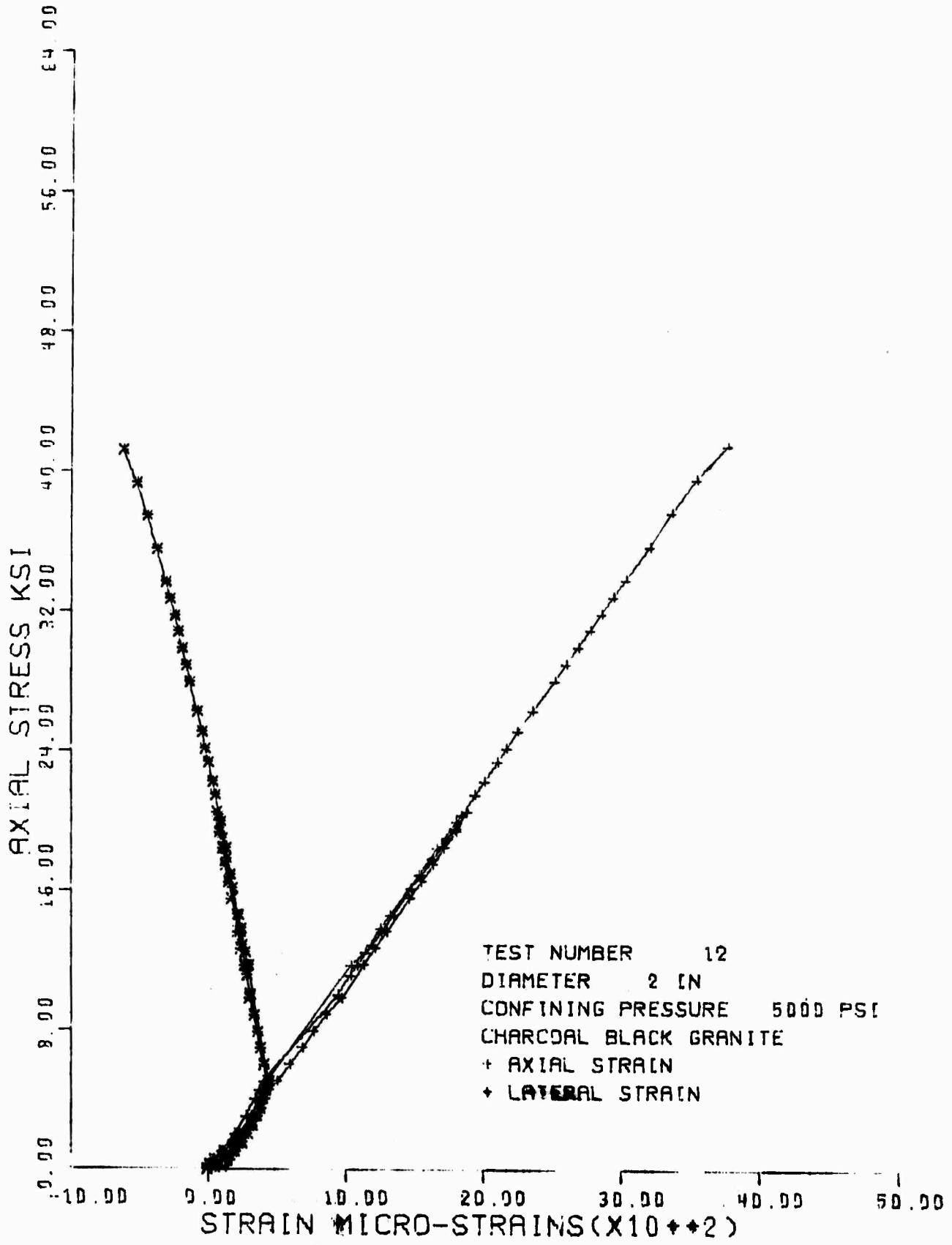
AXIAL STRESS KSI
0.00
8.00
16.00
24.00
32.00
40.00
48.00
56.00
64.00
-10.00
0.00
10.00
20.00
30.00
40.00
50.00
STRAIN MICRO-STRAINS(X10**2)
TEST NUMBER 12
DIAMETER 2 IN
CONFINING PRESSURE 5000 PSI
CHARCOAL BLACK GRANITE
+ AXIAL STRAIN
+ LATERAL STRAIN

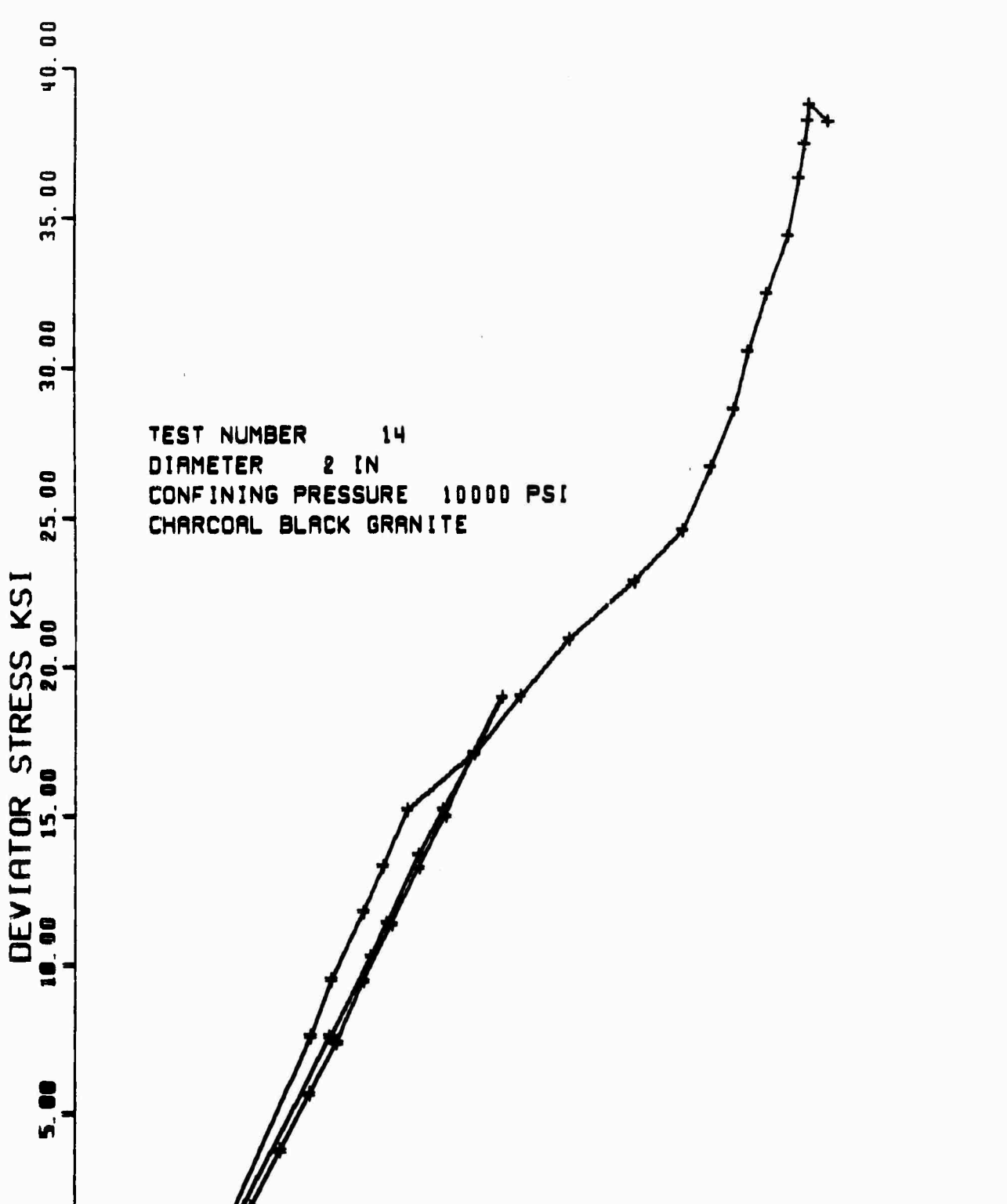
TEST NUMBER 14
DIAMETER 2 IN
CONFINING PRESSURE 10000 PSI
CHARCOAL BLACK GRANITE
DEVIATOR STRESS KSI
0.00
5.00
10.00
15.00
20.00
25.00
30.00
35.00
40.00
-10.00
0.00
10.00
20.00
30.00
40.00
50.00
SHEAR STRAIN MICRO-STRAINS(X10**2)

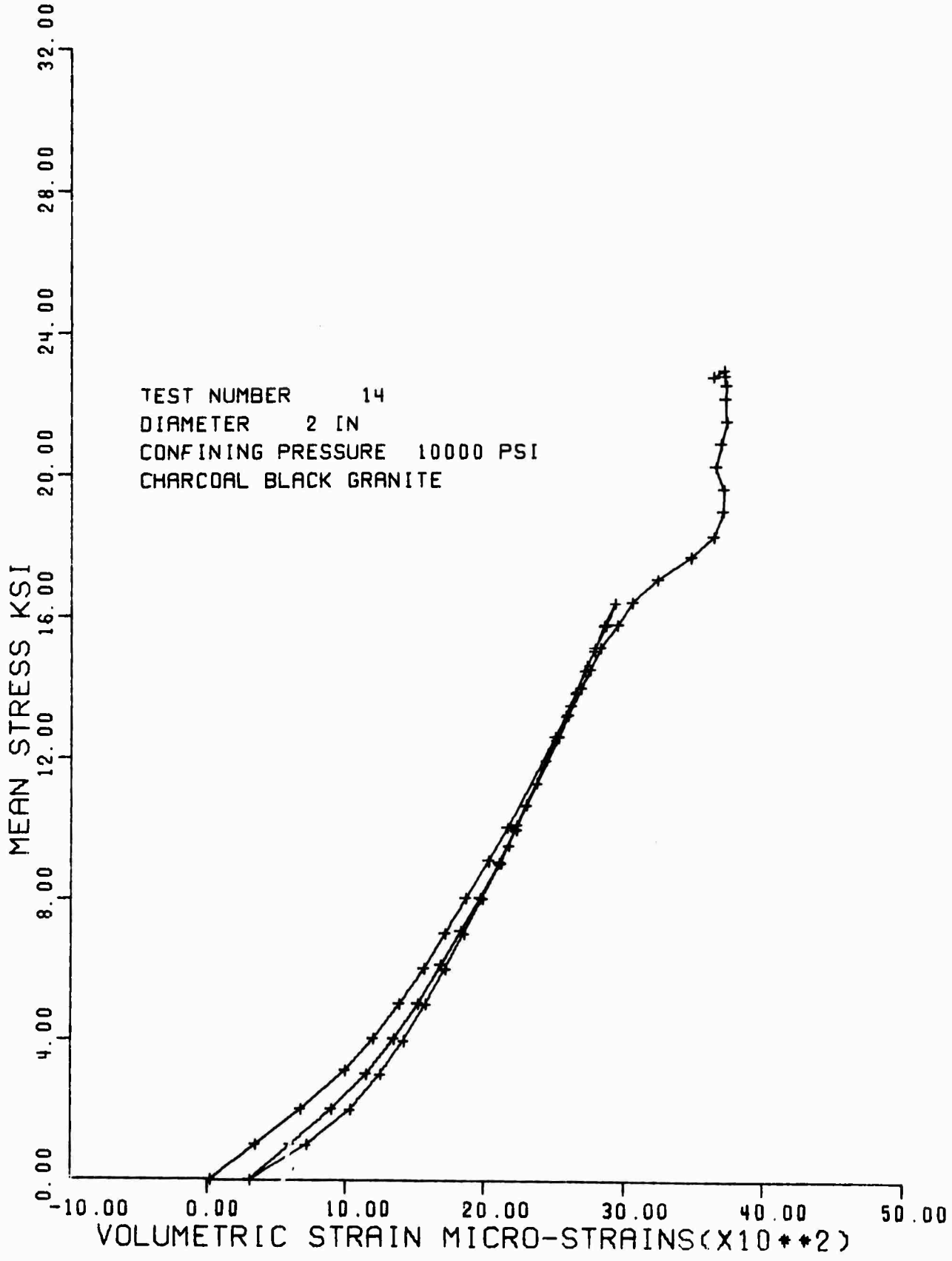
TEST NUMBER 14
DIAMETER 2 IN
CONFINING PRESSURE 10000 PSI
CHARCOAL BLACK GRANITE
MEAN STRESS KSI
0.00
4.00
8.00
12.00
16.00
20.00
24.00
28.00
32.00
-10.00
0.00
10.00
20.00
30.00
40.00
50.00
VOLUMETRIC STRAIN MICRO-STRAINS(X10**2)

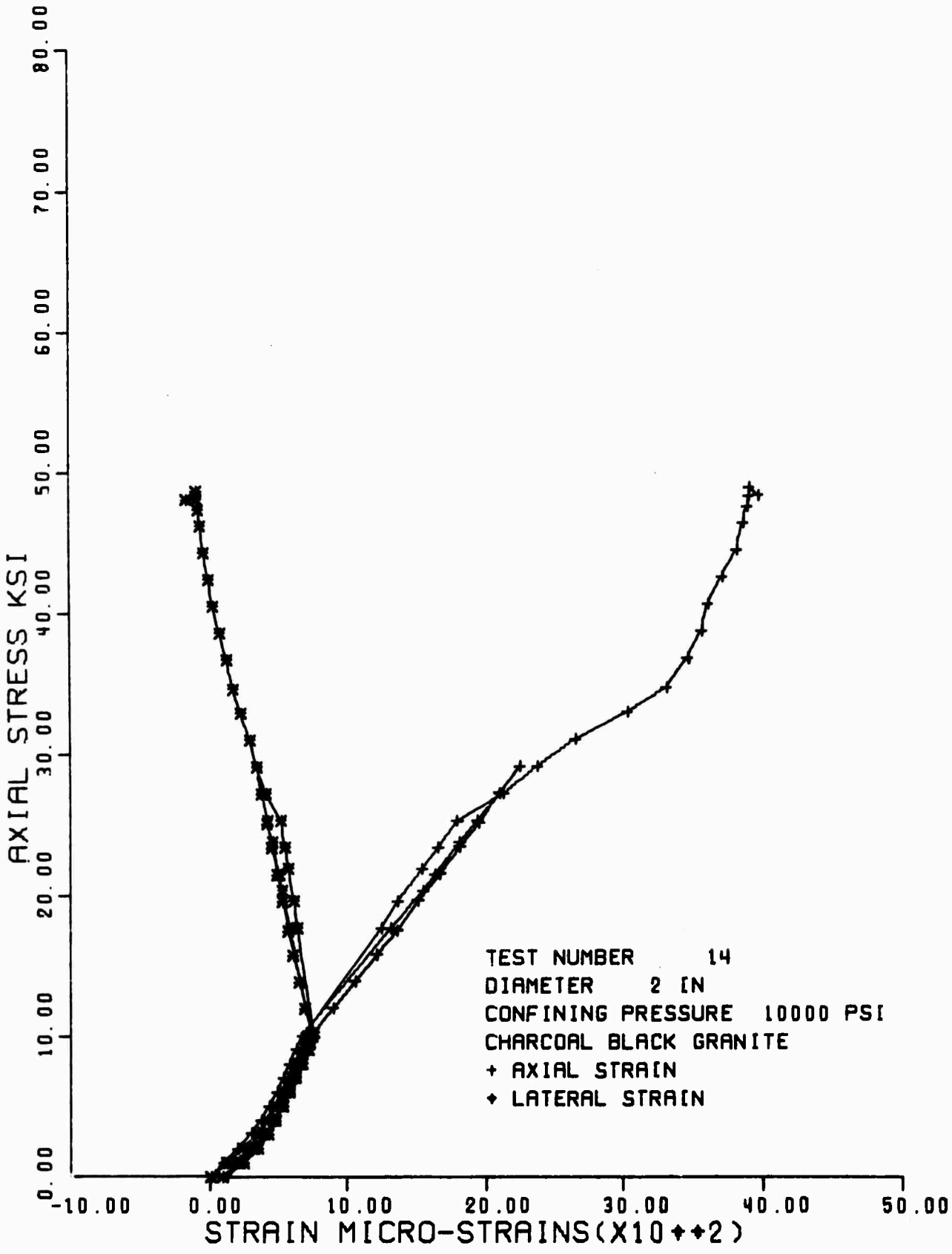
AXIAL STRESS KSI
0.00
10.00
20.00
30.00
40.00
50.00
60.00
70.00
80.00
-10.00
0.00
10.00
20.00
30.00
40.00
50.00
STRAIN MICRO-STRAINS(X10**2)
TEST NUMBER 14
DIAMETER 2 IN
CONFINING PRESSURE 10000 PSI
CHARCOAL BLACK GRANITE
+ AXIAL STRAIN
* LATERAL STRAIN

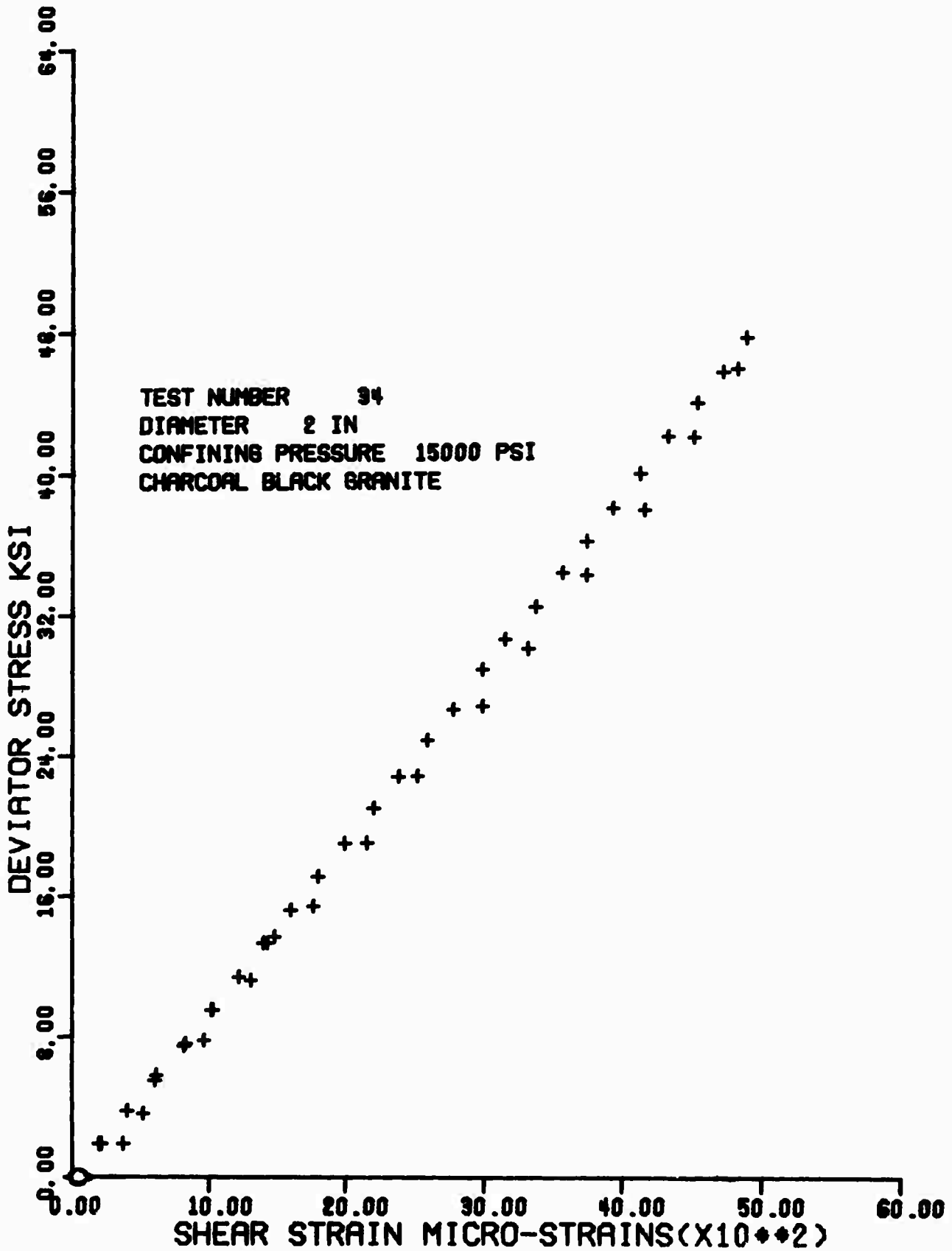
TEST NUMBER 34
DIAMETER 2 IN
CONFINING PRESSURE 15000 PSI
CHARCOAL BLACK GRANITE
DEVIATOR STRESS KSI
0.00
8.00
16.00
24.00
32.00
40.00
48.00
56.00
64.00
0.00
10.00
20.00
30.00
40.00
50.00
60.00
SHEAR STRAIN MICRO-STRAINS(X10**2)

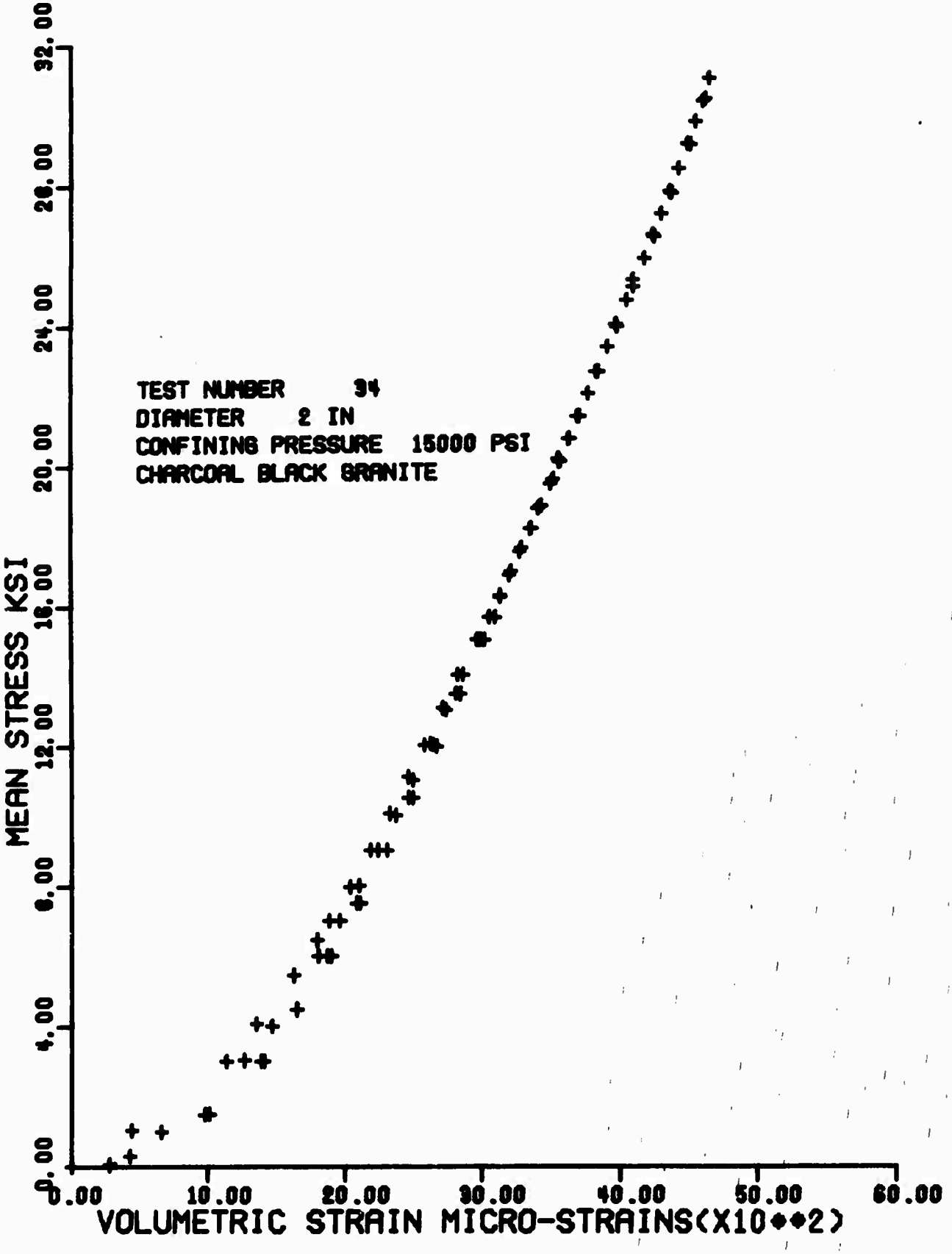
TEST NUMBER 94
DIAMETER 2 IN
CONFINING PRESSURE 15000 PSI
CHARCOAL BLACK GRANITE
MEAN STRESS KSI
0.00
4.00
8.00
12.00
16.00
20.00
24.00
28.00
32.00
0.00
10.00
20.00
30.00
40.00
50.00
60.00
VOLUMETRIC STRAIN MICRO-STRAINS(X10**2)

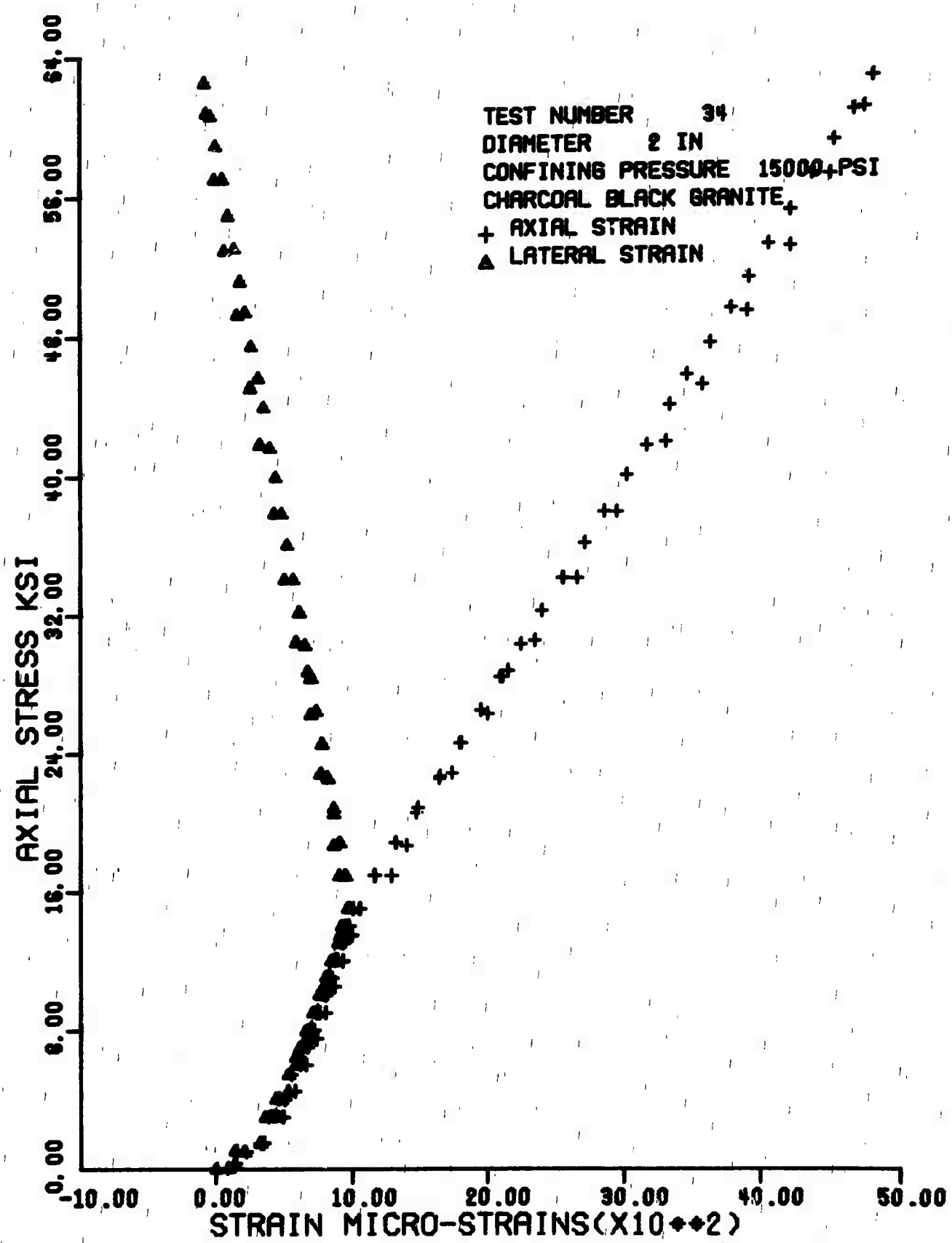
TEST NUMBER 34
DIAMETER 2 IN
CONFINING PRESSURE 15000 PSI
CHARCOAL BLACK GRANITE
+ AXIAL STRAIN
▲ LATERAL STRAIN
AXIAL STRESS KSI
0.00
8.00
16.00
24.00
32.00
40.00
48.00
56.00
64.00
-10.00
0.00
10.00
20.00
30.00
40.00
50.00
STRAIN MICRO-STRAINS(X10**2)

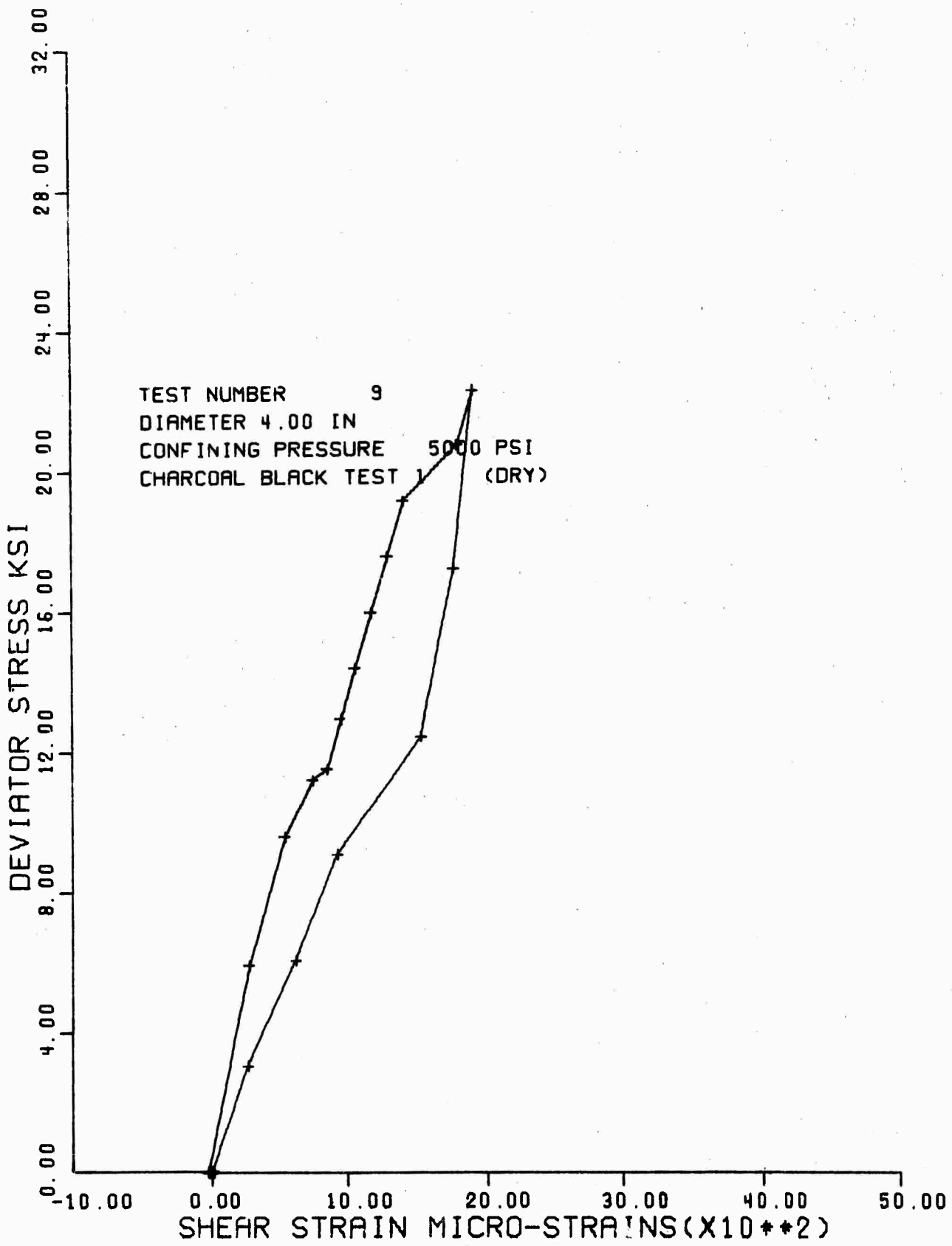
TEST NUMBER 9
DIAMETER 4.00 IN
CONFINING PRESSURE 5000 PSI
CHARCOAL BLACK TEST 1 (DRY)
DEVIATOR STRESS KSI
0.00
4.00
8.00
12.00
16.00
20.00
24.00
28.00
32.00
-10.00
0.00
10.00
20.00
30.00
40.00
50.00
SHEAR STRAIN MICRO-STRAINS(X10**2)

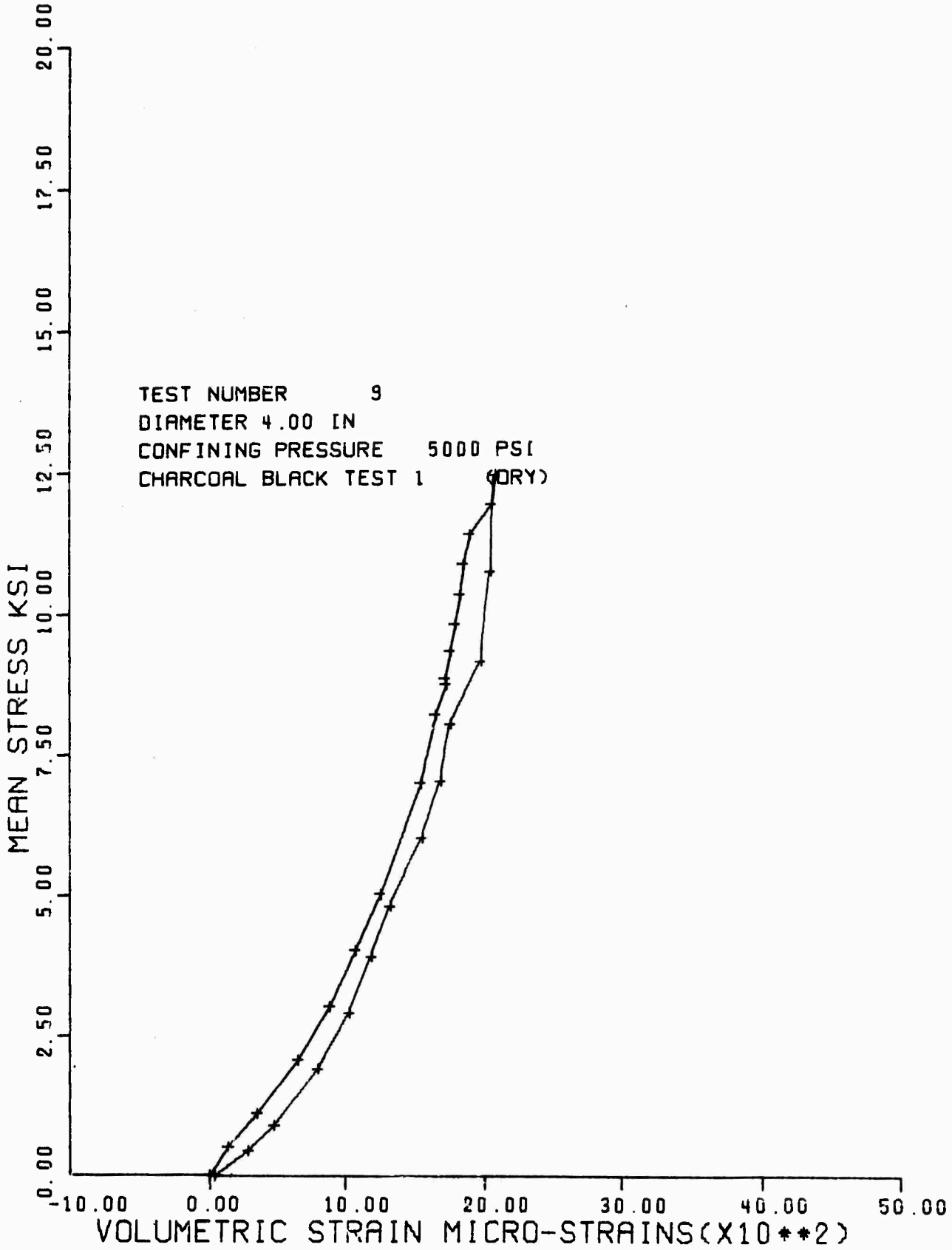
TEST NUMBER 9
DIAMETER 4.00 IN
CONFINING PRESSURE 5000 PSI
CHARCOAL BLACK TEST 1 (DRY)
MEAN STRESS KSI
0.00
2.50
5.00
7.50
10.00
12.50
15.00
17.50
20.00
-10.00
0.00
10.00
20.00
30.00
40.00
50.00
VOLUMETRIC STRAIN MICRO-STRAINS(X10**2)

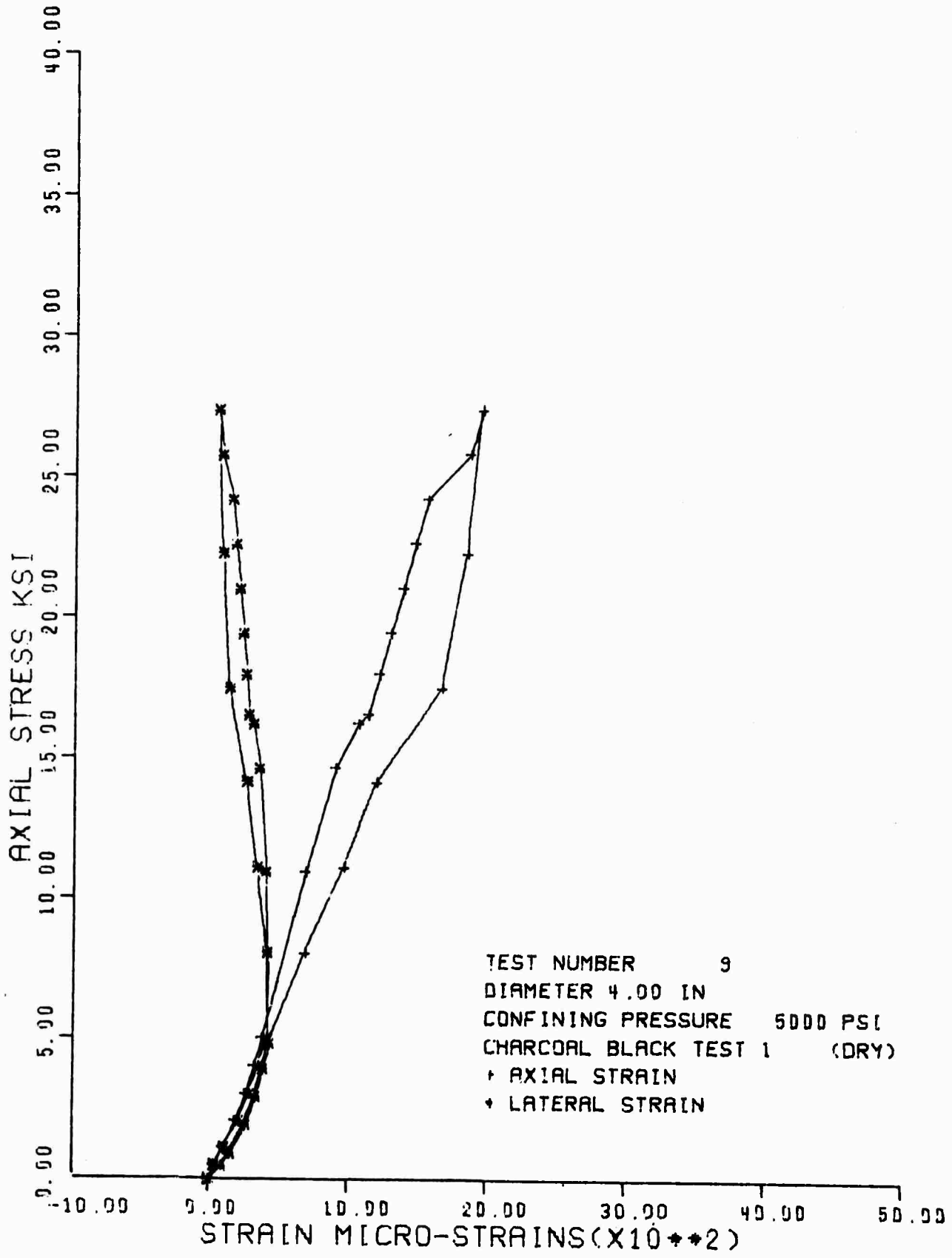
AXIAL STRESS KSI
0.00
5.00
10.00
15.00
20.00
25.00
30.00
35.00
40.00
-10.00
0.00
10.00
20.00
30.00
40.00
50.00
STRAIN MICRO-STRAINS(X10**2)
TEST NUMBER 9
DIAMETER 4.00 IN
CONFINING PRESSURE 5000 PSI
CHARCOAL BLACK TEST 1 (DRY)
+ AXIAL STRAIN
+ LATERAL STRAIN

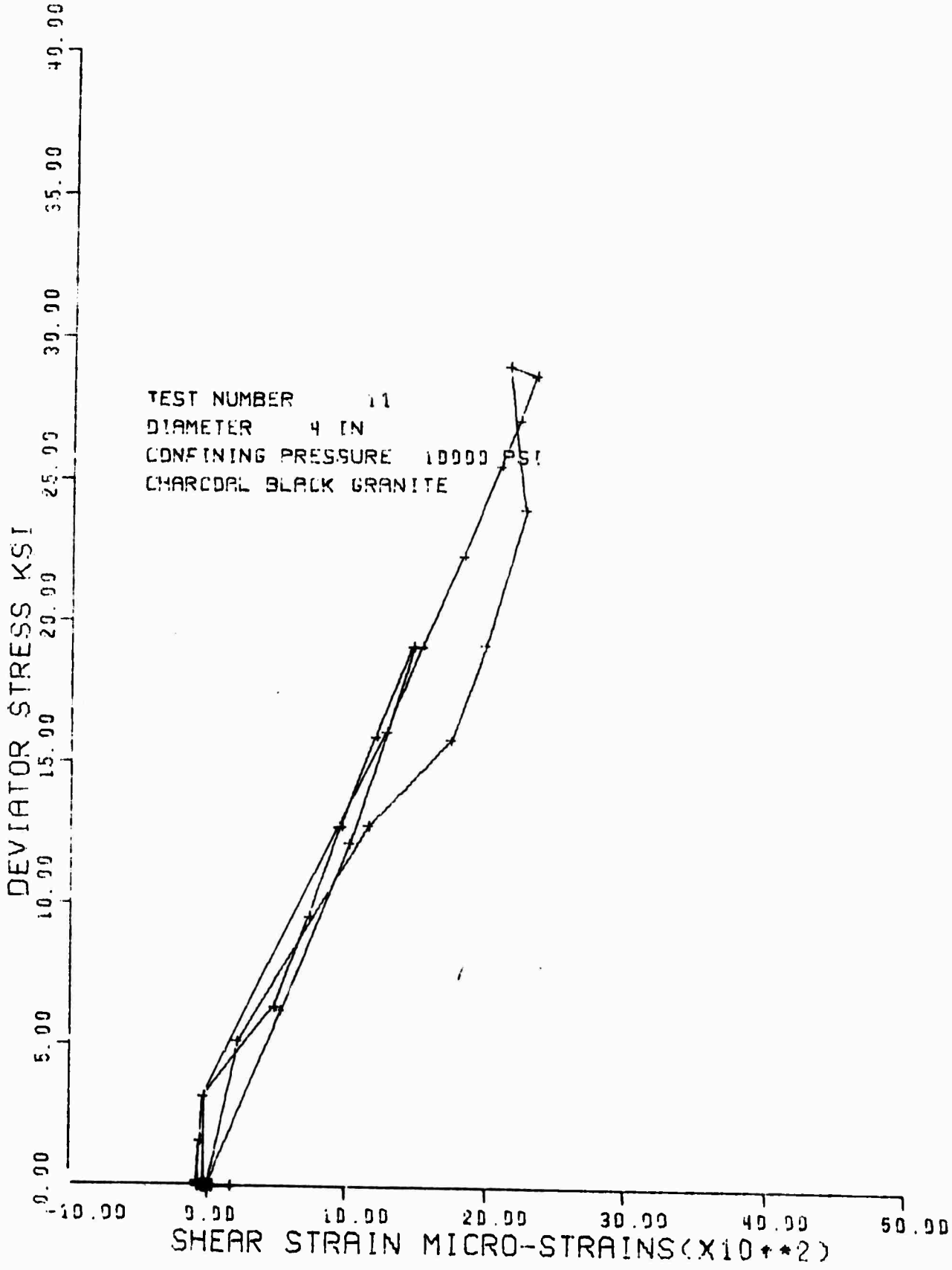
TEST NUMBER 11
DIAMETER 4 IN
CONFINING PRESSURE 10000 PSI
CHARCOAL BLACK GRANITE
DEVIATOR STRESS KSI
0.00
5.00
10.00
15.00
20.00
25.00
30.00
35.00
40.00
-10.00
0.00
10.00
20.00
30.00
40.00
50.00
SHEAR STRAIN MICRO-STRAINS(X10**2)

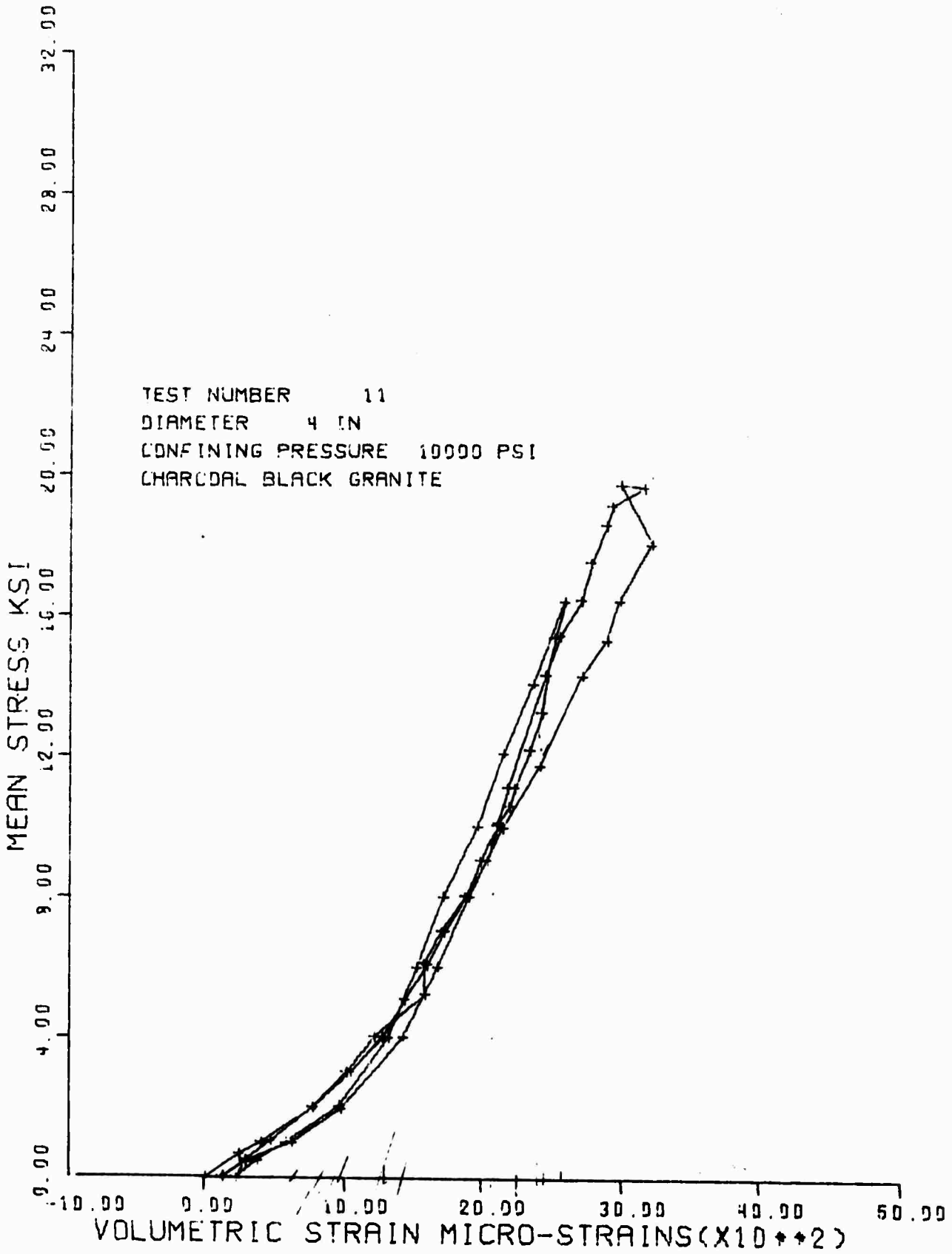
TEST NUMBER 11
DIAMETER 4 IN
CONFINING PRESSURE 10000 PSI
CHARCOAL BLACK GRANITE
MEAN STRESS KSI
0.00
4.00
8.00
12.00
16.00
20.00
24.00
28.00
32.00
-10.00
0.00
10.00
20.00
30.00
40.00
50.00
VOLUMETRIC STRAIN MICRO-STRAINS(X10**2)

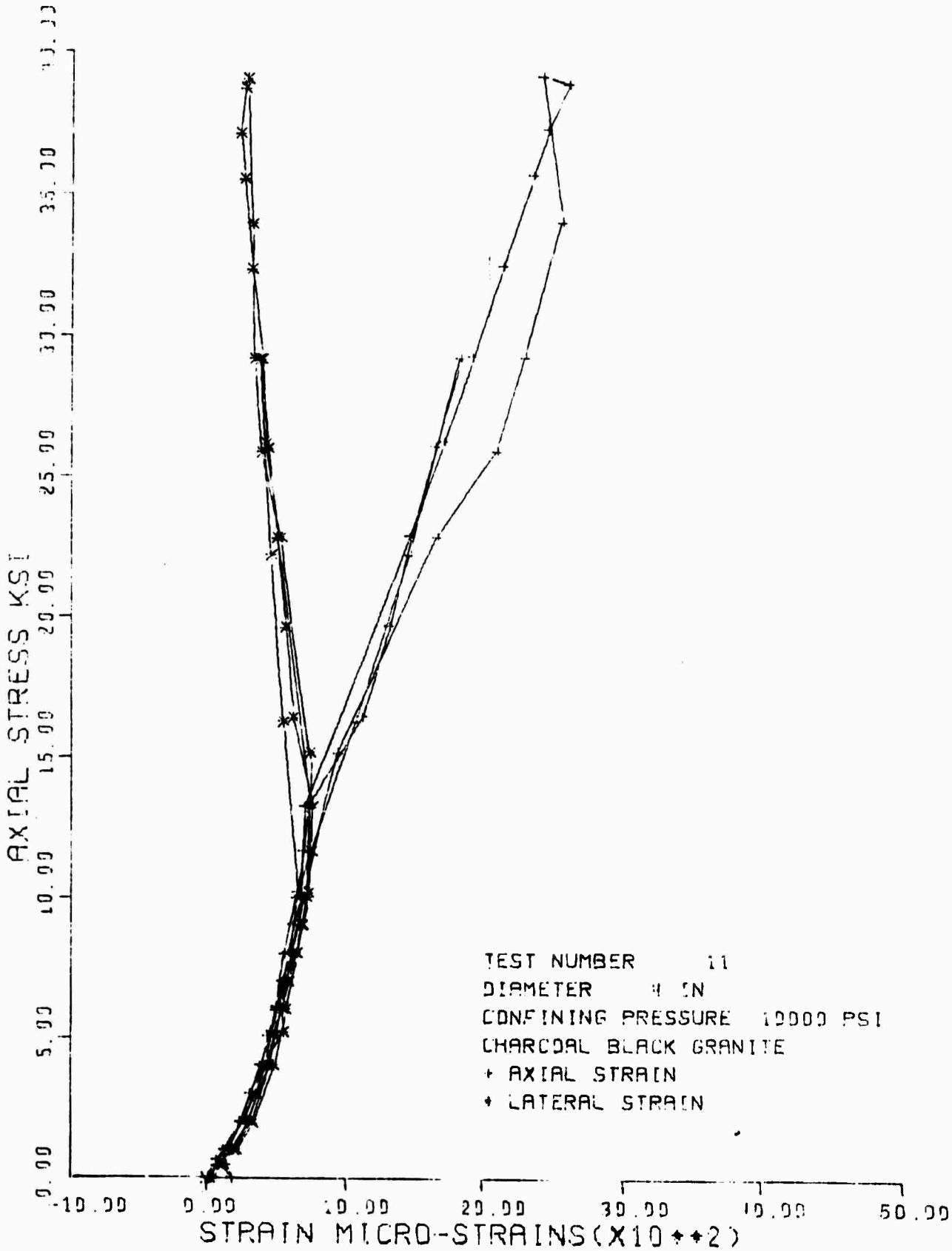
AXIAL STRESS KSI
0.00
5.00
10.00
15.00
20.00
25.00
30.00
35.00
-10.00
0.00
10.00
20.00
30.00
40.00
50.00
STRAIN MICRO-STRAINS(X10**2)
TEST NUMBER 11
DIAMETER 4 IN
CONFINING PRESSURE 10000 PSI
CHARCOAL BLACK GRANITE
+ AXIAL STRAIN
+ LATERAL STRAIN

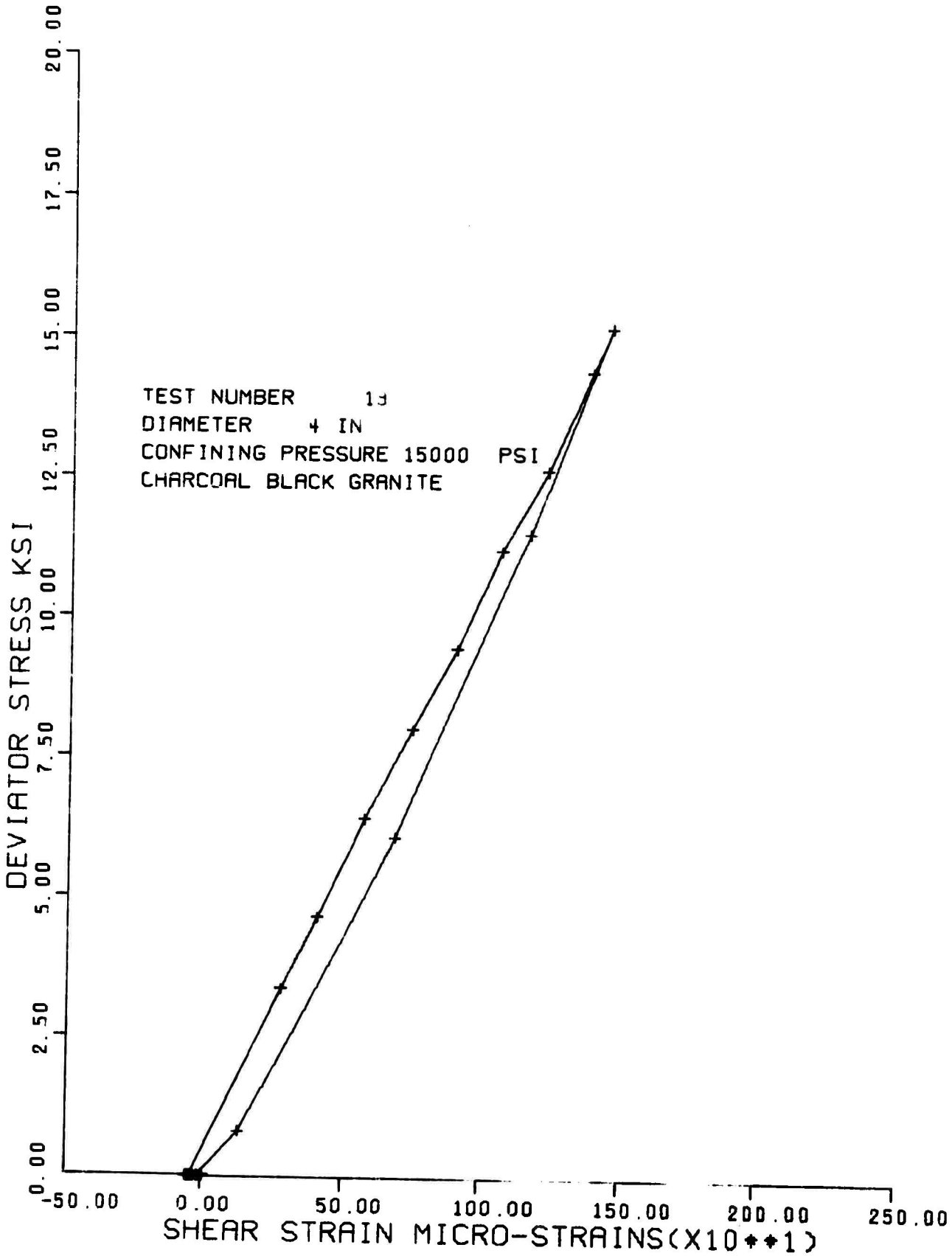
TEST NUMBER 13
DIAMETER 4 IN
CONFINING PRESSURE 15000 PSI
CHARCOAL BLACK GRANITE
DEVIATOR STRESS KSI
0.00
2.50
5.00
7.50
10.00
12.50
15.00
17.50
20.00
-50.00
0.00
50.00
100.00
150.00
200.00
250.00
SHEAR STRAIN MICRO-STRAINS(X10**1)

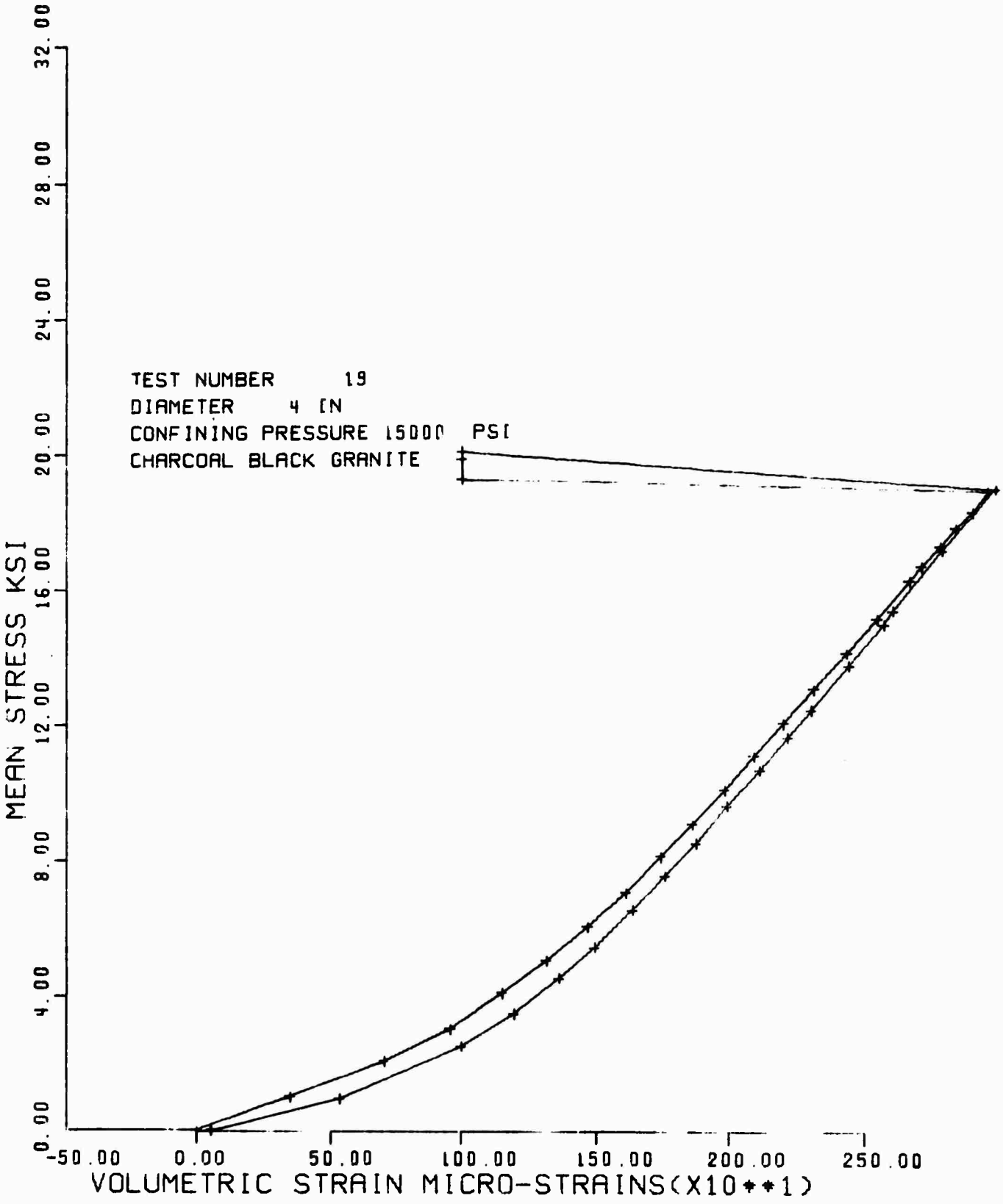
TEST NUMBER 19
DIAMETER 4 IN
CONFINING PRESSURE 15000 PSI
CHARCOAL BLACK GRANITE
MEAN STRESS KSI
0.00
4.00
8.00
12.00
16.00
20.00
24.00
28.00
32.00
-50.00
0.00
50.00
100.00
150.00
200.00
250.00
VOLUMETRIC STRAIN MICRO-STRAINS(X10**1)

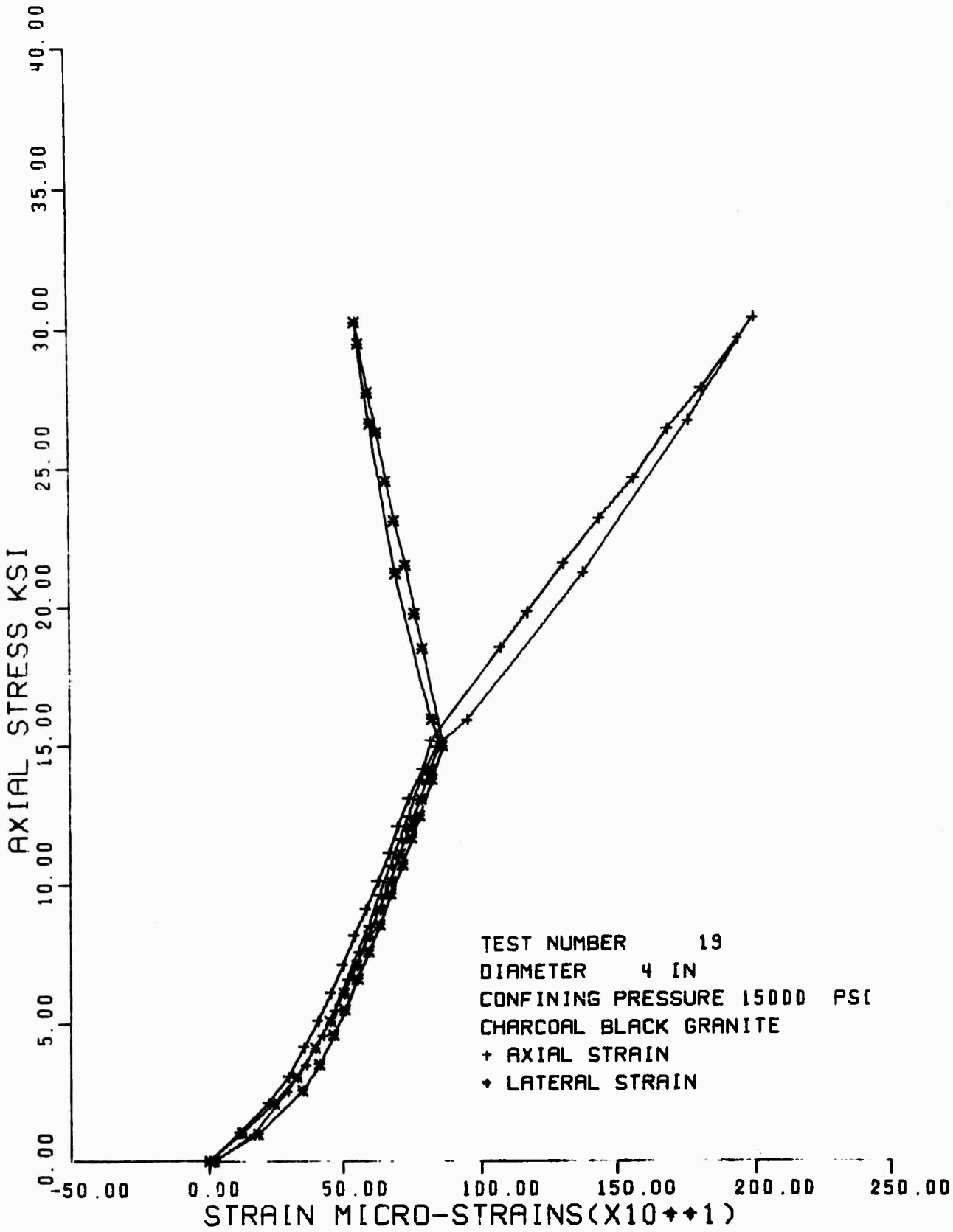
AXIAL STRESS KSI
0.00
5.00
10.00
15.00
20.00
25.00
30.00
35.00
40.00
-50.00
0.00
50.00
100.00
150.00
200.00
250.00
STRAIN MICRO-STRAINS(X10**1)
TEST NUMBER 19
DIAMETER 4 IN
CONFINING PRESSURE 15000 PSI
CHARCOAL BLACK GRANITE
+ AXIAL STRAIN
* LATERAL STRAIN

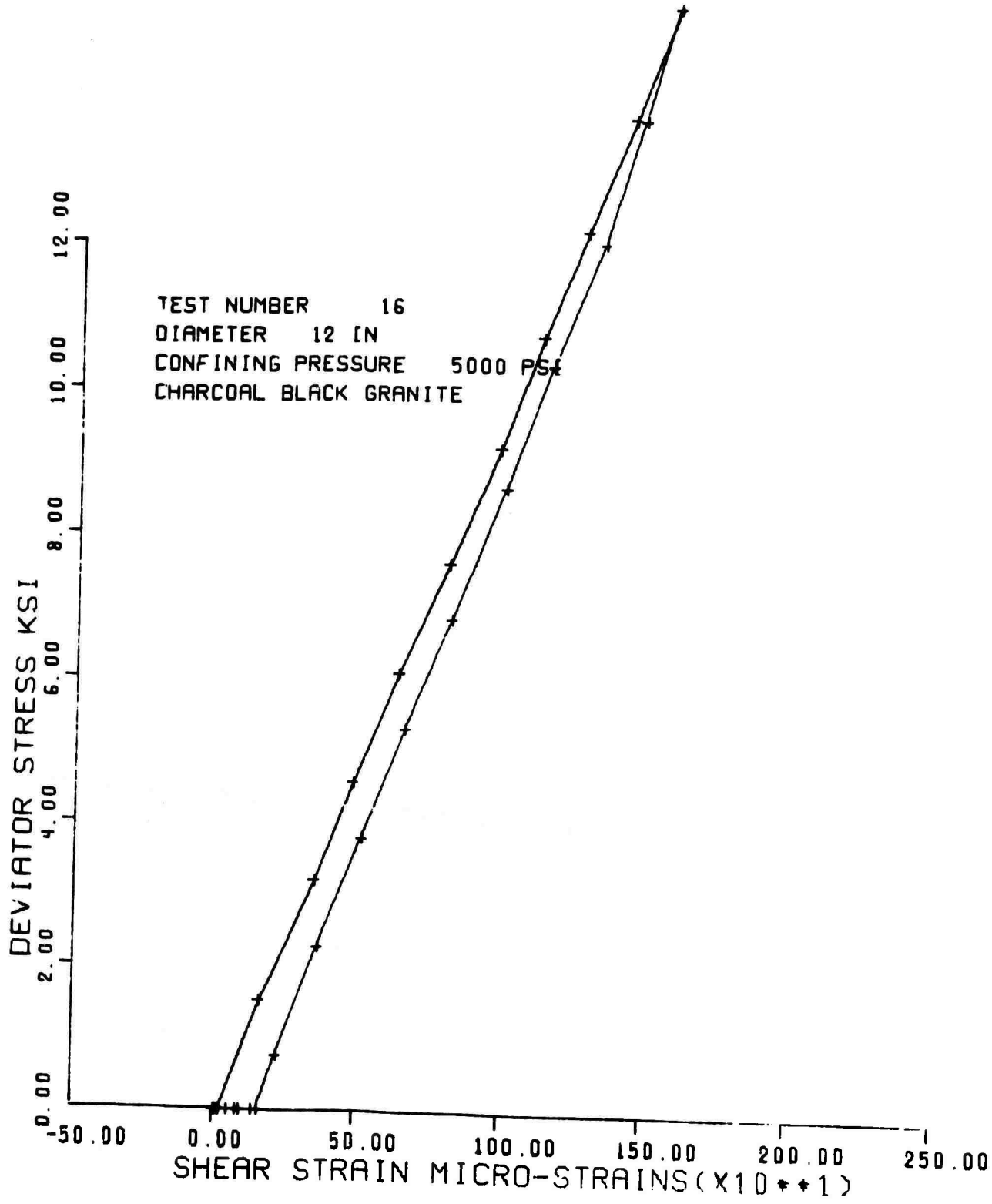
TEST NUMBER 16
DIAMETER 12 IN
CONFINING PRESSURE 5000 PSI
CHARCOAL BLACK GRANITE
DEVIATOR STRESS KSI
0.00
2.00
4.00
6.00
8.00
10.00
12.00
-50.00
0.00
50.00
100.00
150.00
200.00
250.00
SHEAR STRAIN MICRO-STRAINS(X10**1)

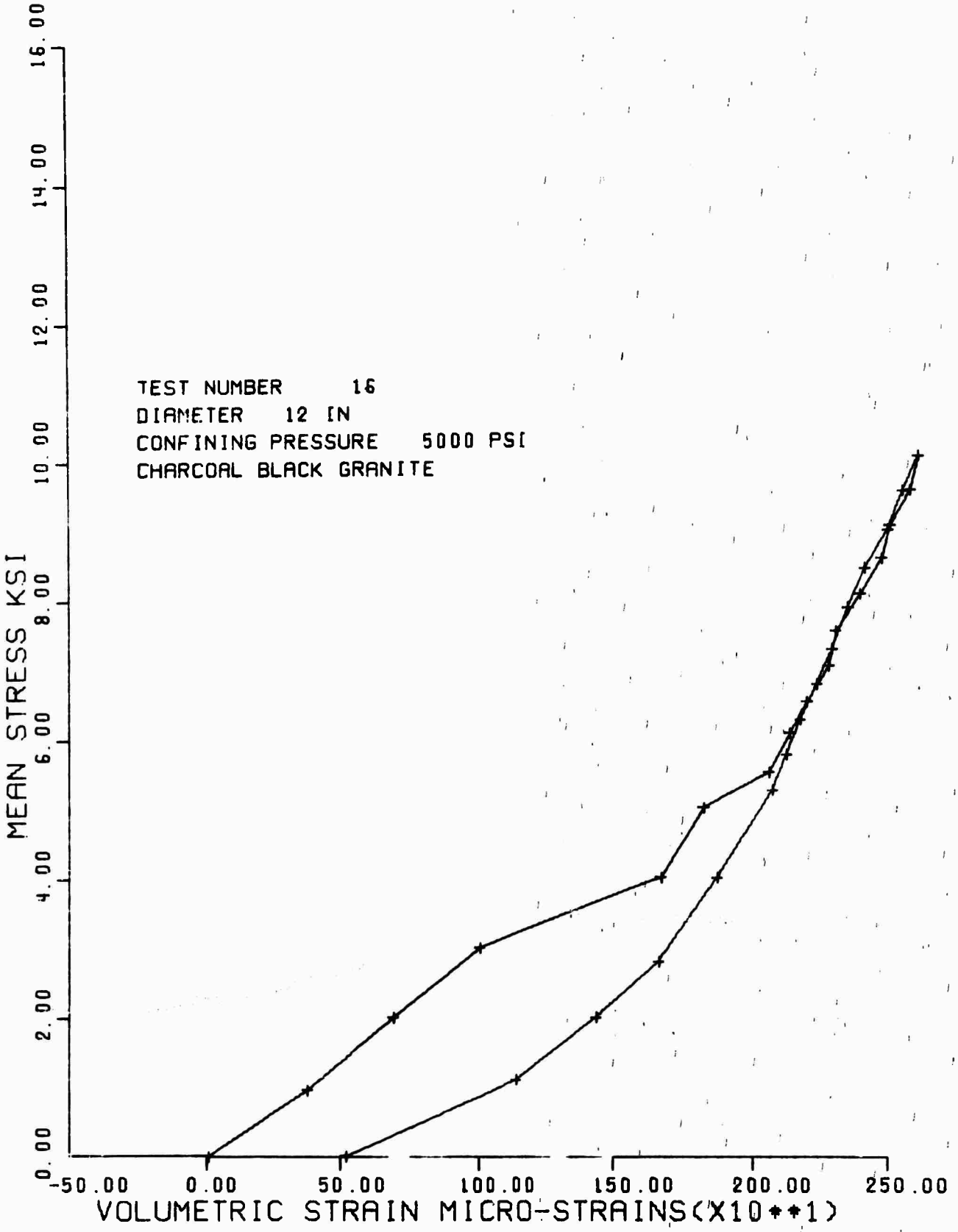
TEST NUMBER 16
DIAMETER 12 IN
CONFINING PRESSURE 5000 PSI
CHARCOAL BLACK GRANITE
MEAN STRESS KSI
0.00
2.00
4.00
6.00
8.00
10.00
12.00
14.00
16.00
-50.00
0.00
50.00
100.00
150.00
200.00
250.00
VOLUMETRIC STRAIN MICRO-STRAINS(X10**1)

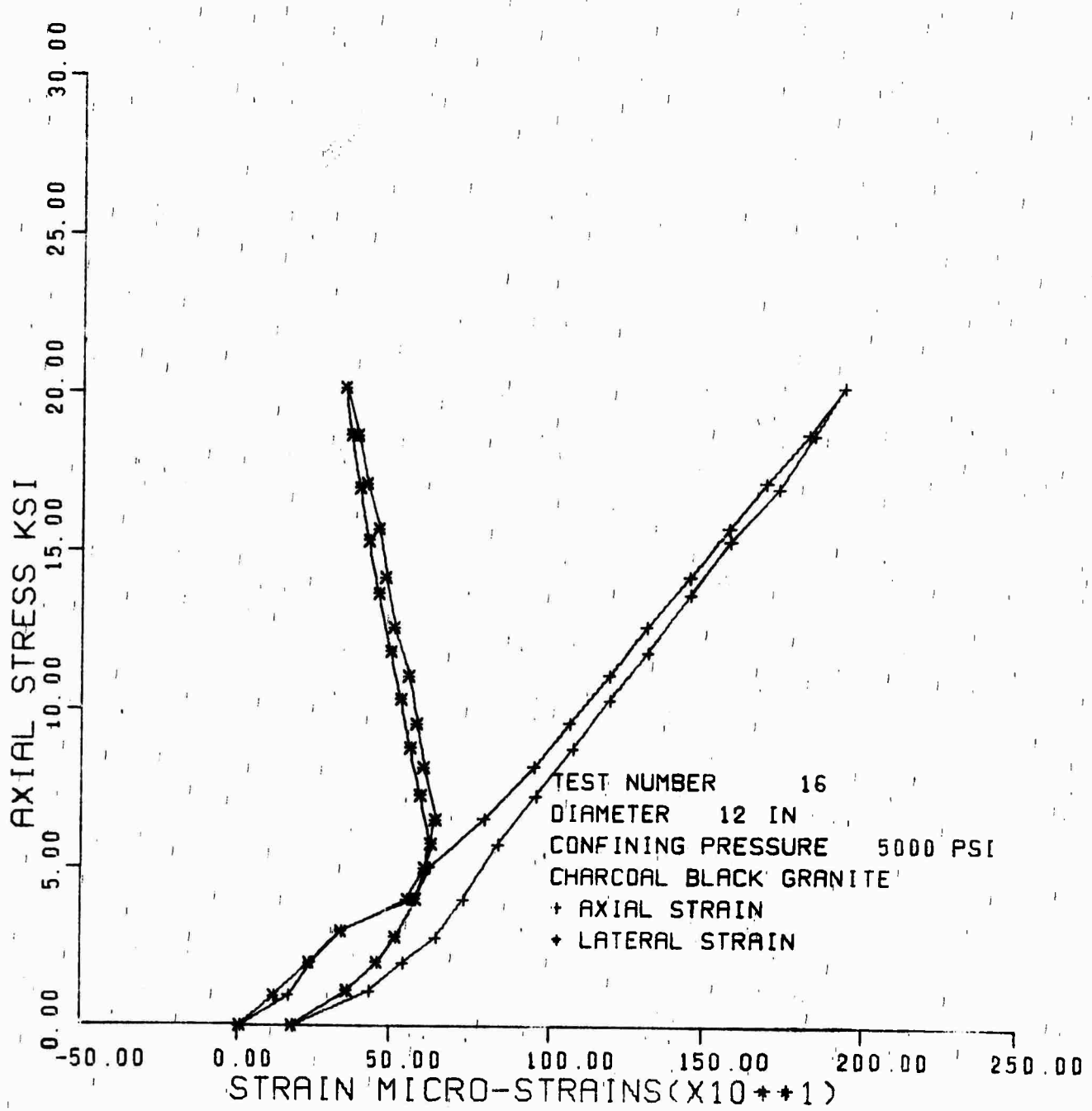
AXIAL STRESS KSI
0.00
5.00
10.00
15.00
20.00
25.00
30.00
-50.00
0.00
50.00
100.00
150.00
200.00
250.00
STRAIN MICRO-STRAINS(X10**1)
TEST NUMBER 16
DIAMETER 12 IN
CONFINING PRESSURE 5000 PSI
CHARCOAL BLACK GRANITE
+ AXIAL STRAIN
+ LATERAL STRAIN

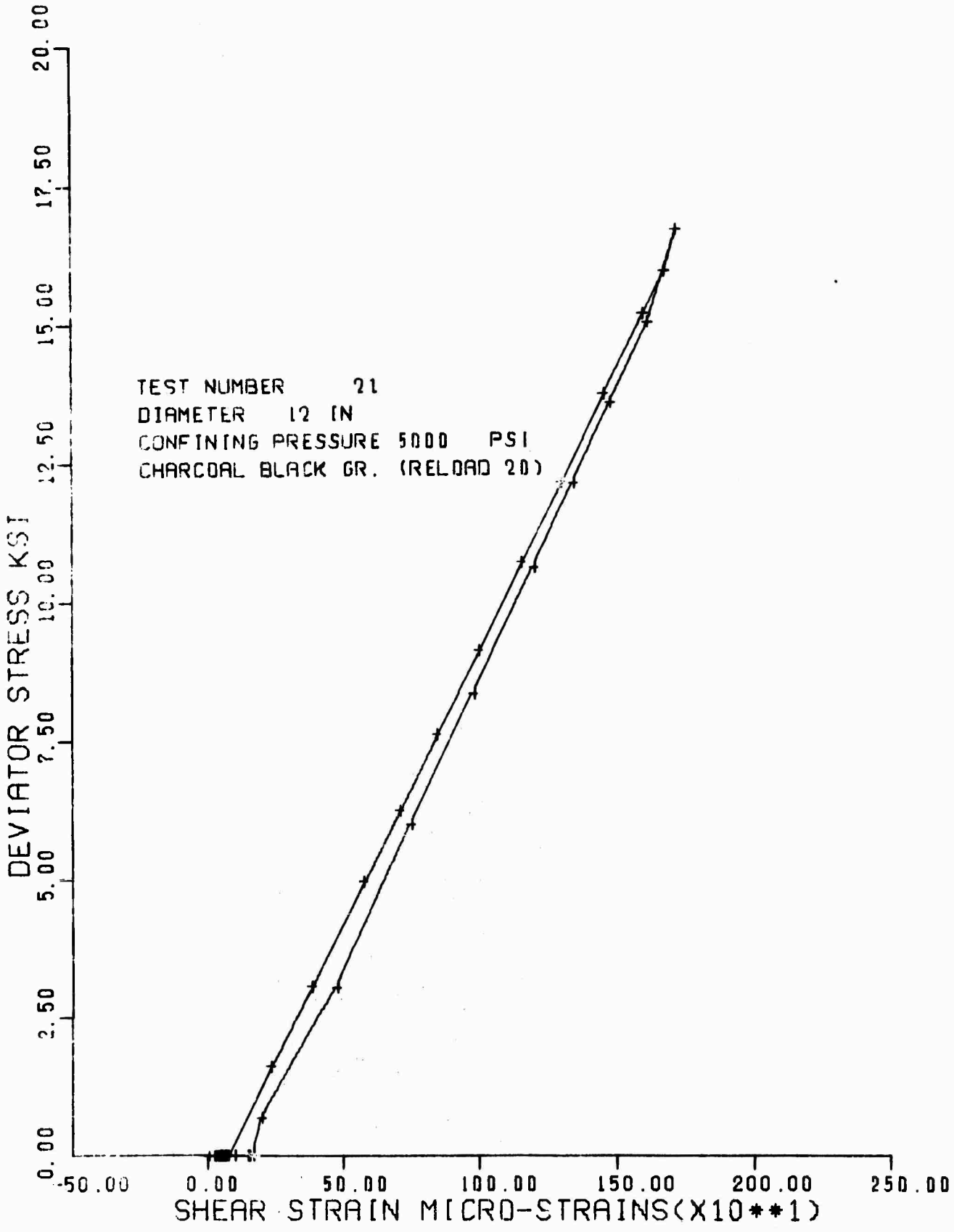
TEST NUMBER 21
DIAMETER 12 IN
CONFINING PRESSURE 5000 PSI
CHARCOAL BLACK GR. (RELOAD 20)
DEVIATOR STRESS KSI
0.00
2.50
5.00
7.50
10.00
12.50
15.00
17.50
20.00
-50.00
0.00
50.00
100.00
150.00
200.00
250.00
SHEAR STRAIN MICRO-STRAINS(X10**1)

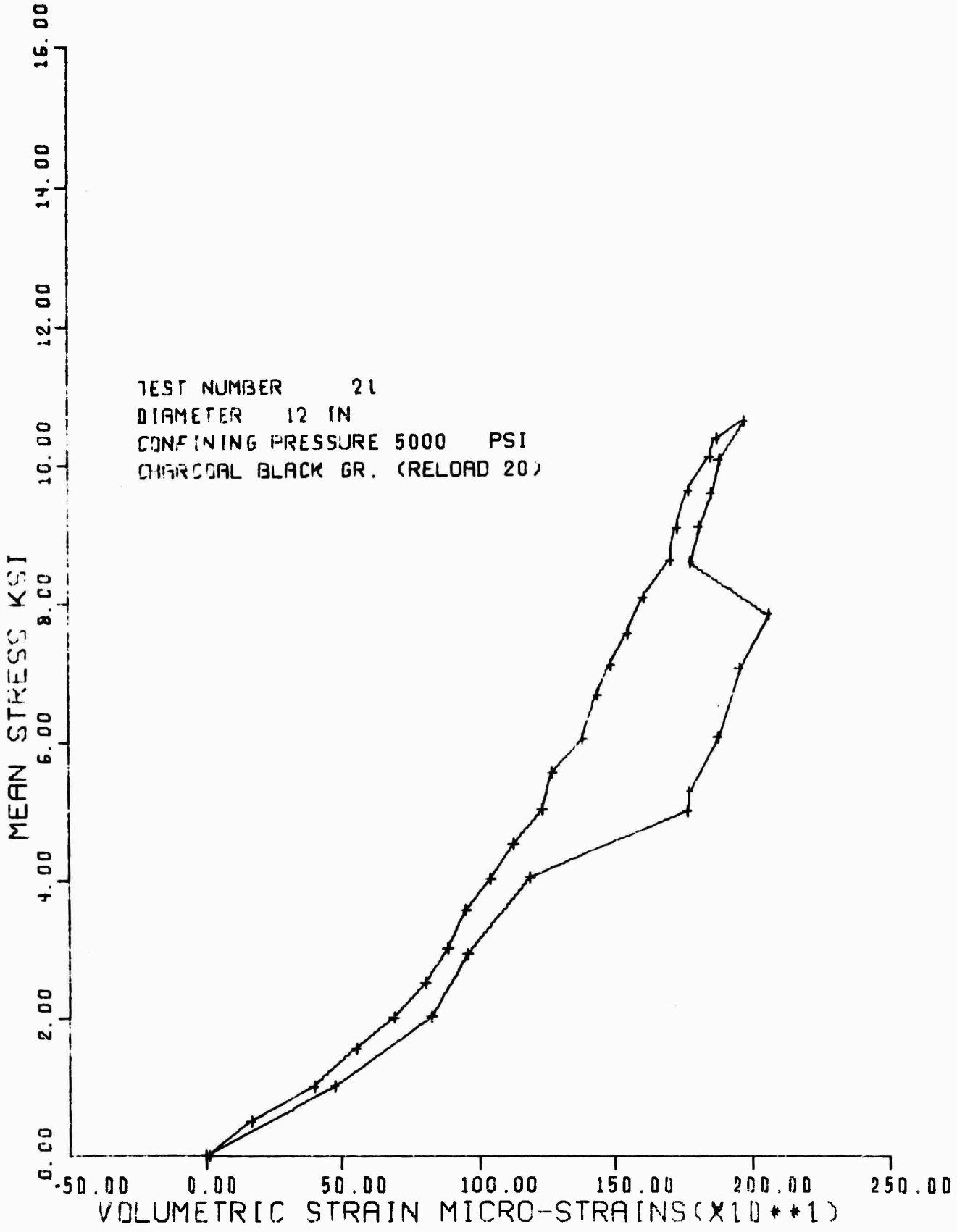
TEST NUMBER 21
DIAMETER 12 IN
CONFINING PRESSURE 5000 PSI
CHARCOAL BLACK GR. (RELOAD 20)
MEAN STRESS KSI
0.00
2.00
4.00
6.00
8.00
10.00
12.00
14.00
16.00
-50.00
0.00
50.00
100.00
150.00
200.00
250.00
VOLUMETRIC STRAIN MICRO-STRAINS(X10**1)

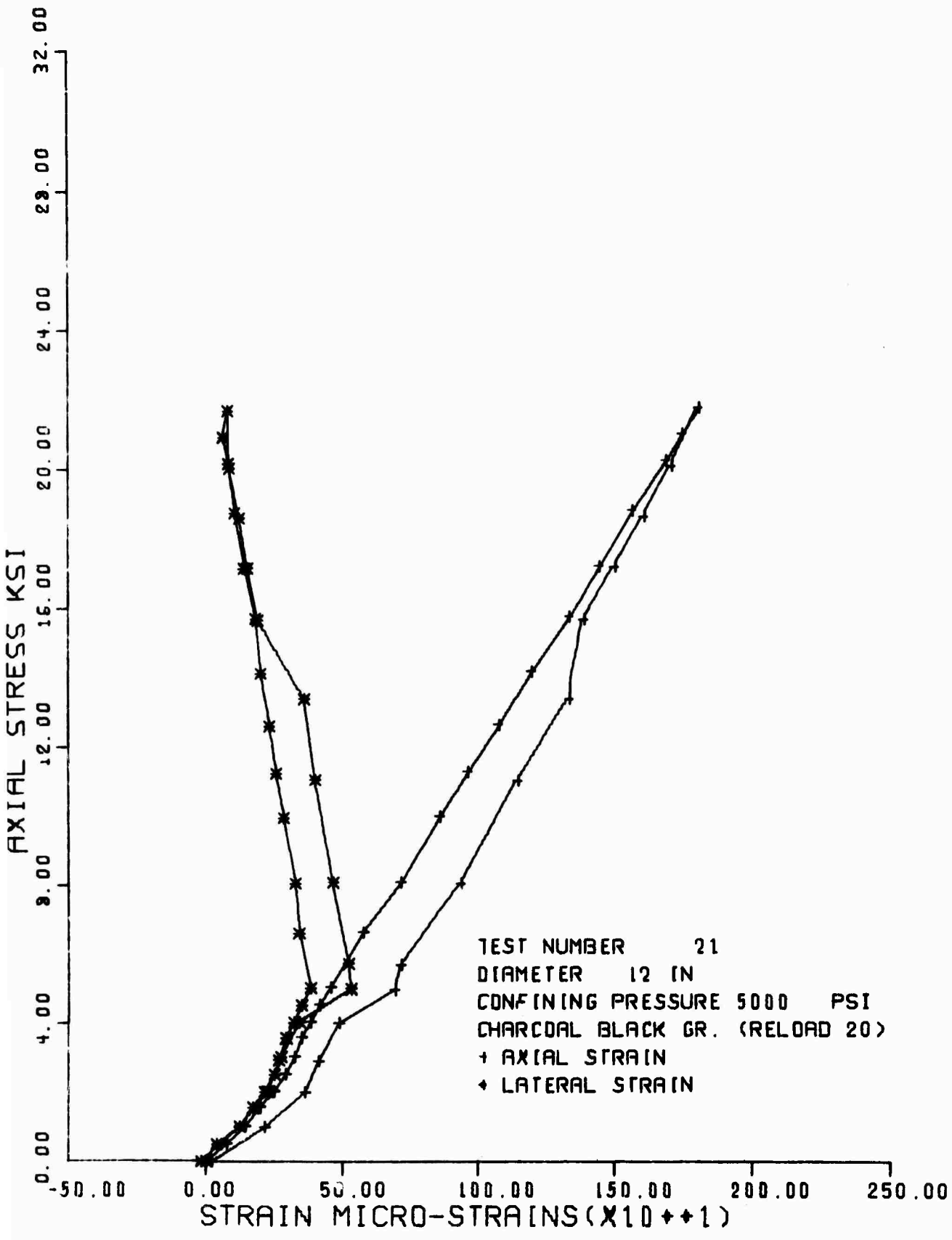
AXIAL STRESS KSI
0.00
4.00
8.00
12.00
16.00
20.00
24.00
28.00
32.00
-50.00
0.00
50.00
100.00
150.00
200.00
250.00
STRAIN MICRO-STRAINS(X10**1)
TEST NUMBER 21
DIAMETER 12 IN
CONFINING PRESSURE 5000 PSI
CHARCOAL BLACK GR. (RELOAD 20)
+ AXIAL STRAIN
* LATERAL STRAIN

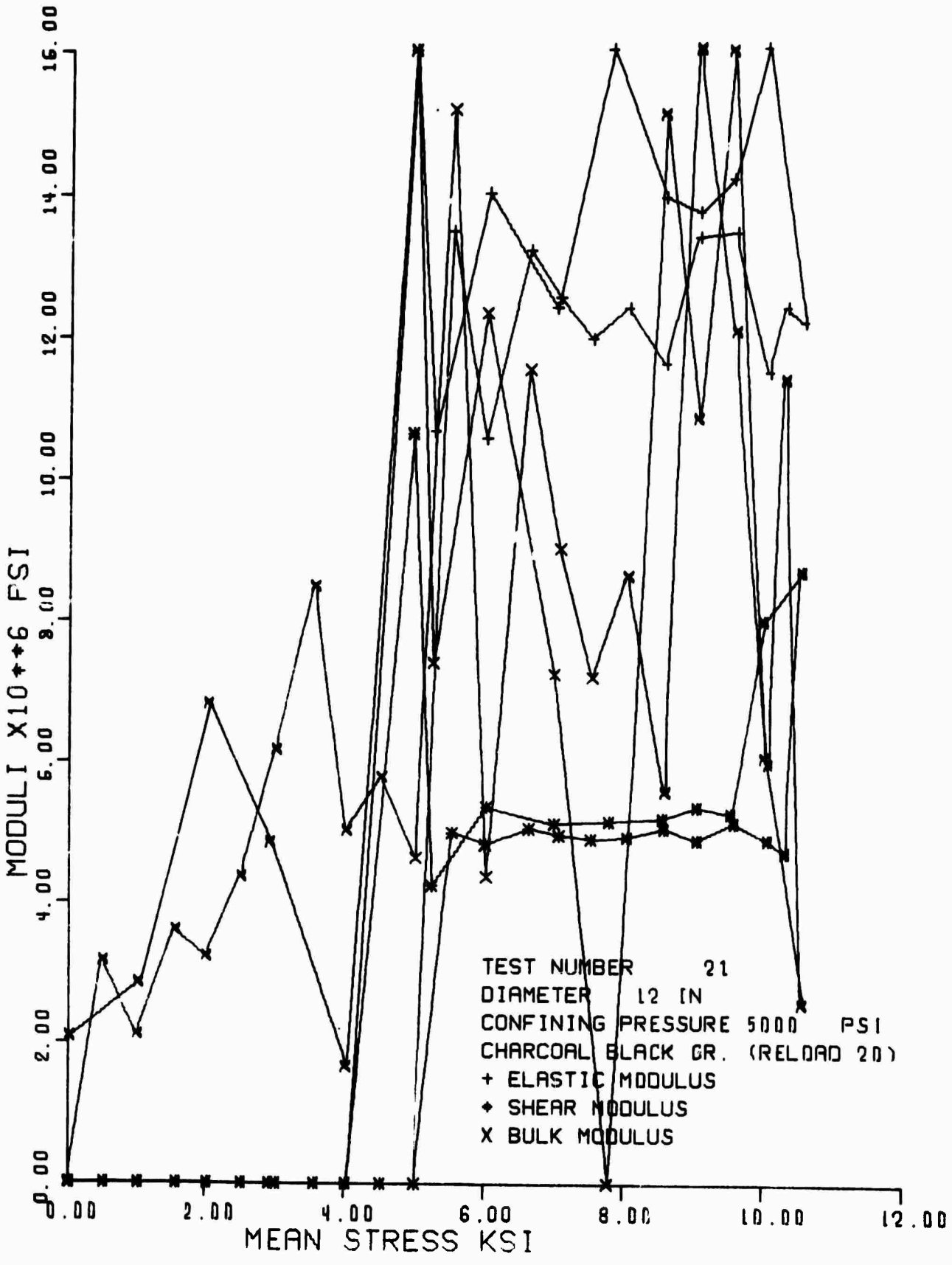
MODULI X10**6 PSI
0.00
2.00
4.00
6.00
8.00
10.00
12.00
14.00
16.00
0.00
2.00
4.00
6.00
8.00
10.00
12.00
MEAN STRESS KSI
TEST NUMBER 21
DIAMETER 12 IN
CONFINING PRESSURE 5000 PSI
CHARCOAL BLACK GR. (RELOAD 20)
+ ELASTIC MODULUS
* SHEAR MODULUS
X BULK MODULUS

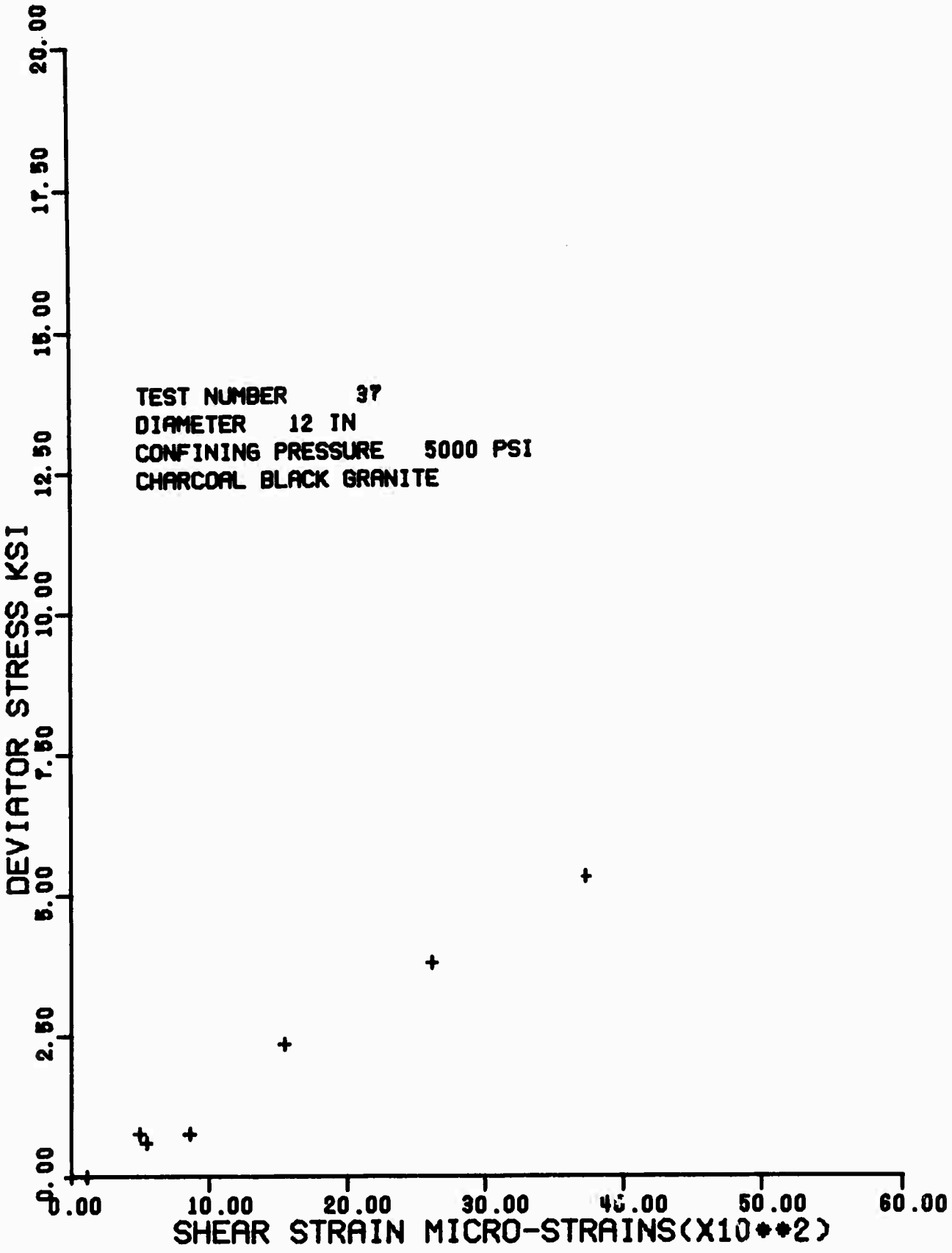
TEST NUMBER 37
DIAMETER 12 IN
CONFINING PRESSURE 5000 PSI
CHARCOAL BLACK GRANITE
DEVIATOR STRESS KSI
0.00
2.50
5.00
7.50
10.00
12.50
15.00
17.50
20.00
0.00
10.00
20.00
30.00
40.00
50.00
60.00
SHEAR STRAIN MICRO-STRAINS(X10**2)

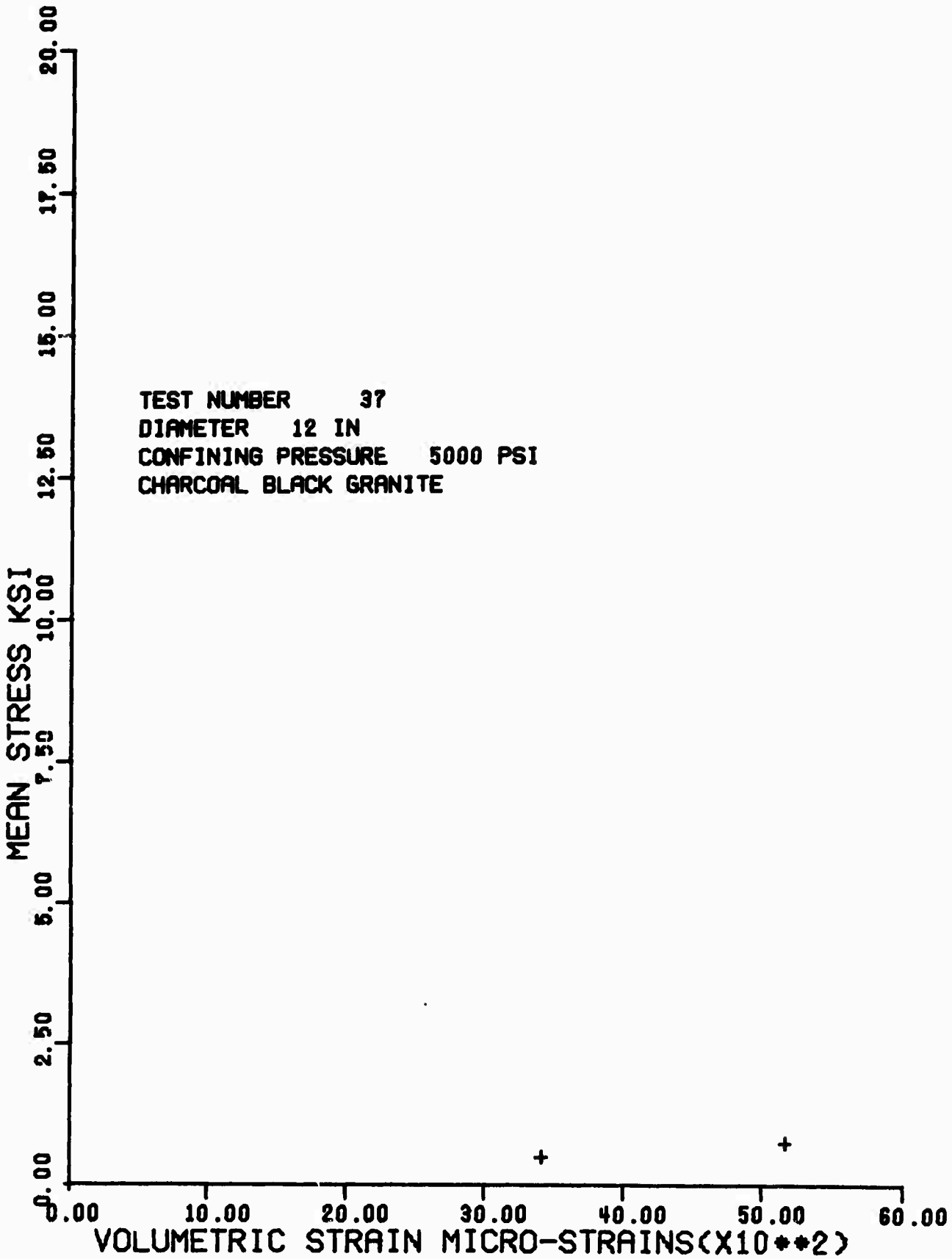
TEST NUMBER 37
DIAMETER 12 IN
CONFINING PRESSURE 5000 PSI
CHARCOAL BLACK GRANITE
MEAN STRESS KSI
0.00
2.50
5.00
7.50
10.00
12.50
15.00
17.50
20.00
0.00
10.00
20.00
30.00
40.00
50.00
60.00
VOLUMETRIC STRAIN MICRO-STRAINS(X10**2)

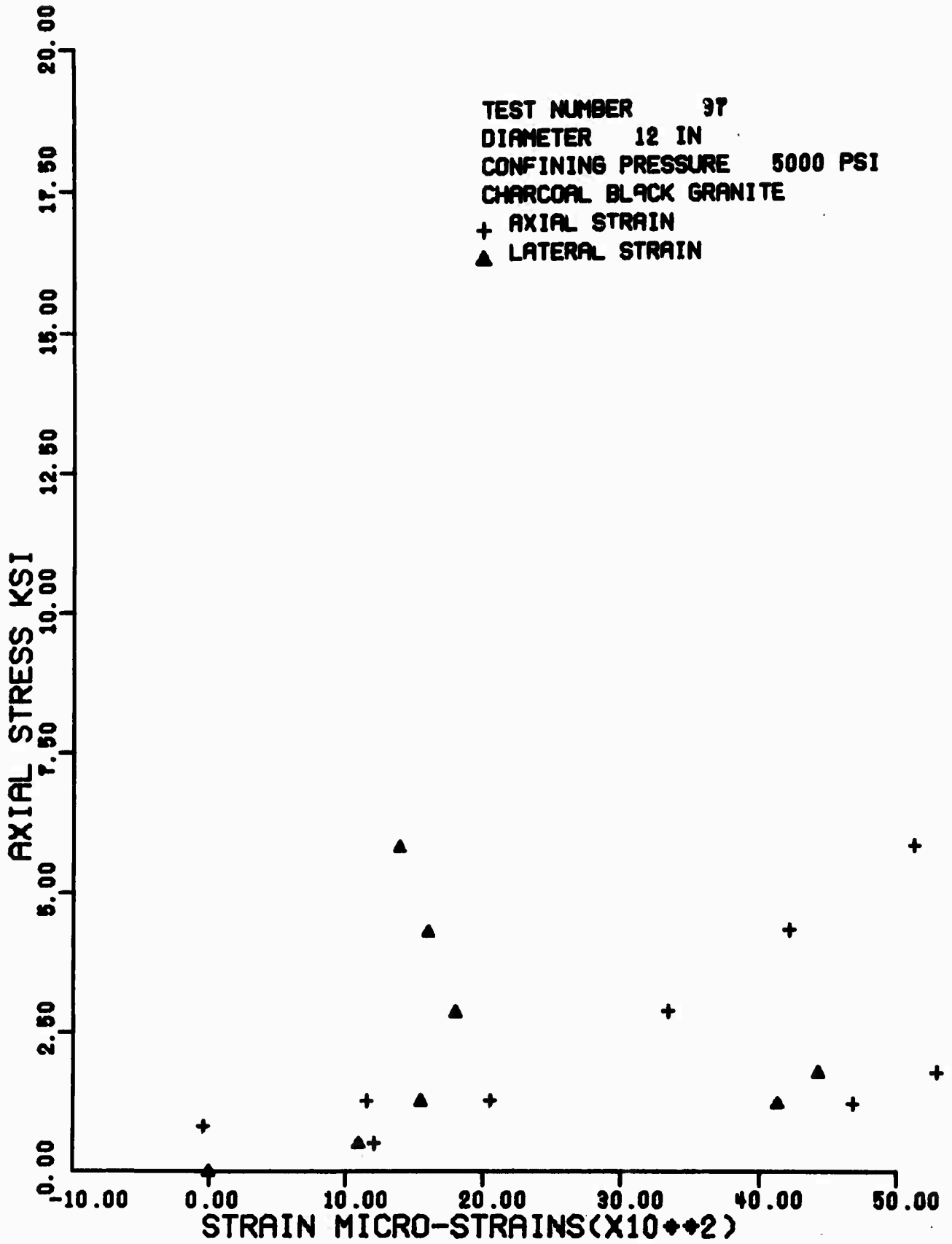
TEST NUMBER 97
DIAMETER 12 IN
CONFINING PRESSURE 5000 PSI
CHARCOAL BLACK GRANITE
+ AXIAL STRAIN
▲ LATERAL STRAIN
AXIAL STRESS KSI
0.00
2.50
5.00
7.50
10.00
12.50
15.00
17.50
20.00
-10.00
0.00
10.00
20.00
30.00
40.00
50.00
STRAIN MICRO-STRAINS(X10**2)

7-13-70

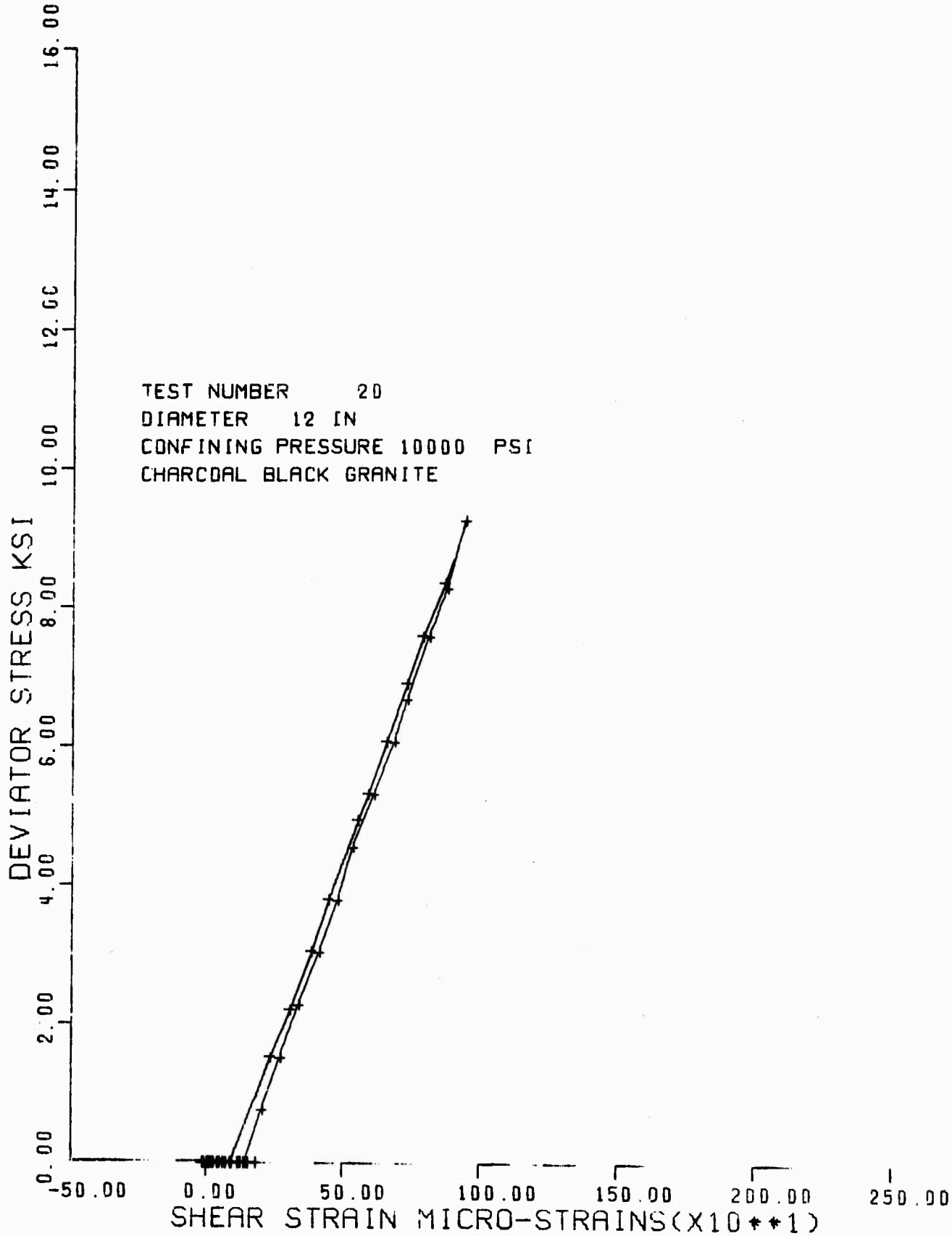
TEST NUMBER 20
DIAMETER 12 IN
CONFINING PRESSURE 10000 PSI
CHARCOAL BLACK GRANITE
DEVIATOR STRESS KSI
0.00
2.00
4.00
6.00
8.00
10.00
12.00
14.00
16.00
-50.00
0.00
50.00
100.00
150.00
200.00
250.00
SHEAR STRAIN MICRO-STRAINS(X10**1)

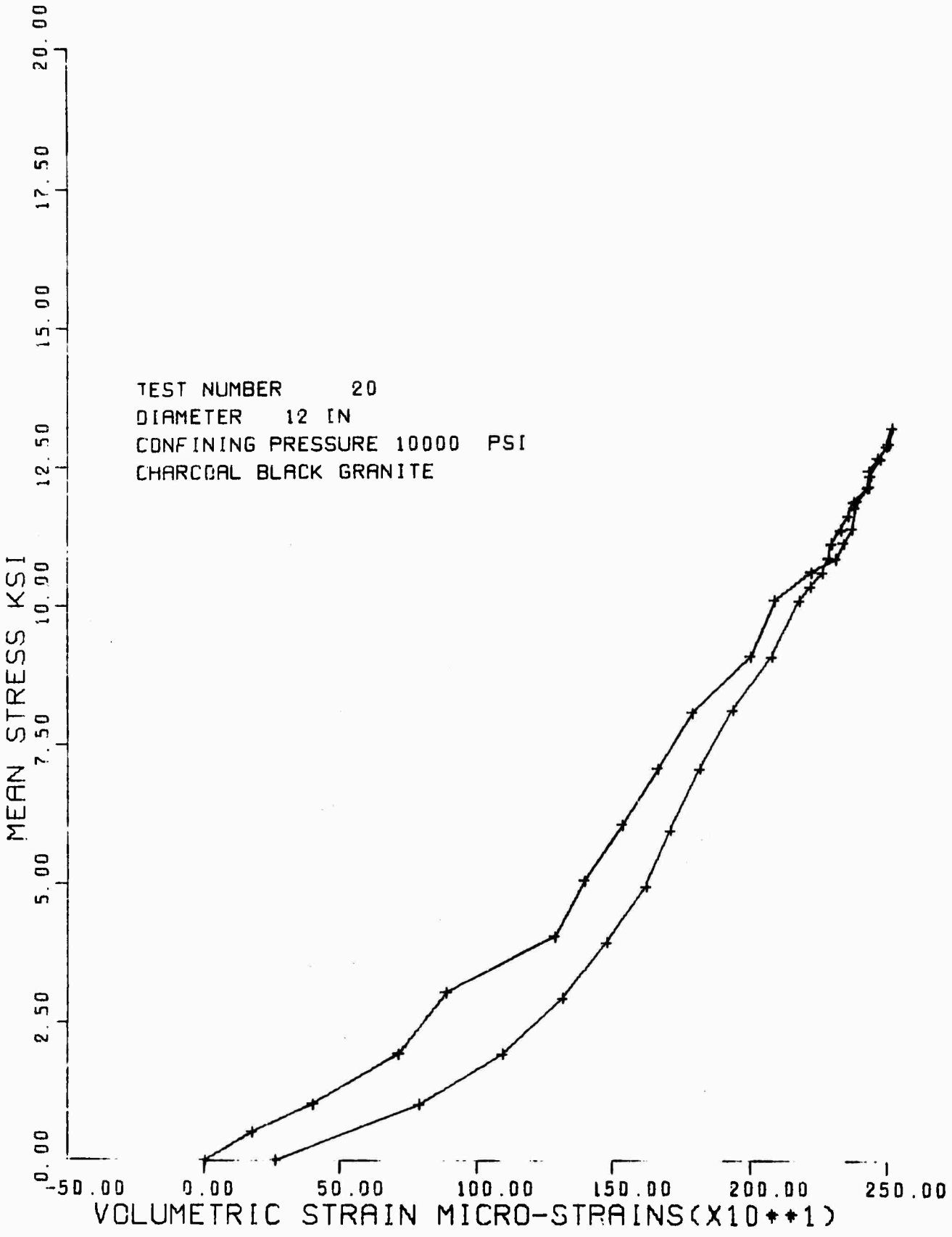
TEST NUMBER 20
DIAMETER 12 IN
CONFINING PRESSURE 10000 PSI
CHARCOAL BLACK GRANITE
MEAN STRESS KSI
0.00
2.50
5.00
7.50
10.00
12.50
15.00
17.50
20.00
-50.00
0.00
50.00
100.00
150.00
200.00
250.00
VOLUMETRIC STRAIN MICRO-STRAINS(X10**1)

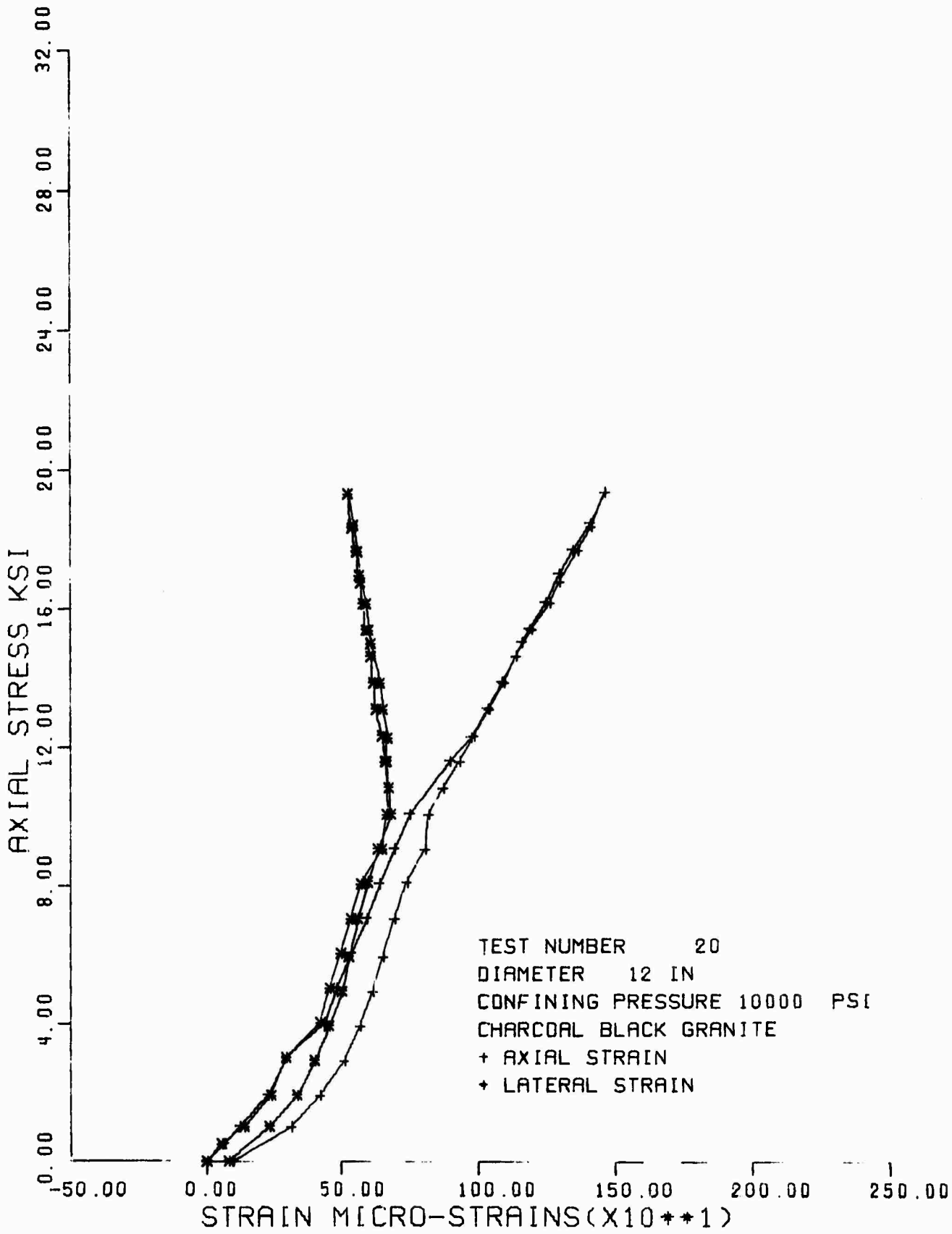
AXIAL STRESS KSI
0.00
4.00
8.00
12.00
16.00
20.00
24.00
28.00
32.00
-50.00
0.00
50.00
100.00
150.00
200.00
250.00
STRAIN MICRO-STRAINS(X10**1)
TEST NUMBER 20
DIAMETER 12 IN
CONFINING PRESSURE 10000 PSI
CHARCOAL BLACK GRANITE
+ AXIAL STRAIN
+ LATERAL STRAIN

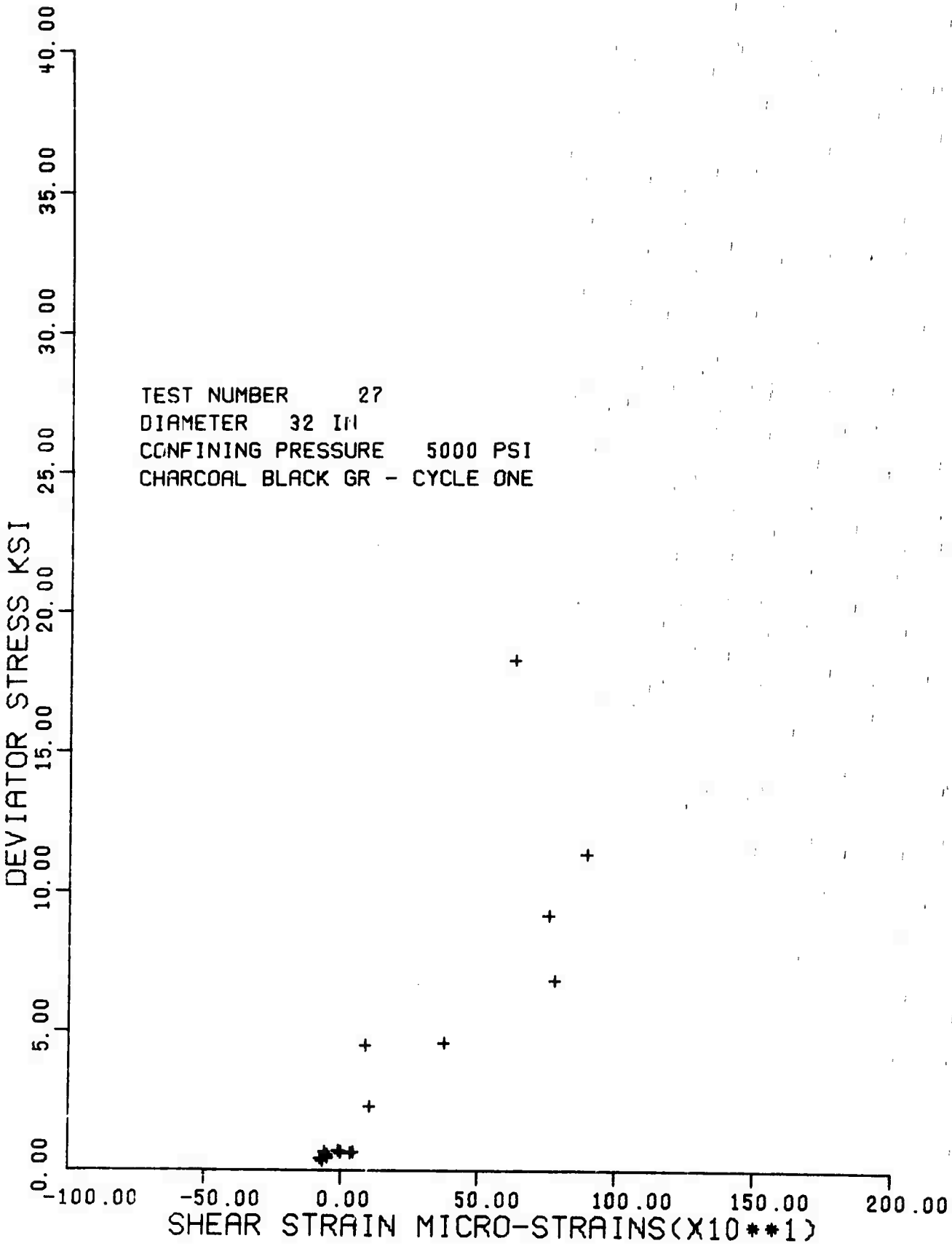
TEST NUMBER 27
DIAMETER 32 IN
CONFINING PRESSURE 5000 PSI
CHARCOAL BLACK GR - CYCLE ONE
DEVIATOR STRESS KSI
0.00
5.00
10.00
15.00
20.00
25.00
30.00
35.00
40.00
-100.00
-50.00
0.00
50.00
100.00
150.00
200.00
SHEAR STRAIN MICRO-STRAINS(X10**1)

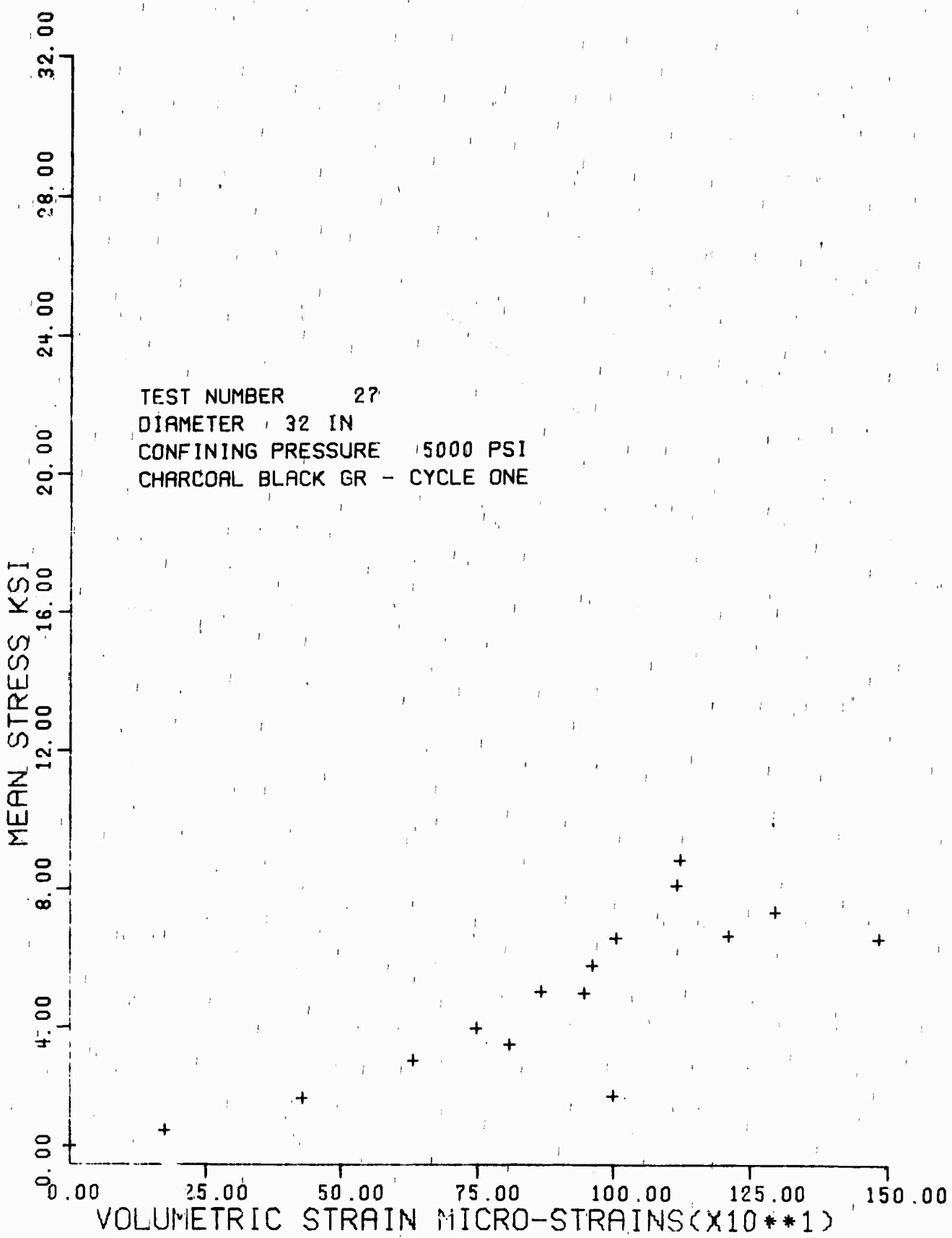
TEST NUMBER 27
DIAMETER 32 IN
CONFINING PRESSURE 5000 PSI
CHARCOAL BLACK GR - CYCLE ONE
MEAN STRESS KSI
0.00
4.00
8.00
12.00
16.00
20.00
24.00
28.00
32.00
0.00
25.00
50.00
75.00
100.00
125.00
150.00
VOLUMETRIC STRAIN MICRO-STRAINS(X10**1)

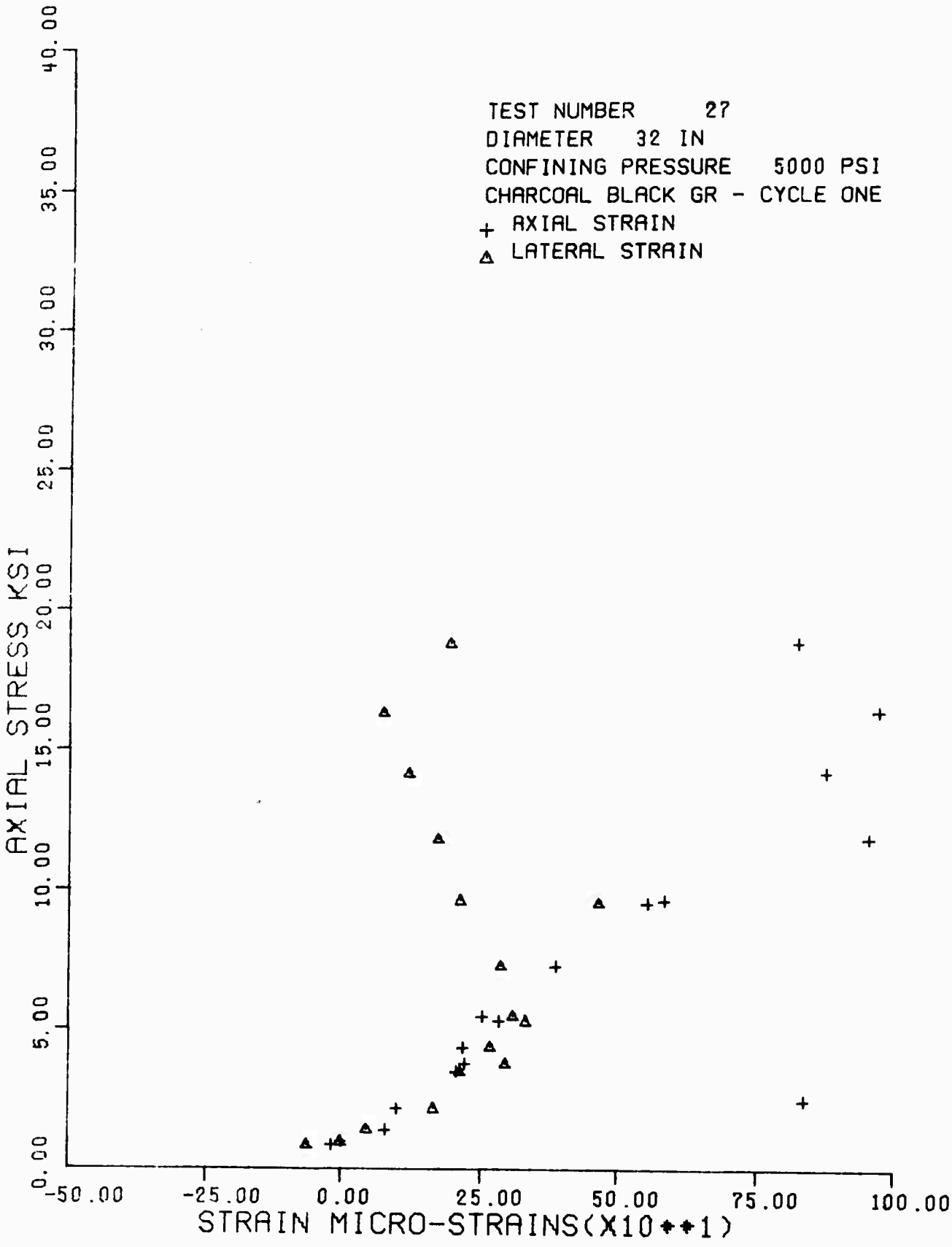
TEST NUMBER 27
DIAMETER 32 IN
CONFINING PRESSURE 5000 PSI
CHARCOAL BLACK GR - CYCLE ONE
+ AXIAL STRAIN
△ LATERAL STRAIN
AXIAL STRESS KSI
0.00
5.00
10.00
15.00
20.00
25.00
30.00
35.00
40.00
-50.00
-25.00
0.00
25.00
50.00
75.00
100.00
STRAIN MICRO-STRAINS(X10**1)

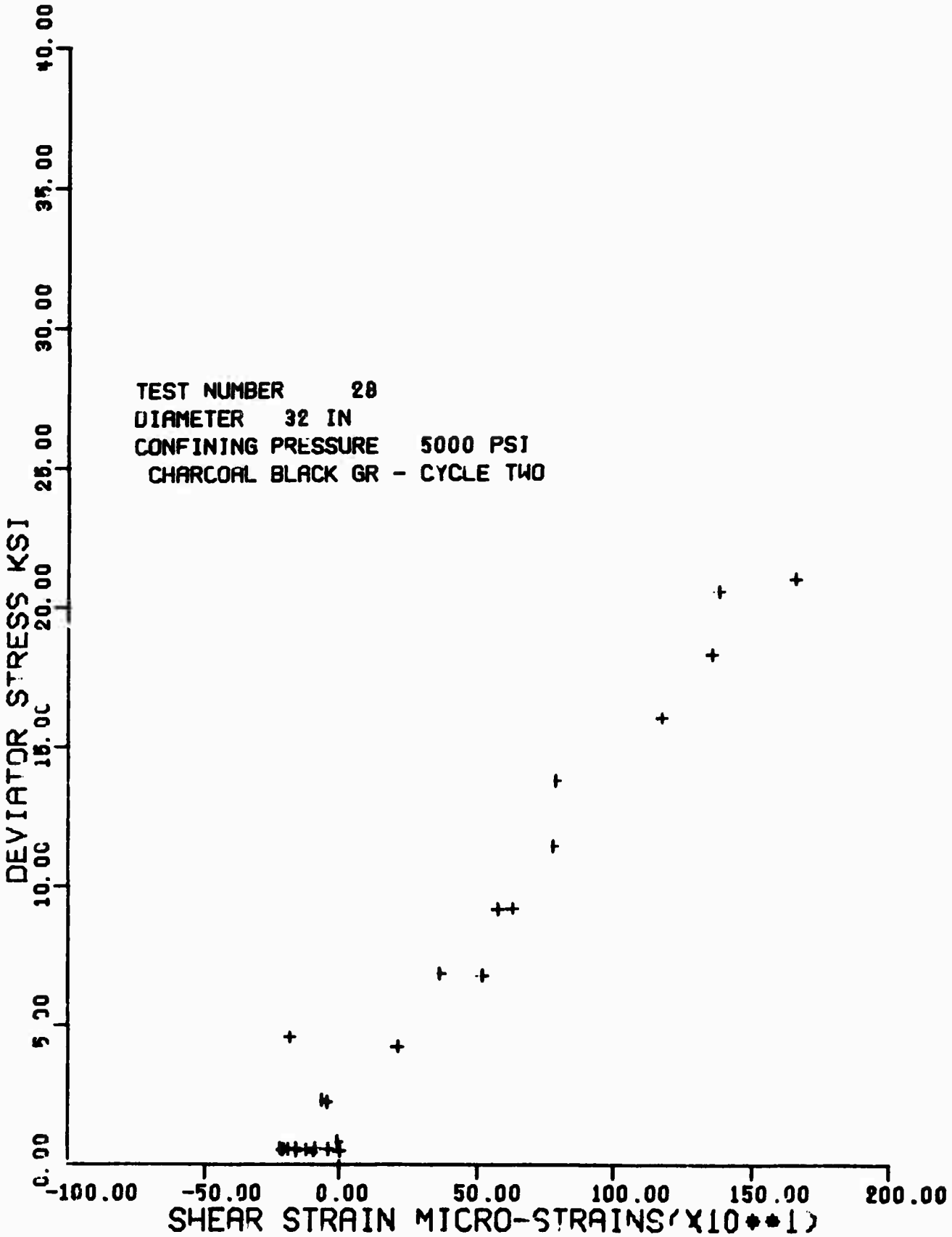
TEST NUMBER 28
DIAMETER 32 IN
CONFINING PRESSURE 5000 PSI
CHARCOAL BLACK GR - CYCLE TWO
DEVIATOR STRESS KSI
0.00
5.00
10.00
15.00
20.00
25.00
30.00
35.00
40.00
-100.00
-50.00
0.00
50.00
100.00
150.00
200.00
SHEAR STRAIN MICRO-STRAINS(X10**1)

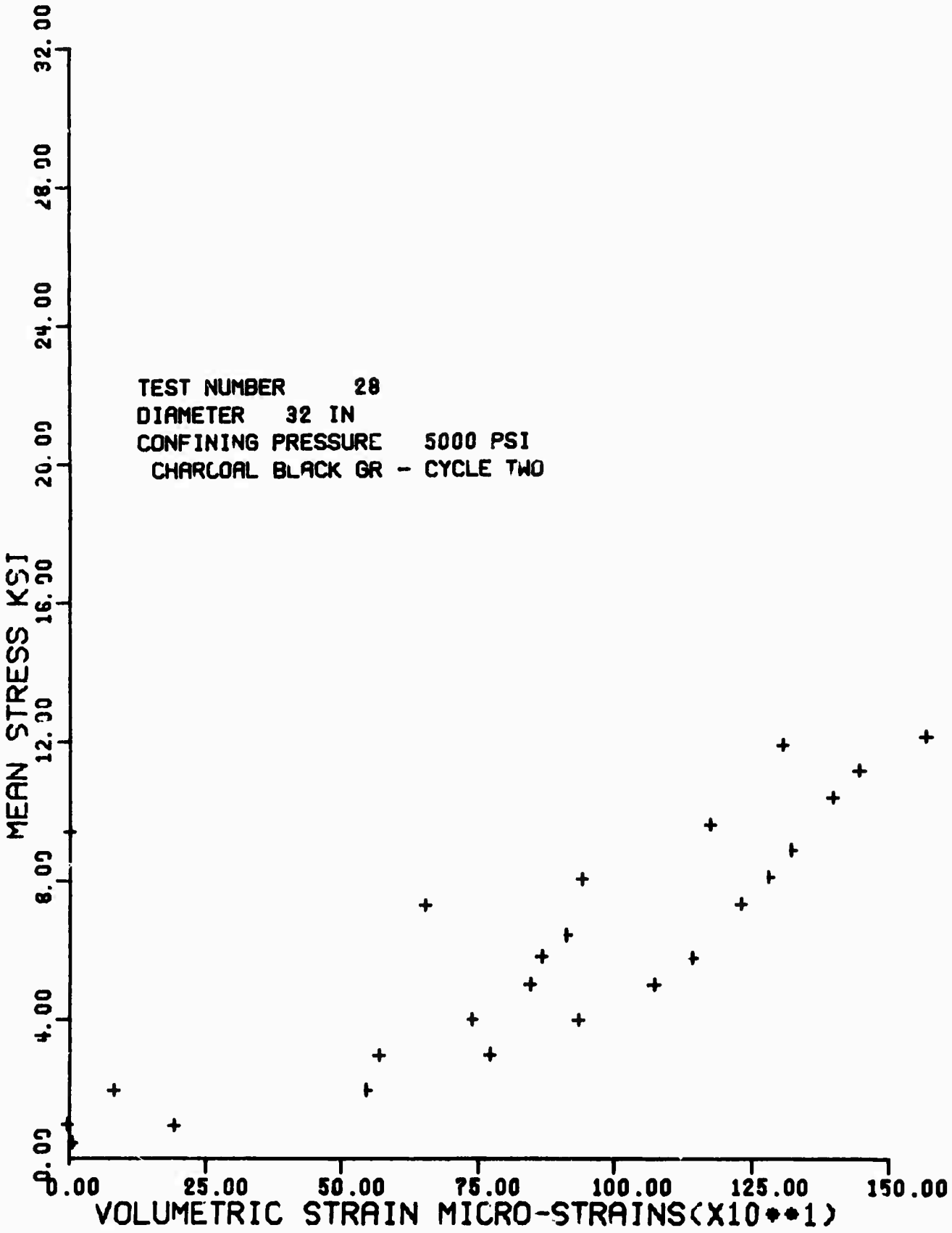
TEST NUMBER 28
DIAMETER 32 IN
CONFINING PRESSURE 5000 PSI
CHARCOAL BLACK GR - CYCLE TWO
MEAN STRESS KSI
0.00
4.00
8.00
12.00
16.00
20.00
24.00
28.00
32.00
0.00
25.00
50.00
75.00
100.00
125.00
150.00
VOLUMETRIC STRAIN MICRO-STRAINS(X10**1)

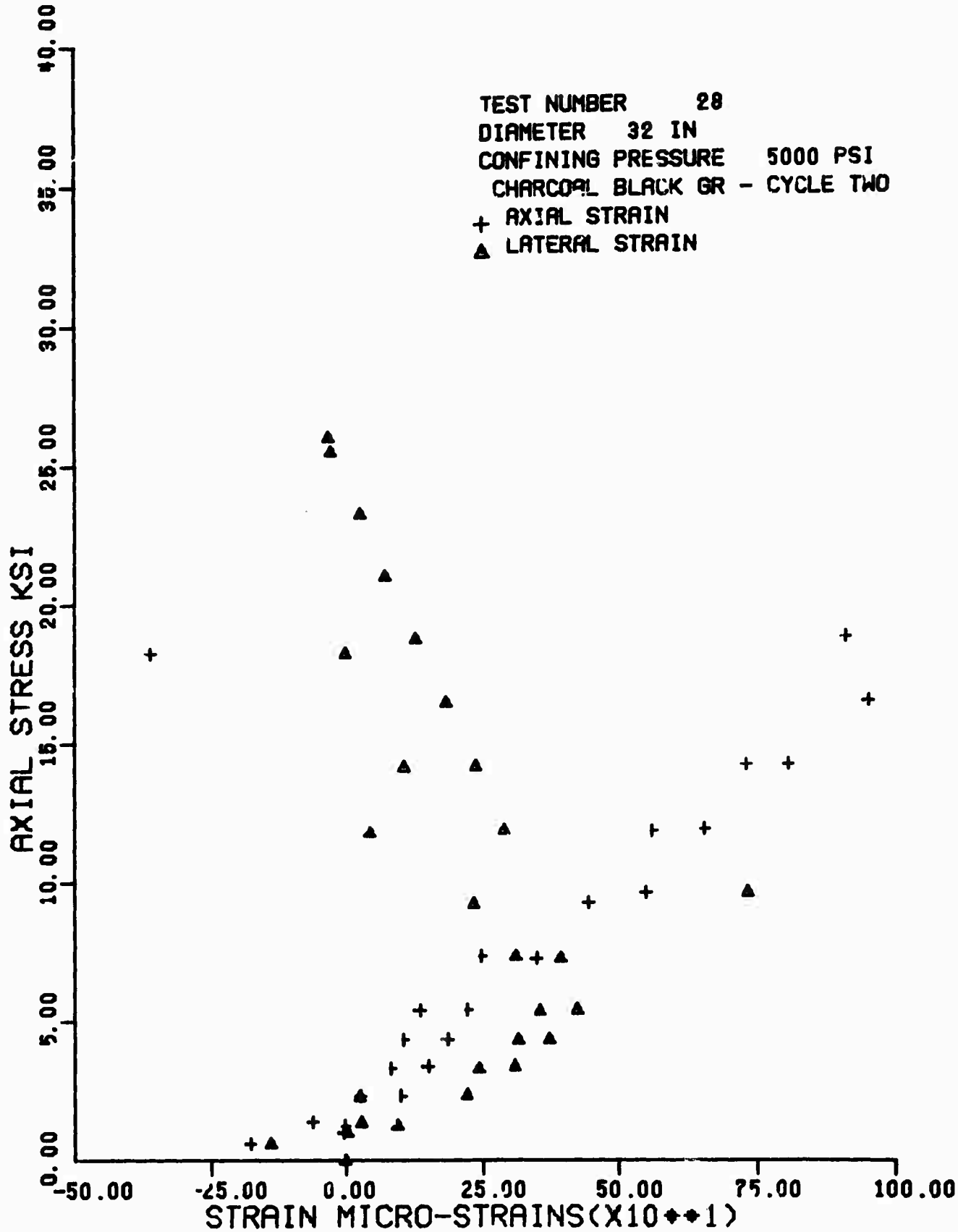
TEST NUMBER 28
DIAMETER 32 IN
CONFINING PRESSURE 5000 PSI
CHARCOAL BLACK GR - CYCLE TWO
+ AXIAL STRAIN
▲ LATERAL STRAIN
AXIAL STRESS KSI
0.00
5.00
10.00
15.00
20.00
25.00
30.00
35.00
40.00
-50.00
-25.00
0.00
25.00
50.00
75.00
100.00
STRAIN MICRO-STRAINS(X10**1)

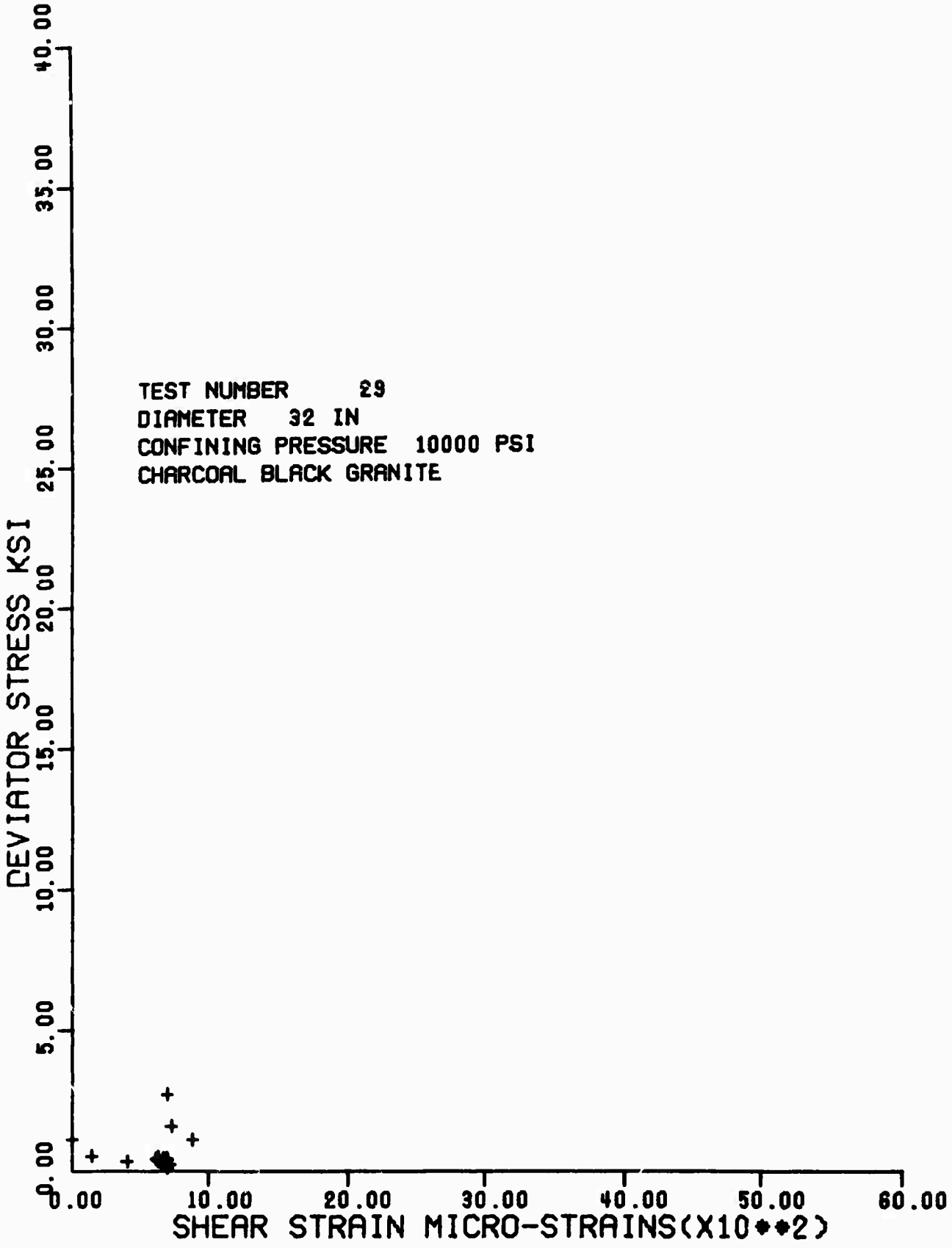
TEST NUMBER 29
DIAMETER 32 IN
CONFINING PRESSURE 10000 PSI
CHARCOAL BLACK GRANITE
DEVIATOR STRESS KSI
0.00
5.00
10.00
15.00
20.00
25.00
30.00
35.00
40.00
0.00
10.00
20.00
30.00
40.00
50.00
60.00
SHEAR STRAIN MICRO-STRAINS(X10**2)

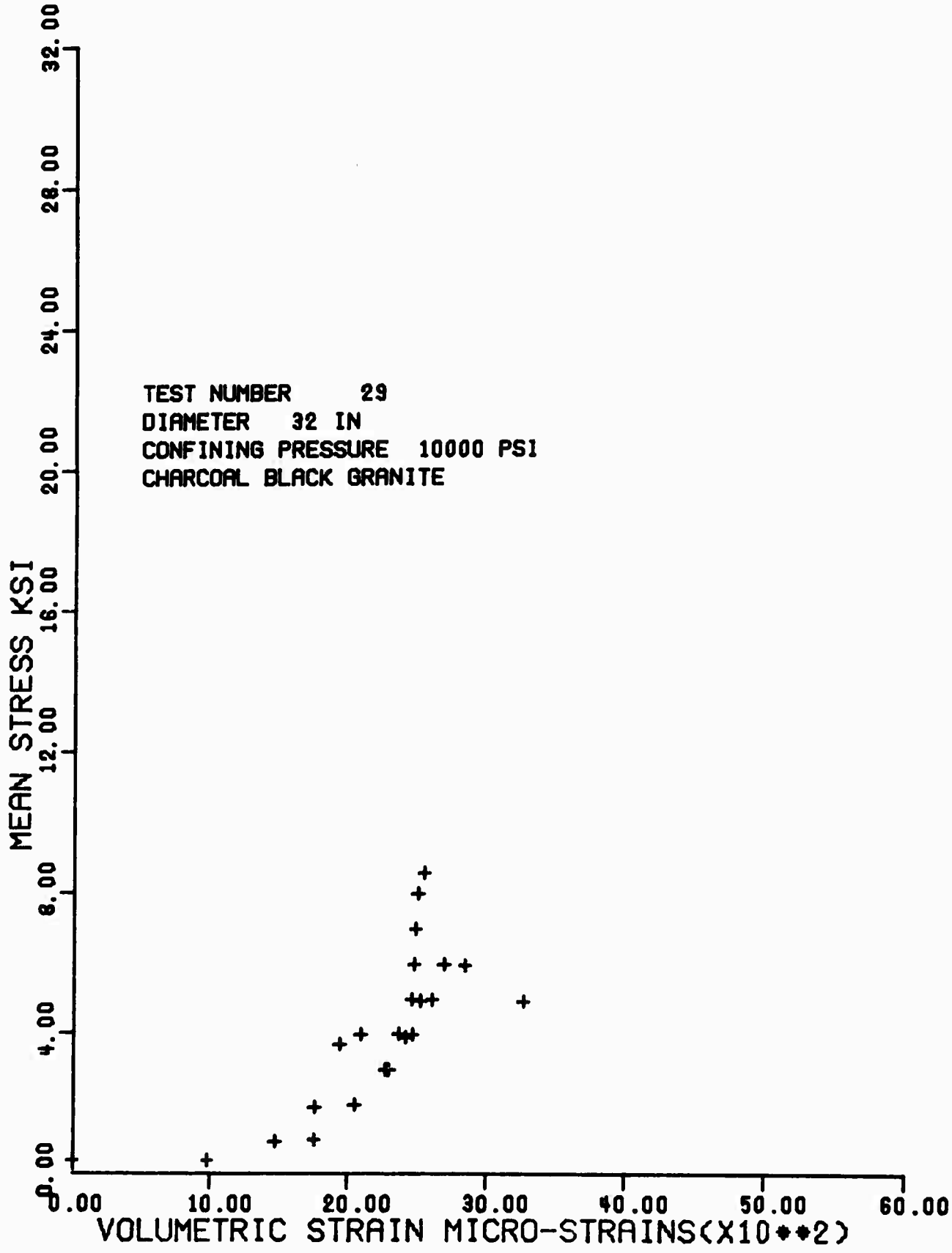
TEST NUMBER 29
DIAMETER 32 IN
CONFINING PRESSURE 10000 PSI
CHARCOAL BLACK GRANITE
MEAN STRESS KSI
0.00
4.00
8.00
12.00
16.00
20.00
24.00
28.00
32.00
0.00
10.00
20.00
30.00
40.00
50.00
60.00
VOLUMETRIC STRAIN MICRO-STRAINS(X10**2)

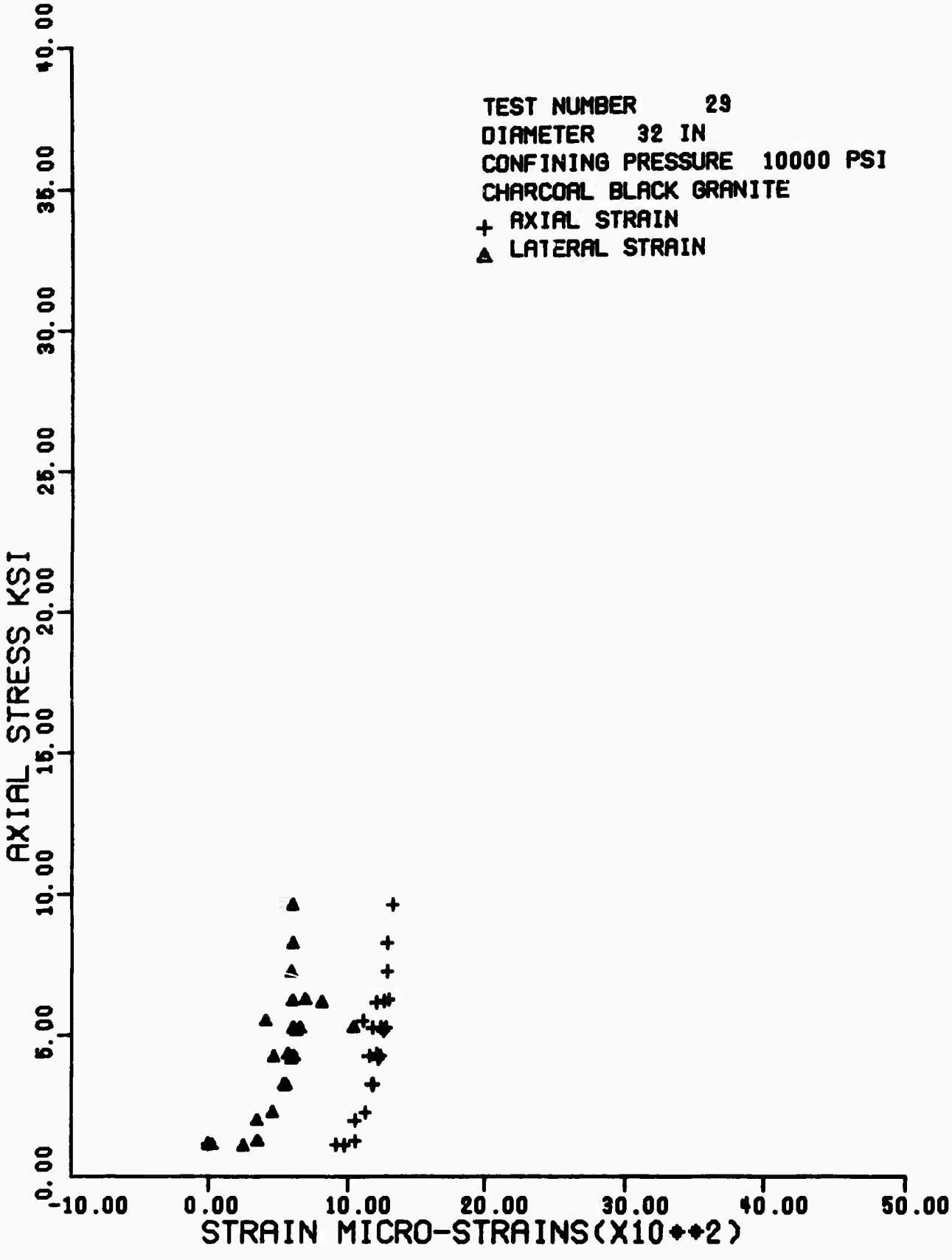
TEST NUMBER 29
DIAMETER 32 IN
CONFINING PRESSURE 10000 PSI
CHARCOAL BLACK GRANITE
+ AXIAL STRAIN
▲ LATERAL STRAIN
AXIAL STRESS KSI
0.00
5.00
10.00
15.00
20.00
25.00
30.00
35.00
40.00
-10.00
0.00
10.00
20.00
30.00
40.00
50.00
STRAIN MICRO-STRAINS(X10**2)

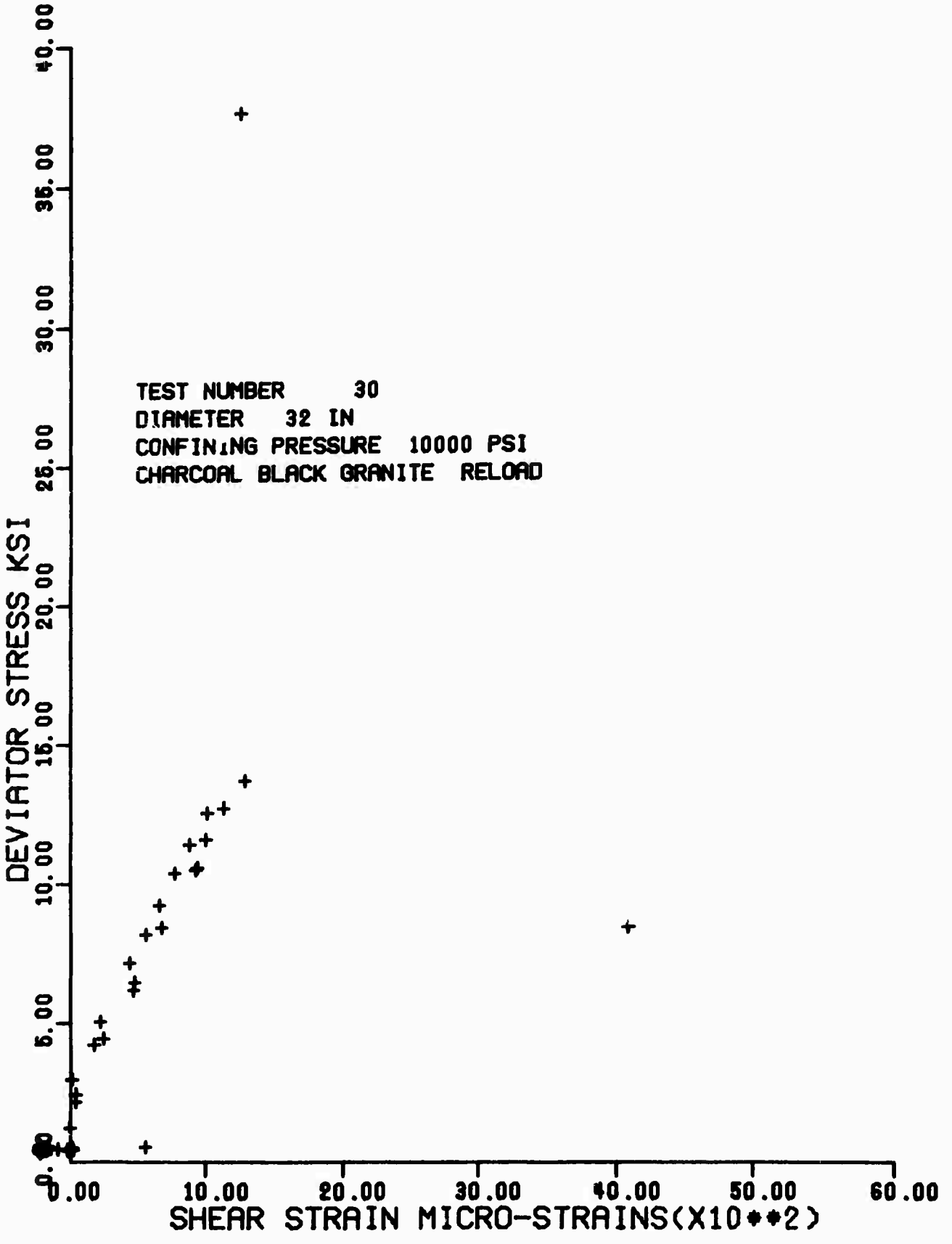
TEST NUMBER 30
DIAMETER 32 IN
CONFINING PRESSURE 10000 PSI
CHARCOAL BLACK GRANITE RELOAD
DEVIATOR STRESS KSI
0.00
5.00
10.00
15.00
20.00
25.00
30.00
35.00
40.00
0.00
10.00
20.00
30.00
40.00
50.00
60.00
SHEAR STRAIN MICRO-STRAINS(X10**2)

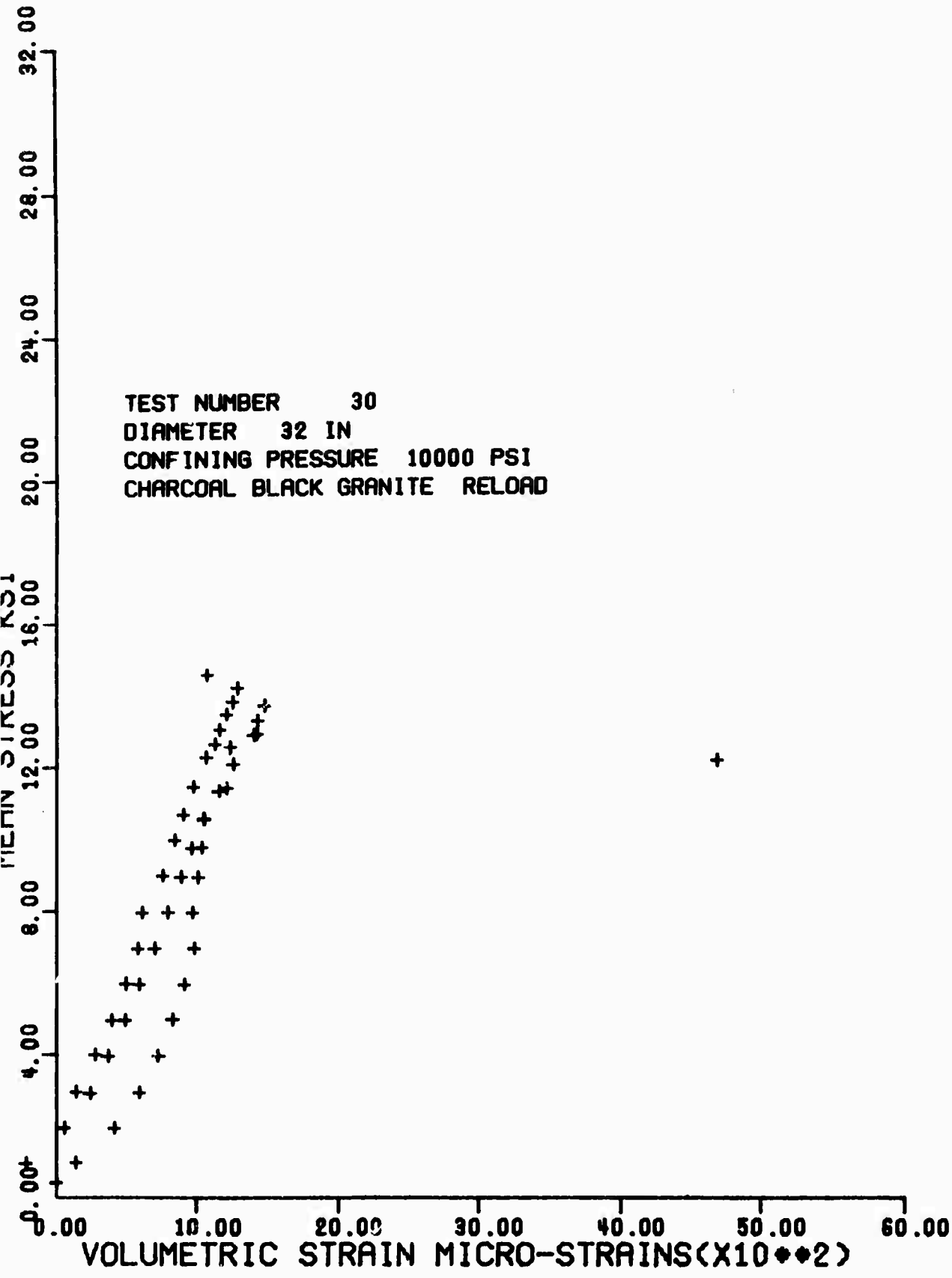
TEST NUMBER 30
DIAMETER 32 IN
CONFINING PRESSURE 10000 PSI
CHARCOAL BLACK GRANITE RELOAD
MEAN STRESS KSI
0.00
4.00
8.00
12.00
16.00
20.00
24.00
28.00
32.00
0.00
10.00
20.00
30.00
40.00
50.00
60.00
VOLUMETRIC STRAIN MICRO-STRAINS(X10**2)

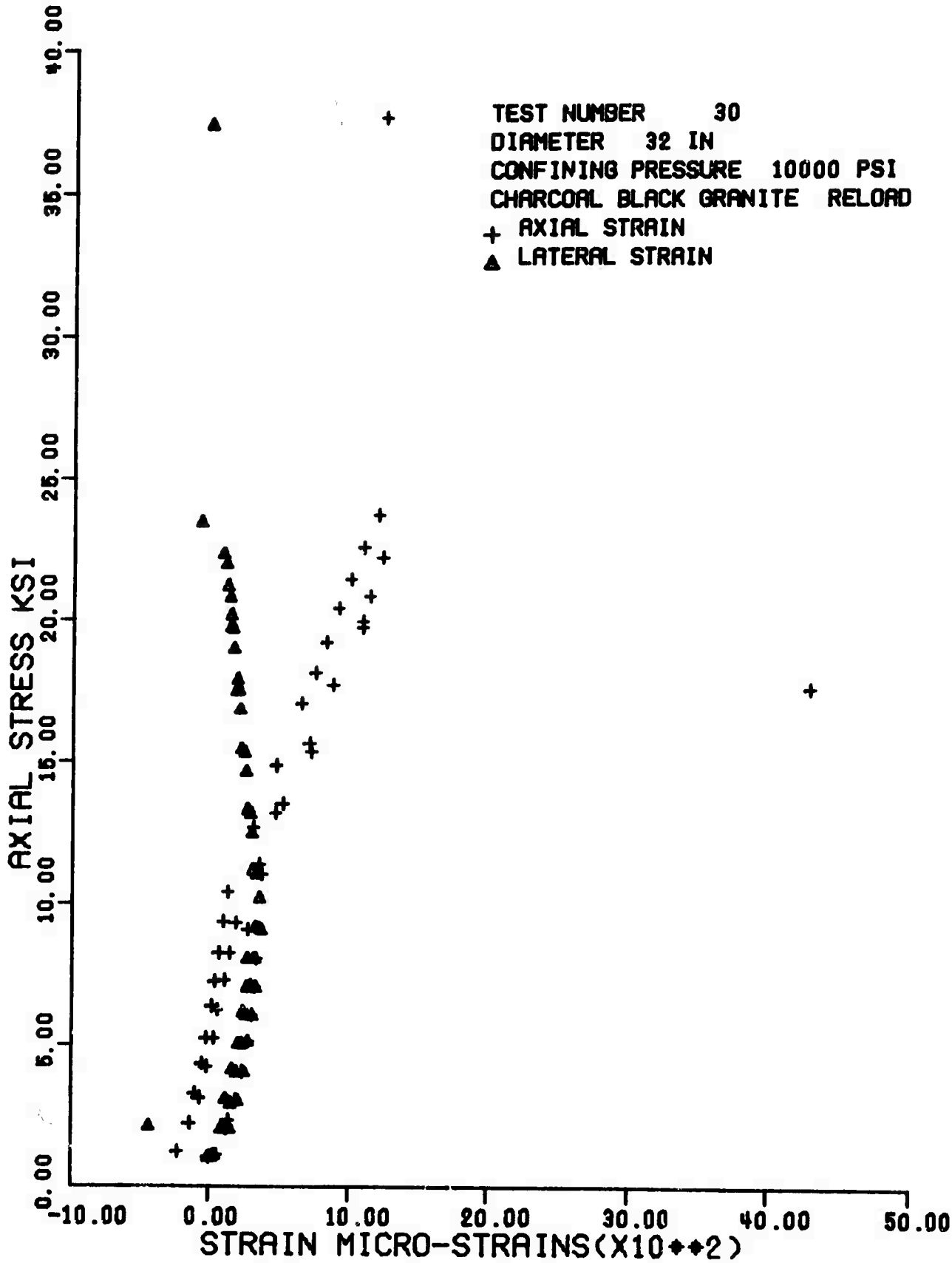
TEST NUMBER 30
DIAMETER 32 IN
CONFINING PRESSURE 10000 PSI
CHARCOAL BLACK GRANITE RELOAD
+ AXIAL STRAIN
▲ LATERAL STRAIN
AXIAL STRESS KSI
0.00
5.00
10.00
15.00
20.00
25.00
30.00
35.00
40.00
-10.00
0.00
10.00
20.00
30.00
40.00
50.00
STRAIN MICRO-STRAINS(X10**2)

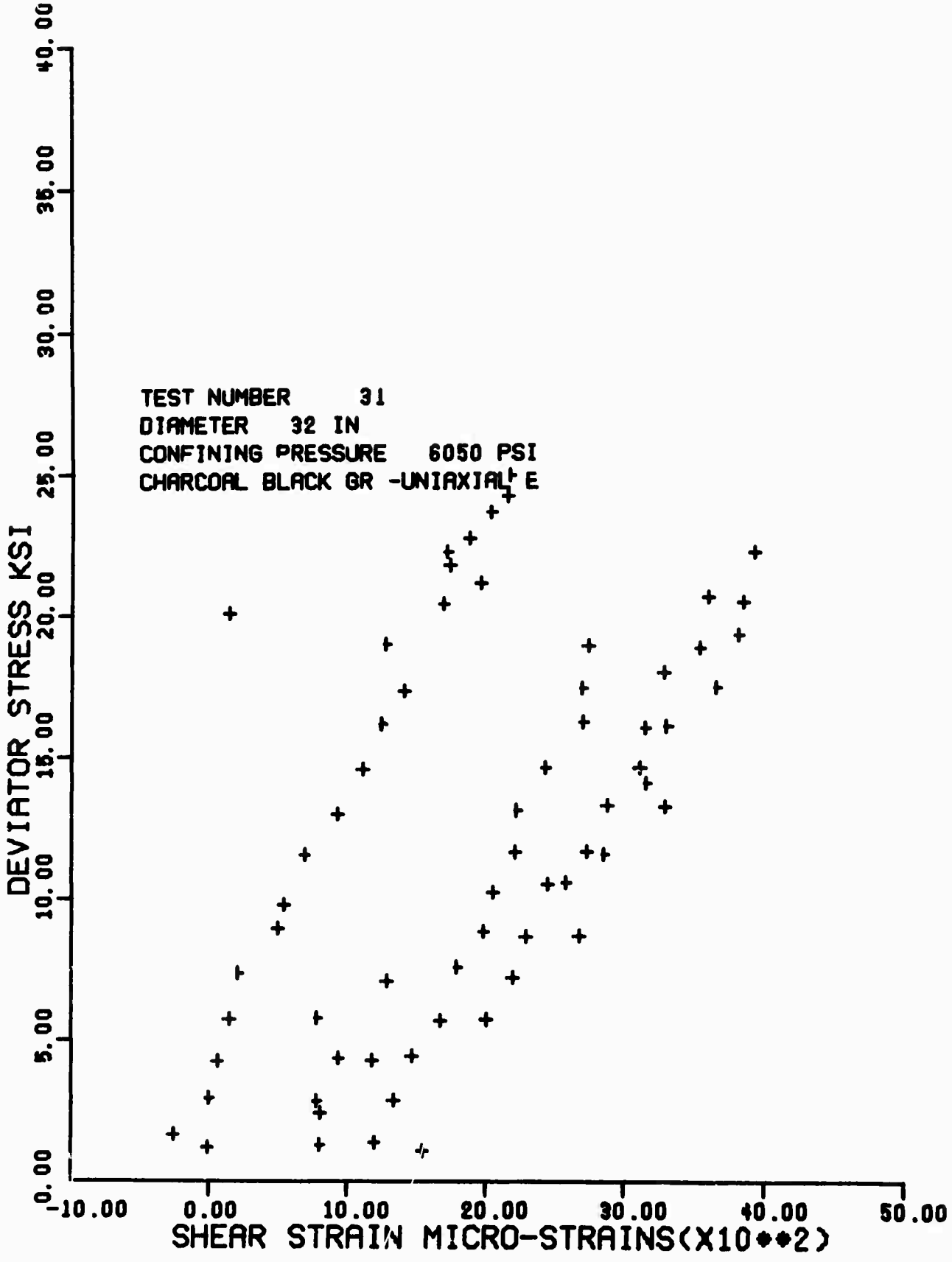
TEST NUMBER 31
DIAMETER 32 IN
CONFINING PRESSURE 6050 PSI
CHARCOAL BLACK GR -UNIAXIAL E
DEVIATOR STRESS KSI
0.00
5.00
10.00
15.00
20.00
25.00
30.00
35.00
40.00
-10.00
0.00
10.00
20.00
30.00
40.00
50.00
SHEAR STRAIN MICRO-STRAINS(X10**2)

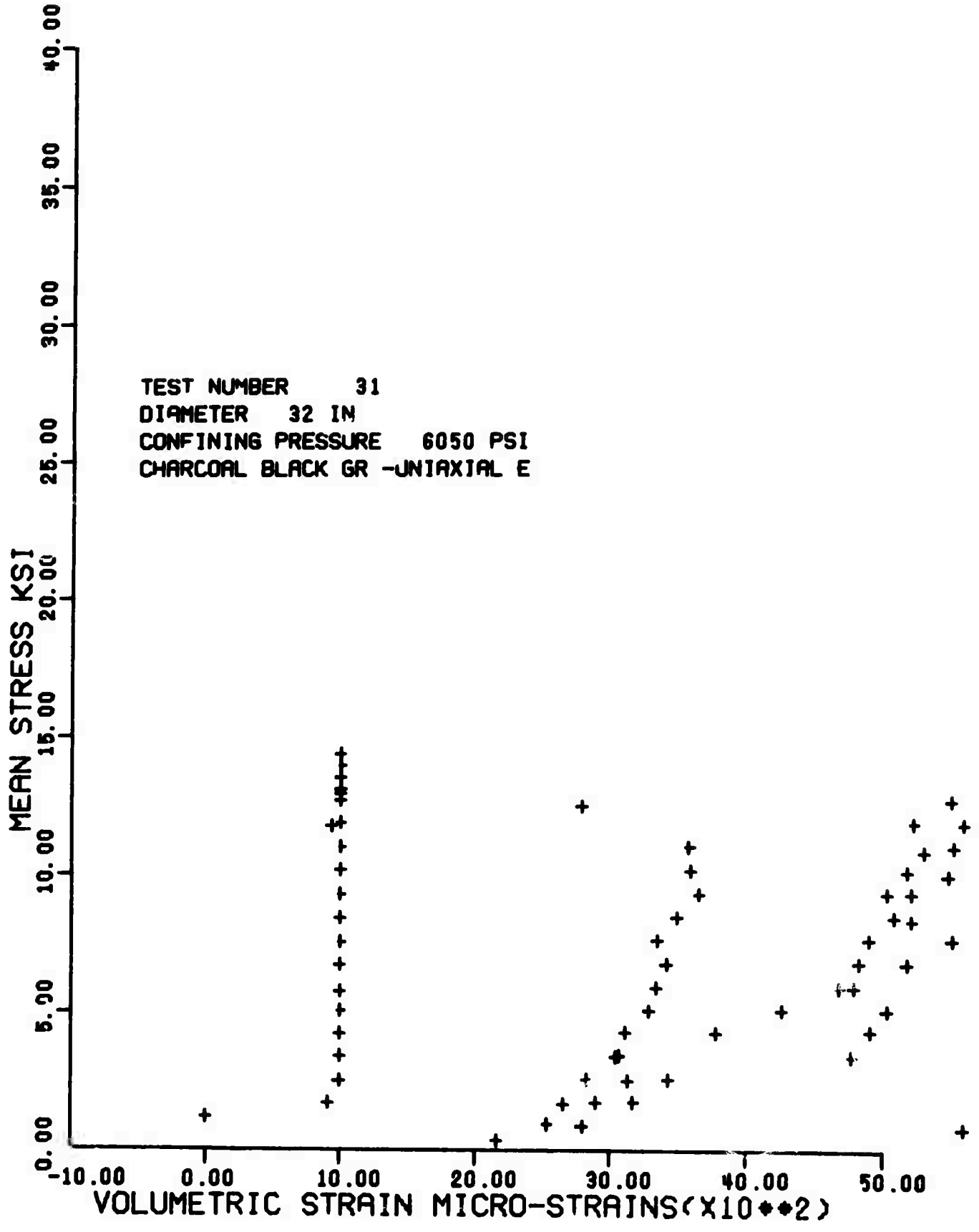
TEST NUMBER 31
DIAMETER 32 IN
CONFINING PRESSURE 6050 PSI
CHARCOAL BLACK GR -UNIAXIAL E
MEAN STRESS KSI
0.00
5.00
10.00
15.00
20.00
25.00
30.00
35.00
40.00
-10.00
0.00
10.00
20.00
30.00
40.00
50.00
VOLUMETRIC STRAIN MICRO-STRAINS(X10**2)

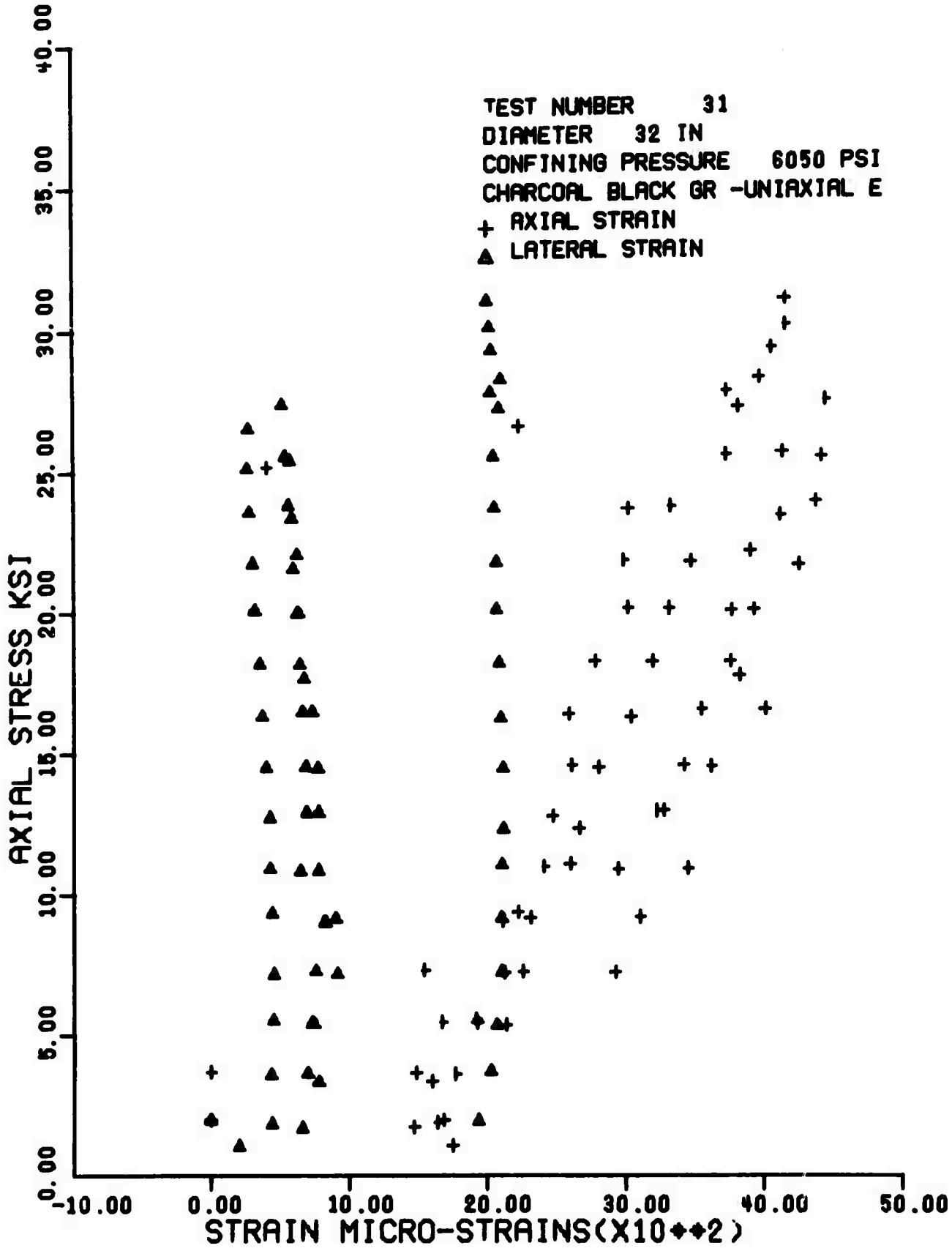
TEST NUMBER 31
DIAMETER 32 IN
CONFINING PRESSURE 6050 PSI
CHARCOAL BLACK GR -UNIAXIAL E
+ AXIAL STRAIN
▲ LATERAL STRAIN
AXIAL STRESS KSI
0.00
5.00
10.00
15.00
20.00
25.00
30.00
35.00
40.00
-10.00
0.00
10.00
20.00
30.00
40.00
50.00
STRAIN MICRO-STRAINS(X10**2)

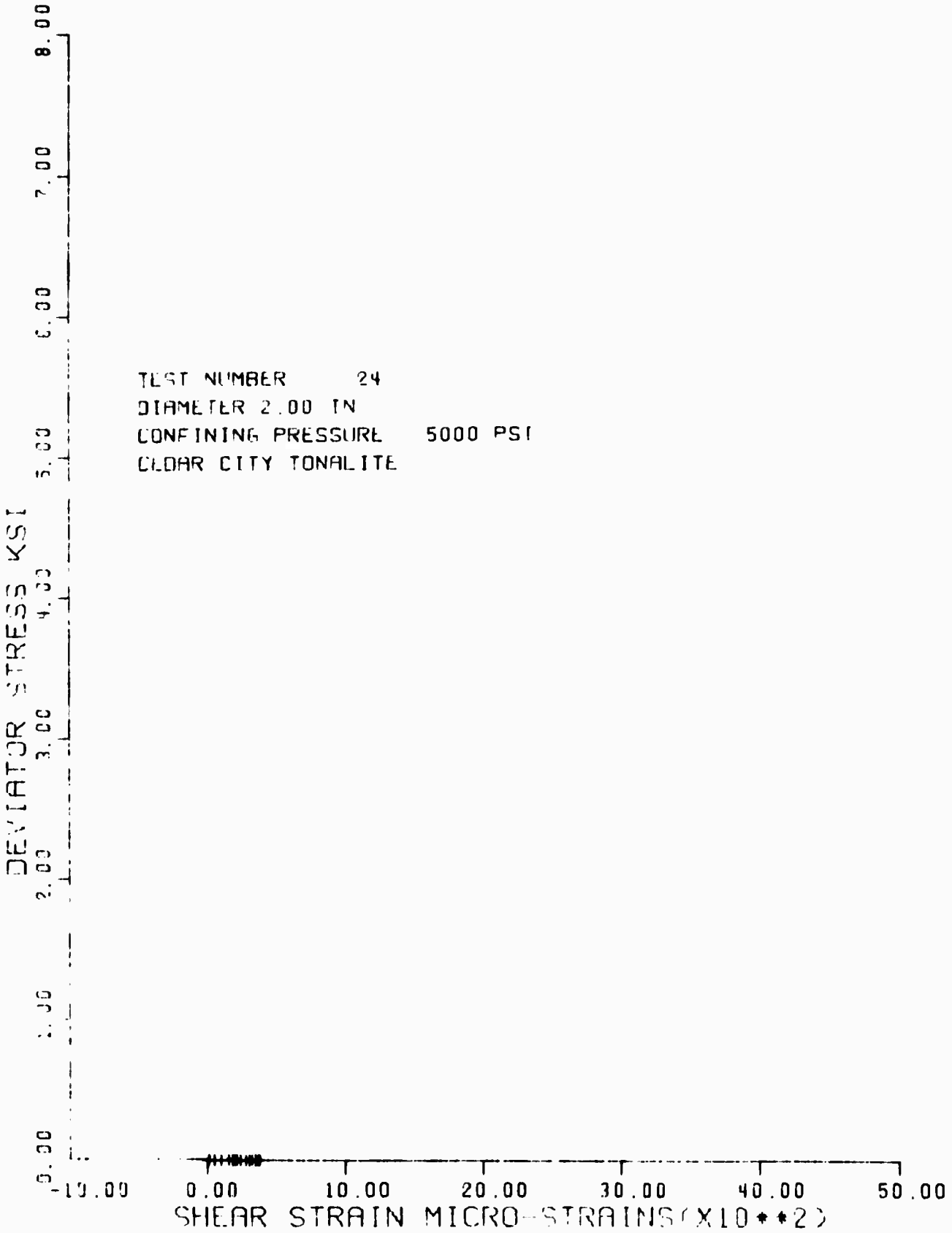
TEST NUMBER 24
DIAMETER 2.00 IN
CONFINING PRESSURE 5000 PSI
CLEAR CITY TONALITE
DEVIATOR STRESS KSI
8.00
7.00
6.00
5.00
4.00
3.00
2.00
1.00
0.00
-10.00
0.00
10.00
20.00
30.00
40.00
50.00
SHEAR STRAIN MICRO-STRAINS(X10**2)

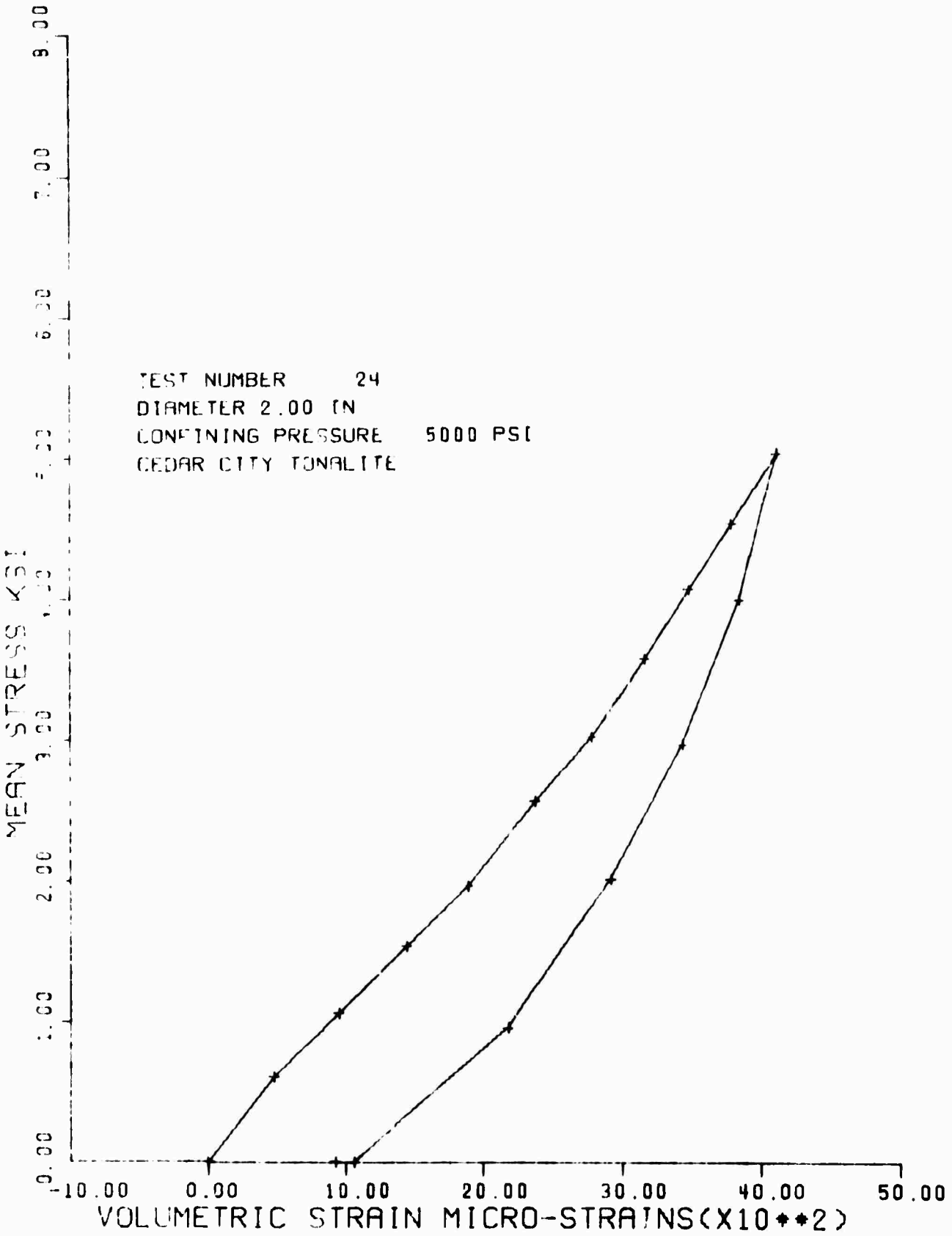
TEST NUMBER 24
DIAMETER 2.00 IN
CONFINING PRESSURE 5000 PSI
CEDAR CITY TONALITE
MEAN STRESS KSI
0.00
2.00
3.00
7.00
8.00
-10.00
0.00
10.00
20.00
30.00
40.00
50.00
VOLUMETRIC STRAIN MICRO-STRAINS(X10**2)

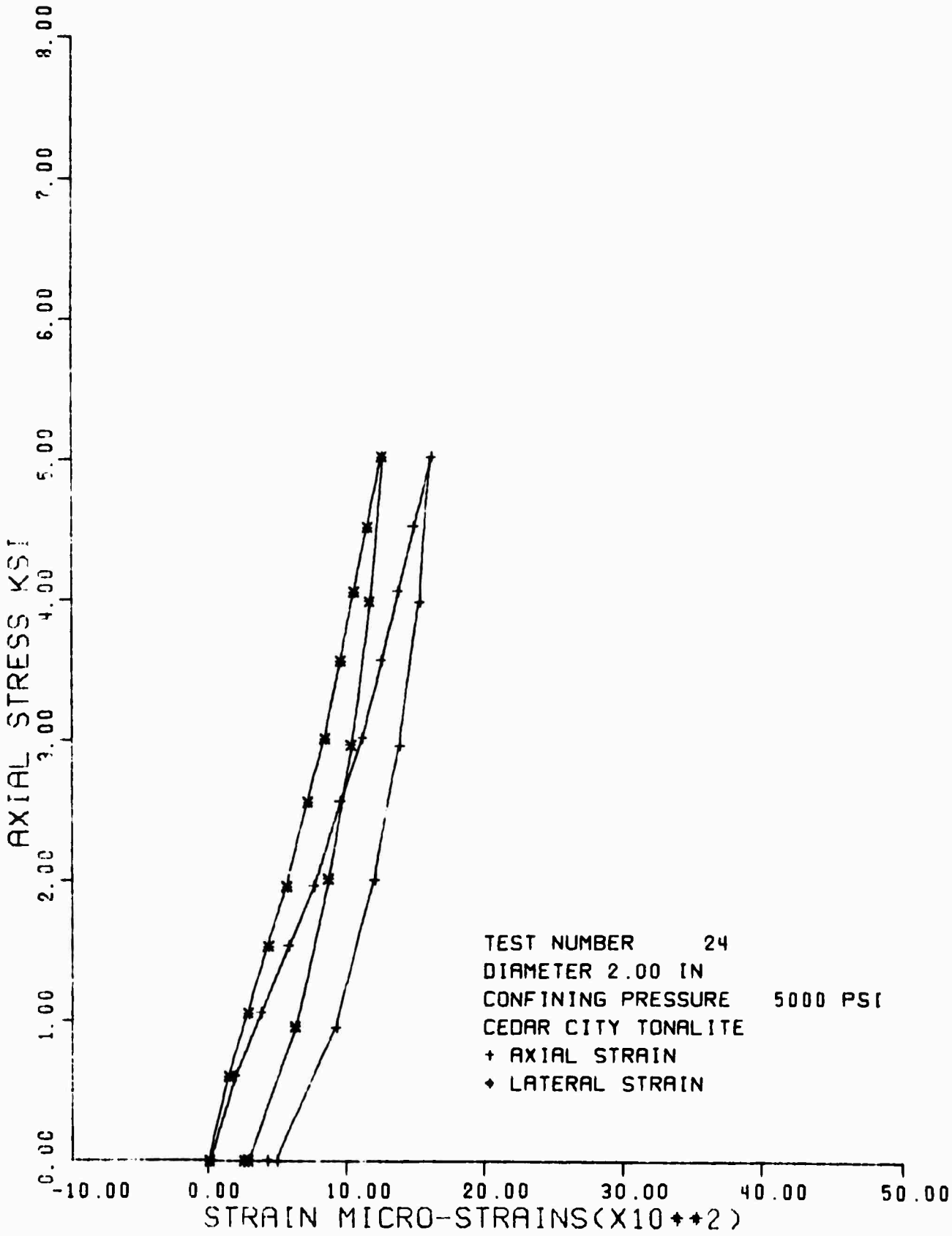
AXIAL STRESS KSI
0.00
1.00
2.00
3.00
4.00
5.00
6.00
7.00
8.00
-10.00
0.00
10.00
20.00
30.00
40.00
50.00
STRAIN MICRO-STRAINS(X10**2)
TEST NUMBER 24
DIAMETER 2.00 IN
CONFINING PRESSURE 5000 PSI
CEDAR CITY TONALITE
+ AXIAL STRAIN
* LATERAL STRAIN

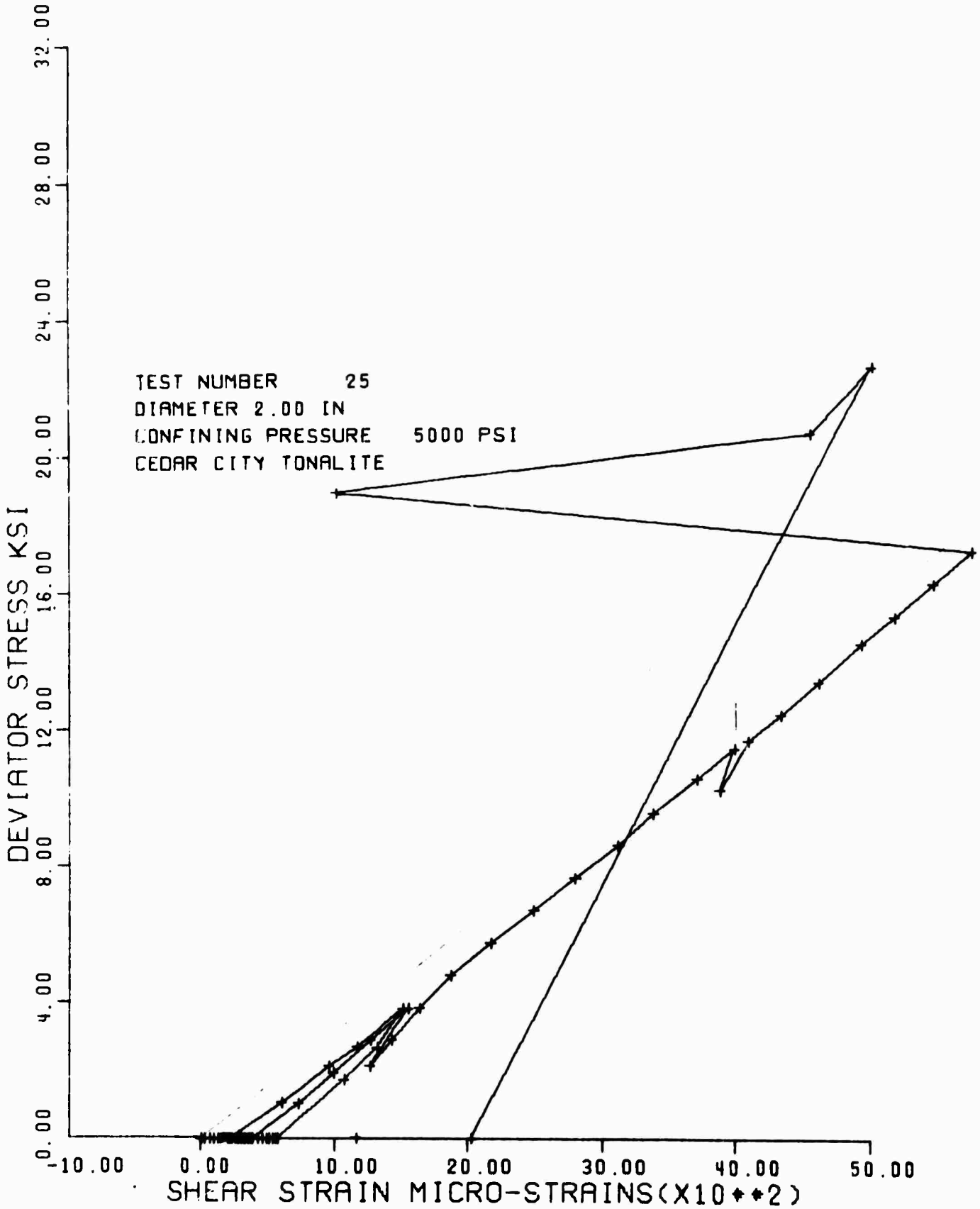
TEST NUMBER 25
DIAMETER 2.00 IN
CONFINING PRESSURE 5000 PSI
CEDAR CITY TONALITE
DEVIATOR STRESS KSI
0.00
4.00
8.00
12.00
16.00
20.00
24.00
28.00
32.00
-10.00
0.00
10.00
20.00
30.00
40.00
50.00
SHEAR STRAIN MICRO-STRAINS(X10**2)

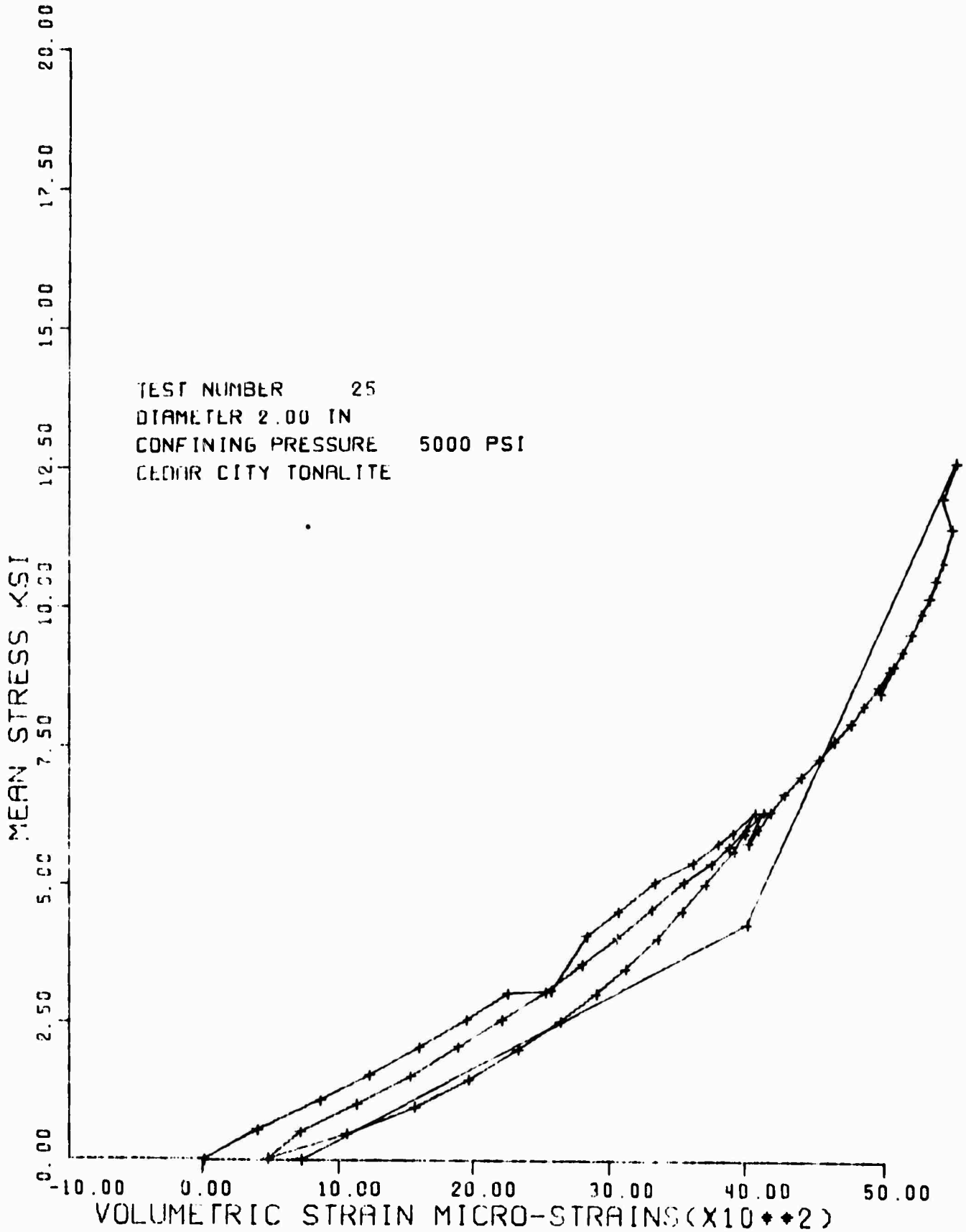
TEST NUMBER 25
DIAMETER 2.00 IN
CONFINING PRESSURE 5000 PSI
CEDAR CITY TONALITE
MEAN STRESS KSI
0.00
2.50
5.00
7.50
10.00
12.50
15.00
17.50
20.00
-10.00
0.00
10.00
20.00
30.00
40.00
50.00
VOLUMETRIC STRAIN MICRO-STRAINS(X10**2)

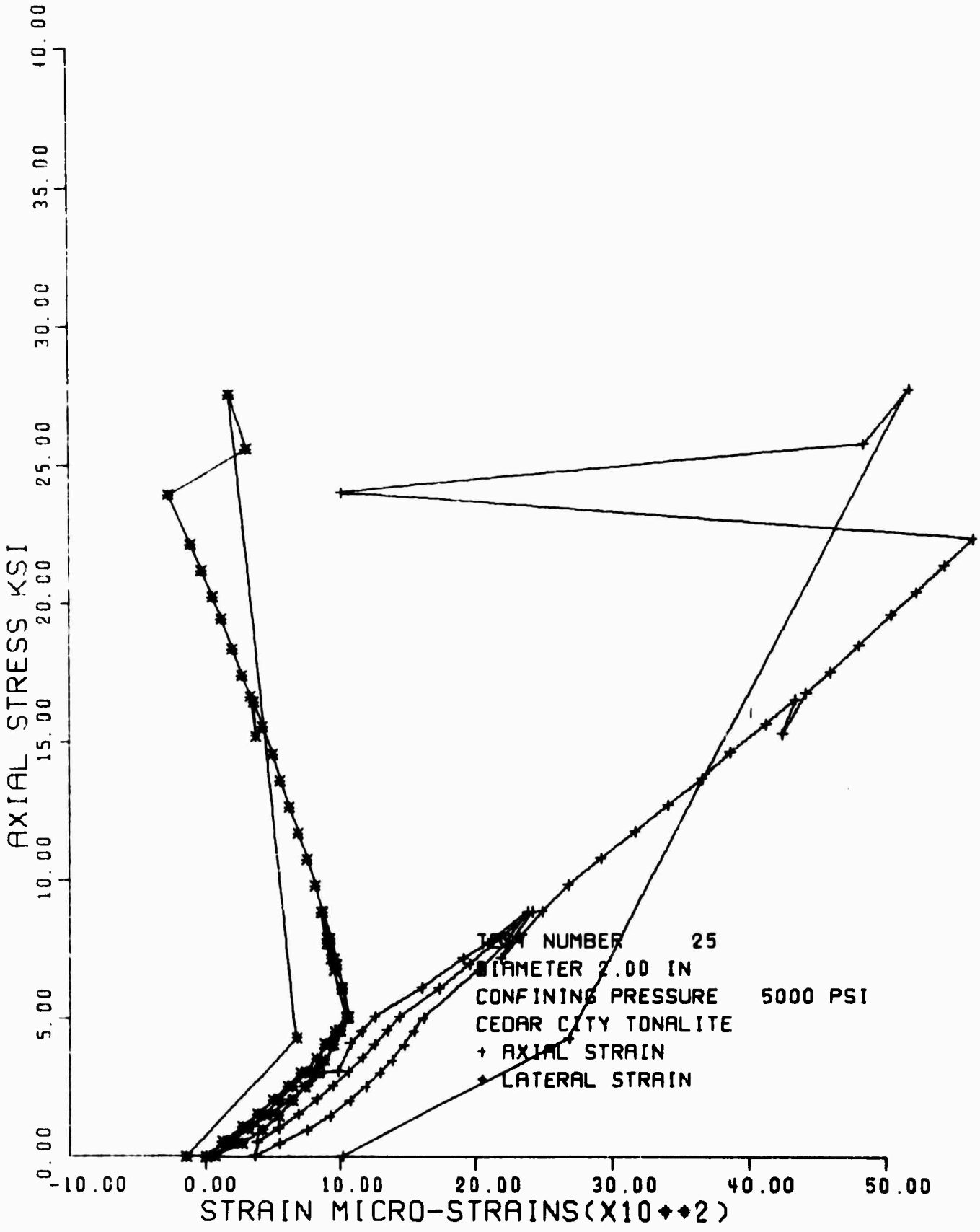
AXIAL STRESS KSI
0.00
5.00
10.00
15.00
20.00
25.00
30.00
35.00
40.00
-10.00
0.00
10.00
20.00
30.00
40.00
50.00
STRAIN MICRO-STRAINS(X10**2)
TEST NUMBER 25
DIAMETER 2.00 IN
CONFINING PRESSURE 5000 PSI
CEDAR CITY TONALITE
+ AXIAL STRAIN
* LATERAL STRAIN

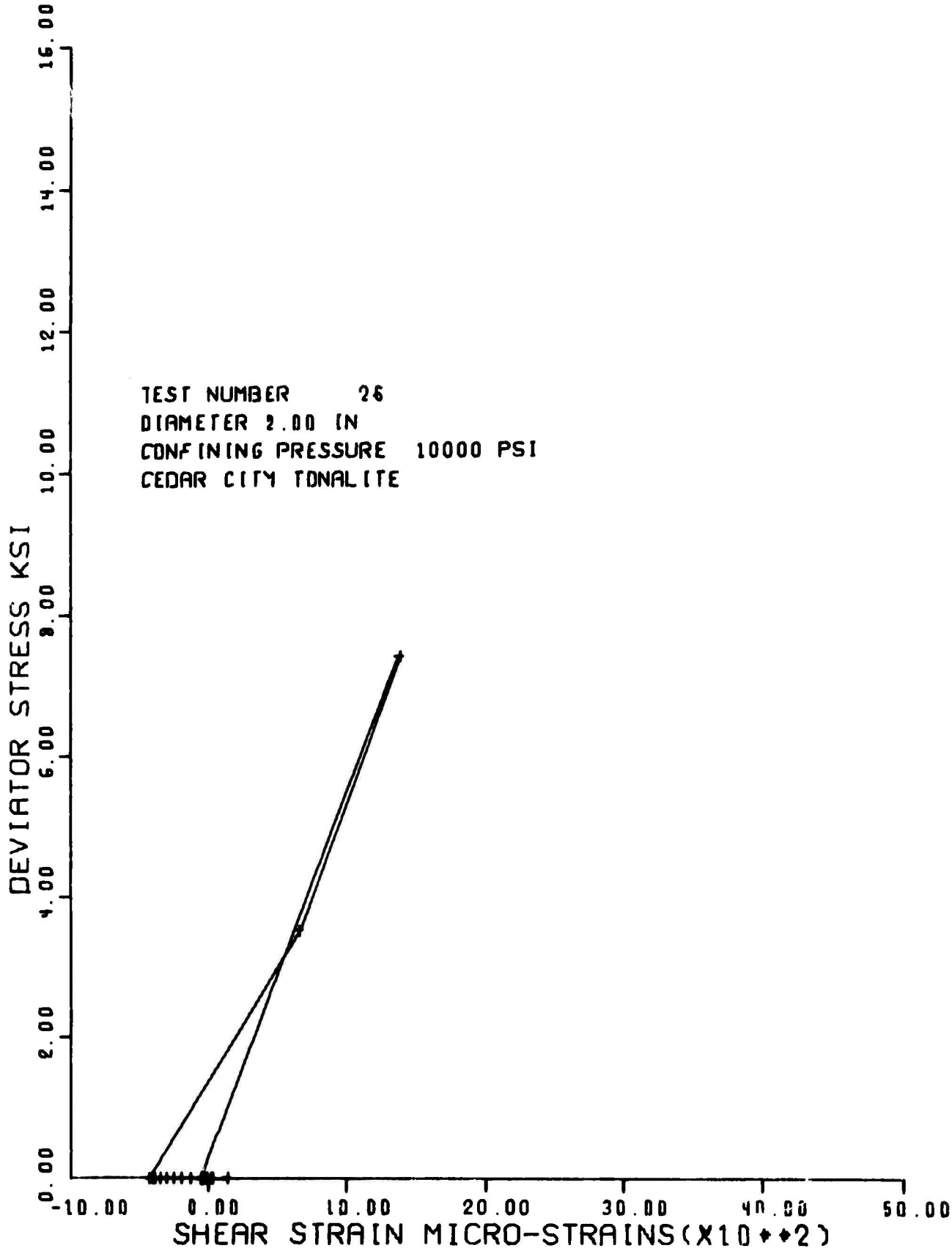
TEST NUMBER 26
DIAMETER 2.00 IN
CONFINING PRESSURE 10000 PSI
CEDAR CITY TONALITE
DEVIATOR STRESS KSI
0.00
2.00
4.00
6.00
8.00
10.00
12.00
14.00
16.00
-10.00
0.00
10.00
20.00
30.00
40.00
50.00
SHEAR STRAIN MICRO-STRAINS(X10**2)

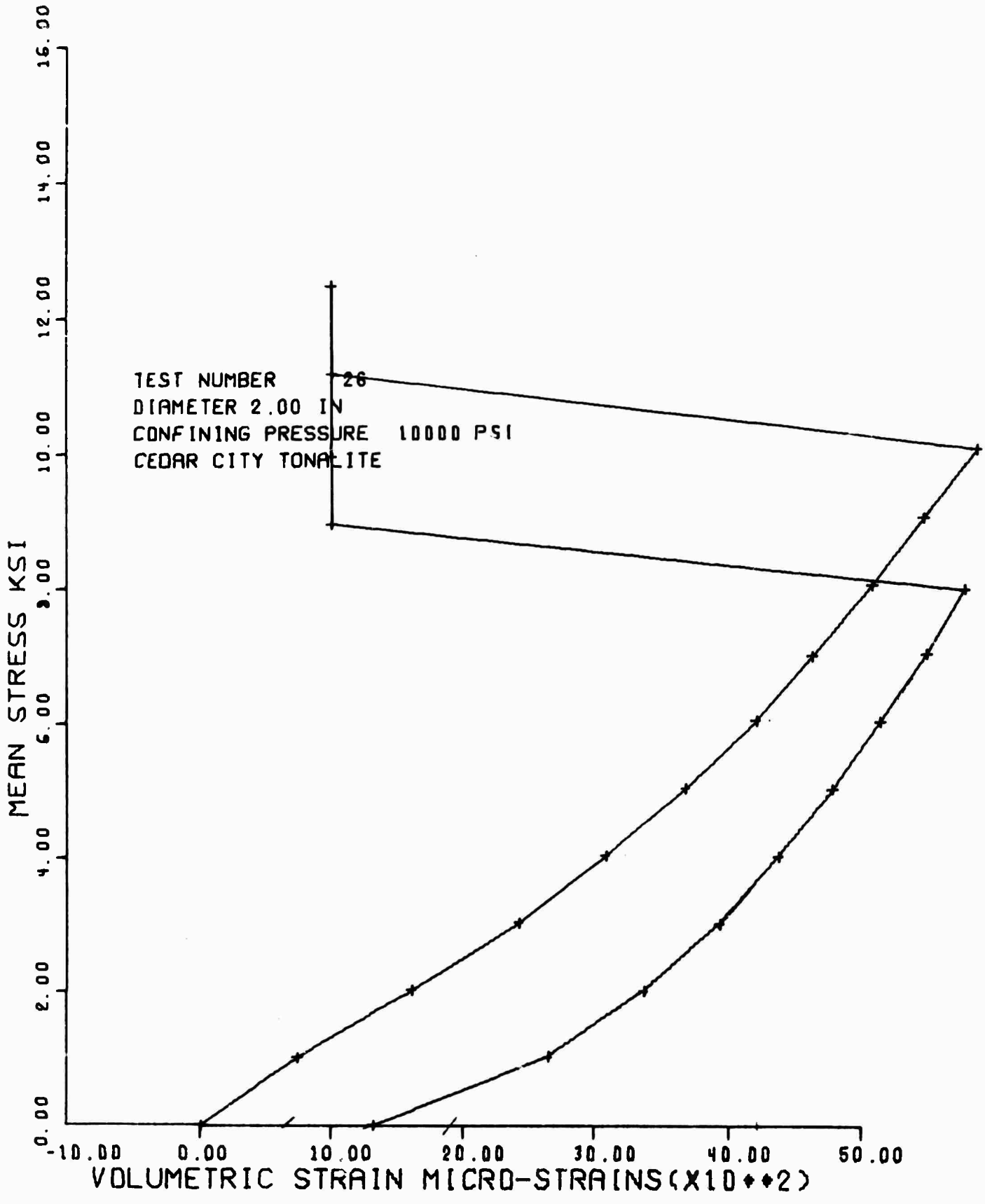
TEST NUMBER 26
DIAMETER 2.00 IN
CONFINING PRESSURE 10000 PSI
CEDAR CITY TONALITE
MEAN STRESS KSI
0.00
2.00
4.00
6.00
8.00
10.00
12.00
14.00
16.00
-10.00
0.00
10.00
20.00
30.00
40.00
50.00
VOLUMETRIC STRAIN MICRO-STRAINS(X10**2)

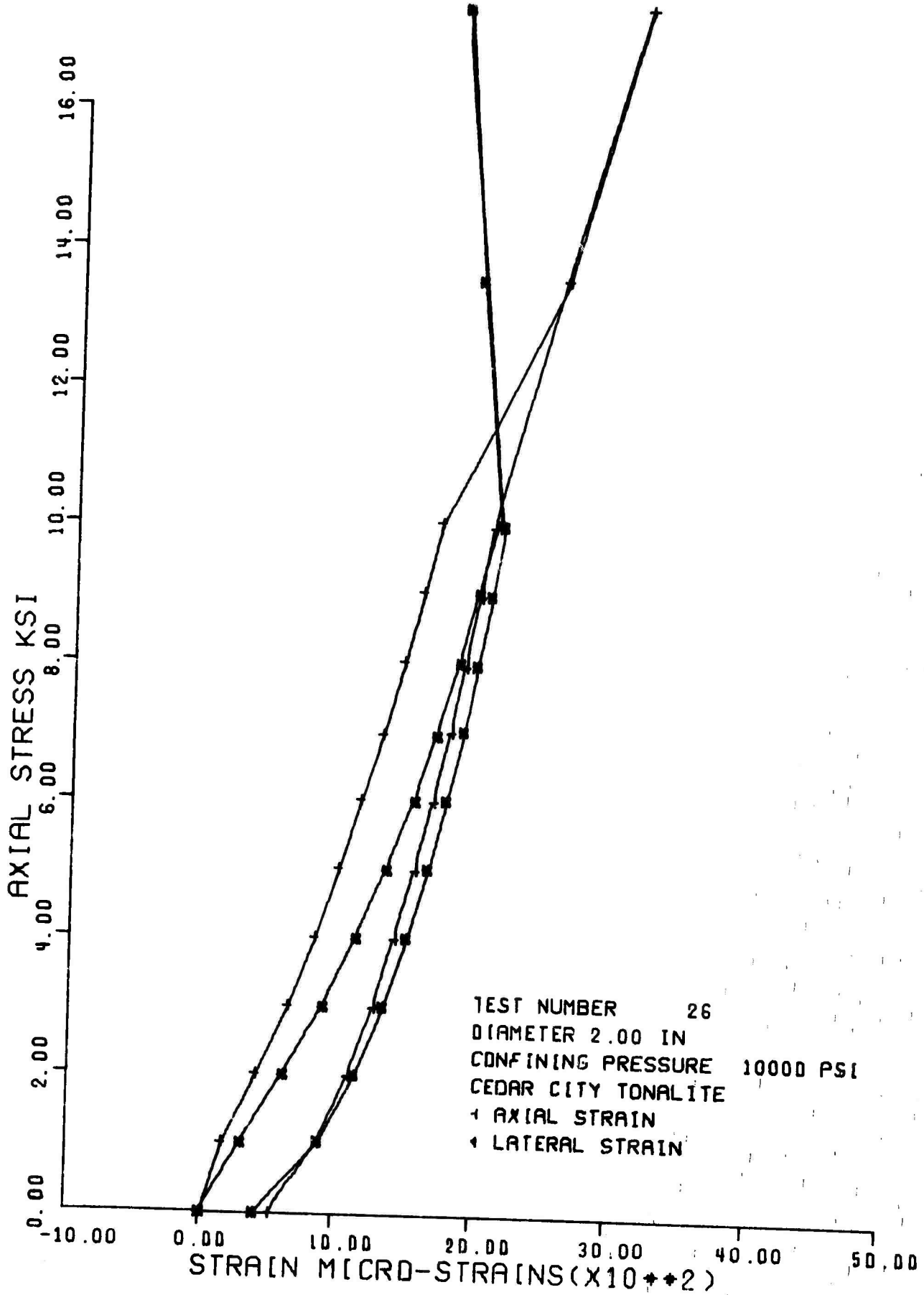
AXIAL STRESS KSI
0.00
2.00
4.00
6.00
8.00
10.00
12.00
14.00
16.00
-10.00
0.00
10.00
20.00
30.00
40.00
50.00
STRAIN MICRO-STRAINS(X10**2)
TEST NUMBER 26
DIAMETER 2.00 IN
CONFINING PRESSURE 10000 PSI
CEDAR CITY TONALITE
1 AXIAL STRAIN
1 LATERAL STRAIN

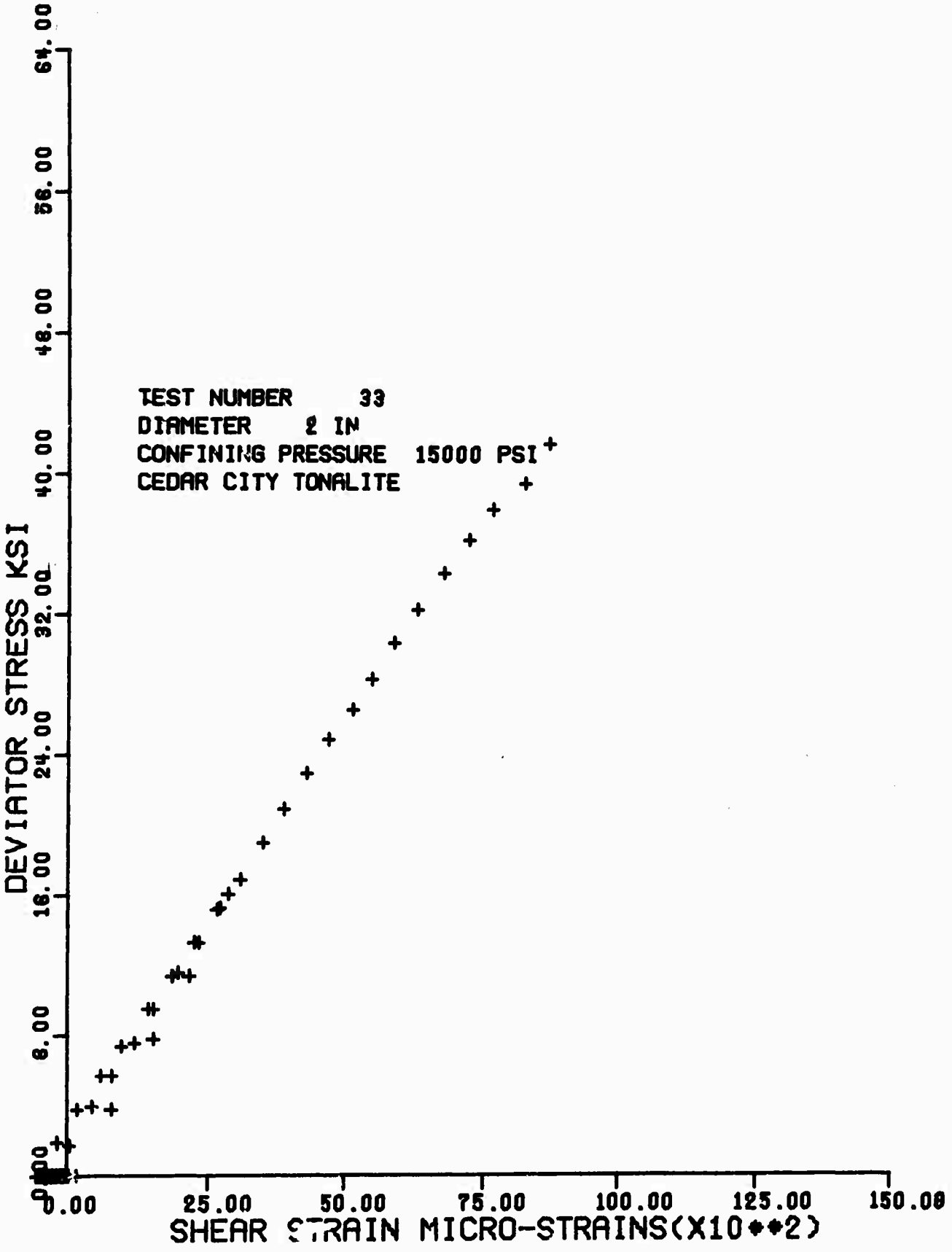
TEST NUMBER 33
DIAMETER 2 IN
CONFINING PRESSURE 15000 PSI
CEDAR CITY TONALITE
DEVIATOR STRESS KSI
64.00
56.00
48.00
40.00
32.00
24.00
16.00
8.00
0.00
0.00
25.00
50.00
75.00
100.00
125.00
150.00
SHEAR STRAIN MICRO-STRAINS(X10**2)

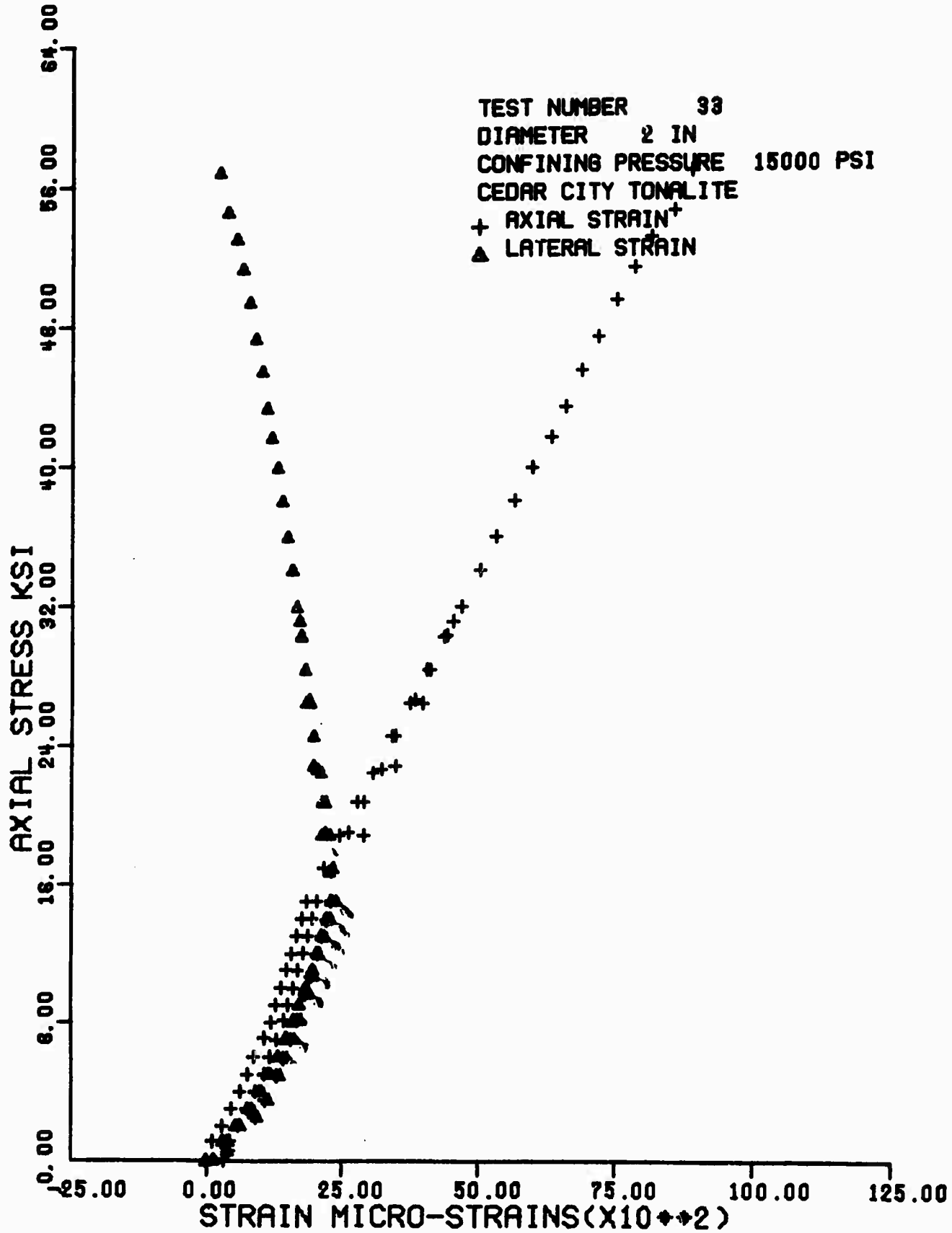
TEST NUMBER 33
DIAMETER 2 IN
CONFINING PRESSURE 15000 PSI
CEDAR CITY TONALITE
+ AXIAL STRAIN
▲ LATERAL STRAIN
AXIAL STRESS KSI
0.00
8.00
16.00
24.00
32.00
40.00
48.00
56.00
64.00
-25.00
0.00
25.00
50.00
75.00
100.00
125.00
STRAIN MICRO-STRAINS(X10**2)

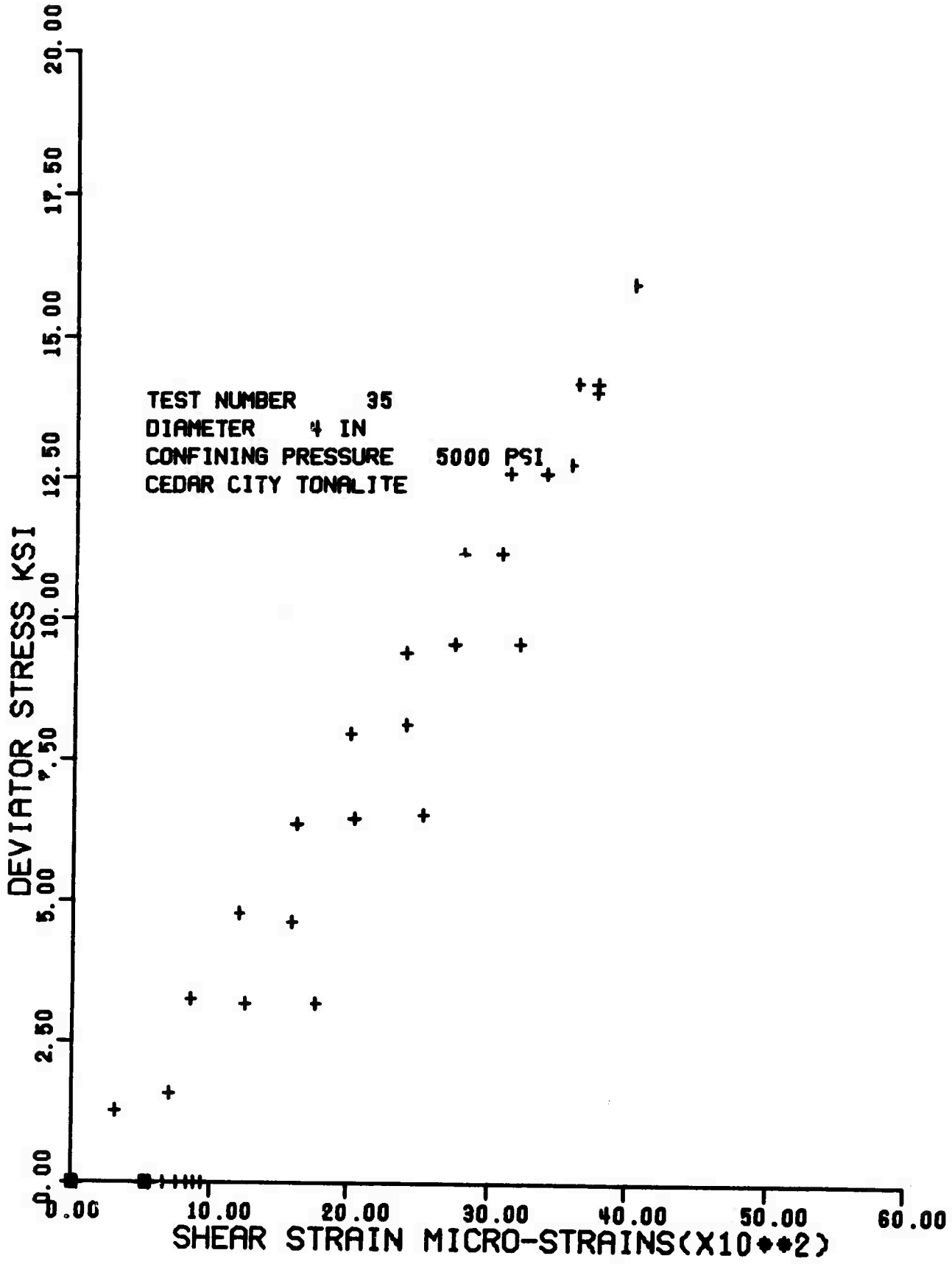
TEST NUMBER 35
DIAMETER 4 IN
CONFINING PRESSURE 5000 PSI
CEDAR CITY TONALITE
DEVIATOR STRESS KSI
0.00
2.50
5.00
7.50
10.00
12.50
15.00
17.50
20.00
0.00
10.00
20.00
30.00
40.00
50.00
60.00
SHEAR STRAIN MICRO-STRAINS(X10**2)

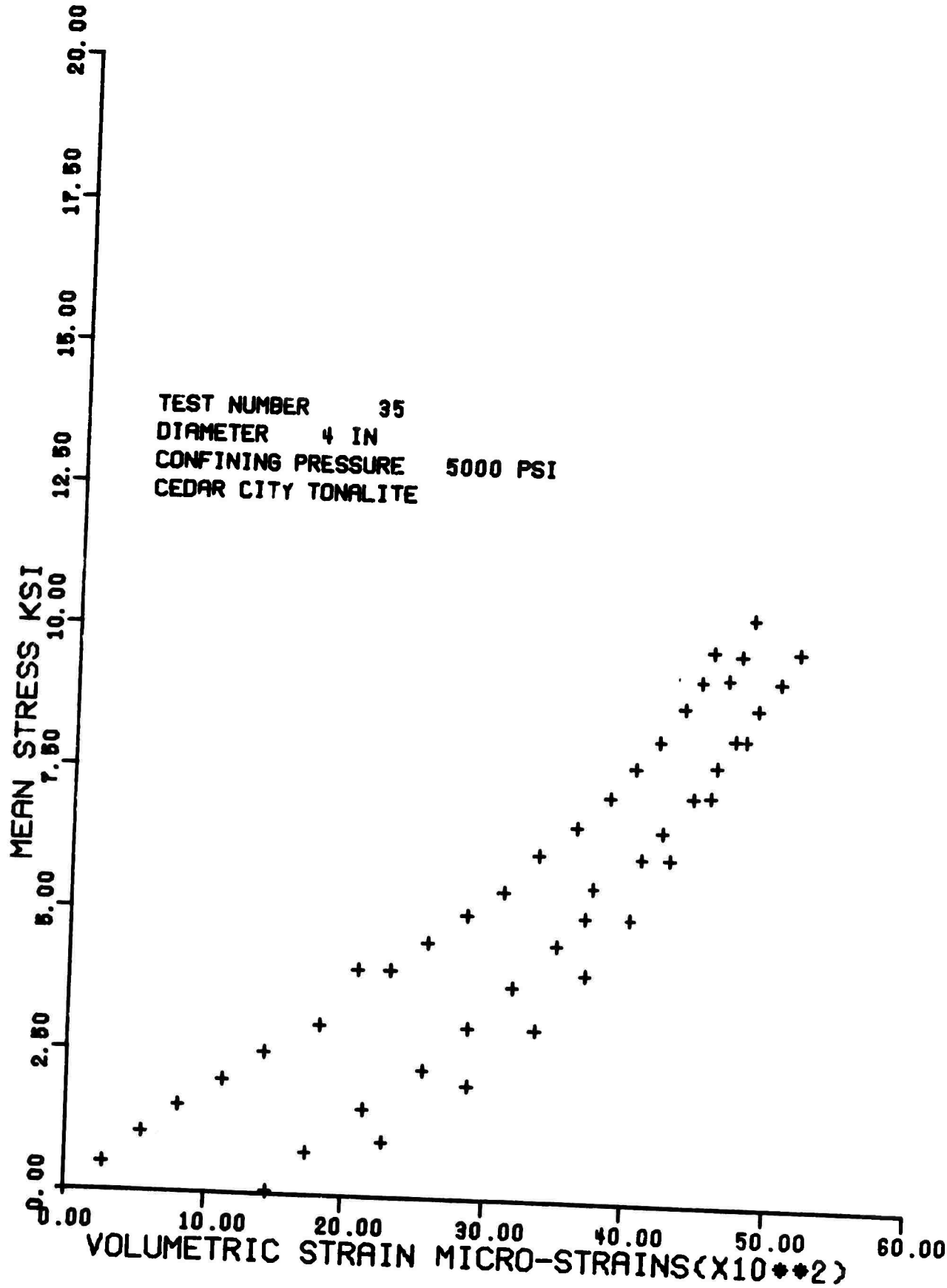
TEST NUMBER 35
DIAMETER 4 IN
CONFINING PRESSURE 5000 PSI
CEDAR CITY TONALITE
MEAN STRESS KSI
0.00
2.50
5.00
7.50
10.00
12.50
15.00
17.50
20.00
0.00
10.00
20.00
30.00
40.00
50.00
60.00
VOLUMETRIC STRAIN MICRO-STRAINS(X10**2)

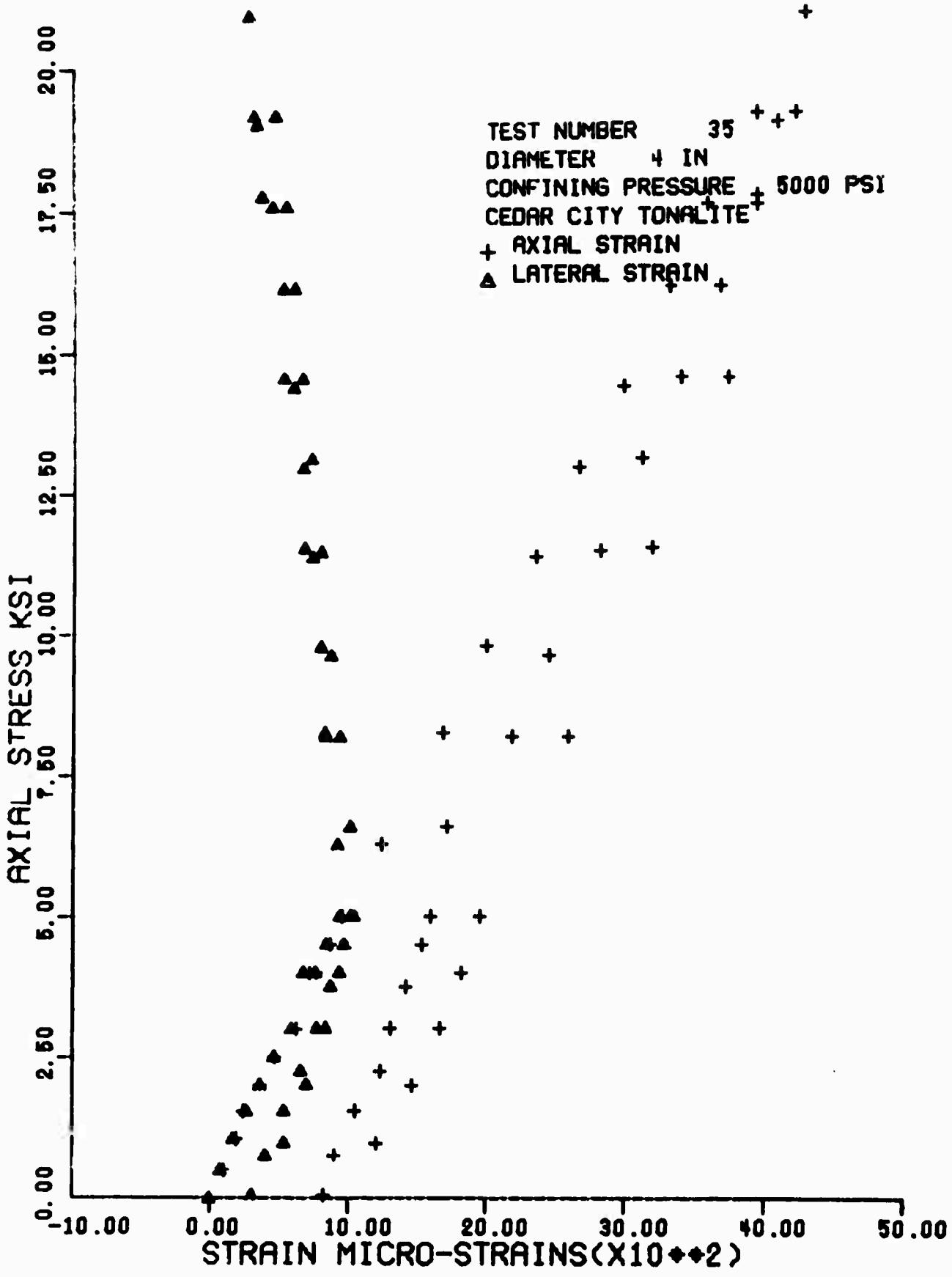
TEST NUMBER 35
DIAMETER 4 IN
CONFINING PRESSURE 5000 PSI
CEDAR CITY TONALITE
+ AXIAL STRAIN
△ LATERAL STRAIN
AXIAL STRESS KSI
0.00
2.50
5.00
7.50
10.00
12.50
15.00
17.50
20.00
-10.00
0.00
10.00
20.00
30.00
40.00
50.00
STRAIN MICRO-STRAINS(X10**2)

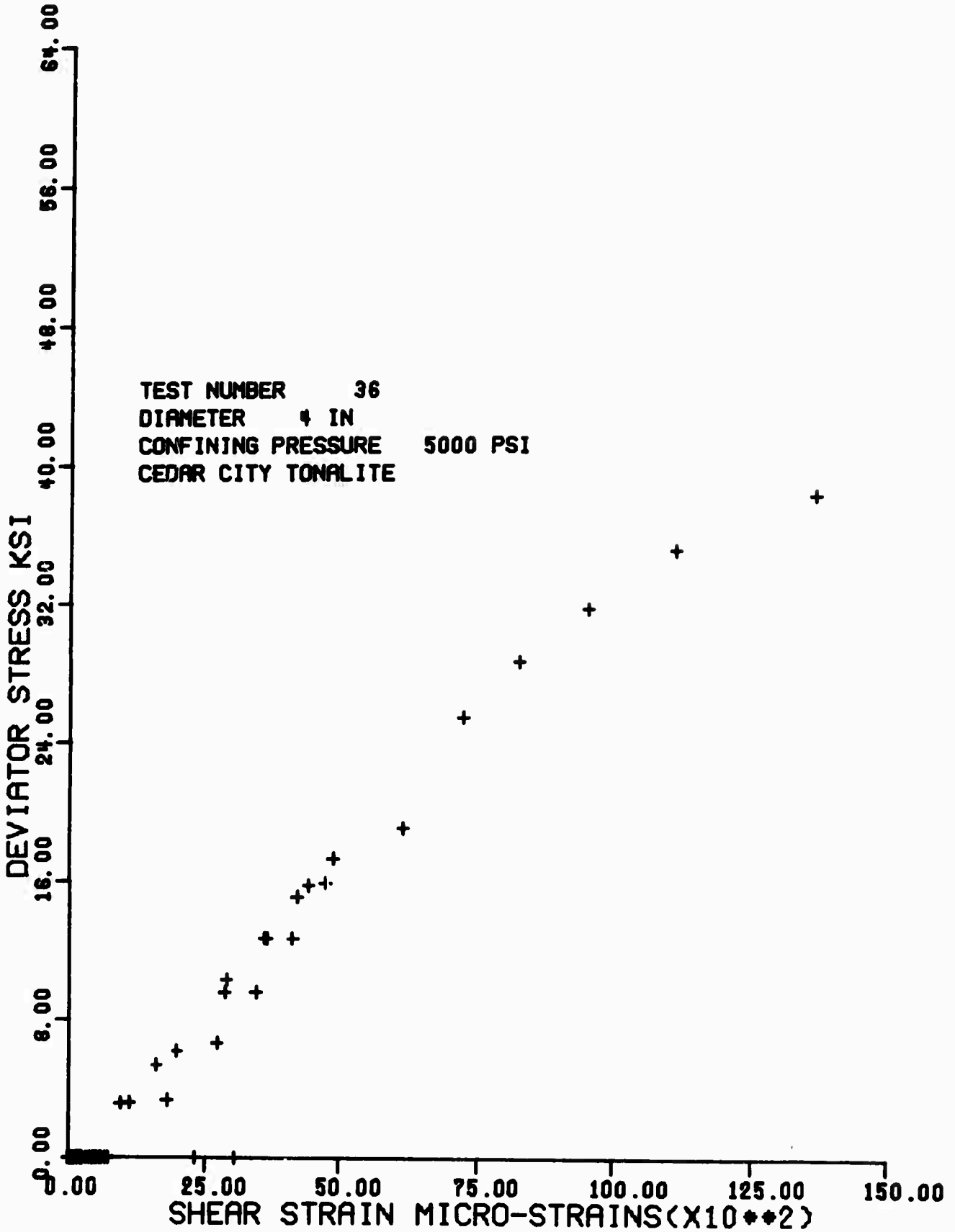
TEST NUMBER 36
DIAMETER 4 IN
CONFINING PRESSURE 5000 PSI
CEDAR CITY TONALITE
DEVIATOR STRESS KSI
0.00
8.00
16.00
24.00
32.00
40.00
48.00
56.00
64.00
0.00
25.00
50.00
75.00
100.00
125.00
150.00
SHEAR STRAIN MICRO-STRAINS(X10**2)

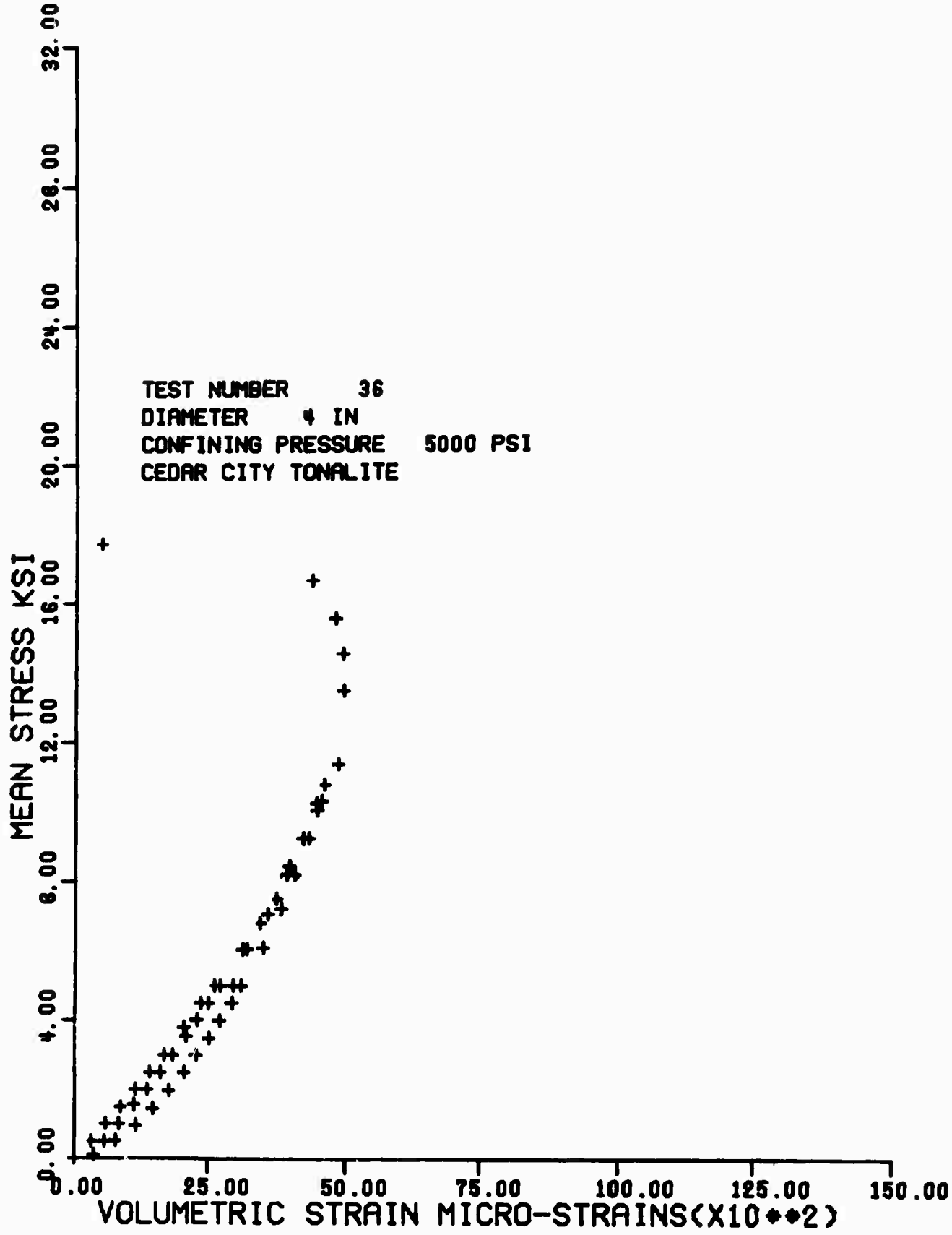
TEST NUMBER 36
DIAMETER 4 IN
CONFINING PRESSURE 5000 PSI
CEDAR CITY TONALITE
MEAN STRESS KSI
0.00
4.00
8.00
12.00
16.00
20.00
24.00
28.00
32.00
0.00
25.00
50.00
75.00
100.00
125.00
150.00
VOLUMETRIC STRAIN MICRO-STRAINS(X10**2)

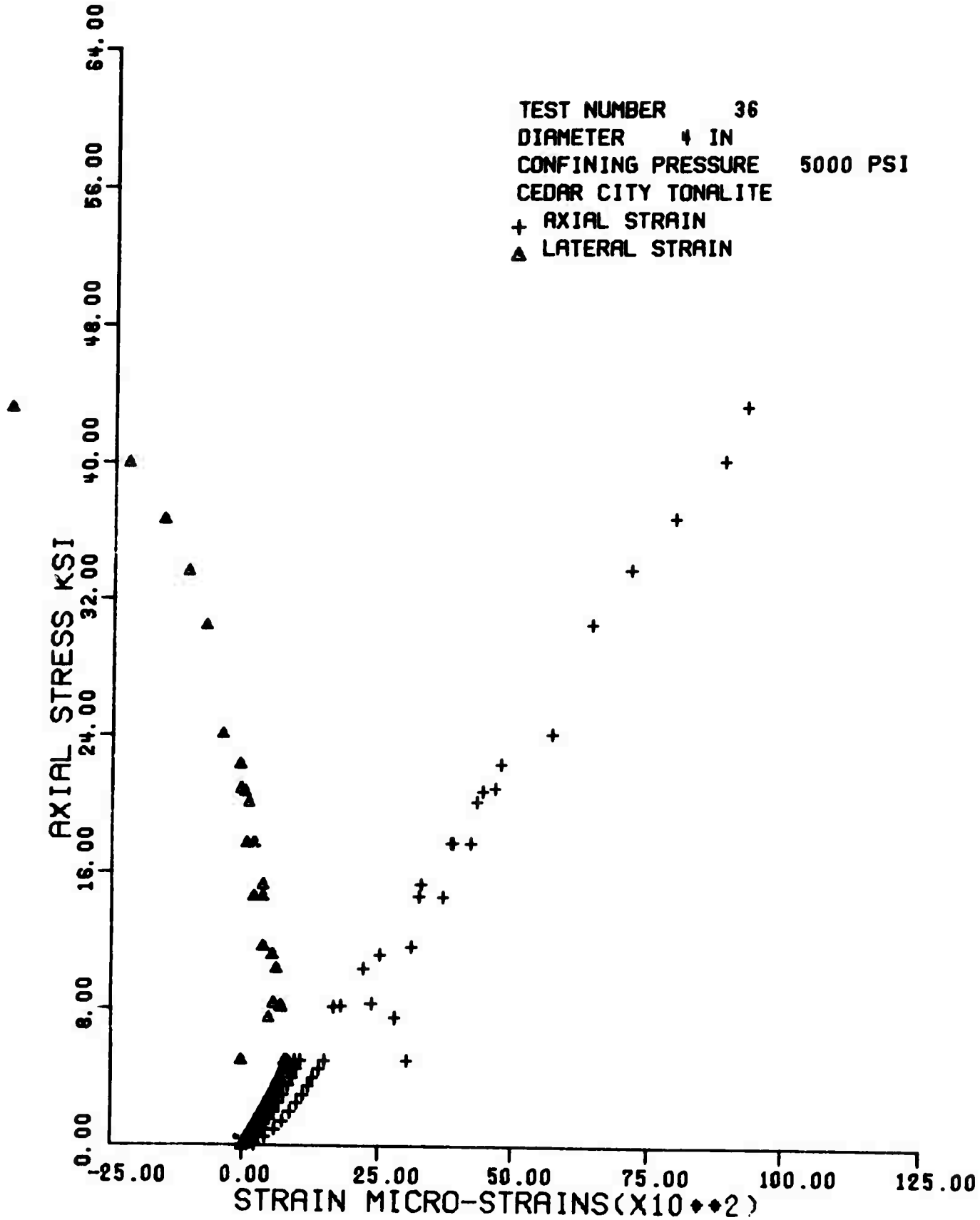
TEST NUMBER 36
DIAMETER 4 IN
CONFINING PRESSURE 5000 PSI
CEDAR CITY TONALITE
+ AXIAL STRAIN
▲ LATERAL STRAIN
AXIAL STRESS KSI
0.00
8.00
16.00
24.00
32.00
40.00
48.00
56.00
64.00
-25.00
0.00
25.00
50.00
75.00
100.00
125.00
STRAIN MICRO-STRAINS(X10**2)

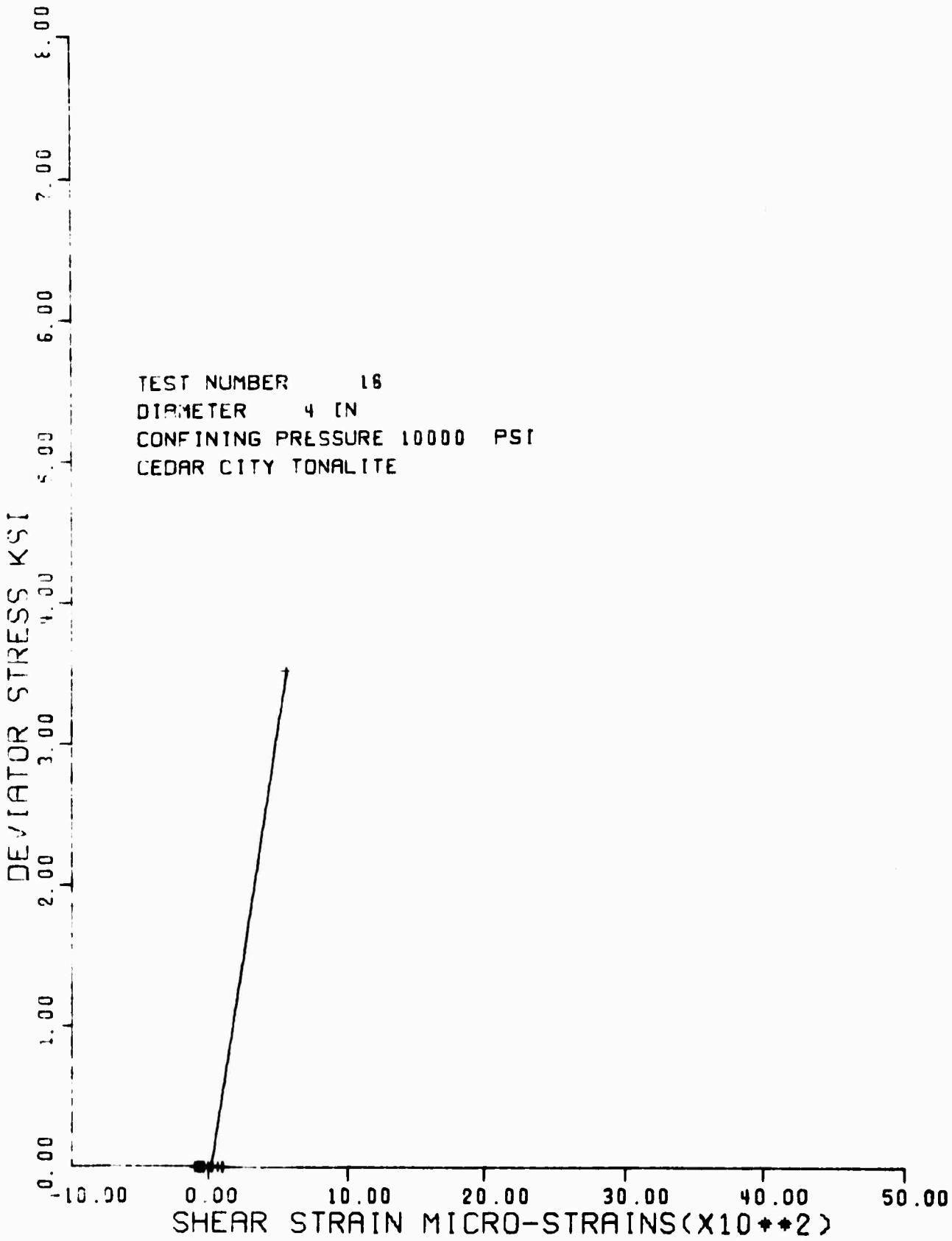
TEST NUMBER 16
DIAMETER 4 IN
CONFINING PRESSURE 10000 PSI
CEDAR CITY TONALITE
DEVIATOR STRESS KSI
0.00
1.00
2.00
3.00
4.00
5.00
6.00
7.00
8.00
-10.00
0.00
10.00
20.00
30.00
40.00
50.00
SHEAR STRAIN MICRO-STRAINS(X10**2)

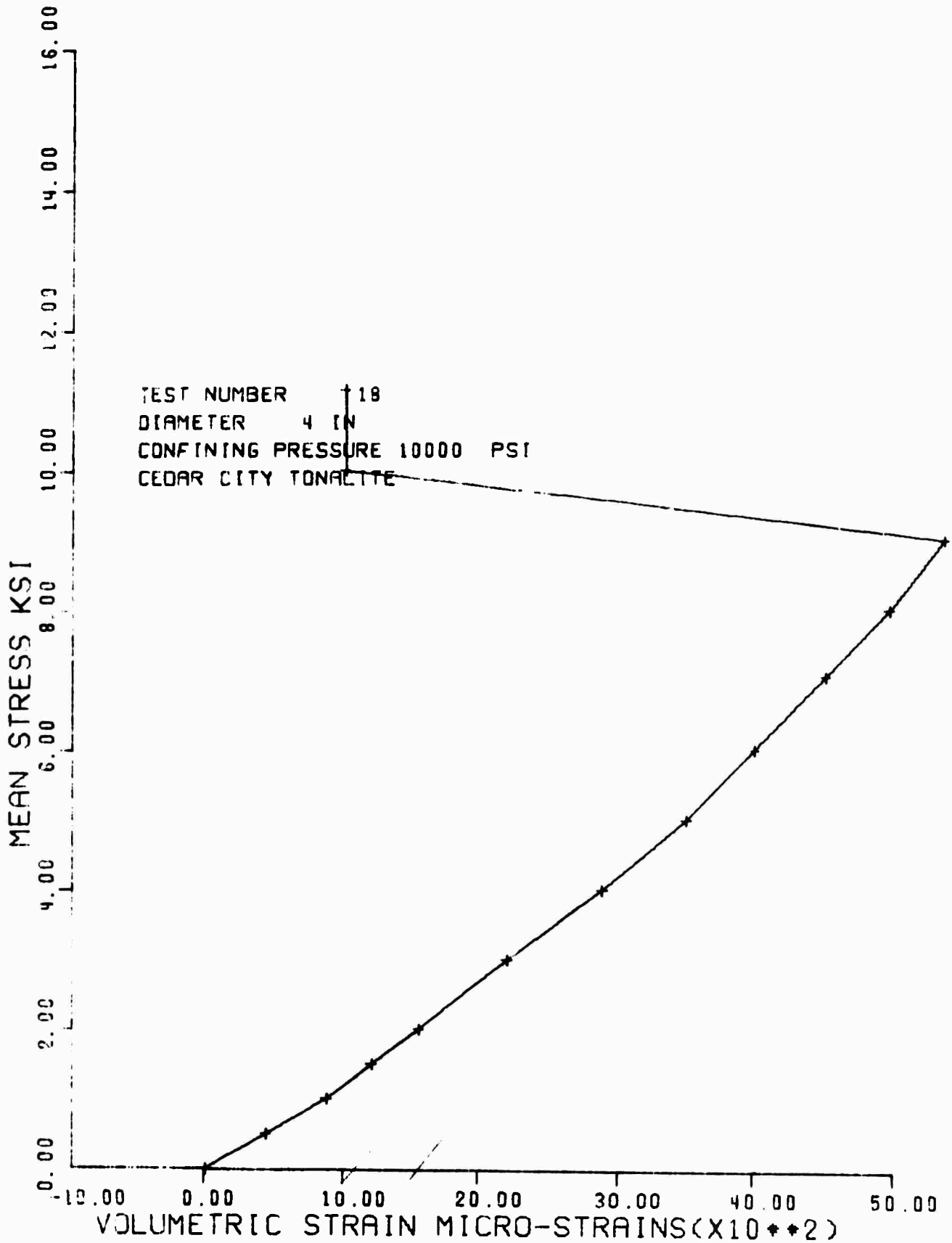
TEST NUMBER 18
DIAMETER 4 IN
CONFINING PRESSURE 10000 PSI
CEDAR CITY TONALITE
MEAN STRESS KSI
0.00
2.00
4.00
6.00
8.00
10.00
12.00
14.00
16.00
-10.00
0.00
10.00
20.00
30.00
40.00
50.00
VOLUMETRIC STRAIN MICRO-STRAINS(X10**2)

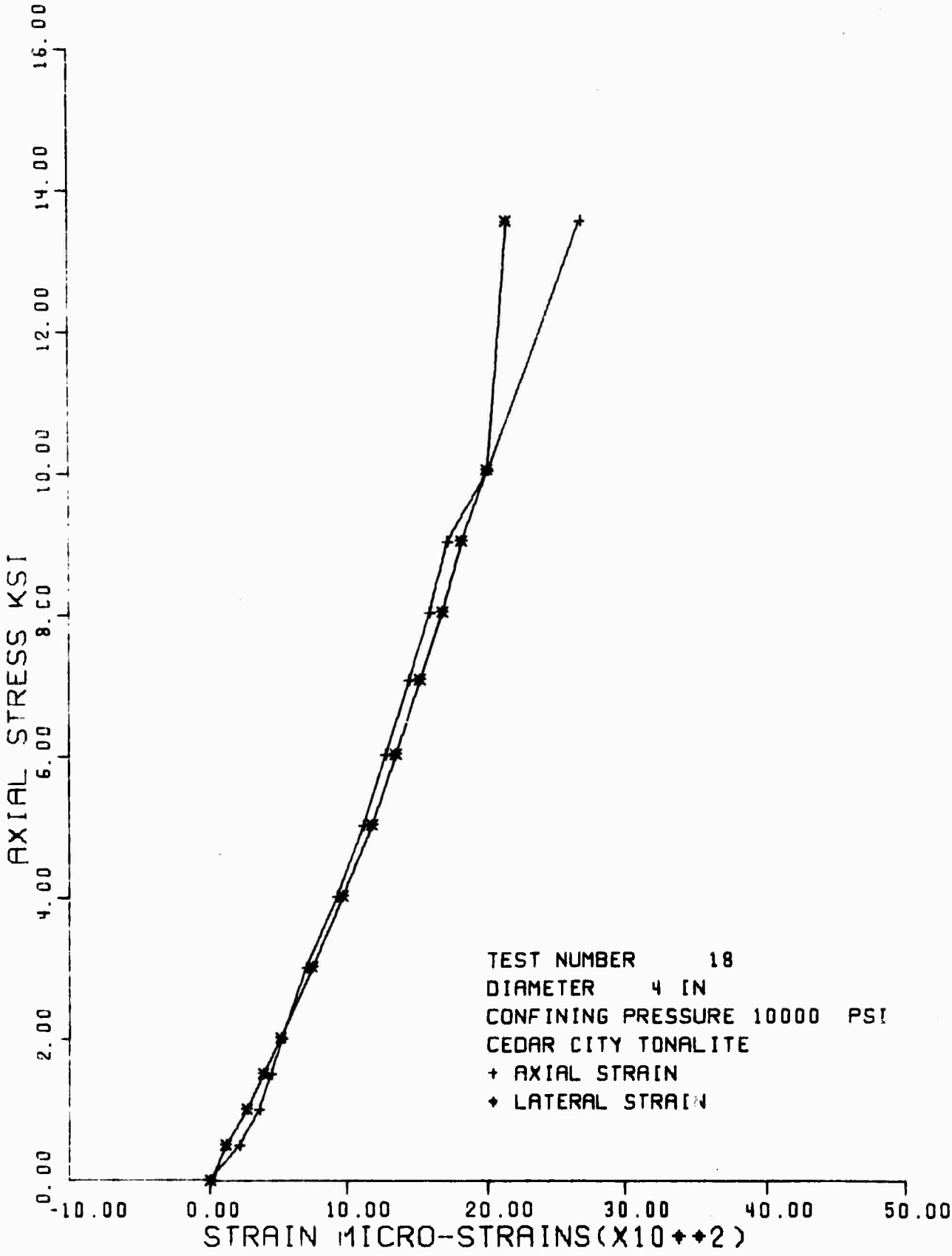
AXIAL STRESS KSI
0.00
2.00
4.00
6.00
8.00
10.00
12.00
14.00
16.00
-10.00
0.00
10.00
20.00
30.00
40.00
50.00
STRAIN MICRO-STRAINS(X10**2)
TEST NUMBER 18
DIAMETER 4 IN
CONFINING PRESSURE 10000 PSI
CEDAR CITY TONALITE
+ AXIAL STRAIN
* LATERAL STRAIN

7.3.79

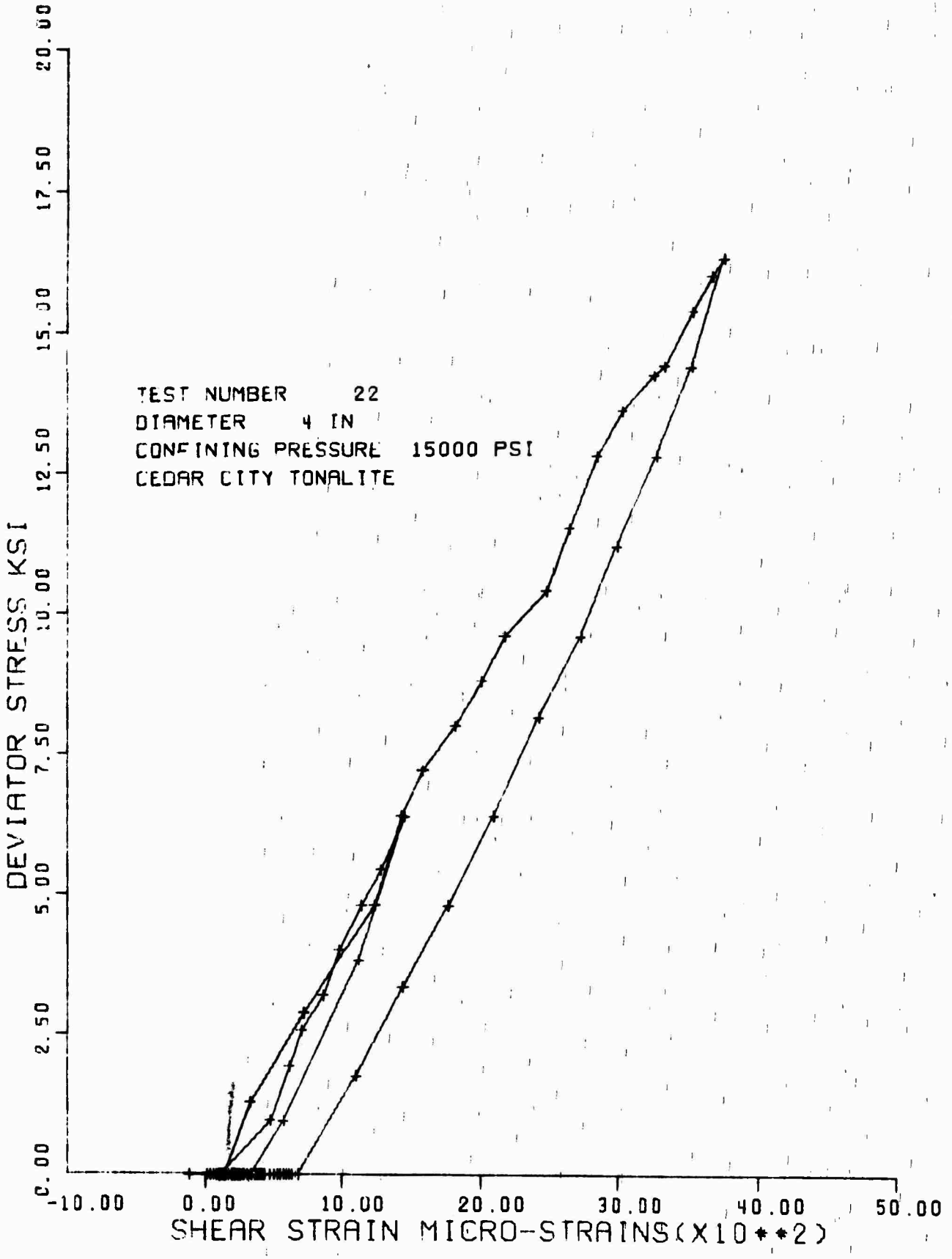
TEST NUMBER 22
DIAMETER 4 IN
CONFINING PRESSURE 15000 PSI
CEDAR CITY TONALITE
DEVIATOR STRESS KSI
0.00
2.50
5.00
7.50
10.00
12.50
15.00
17.50
20.00
-10.00
0.00
10.00
20.00
30.00
40.00
50.00
SHEAR STRAIN MICRO-STRAINS(X10**2)

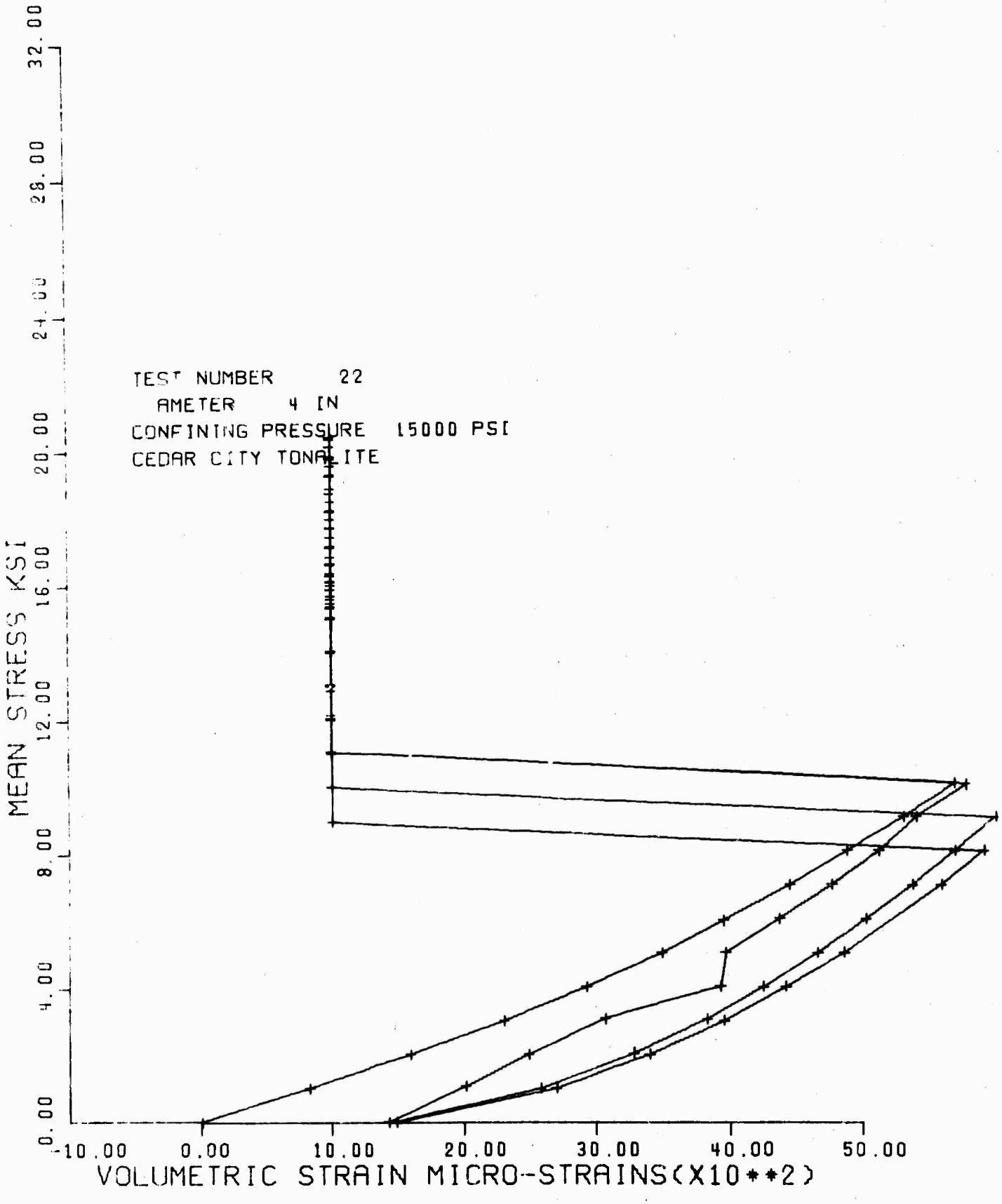
TEST NUMBER 22
AMETER 4 IN
CONFINING PRESSURE 15000 PSI
CEDAR CITY TONALITE
MEAN STRESS KSI
0.00
4.00
8.00
12.00
16.00
20.00
24.00
28.00
32.00
-10.00
0.00
10.00
20.00
30.00
40.00
50.00
VOLUMETRIC STRAIN MICRO-STRAINS(X10**2)

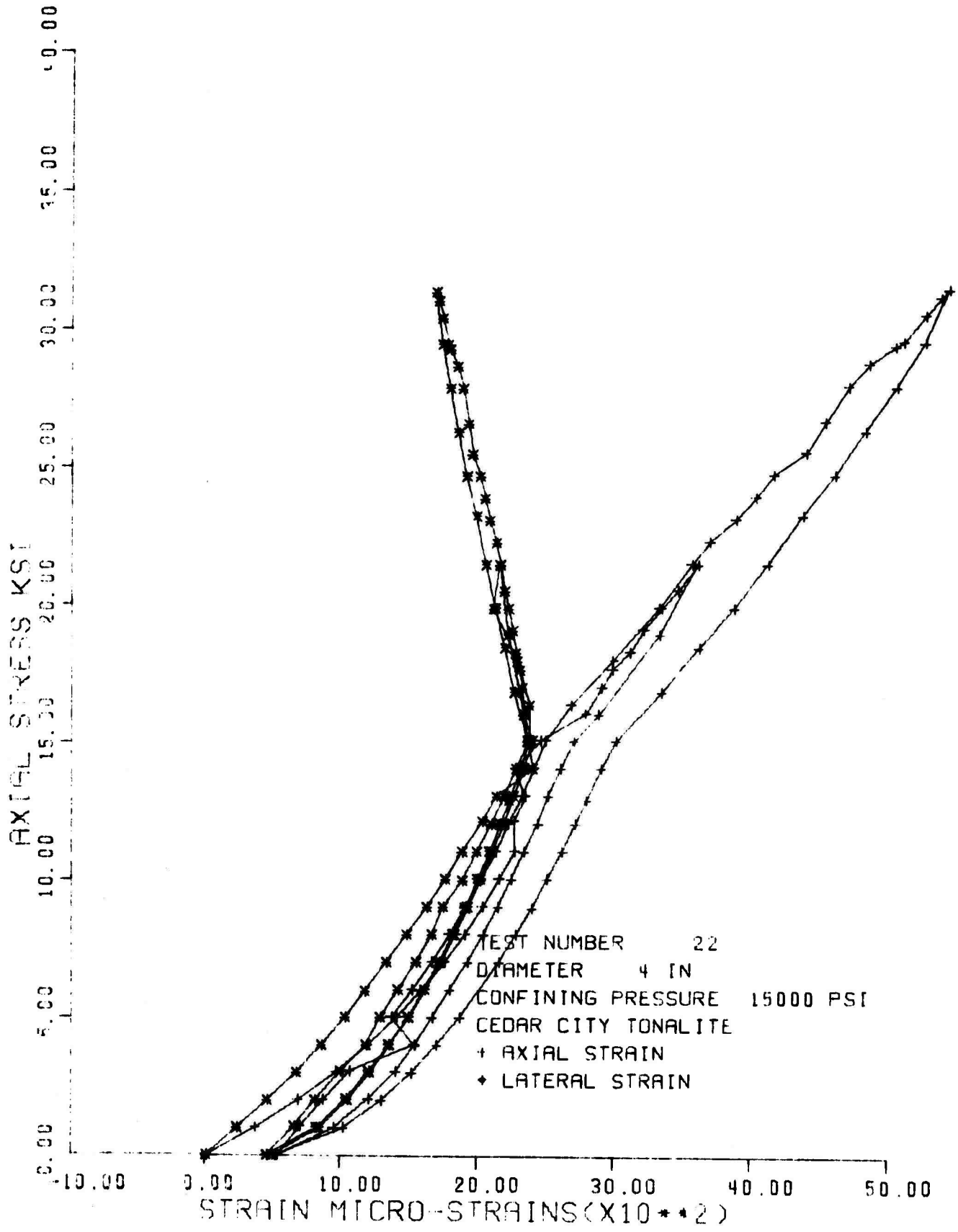
AXIAL STRESS KSI
STRAIN MICRO-STRAINS(X10**2)
-10.00
0.00
10.00
20.00
30.00
40.00
50.00
TEST NUMBER 22
DIAMETER 4 IN
CONFINING PRESSURE 15000 PSI
CEDAR CITY TONALITE
+ AXIAL STRAIN
* LATERAL STRAIN

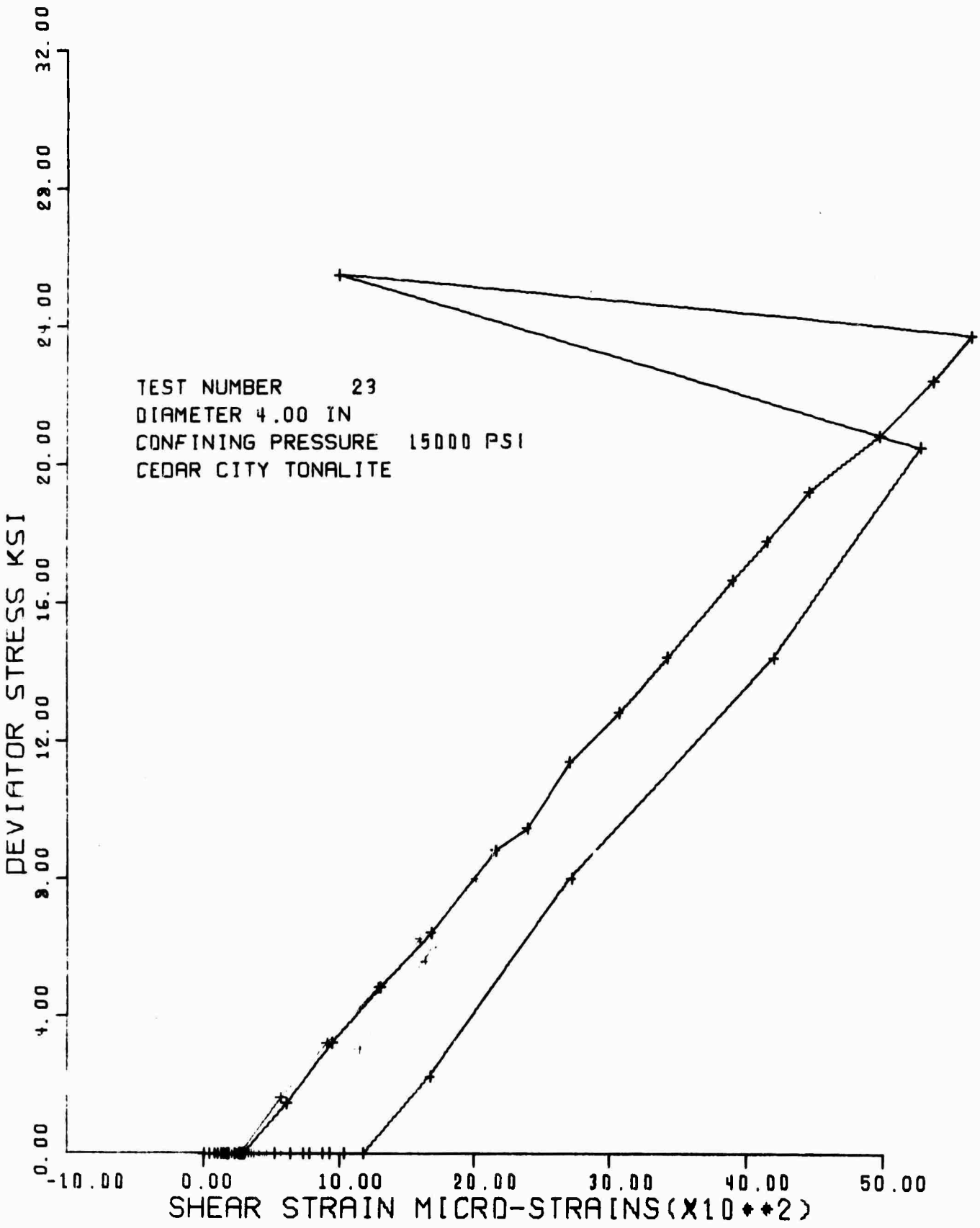
TEST NUMBER 23
DIAMETER 4.00 IN
CONFINING PRESSURE 15000 PSI
CEDAR CITY TONALITE
DEVIATOR STRESS KSI
0.00
4.00
8.00
12.00
16.00
20.00
24.00
28.00
32.00
-10.00
0.00
10.00
20.00
30.00
40.00
50.00
SHEAR STRAIN MICRO-STRAINS(X10**2)

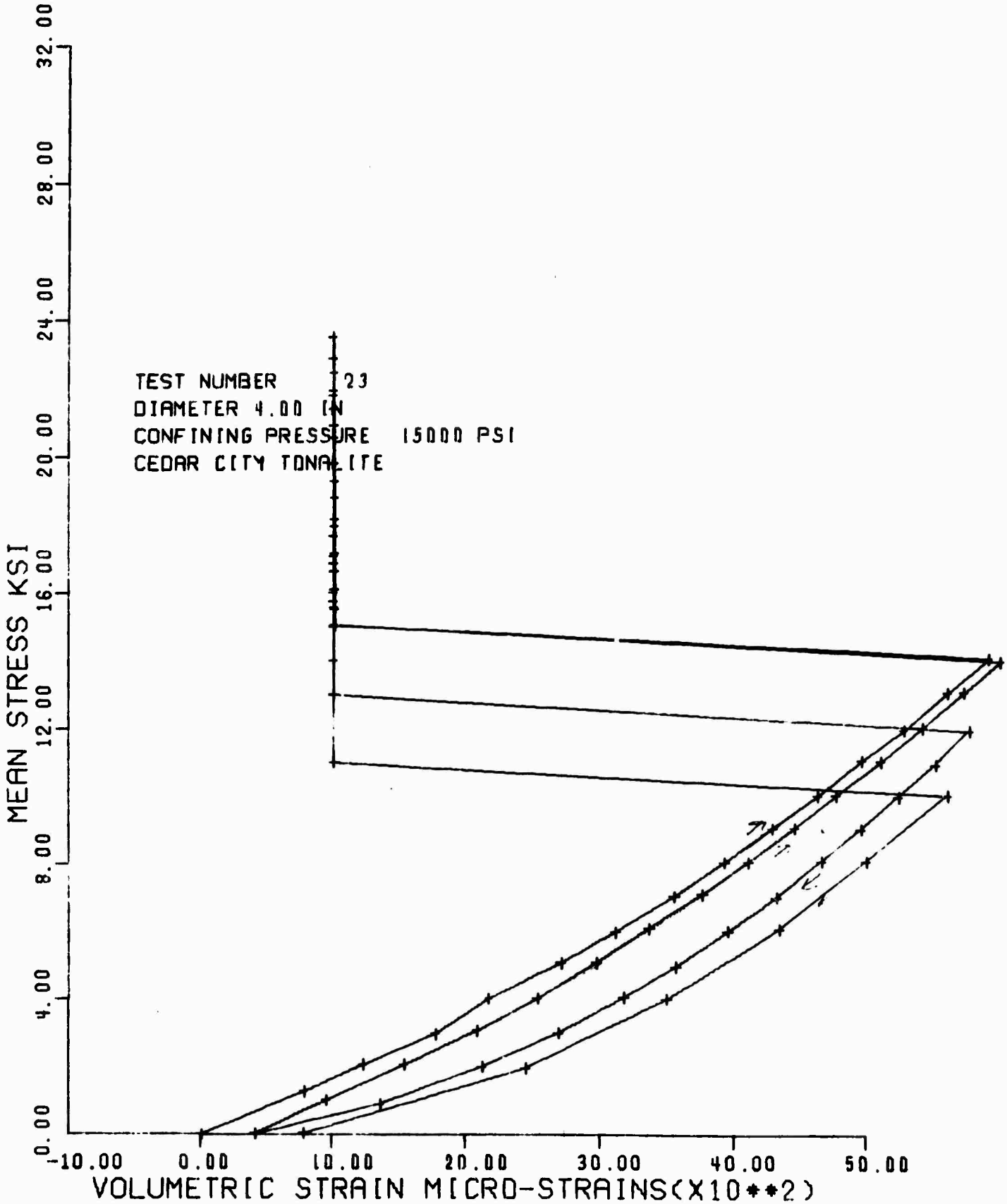
TEST NUMBER 23
DIAMETER 4.00 IN
CONFINING PRESSURE 15000 PSI
CEDAR CITY TONALITE
MEAN STRESS KSI
0.00
4.00
8.00
12.00
16.00
20.00
24.00
28.00
32.00
-10.00
0.00
10.00
20.00
30.00
40.00
50.00
VOLUMETRIC STRAIN MICRO-STRAINS(X10**2)

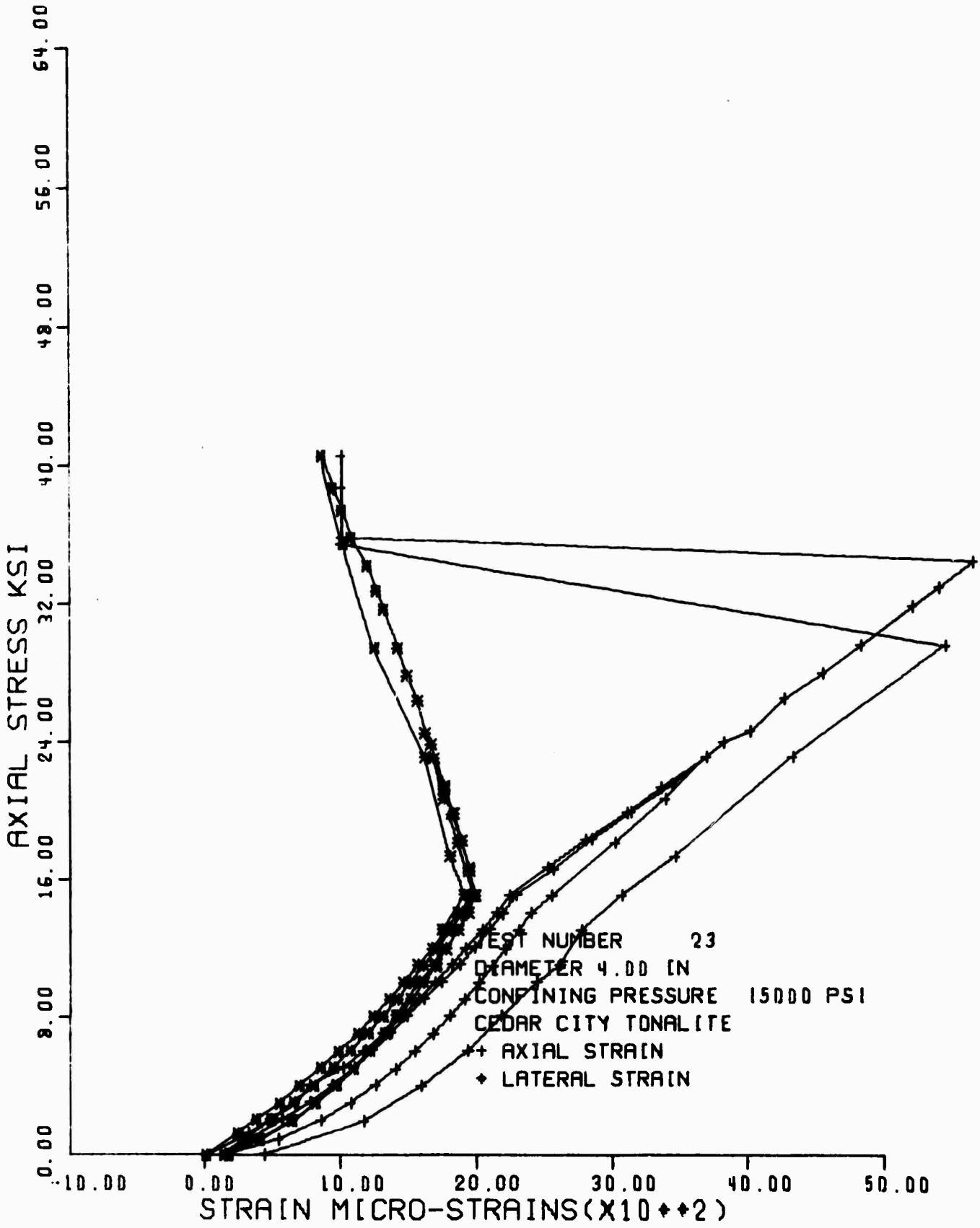
AXIAL STRESS KSI
0.00
8.00
16.00
24.00
32.00
40.00
48.00
56.00
64.00
-10.00
0.00
10.00
20.00
30.00
40.00
50.00
STRAIN M[CRO-STRAINS(X10**2)
TEST NUMBER 23
DIAMETER 4.00 IN
CONFINING PRESSURE 15000 PSI
CEDAR CITY TONALITE
+ AXIAL STRAIN
* LATERAL STRAIN

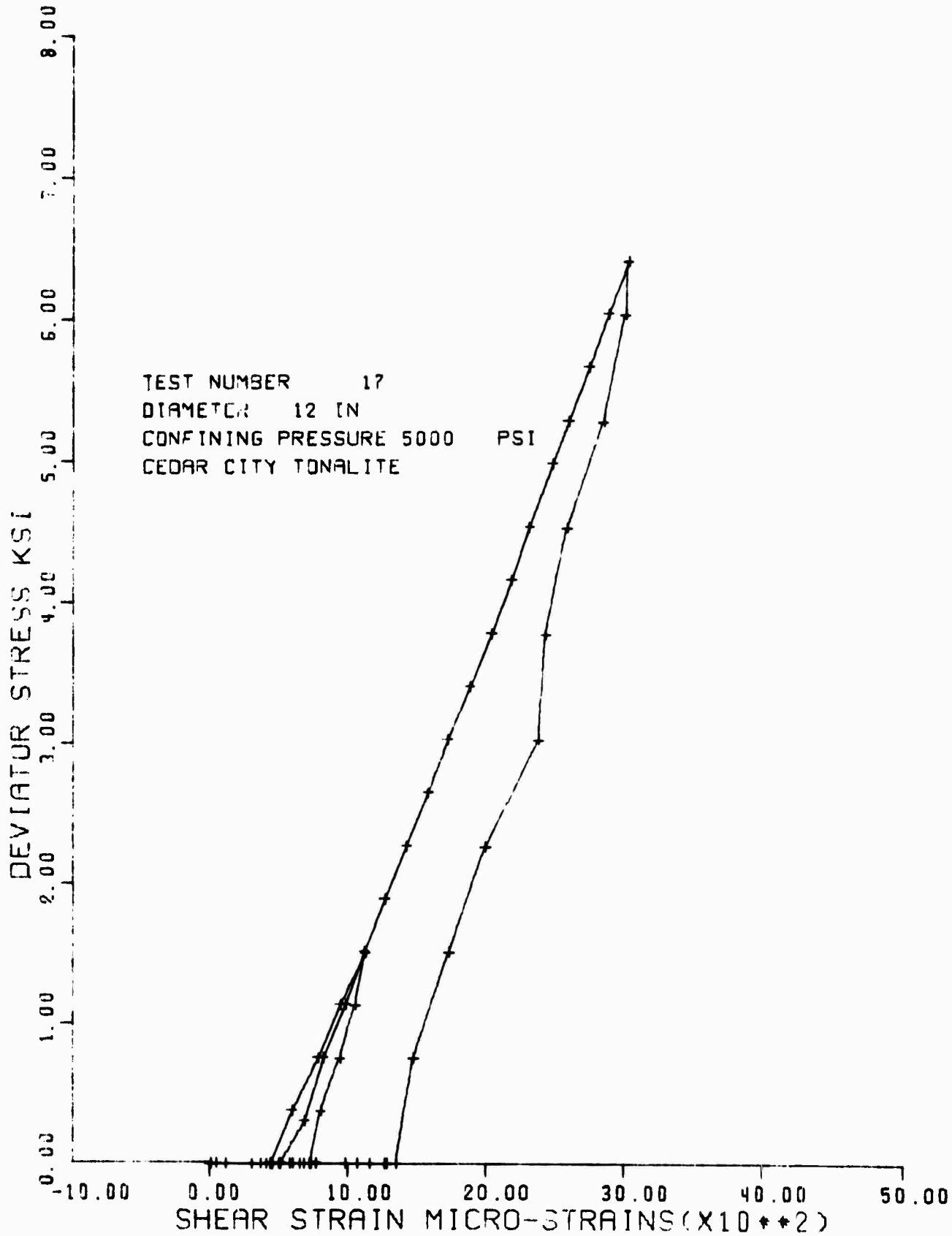
TEST NUMBER 17
DIAMETER 12 IN
CONFINING PRESSURE 5000 PSI
CEDAR CITY TONALITE
DEVIATOR STRESS KSI
0.00
1.00
2.00
3.00
4.00
5.00
6.00
7.00
8.00
-10.00
0.00
10.00
20.00
30.00
40.00
50.00
SHEAR STRAIN MICRO-STRAINS(X10**2)

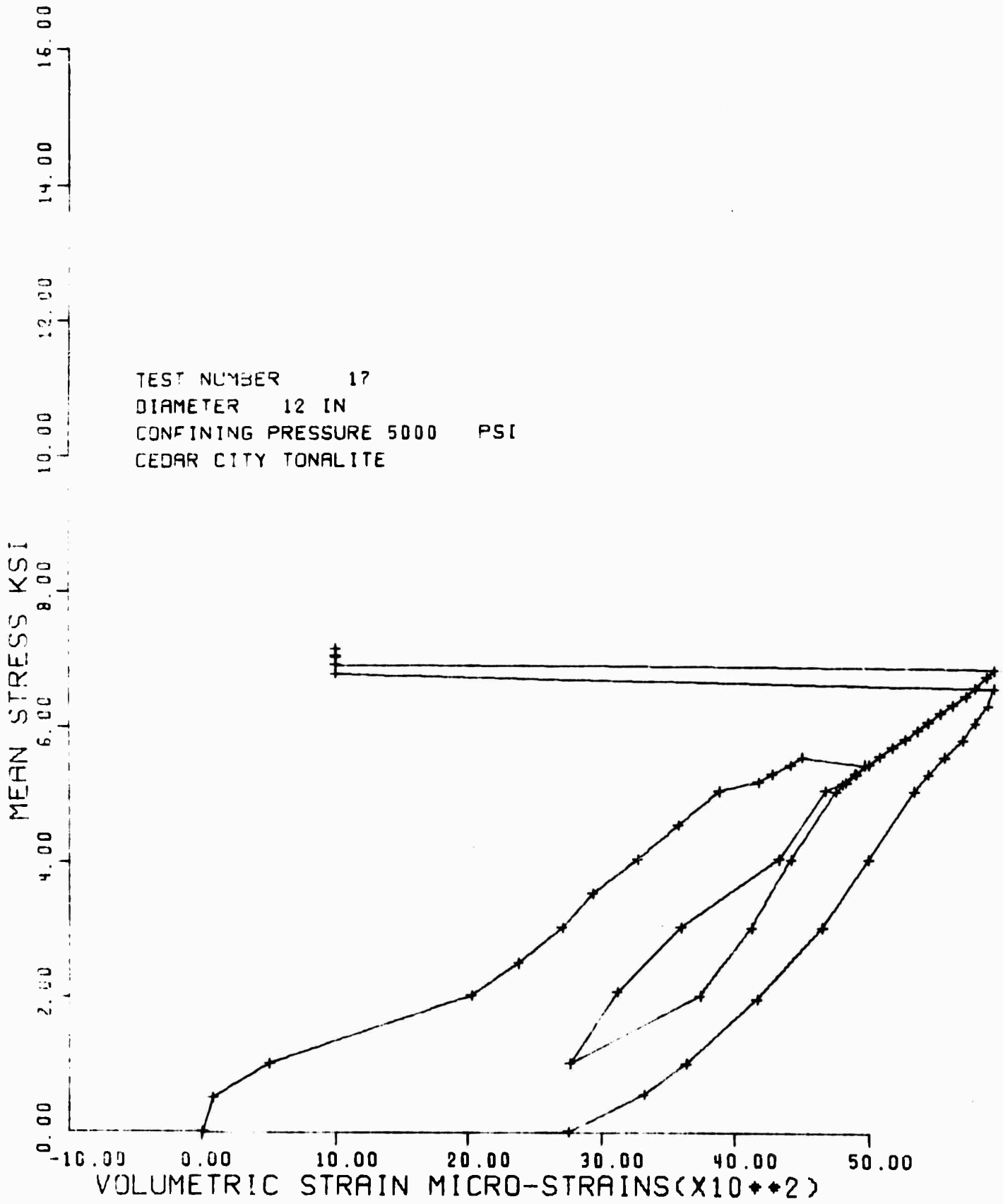
TEST NUMBER 17
DIAMETER 12 IN
CONFINING PRESSURE 5000 PSI
CEDAR CITY TONALITE
MEAN STRESS KSI
0.00
2.00
4.00
6.00
8.00
10.00
12.00
14.00
16.00
-10.00
0.00
10.00
20.00
30.00
40.00
50.00
VOLUMETRIC STRAIN MICRO-STRAINS(X10**2)

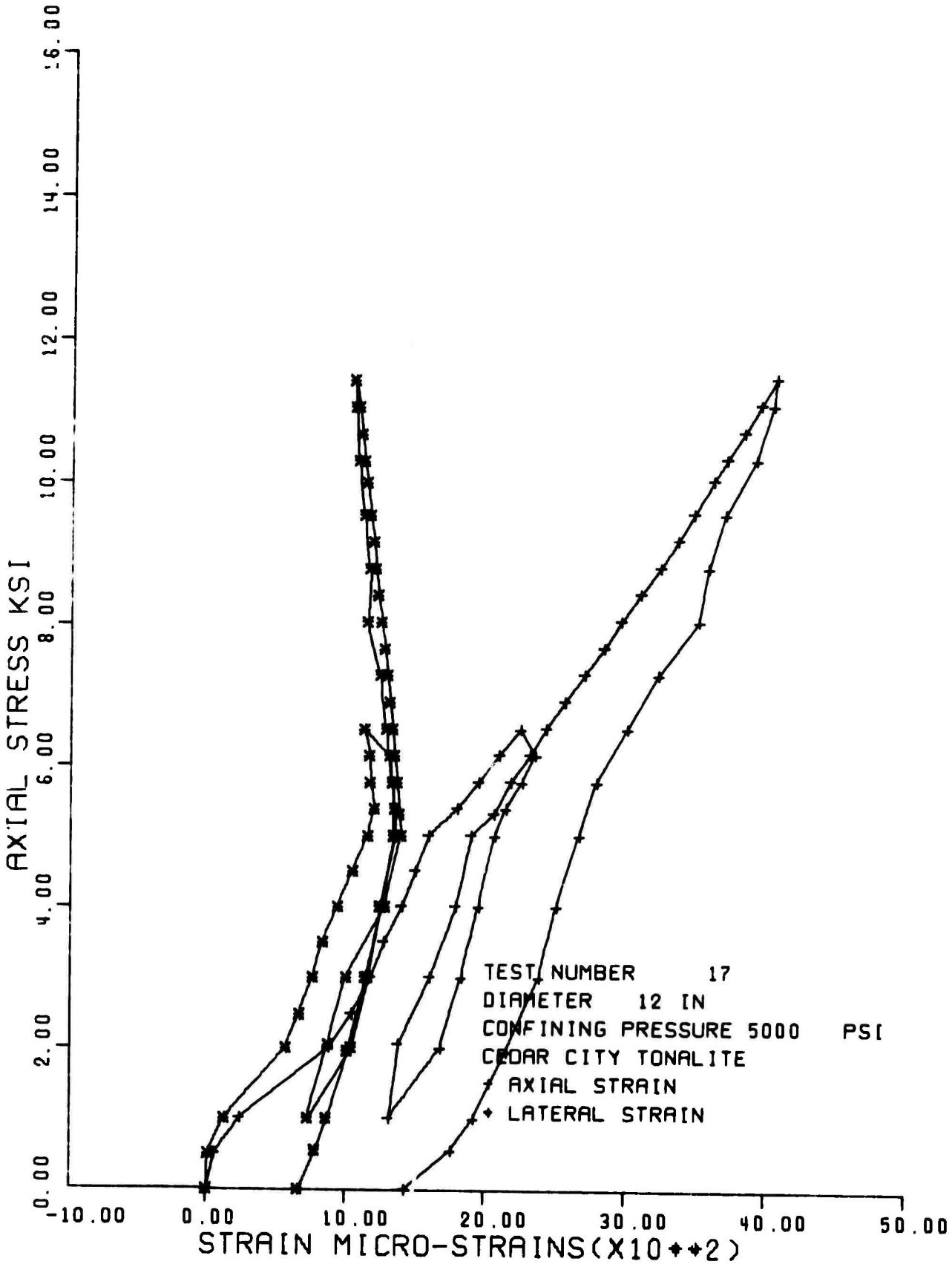
AXIAL STRESS KSI
0.00
2.00
4.00
6.00
8.00
10.00
12.00
14.00
16.00
-10.00
0.00
10.00
20.00
30.00
40.00
50.00
STRAIN MICRO-STRAINS(X10**2)
TEST NUMBER 17
DIAMETER 12 IN
CONFINING PRESSURE 5000 PSI
CEDAR CITY TONALITE
AXIAL STRAIN
LATERAL STRAIN

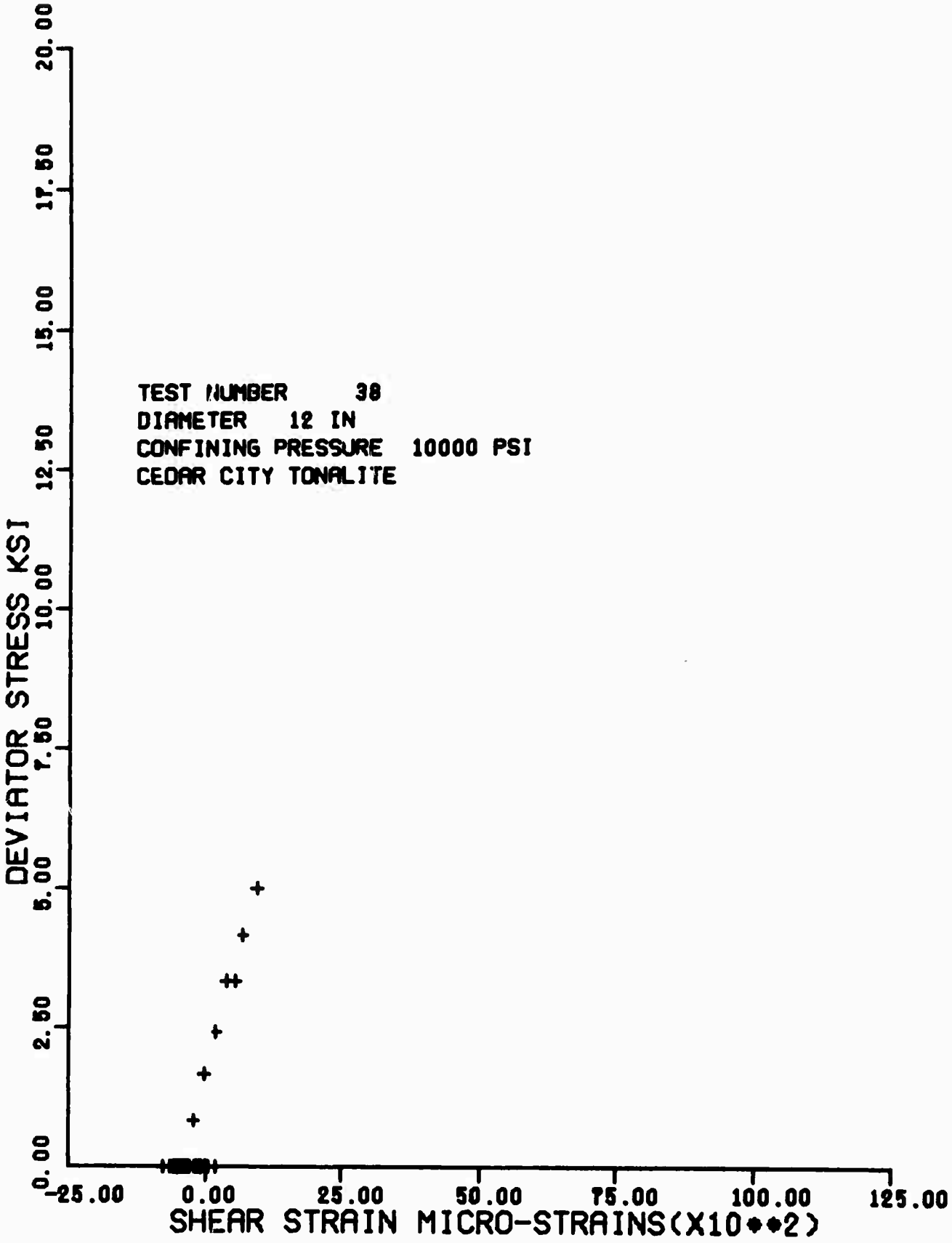
TEST NUMBER 38
DIAMETER 12 IN
CONFINING PRESSURE 10000 PSI
CEDAR CITY TONALITE
DEVIATOR STRESS KSI
0.00
2.50
5.00
7.50
10.00
12.50
15.00
17.50
20.00
-25.00
0.00
25.00
50.00
75.00
100.00
125.00
SHEAR STRAIN MICRO-STRAINS(X10**2)

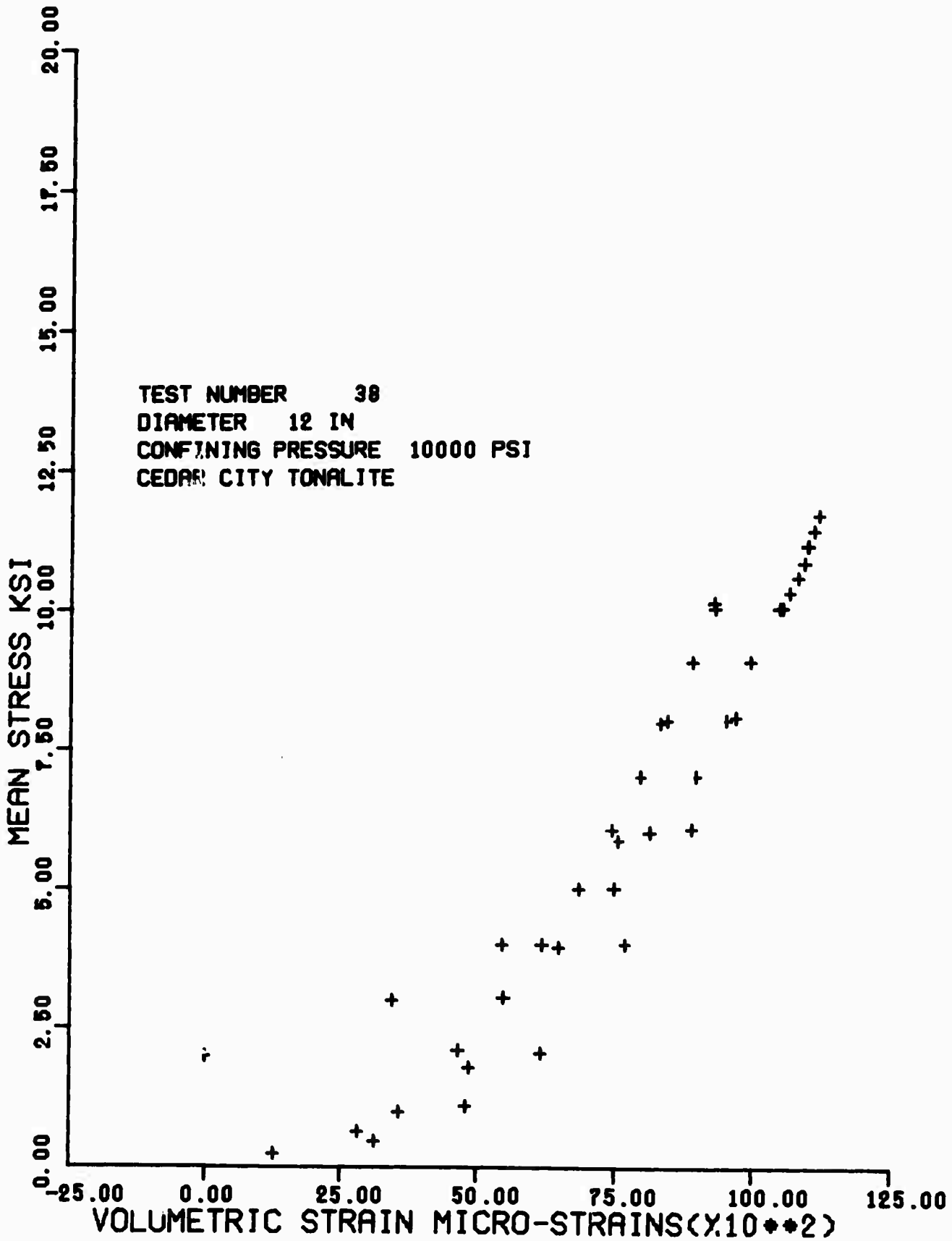
TEST NUMBER 38
DIAMETER 12 IN
CONFINING PRESSURE 10000 PSI
CEDAR CITY TONALITE
MEAN STRESS KSI
0.00
2.50
5.00
7.50
10.00
12.50
15.00
17.50
20.00
-25.00
0.00
25.00
50.00
75.00
100.00
125.00
VOLUMETRIC STRAIN MICRO-STRAINS(X10**2)

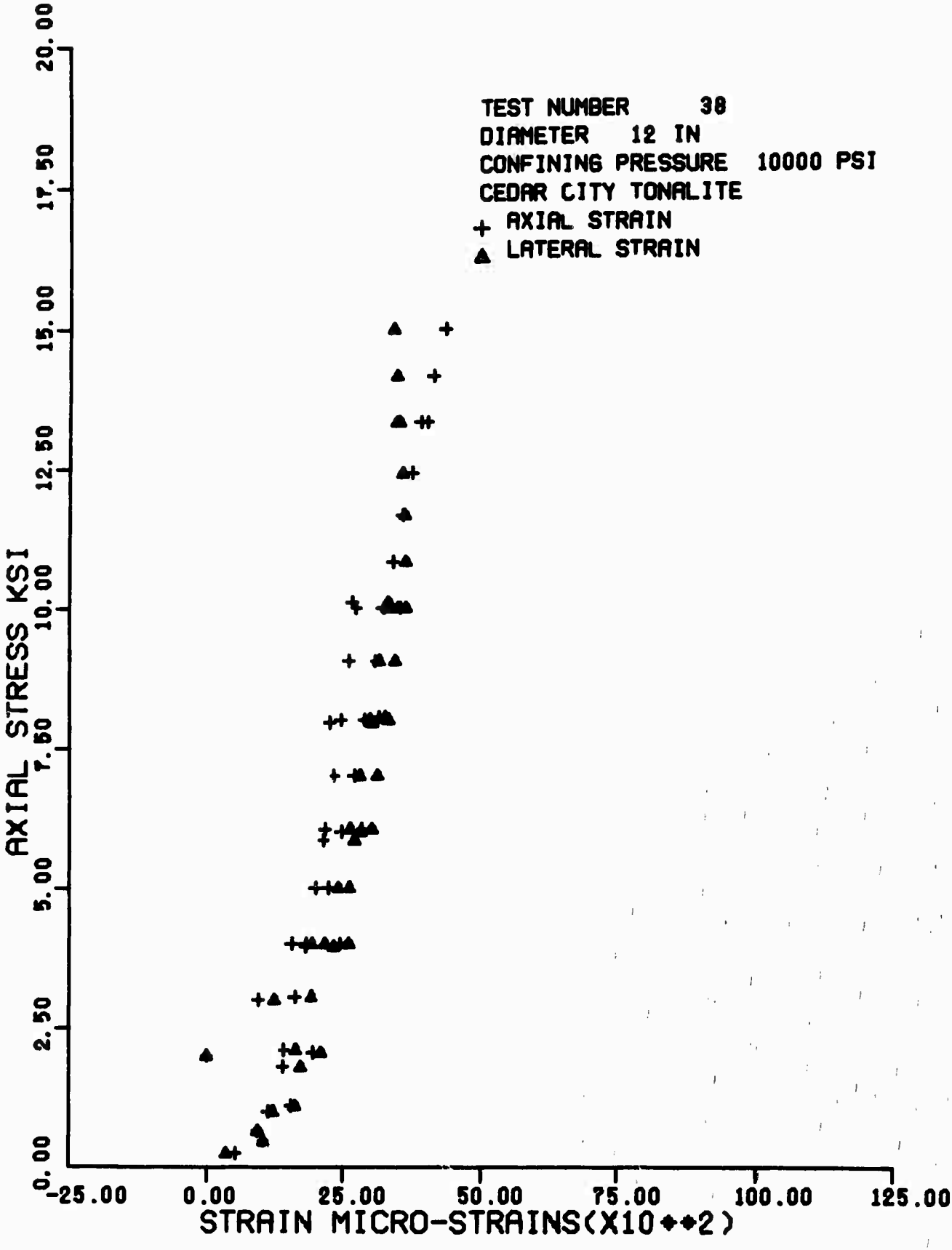
TEST NUMBER 38
DIAMETER 12 IN
CONFINING PRESSURE 10000 PSI
CEDAR CITY TONALITE
+ AXIAL STRAIN
▲ LATERAL STRAIN
AXIAL STRESS KSI
0.00
2.50
5.00
7.50
10.00
12.50
15.00
17.50
20.00
-25.00
0.00
25.00
50.00
75.00
100.00
125.00
STRAIN MICRO-STRAINS(X10**2)

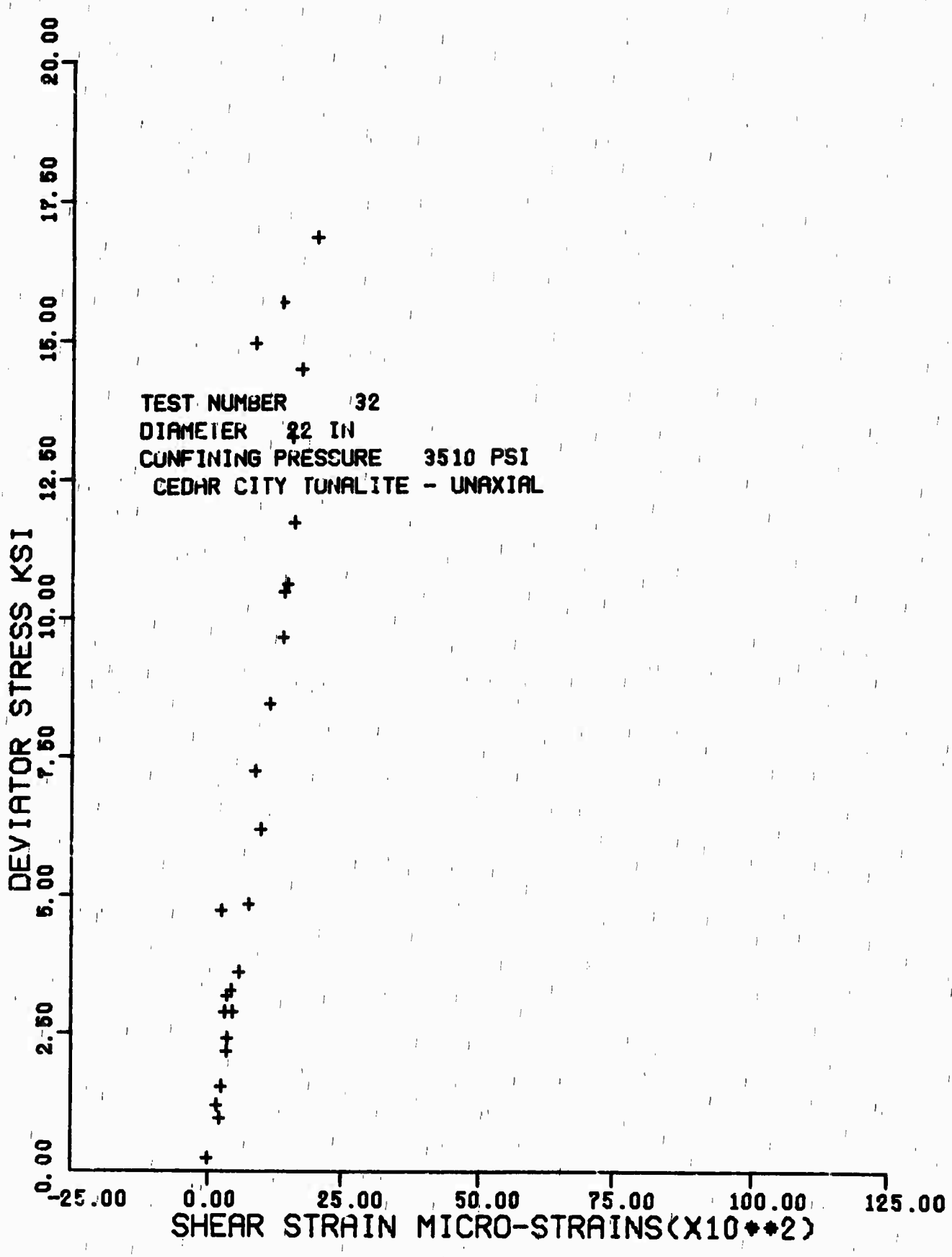
TEST NUMBER 32
DIAMETER 2.2 IN
CONFINING PRESSURE 3510 PSI
CEDAR CITY TONALITE - UNAXIAL
DEVIATOR STRESS KSI
0.00
2.50
5.00
7.50
10.00
12.50
15.00
17.50
20.00
-25.00
0.00
25.00
50.00
75.00
100.00
125.00
SHEAR STRAIN MICRO-STRAINS(X10**2)

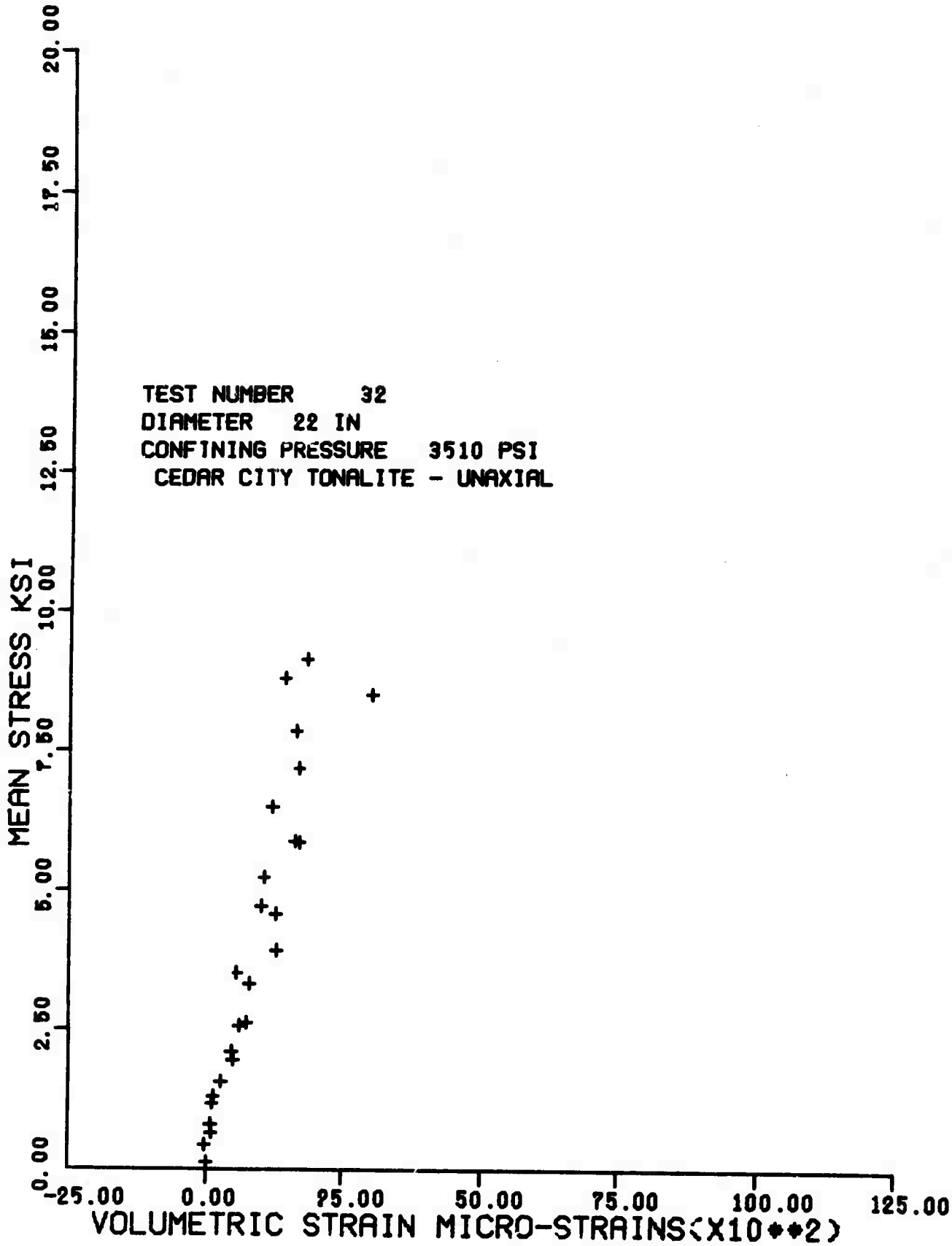
TEST NUMBER 32
DIAMETER 22 IN
CONFINING PRESSURE 3510 PSI
CEDAR CITY TONALITE - UNAXIAL
MEAN STRESS KSI
0.00
2.50
5.00
7.50
10.00
12.50
15.00
17.50
20.00
-25.00
0.00
25.00
50.00
75.00
100.00
125.00
VOLUMETRIC STRAIN MICRO-STRAINS(X10**2)

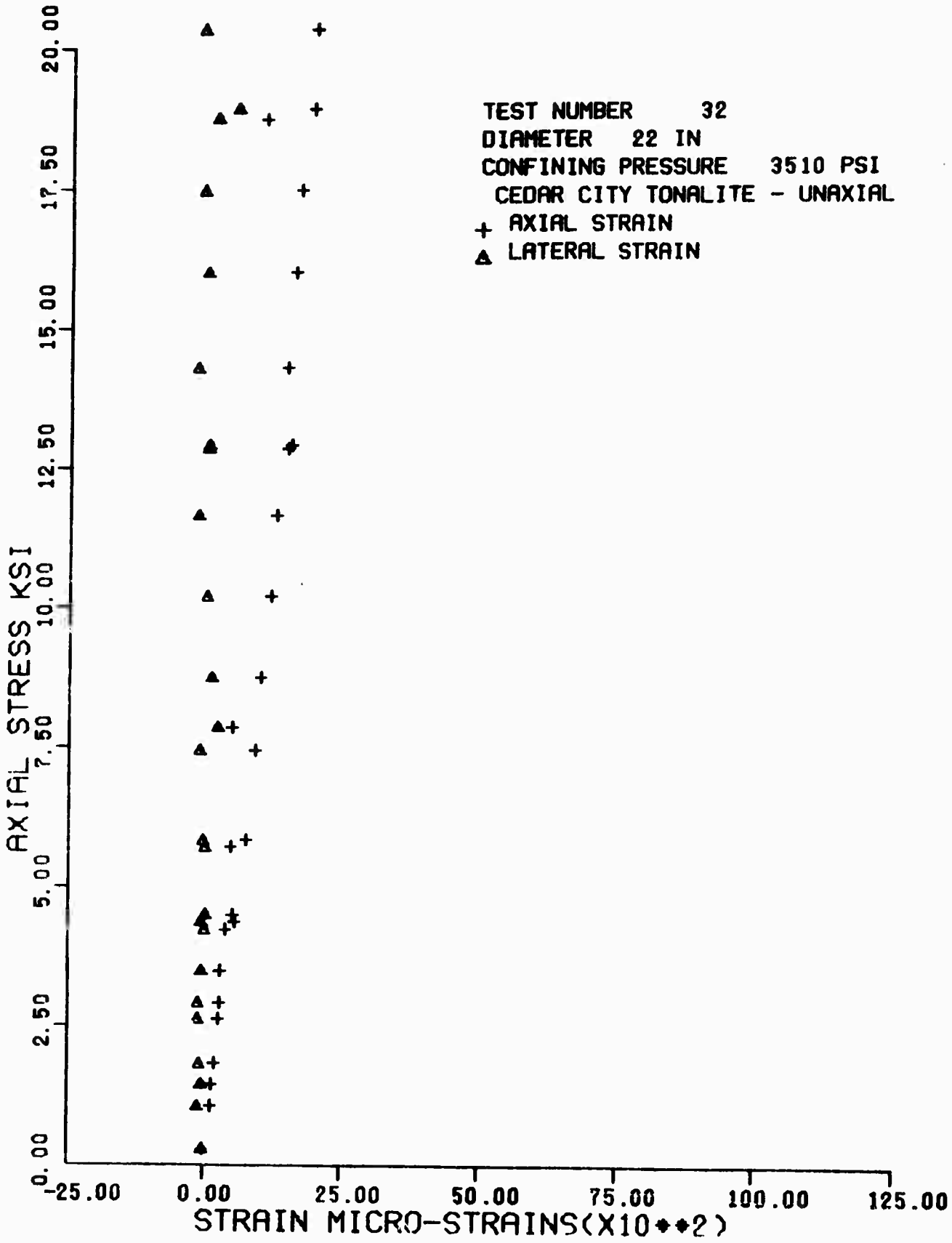
TEST NUMBER 32
DIAMETER 22 IN
CONFINING PRESSURE 3510 PSI
CEDAR CITY TONALITE - UNAXIAL
+ AXIAL STRAIN
△ LATERAL STRAIN
AXIAL STRESS KSI
0.00
2.50
5.00
7.50
10.00
12.50
15.00
17.50
20.00
-25.00
0.00
25.00
50.00
75.00
100.00
125.00
STRAIN MICRO-STRAINS(X10**2)